



University
of Glasgow

Collins, Louise L. (2010) *Analysis of the role of rab11-FIP3 phosphorylation during cytokinesis*. PhD thesis.

<http://theses.gla.ac.uk/1682/>

Copyright and moral rights for this thesis are retained by the author

A copy can be downloaded for personal non-commercial research or study, without prior permission or charge

This thesis cannot be reproduced or quoted extensively from without first obtaining permission in writing from the Author

The content must not be changed in any way or sold commercially in any format or medium without the formal permission of the Author

When referring to this work, full bibliographic details including the author, title, awarding institution and date of the thesis must be given.

Analysis of the Role of Rab11-FIP3 Phosphorylation During Cytokinesis

A thesis submitted to the
FACULTY OF BIOMEDICAL AND LIFE SCIENCES

For the degree of
DOCTOR OF PHILOSOPHY

By
LOUISE LARMOUR COLLINS

Division of Molecular and Cellular Biology
Faculty of Biomedical and Life Sciences
University of Glasgow
March 2010

Abstract

Cytokinesis involves abscission of the intracellular bridge between two daughter cells, thus completing mitosis. Membrane traffic is at the heart of mammalian cytokinesis. Rab11-FIP3 (also referred to as FIP3) in complex with Rab11 plays a key role in the delivery and targeting of recycling endosomes to the furrow; this is essential for completion of cytokinesis. FIP3 undergoes spatial and temporal dynamics during mitosis. During metaphase and early anaphase, FIP3 is largely cytosolic, with some localised to endosomal membrane structures. During late anaphase, following furrow initiation, FIP3 localises to the centrosome. At late cytokinesis, FIP3 relocates to the cleavage furrow and midbody. On separation of the daughter cells, FIP3 returns to the centrosome. The regulatory mechanisms governing the dynamics of FIP3 during mitosis are unknown. This work aims to determine if FIP3 can be phosphorylated by the cell-cycle kinases which regulate mitosis, and whether this has an impact on the spatial and temporal dynamics of FIP3.

In vitro phosphorylation assays show that FIP3 can be phosphorylated by cyclin B-CDK1, Plk1, Aurora A and weakly by Aurora B. A proteomic approach revealed that, within the limits of our experimental approach, only cyclin B-CDK1 phosphorylated FIP3 significantly, at serine 102. Interestingly, proteomic analysis of FIP3 immunoprecipitated from metaphase cells has identified serine 102, 281, 348 and 451 as sites of potential phosphorylation. Data from this and a collaborating lab offers the hypothesis that FIP3 is phosphorylated during the early stages of the cell-cycle, and that dephosphorylation of FIP3 is the trigger for the association of FIP3 with membranes. A phospho-specific antibody to serine 102 (pS102) detects CDK1 phosphorylated FIP3. Serine 102 is phosphorylated in metaphase and becomes dephosphorylated as the cell progresses through to telophase. Further analysis reveals that cytosolic levels of pS102 peak in metaphase and decrease towards telophase to negligible levels. pS102 is absent in the membrane fraction. This work suggests that FIP3 may be directly phosphorylated by CDK1, at serine 102, in early mitosis. Kinase inhibition studies show that inhibition of CDK1, by the inhibitor BMI-1026, results in a mis-localisation of GFP-FIP3 in HeLa cells. This could also be interpreted as a delay in cytokinesis, since CDK1 inhibition resulted in more cells in telophase

displaying GFP-FIP3 in a localisation characteristic of an earlier stage of telophase, compared to the controls.

The role of phosphorylation at serines 102, 281, 348 and 451 of FIP3 was investigated by creating phospho-null and phospho-mimetic mutants in the context of GFP-FIP3. It would appear that when mutated singly, the potential phospho-sites of serines 102, 281, 348 and 451 (phospho-mimetic mutant only for serine 451) have no significant effect on the localisation of FIP3 during mitosis, nor do they affect cytokinesis. A phospho-null mutation of serine 451 resulted in poor expression of the protein and an unhealthy population of cells.

In summary, the spatial and temporal dynamics of FIP3 may be regulated by phosphorylation. We hypothesise that during prometaphase and metaphase FIP3 is phosphorylated, preventing its association with endosomes. FIP3 is dephosphorylated in late anaphase, allowing it to associate with endosomes and subsequently traffic to the furrow and midbody. We suggest that CDK1 phosphorylates FIP3 in the early stages of mitosis, at serine 102. In conclusion, membrane traffic is central to mammalian cytokinesis and data from this thesis suggests that it may be regulated by the cell-cycle kinases.

Table of Contents

Chapter 1 Introduction

1	Introduction.....	17
1.1	Cell division	18
1.2	Cytokinesis.....	20
1.2.1	Cytokinesis specialisations	20
1.2.1.1	Animal cells.....	20
1.2.1.2	Plant cells.....	20
1.2.1.3	Fission Yeast.....	21
1.2.1.4	Budding Yeast	21
1.2.1.5	<i>Drosophila melanogaster</i> cellularisation	21
1.2.2	Stages of mammalian cytokinesis.....	22
1.2.2.1	Cleavage plane specification.....	22
1.2.2.2	Contractile ring assembly.....	23
1.2.2.3	Molecular mechanisms of furrow ingression	24
1.2.2.4	The midbody.....	26
1.2.2.5	Completion of cytokinesis	27
1.3	Membrane trafficking	27
1.3.1	Intracellular membrane-trafficking pathways	27
1.3.2	Rab GTPase family	28
1.3.3	The ADP-ribosylation factor (ARF) family.....	29
1.3.4	SNARE proteins	29
1.3.5	Vesicle-tethering factors.....	30
1.4	Membrane trafficking in cytokinesis	30
1.4.1	The role of membrane trafficking in cytokinesis	30
1.4.2	Origin of the membrane delivered to the cleavage furrow	32
1.4.2.1	The secretory pathway.....	32
1.4.2.2	The endosomal pathway	33
1.5	Rab11-FIP3.....	36
1.5.1	Rab11-family interacting proteins (Rab11-FIPs)	36
1.5.2	Nuf protein is a <i>D. melanogaster</i> homologue of FIP3	37
1.5.3	Cellular functions of FIP3	38
1.5.4	Subcellular localisation of FIP3	39
1.5.5	Structure of FIP3	40
1.5.6	Interacting partners of FIP3	41
1.5.6.1	FIP3 interacts with members of the Rab GTPase family	41
1.5.6.2	FIP3 interacts with members of the ARF GTPase family	42
1.5.6.3	FIP3 interacts with CYK-4.....	43
1.5.6.4	FIP3 interacts with ASAP1	44
1.5.6.5	FIP3 interacts with molecular motor proteins.....	44
1.5.7	Model for membrane traffic during cytokinesis.....	45
1.5.8	Regulation of FIP3.....	48
1.6	Cell-cycle kinases.....	49
1.6.1	Cell-cycle overview	49
1.6.2	Cyclin-dependent kinase 1 (CDK1).....	50
1.6.3	Polo-like kinase 1 (Plk1).....	54
1.6.4	Aurora A kinase	56
1.6.5	Aurora B kinase	57

1.7	Aims	59
-----	------------	----

Chapter 2 Materials and Methods

2	Materials and Methods.....	60
2.1	Materials	61
2.1.1	General reagents.....	61
2.1.2	Cell culture reagents	66
2.1.3	Primary antibodies	66
2.1.4	<i>Escherichia coli</i> (<i>E. coli</i>) strains.....	67
2.1.5	Plasmids	67
2.1.6	Primers.....	68
2.1.7	Rab11-FIP3 phospho-peptides	69
2.1.8	Radiochemicals	70
2.1.9	Kinase Inhibitors.....	70
2.1.10	General solutions.....	71
2.2	General laboratory procedures	73
2.2.1	Protein assays.....	73
2.2.2	SDS-polyacrylamide gel electrophoresis (SDS-PAGE)	73
2.2.3	Western blotting	74
2.2.4	Immunodetection of proteins.....	74
2.2.5	Stripping of nitrocellulose membranes.....	75
2.2.6	Coomassie blue staining of SDS polyacrylamide gels.....	75
2.2.7	Brilliant Blue G-Colloidal Coomassie	75
2.3	General molecular biology	76
2.3.1	Site directed mutagenesis	76
2.3.2	Transformation of <i>Escherichia coli</i>	77
2.3.3	Small scale DNA preparations (miniprep).....	77
2.3.4	Large-scale DNA preparation (maxiprep)	78
2.3.5	DNA restriction digests	79
2.3.6	Ligation	79
2.3.7	Agarose gel electrophoresis	80
2.3.8	Gel extraction of DNA	80
2.3.9	Alkaline phosphatase treatment of linearised plasmid DNA	81
2.3.10	DNA sequencing.....	81
2.4	Mammalian cell culture.....	81
2.4.1	Cell culture conditions	81
2.4.2	Passage of cells	82
2.4.3	Cryopreservation of cells.....	82
2.4.4	Resurrecting cells	83
2.4.5	HeLa cell synchronisation.....	83
2.4.5.1	Thymidine, nocodazole block	83
2.4.5.2	Thymidine, nocodazole and MG132 block	83
2.4.6	Plasmid DNA transfection	84
2.4.7	Cell lysis	84
2.4.8	Membrane and cytosol fractionation	85
2.4.9	Density gradient fractionation	86
2.5	Immunofluorescence	88
2.5.1	Immunofluorescence.....	88
2.5.2	Confocal microscopy.....	89

2.6	<i>In vitro</i> phosphorylation assays	89
2.7	Proteomics.....	90
2.7.1	Phosphorylation site mapping of Rab11-FIP3.....	90
2.7.2	Proteomic analysis of recombinant Rab11-FIP3.....	91
2.8	Phospho-specific antibody production.....	92
2.8.1	Phospho-specific antibody generation	92
2.8.2	Phospho-specific antibody purification	93
2.8.3	Peptide competition assay (PCA)	93

Chapter 3 *In vitro* phosphorylation of Rab11-FIP3

3	<i>In vitro</i> phosphorylation of Rab11-FIP3	95
3.1	Introduction	96
3.2	Aims	97
3.3	Results.....	99
3.3.1	Generic (non kinase specific) phosphorylation predictions	99
3.3.2	Kinase specific phosphorylation predictions	101
3.3.3	<i>In vitro</i> phosphorylation of FIP3 by mitotic kinases.....	102
3.3.4	Analysis of recombinant FIP3's capacity to autophosphorylate ...	104
3.3.5	<i>In vitro</i> phosphorylation of heat-treated FIP3 by mitotic kinases.	106
3.3.6	Phosphorylation site mapping of FIP3	107
3.3.7	<i>In vitro</i> phosphorylation of FIP3 by Aurora B (co-expressed with INCENP and survivin).....	113
3.3.8	<i>In vitro</i> phosphorylation of CDK1 and Aurora A primed FIP3.....	113
3.3.9	<i>In vitro</i> phosphorylation of Alkaline Phosphatase treated FIP3 by mitotic kinases.....	116
3.3.10	Proteomic analysis of recombinant FIP3	117
3.3.11	Immunoblot analysis of recombinant FIP3.....	121
3.3.12	FIP3 autophosphorylation in the presence of kinase inhibitors....	123
3.3.13	HeLa cytoplasmic S100 fraction phosphorylation of FIP3	124
3.4	Conclusions	126

Chapter 4 Consequences of Rab11-FIP3 phosphorylation

4	Consequences of Rab11-FIP3 phosphorylation	130
4.1	Introduction	131
4.2	Aims	133
4.3	Results.....	133
4.3.1	Membrane and cytosol fractionation of synchronised GFP-FIP3 expressing HeLa cells	133
4.3.2	Phospho-specific antibody validation via peptide competition assays (PCAs)	136
4.3.3	Phospho-specific antibody analysis of membrane and cytosol fractions from synchronised GFP-FIP3 expressing HeLa cells	143
4.3.4	Density gradient analysis of FIP3's association with HeLa membranes.....	147
4.3.5	Effect of kinase inhibition on GFP-FIP3 localisation in HeLa cells	149
4.4	Conclusions	154

Chapter 5 Analysis of Rab11-FIP3 phosphosites

5	Analysis of Rab11-FIP3 phosphosites	158
5.1	Introduction	159
5.2	Aims	159
5.3	Methods	159
5.3.1	Site directed mutagenesis	159
5.3.2	Validation of mutant plasmids	161
5.3.3	Cloning of BamHI fragments into GFP-FIP3 or pCR3.1	161
5.3.4	Generation of phospho-mutant GFP-FIP3 plasmids.....	163
5.3.4.1	Generation of GFP-FIP3-S102A and GFP-FIP3-S102D plasmids	163
5.3.4.2	Generation of GFP-FIP3-S281A and GFP-FIP3-S281D plasmids	163
5.3.4.3	Generation of GFP-FIP3-S348A and GFP-FIP3-S348D plasmids	165
5.3.4.4	Generation of GFP-FIP3-S451A and GFP-FIP3-S451D plasmids	166
5.4	Results.....	167
5.4.1	Restriction digest analysis of phospho-mutant GFP-FIP3 plasmids	167
5.4.2	Immunoblot analysis of HeLa lysates from cells expressing phospho-mutant GFP-FIP3 plasmids	169
5.4.3	Immunofluorescence analysis of HeLa cells expressing phospho-mutant GFP-FIP3 plasmids	172
5.4.4	Binuclear cell count analysis of HeLa cells expressing phospho-mutant GFP-FIP3 plasmids	174
5.5	Conclusions	178

Chapter 6 Discussion

6	Discussion	201
---	------------------	-----

Chapter 7 Appendix

7	Appendix	206
7.1	Rab11-FIP3 Proteomic Data	206
7.1.1	Rab11-FIP3 solution analysed via nLC-ESI-MS/MS by Sir Henry Wellcome Functional Genomics Facility (SHWFGF), University of Glasgow	206
7.1.2	Rab11-FIP3 gel slices analysed via nLC-ESI-MS/MS by Sir Henry Wellcome Functional Genomics Facility (SHWFGF), University of Glasgow	209
7.1.3	Rab11-FIP3 gel slices analysed via LC-MS/MS by Aberdeen Proteomics, University of Aberdeen.....	219
	List of References	221

List of Tables

Table 3.1 Generic (non kinase specific) phosphorylation predictions for serine residues of human Rab11-FIP3.....	101
Table 7.1 Protein identification of recombinant FIP3 solution by nLC-ESI-MS/MS, searching the <i>Mammalia</i> database, performed by SHWFGF, University of Glasgow.	208
Table 7.2 Protein identification of recombinant FIP3 solution by nLC-ESI-MS/MS, searching the <i>Drosophila</i> database, performed by SHWFGF, University of Glasgow.	209
Table 7.3 Protein identification of recombinant FIP3 gel slice 1 by nLC-ESI-MS/MS searching the <i>Mammalia</i> database, performed by SHWFGF, University of Glasgow.	210
Table 7.4 Protein identification of recombinant FIP3 gel slice 1 by nLC-ESI-MS/MS searching the <i>Drosophila</i> database, performed by SHWFGF, University of Glasgow.	211
Table 7.5 Protein identification of recombinant FIP3 gel slice 2 by nLC-ESI-MS/MS searching the <i>Mammalia</i> database, performed by SHWFGF, University of Glasgow.	213
Table 7.6 Protein identification of recombinant FIP3 gel slice 2 by nLC-ESI-MS/MS searching the <i>Drosophila</i> database, performed by SHWFGF, University of Glasgow.	213
Table 7.7 Protein identification of recombinant FIP3 gel slice 3 by nLC-ESI-MS/MS searching the <i>Mammalia</i> database, performed by SHWFGF, University of Glasgow.	215
Table 7.8 Protein identification of recombinant FIP3 gel slice 3 by nLC-ESI-MS/MS searching the <i>Drosophila</i> database, performed by SHWFGF, University of Glasgow.	215
Table 7.9 Protein identification of recombinant FIP3 gel slice 4 by nLC-ESI-MS/MS searching the <i>Mammalia</i> database, performed by SHWFGF, University of Glasgow.	216
Table 7.10 Protein identification of recombinant FIP3 gel slice 4 by nLC-ESI-MS/MS searching the <i>Drosophila</i> database, performed by SHWFGF, University of Glasgow.	217
Table 7.11 Protein identification of recombinant FIP3 gel slice 5 by nLC-ESI-MS/MS searching the <i>Mammalia</i> database, performed by SHWFGF, University of Glasgow.	218
Table 7.12 Protein identification of recombinant FIP3 gel slice 5 by nLC-ESI-MS/MS searching the <i>Drosophila</i> database, performed by SHWFGF, University of Glasgow.	218
Table 7.13 Protein identification of recombinant FIP3 gel slices by LC-MS/MS searching Human and <i>Spodoptera Frugiperda</i> databases, performed by Aberdeen Proteomics at the University of Aberdeen.	220

List of Figures

Figure 1-1 The stages of cell division.....	19
Figure 1-2 Schematic diagram of the molecular mechanisms of furrow ingression	25
Figure 1-3 Schematic representation of predicted domains and classification of the FIPs	37
Figure 1-4 Temporal and spatial dynamics of GFP-FIP3 during mitosis.....	40
Figure 1-5 Model for membrane traffic during cytokinesis.....	48
Figure 1-6 Cell-cycle regulation of the central spindle.....	50
Figure 3-1 Identification of FIP3 phosphosites from metaphase HeLa lysates....	98
Figure 3-2 <i>In vitro</i> phosphorylation of FIP3 by mitotic kinases	103
Figure 3-3 Analysis of recombinant FIP3's capacity to autophosphorylate	105
Figure 3-4 <i>In vitro</i> phosphorylation of heat-treated FIP3 by mitotic kinases....	107
Figure 3-5 Phosphorylation site mapping of non-phosphorylated FIP3	109
Figure 3-6 <i>In vitro</i> phosphorylation of CDK1 and Aurora A primed FIP3	115
Figure 3-7 Recombinant FIP3 separated by SDS-PAGE and stained with Coomassie Blue Stain.	117
Figure 3-8 Immunoblot analysis of recombinant FIP3	122
Figure 3-9 FIP3 autophosphorylation in the presence of kinase inhibitors.....	124
Figure 3-10 HeLa cytoplasmic S100 fraction phosphorylation of FIP3	126
Figure 4-1 Analysis of the role of phosphorylation in the membrane and cytosol distribution of FIP3 throughout the cell-cycle.	132
Figure 4-2 Membrane and cytosol fractionation of synchronised GFP-FIP3 expressing HeLa cells	135
Figure 4-3 Quantification of GFP levels in the membrane and cytosol fractions of synchronised GFP-FIP3 expressing HeLa cells.	136
Figure 4-4 FIP3 pS102 peptide competition assay	139
Figure 4-5 FIP3 pS281 peptide competition assay	140
Figure 4-6 FIP3 pS348 peptide competition assay	141
Figure 4-7 FIP3 pS451 peptide competition assay	142
Figure 4-8 Analysis of phosphorylated serine 102 in membrane and cytosol fractionated synchronised GFP-FIP3 expressing HeLa cells	144
Figure 4-9 Quantification of pS102 expression in the input, membrane and cytosol fractions of synchronised GFP-FIP3 expressing HeLa cells.	145
Figure 4-10 Phospho-specific antibody analysis of crude cell homogenate from synchronised GFP-FIP3 expressing HeLa cells	146
Figure 4-11 Density gradient analysis of FIP3's association with HeLa membranes	148
Figure 4-12 Telophase localisations of GFP-FIP3 in HeLa cells	150
Figure 4-13 Effect of kinase inhibition on the localisation of GFP-FIP3 in non- synchronised HeLa cells	151
Figure 4-14 Effect of kinase inhibition on the localisation of GFP-FIP3 in synchronised HeLa cells	153
Figure 5-1 Schematic figure of the GFP-FIP3 plasmid.....	160
Figure 5-2 Restriction digest analysis of GFP-FIP3-S102A and GFP-FIP3-S102D plasmids.....	168

Figure 5-3 Immunoblot analysis of HeLa lysates from cells expressing GFP-FIP3-S102A and GFP-FIP3-S102D plasmids	170
Figure 5-4 Immunoblot analysis of HeLa lysates from cells expressing GFP-FIP3-S281A and GFP-FIP3-S281D plasmids.....	171
Figure 5-5 Immunoblot analysis of HeLa lysates from cells expressing GFP-FIP3-S348A and GFP-FIP3-S348D plasmids	171
Figure 5-6 Immunoblot analysis of HeLa lysates from cells expressing GFP-FIP3-S451A and GFP-FIP3-S451D plasmids.....	172
Figure 5-7 Binuclear cell count of HeLa cells expressing GFP-FIP3-S102A and GFP-FIP3-S102D plasmids for 48 hours	176
Figure 5-8 Binuclear cell count of HeLa cells expressing GFP-FIP3-S281A and GFP-FIP3-S281D plasmids for 24 hours	176
Figure 5-9 Binuclear cell count of HeLa cells expressing GFP-FIP3-S348A and GFP-FIP3-S348D plasmids for 72 hours	177
Figure 5-10 Binuclear cell count of HeLa cells expressing GFP-FIP3-S451A and GFP-FIP3-S451D plasmids for 24 hours	177
Figure 5-11 Immunofluorescence analysis of HeLa cells in interphase expressing GFP-FIP3-S102A/D and GFP-FIP3-S281A/D plasmids for 48 hours.	183
Figure 5-12 Immunofluorescence analysis of HeLa cells in interphase expressing GFP-FIP3-S348A/D and GFP-FIP3-S451A/D plasmids for 48 hours.	184
Figure 5-13 Immunofluorescence analysis of HeLa cells in interphase expressing wild-type GFP-FIP3 and GFP-FIP3-I737E plasmids, in addition to Lipofectamine 2000 only and untransfected controls, for 48 hours.....	185
Figure 5-14 Immunofluorescence analysis of HeLa cells in metaphase expressing GFP-FIP3-S102A/D and GFP-FIP3-S281A/D plasmids for 48 hours.	186
Figure 5-15 Immunofluorescence analysis of HeLa cells in metaphase expressing GFP-FIP3-S348A/D and GFP-FIP3-S451D plasmids for 48 hours.	187
Figure 5-16 Immunofluorescence analysis of HeLa cells in metaphase expressing wild-type GFP-FIP3 and GFP-FIP3-I737E plasmids, in addition to Lipofectamine 2000 only and untransfected controls, for 48 hours.....	188
Figure 5-17 Immunofluorescence analysis of HeLa cells in anaphase expressing GFP-FIP3-S102A/D and GFP-FIP3-S281A/D plasmids for 48 hours.	189
Figure 5-18 Immunofluorescence analysis of HeLa cells in anaphase expressing GFP-FIP3-S348A/D and GFP-FIP3-S451D plasmids for 48 hours.	190
Figure 5-19 Immunofluorescence analysis of HeLa cells in anaphase expressing wild-type GFP-FIP3 and GFP-FIP3-I737E plasmids, in addition to Lipofectamine 2000 only and untransfected controls, for 48 hours.....	191
Figure 5-20 Immunofluorescence analysis of HeLa cells in early telophase expressing GFP-FIP3-S102A/D and GFP-FIP3-S281A/D plasmids for 48 hours.	192
Figure 5-21 Immunofluorescence analysis of HeLa cells in early telophase expressing GFP-FIP3-S348A/D and GFP-FIP3-S451D plasmids for 48 hours.	193
Figure 5-22 Immunofluorescence analysis of HeLa cells in early telophase expressing wild-type GFP-FIP3 and GFP-FIP3-I737E plasmids, in addition to Lipofectamine 2000 only and untransfected controls, for 48 hours.	194
Figure 5-23 Immunofluorescence analysis of HeLa cells in late telophase expressing GFP-FIP3-S102A/D and GFP-FIP3-S281A/D plasmids for 48 hours.	195
Figure 5-24 Immunofluorescence analysis of HeLa cells in late telophase expressing GFP-FIP3-S348A/D and GFP-FIP3-S451D plasmids for 48 hours.	196
Figure 5-25 Immunofluorescence analysis of HeLa cells in late telophase expressing wild-type GFP-FIP3 and GFP-FIP3-I737E plasmids, in addition to Lipofectamine 2000 only and untransfected controls, for 48 hours.	197
Figure 5-26 Immunofluorescence analysis of HeLa cells expressing GFP-FIP3-S451A/D plasmids for 48 hours	198

Figure 5-27 Immunofluorescence analysis of HeLa cells expressing wild-type GFP-FIP3 and GFP-FIP3-I737E plasmids for 48 hours. 199

Figure 5-28 Immunofluorescence analysis HeLa cells treated with control transfections for 48 hours.....200

Acknowledgements

First and foremost I'd like to thank Prof. Gwyn W. Gould for giving me the opportunity to work in his lab and for his patience, support and encouragement throughout my PhD. I'd also like to thank him for his faith in my abilities and giving me the opportunity to continue my work in his lab.

I'd also like to thank Dr. Nia J. Bryant for her encouragement throughout my time in the lab. Dr. Johanne Matheson provided great friendship and support throughout my PhD which I value greatly. I'm indebted to Dr. Hélia Neto for her advice, encouragement and scientific discussion throughout this work, for which I am truly grateful. I'd like to thank all members of lab 241, past and present, for their technical help and moral support. In particular I'd like to thank Dr. Scott Shanks for his help and friendship throughout my PhD.

I'd like to thank all my lovely friends who have helped me along the way. I'd especially like to thank Aparna Barua, Sara Stevenson, Helen McArdle and Sarah Jones for their friendship.

Finally, I'm indebted to my parents for their patience, understanding and support, not only during my PhD, but throughout my lifetime. None of this would have been possible without them and I would like to take this opportunity to thank them with all my love. It remains for me to thank Sunny, Bailey and Finty, without whom none of this work would have been possible.

Author's declaration

I declare that the work described in this thesis has been carried out by myself unless otherwise cited or acknowledged. It is entirely of my own composition and has not, in whole or in part, been submitted for any other degree.

Louise Larmour Collins

2009

Abbreviations

Ab	Antibody
ABD	ARF-binding domain
ADP	Adenosine 5'-diphosphate
AIS	Aurora B-INCENP-Survivin complex
APC/C	Anaphase promoting complex/cyclosome
APS	Ammonium persulphate
ARF	ADP-ribosylation factor
ATP	Adenosine 5'-triphosphate
ATP- γ - ³² P	Adenosine 5'-triphosphate [γ - ³² P]
ATP.Mg ²⁺	Adenosine 5'-triphosphate magnesium salt
bp	Base pair
BFA	Brefeldin A
BSA	Bovine serum albumin
Cdc	Cell division control protein
CDK	Cyclin-dependent kinase
<i>C. elegans</i>	<i>Caenorhabditis elegans</i>
CHO	Chinese hamster ovary cells
CK2	Casein kinase 2
CPC	Chromosomal passenger complex
Da	Dalton
DAPI	4',6-Diamidino-2-phenylindole, dilactate
DEPC	Diethylpyrocarbonate
DMEM	Dulbecco's Modified Eagle's Medium
DMSO	Dimethyl sulphoxide
DNA	Deoxyribonucleic acid
dNTP	Deoxynucleoside 5'-triphosphate
DOPS	1,2-dioleoyl phosphatidylserine
DTT	Dithiothreitol
ECL	Enhanced chemiluminescence
<i>E. coli</i>	<i>Escherichia coli</i>
EDTA	Ethylenediaminetetraacetic acid
EE	Early endosome
Eferin	EF-hands-containing Rab11-interacting protein
EGFP	Enhanced green fluorescence protein

EGTA	Ethylene glycol-bis(2-aminoethylether)-N,N,N',N'-tetraacetic acid
ER	Endoplasmic reticulum
FIP	Rab11-family interacting protein
FIP3	Rab11-FIP3
GAP	GTPase activating protein
GAPDH	Glyceraldehyde 3-phosphate dehydrogenase
GEF	Guanine nucleotide exchange factor
GFP	Green fluorescent protein
GTP	Guanosine 5'-triphosphate
HEPES	N-(2-Hydroxyethyl)piperazine-N'-2-ethanesulphonic acid
HCl	Hydrochloric acid
HIS-tag	Hexa-histidine tag
HRP	Horseradish peroxidase
IgG	Immunoglobulin G
INCENP	Inner centromere protein
kb	Kilobase
kDa	Kilo Dalton
LE	Late endosome
m	Milli
M	Molar
mA	Milliamps
MAP	Microtubule-associated protein
MBP	Myelin basic protein
MEM	Minimum Essential Medium
MES	2-(N-Morpholino)ethanesulphonic acid
MG132	Z-Leu-Leu-Leu-al
min	Minute
MKLP	Mitotic kinesin-like protein
MOPS	3-(N-Morpholino)propanesulphonic acid
MT	Microtubule
MTOC	Microtubule-organising centre
nLC-ESI-MS/MS	Nanoflow HPLC electrospray tandem mass spectrometry
nLC-MS/MS	Nano-liquid chromatography-tandem mass spectrometry
Nuf	Nuclear-fallout
Nycodenz®	5-(N-2,3-Dihydroxypropylacetamido)-2,4,6-triiodo-N,N'-bis(2,3-dihydroxypropyl)isophthalamide
OD	Optical density

PAGE	Polyacrylamide gel electrophoresis
PBS	Phosphate buffered saline
PBST	Phosphate buffered saline with Tween20
PCA	Peptide competition assay
PCR	Polymerase chain reaction
Plk	Polo-like kinase
PM	Plasma membrane
POPC	1-palmitoyl-2-oleoyl phosphatidylcholine
PRC1	MAP protein regulator of cytokinesis 1
Rab	Ras protein in brain
Rab11-FIP	Rab11-family interacting protein
Ras	Rat Sarcoma
RBD	Rab11-binding domain
RCP	Rab-coupling protein
RE	Recycling endosome
RNAi	RNA interference
ROCK	Rho-associated kinase
rpm	Revolutions per minute
SAP	Shrimp alkaline phosphatase
<i>S. cerevisiae</i>	<i>Saccharomyces cerevisiae</i>
SDM	Site directed mutagenesis
SDS	Sodium dodecyl sulphate
SDS-PAGE	Sodium dodecyl sulphate polyacrylamide gel electrophoresis
Sf	<i>Spodoptera frugiperda</i>
<i>S. pombe</i>	<i>Schizosaccharomyces pombe</i>
SNARE	Soluble N-ethylmaleimide-sensitive factor attachment protein receptor
TAE	Tris-acetate-EDTA
TCA	Trichloroacetic acid
TEMED	N,N,N',N'-Tetramethylethylenediamine
Tf	Transferrin
TfR	Transferrin Receptor
TGN	Trans-Golgi network
Tris	Tris(hydroxymethyl)aminoethane
Tween 20	Polyethylene glycol sorbitan monolaurate
v/v	volume/volume ratio
w/v	weight/volume ratio

1 Introduction

1.1 Cell division

Cell division involves two key stages. Firstly the nucleus divides through a process known as mitosis, separating replicated chromosomes into two daughter nuclei. This is directly followed by partitioning of the cytoplasm via cytokinesis, forming two daughter cells (Barr and Gruneberg, 2007).

A cell divides via a series of stages, as shown in figure 1.1 (reproduced from Scholey *et al.*, 2003). Interphase is the period in the cell-cycle between one mitotic cycle and the next. At this stage chromosomes are uncondensed, allowing replication of genetic material, thus producing two copies of each chromosome, known as sister chromatids. The centrosome is also duplicated during interphase. The centrosome is composed of a pair of centrioles surrounded by pericentriolar material. This structure is the microtubule-organising centre (MTOC), responsible for microtubule nucleation leading to the formation of the spindle poles during mitosis. Prophase (figure 1.1A) follows, where replicated chromosomes, each consisting of two sister chromatids, condense. Outside of nucleus, the replicated centrosomes migrate around the nucleus. The cytoskeleton reorganises, allowing the microtubules of the mitotic spindle to assemble between the two centrosomes. During prometaphase (figure 1.1B), the nuclear envelope breaks down, allowing the spindle microtubules to interact with the fully condensed chromosomes via their kinetochores. Under the influence of the mitotic spindle, chromosomes align to the equator of the cell, in a process termed congression. At metaphase the chromosomes are aligned at the equator of the cell (indicated in figure 1.1C as 'e'), midway between the spindle poles (indicated in figure 1.1C as 'p'). During anaphase A (figure 1.1D), cohesion is lost between sister chromatids and they are pulled towards either pole of the cell under the influence of the spindle microtubules. In anaphase B (figure 1.1E), the spindle poles move apart which also aids chromosome separation. During anaphase the division plane is determined by the spindle which sends a signal to the cortex, marking the location for contractile ring assembly. Constriction of this structure in late anaphase forms a cleavage furrow, thus driving cytokinesis. At telophase (figure 1.1F), the two sets of

daughter chromosomes arrive at the poles of the spindle and decondense. A new nuclear envelope reassembles around each set, completing the formation of two daughter nuclei. The cleavage furrow continues to ingress, forming a barrier between the two daughter cells. Abscission occurs to seal the furrow, thus creating two separate daughter cells, each with one complement of chromosomes. Cytokinesis is complete by the end of telophase; the nucleus and cytoplasm of each of the daughter cells then return to interphase, marking the end of mitosis.

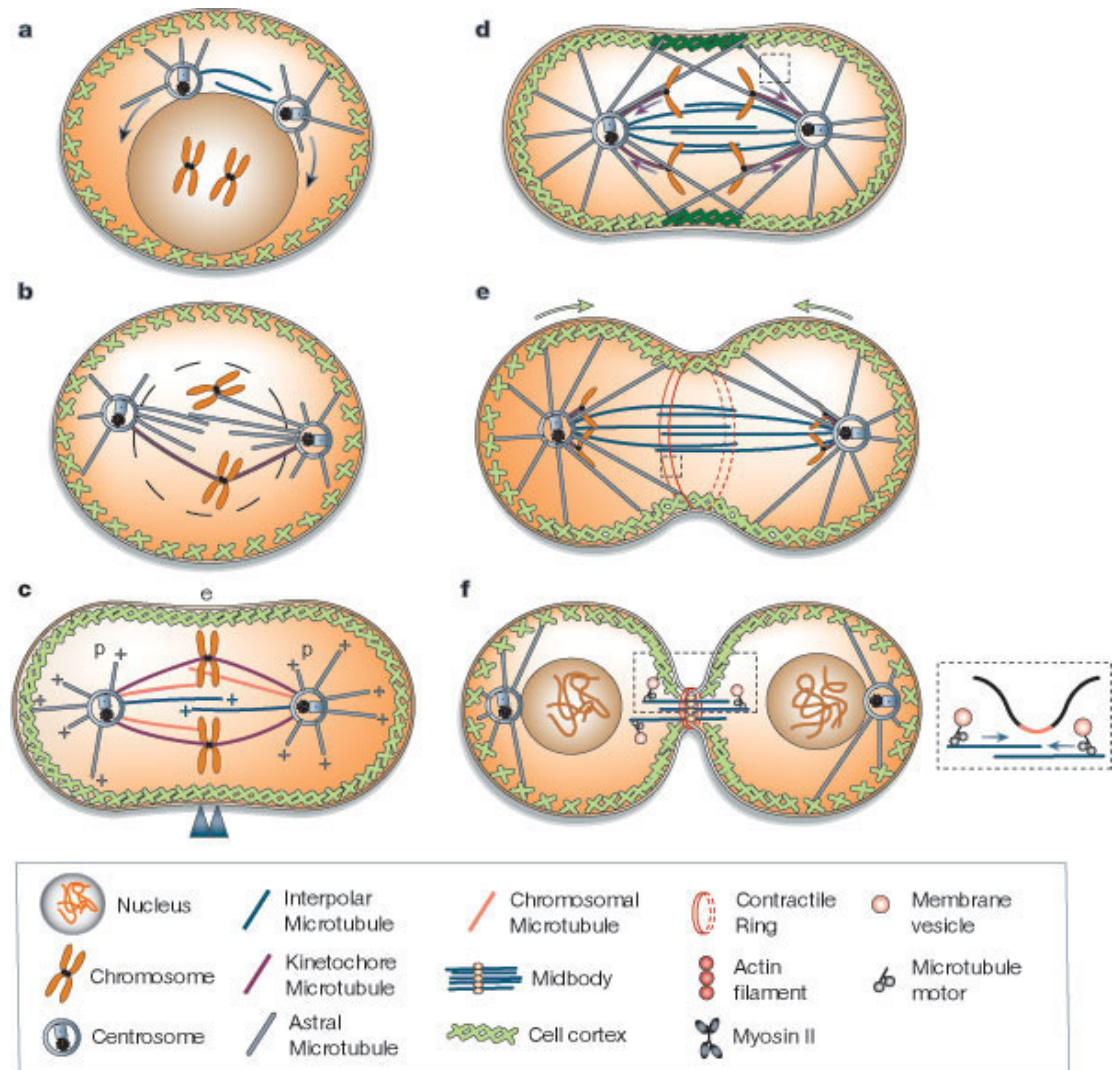


Figure 1-1 The stages of cell division (modified from Scholey *et al.*, 2003)
a, Prophase; b, Prometaphase; c, Metaphase; d, Anaphase A; e, Anaphase B; f, telophase/cytokinesis. Key: 'e' denotes the equator and 'p' marks each pole of the cell.

1.2 Cytokinesis

1.2.1 Cytokinesis specialisations

The overall approach to cell division is well conserved. However, species specific variations exist in the mechanics of cytokinesis. Plant cells divide by creating a Golgi-derived membrane partition between separating nuclei, known as the phragmoplast. Animal cells and yeast both employ an actomyosin based-contractile ring to separate dividing cells (Guertin *et al.*, 2002).

1.2.1.1 Animal cells

In animal cells, cytokinesis commences with the formation of the actomyosin contractile ring. The contractile ring is composed of actin, myosin-II and other structural and regulatory proteins. It forms beneath the plasma membrane, around the equator of the cell, at the mid-point between the two mitotic spindle poles. This structure constricts at the end of anaphase, inducing invagination of the cell membrane. This forms a cleavage furrow which continues to ingress until the two daughter cells are pinched apart (Eggert *et al.*, 2006). The mechanics of animal cell cytokinesis will be discussed in more detail in section 1.2.2.

1.2.1.2 Plant cells

Plant cells are surrounded by a rigid cell wall, thus cell division cannot occur via the formation of an actomyosin-contractile ring or furrow ingression. Indeed, it has been found that the Arabidopsis genome sequence lacks the gene for myosin II (The Arabidopsis Genome Initiative, 2000). Instead plant cells divide by forming a new membrane compartment between the two daughter nuclei. In somatic cells, a structure known as the phragmoplast forms between divided nuclei and is believed to guide the formation of the membrane partition and the new cell wall (Jürgens, 2005). The phragmoplast is a cylindrical structure containing two opposing groups of actin filaments and microtubules. It forms in late anaphase. The phragmoplast is formed by the fusion of Golgi-derived vesicles, containing cell wall material, which have been transported along the microtubules to the plane of cell division. The continuous fusion of vesicles

generates a membrane compartment at the plane of division, forming a structure known as the cell plate. During cytokinesis the cell plate grows from the interior of the cell, outwards to the cell cortex. The fusion of later-arriving vesicles with the margin of the cell plate causes it to expand towards the periphery of the cell, resulting in the fusion of the cell plate with the plasma membrane, thus dividing the cytoplasm of the cell (Otegui *et al.*, 2005).

1.2.1.3 Fission Yeast

Fission yeast *Schizosaccharomyces pombe* (*S. pombe*) divides by employing the actomyosin-contractile ring, which is positioned at the equator of the dividing yeast. As the contractile ring constricts, *S. pombe* synthesises a division septum behind the ring. This leads to the formation of a cell wall and membrane between the two daughter cells. Digestive enzymes then degrade the septum, thus completing cytokinesis and separating the daughter cells (Guertin *et al.*, 2002).

1.2.1.4 Budding Yeast

Contrastingly, *Saccharomyces cerevisiae* (*S. cerevisiae*) division is asymmetric and occurs by budding. A bud grows out from the mother cell cortex via polarised cell growth. An actomyosin based-contractile ring is then formed at the bud neck, and similar to *S. pombe*, a division septum is formed behind the constricting ring (Guertin *et al.*, 2002).

1.2.1.5 *Drosophila melanogaster* cellularisation

Drosophila melanogaster (*D. melanogaster*) cellularisation is a specialised form of cytokinesis. During early embryogenesis, the zygote undergoes 13 nuclear divisions without cytokinesis (syncytial divisions). The first nine occur in the interior of the embryo. This results in the syncytial blastoderm containing approximately 6000 somatic nuclei, which migrate to the cortex during interphase of cycle 10. Four more synchronous divisions take place as a monolayer directly below the plasma membrane. During cycle 14, termed cellularisation, membrane furrows develop in between the cortical nuclei,

eventually compartmentalising each nuclei into separate cells (Mazumdar and Mazumdar, 2002).

1.2.2 Stages of mammalian cytokinesis

In mammalian cells, cytokinesis was thought to be driven by an actomyosin-contractile ring. Constriction of the contractile ring induces invagination of the cell membrane into a cleavage furrow which continues to ingress until the two daughter cells are pinched apart (Eggert *et al.*, 2006). However, animal cell cytokinesis is a far more intricate process, involving a series of stages which are precisely timed and a multitude of proteins which are meticulously regulated to ensure accurate cell division (Eggert *et al.*, 2006). On initiation of cytokinesis, the position of the cleavage plane is first specified. Next the contractile ring is assembled and the cleavage furrow ingresses. This leads to the formation of a narrow intracellular bridge linking the two daughter cells, the central region of which is known as the midbody. Cytokinesis reaches completion upon abscission of the intracellular bridge, forming two separate daughter cells (Eggert *et al.*, 2006). Abscission itself is a complicated process, the mechanism of which is currently undergoing intense research (Steigemann and Gerlich, 2009). For cytokinesis to occur, the actomyosin contractile ring must disassemble. Additionally, recent research has placed membrane traffic to the midbody at the heart of abscission (Albertson *et al.*, 2005; Glotzer, 2005; Barr and Gruneberg, 2007; Prekeris and Gould, 2008). The current understanding of the mechanisms behind each stage of cytokinesis is discussed in the following sections.

1.2.2.1 Cleavage plane specification

The first step in cytokinesis is to specify the position of the cleavage plane, where the components of the contractile ring are destined to assemble (Eggert *et al.*, 2006). Research performed by Rappaport has shown that the mitotic spindle specifies the location of the contractile ring, and thereby the position of the cleavage furrow during early anaphase (reviewed in Burgess and Chang, 2005). The cell cleavage plane is perpendicular to the axis of chromosome segregation, usually midway between spindle poles. This ensures that the genome and cytoplasm are equally partitioned between cells. In some situations, the spindle is not positioned centrally, resulting in asymmetric divisions

important during embryonic and stem cell divisions (Siller and Doe, 2009; Neumüller and Knoblich, 2009).

Several models exist to explain which parts of the mitotic spindle define the site of cleavage furrow formation (Eggert *et al.*, 2006). One area of research questions the nature of the signals delivered to the cortex by the astral microtubules. Firstly, the astral relaxation model suggests that astral microtubules, radiating out from the centrosome to the cortex, dampen down cortical contraction everywhere except the furrow. This is due to the greater density of microtubules interacting with the polar regions of the cortex than at the equator (reviewed in Glotzer, 2004). However, the astral stimulation model suggests that astral microtubules at the equatorial region signal the site of cleavage and recruit contractile components to this region. This is potentially due to the fact that the cortex at the equator interacts with two sets of astral microtubules, one from either pole, and therefore the strength of the stimulus is highest in this region (reviewed in Glotzer, 2004). Another area of research has focused on the type of microtubules delivering the signal: astral or central spindle. During anaphase, overlapping microtubules from opposing poles are bundled, forming a structure known as the central spindle, or spindle midzone. Research suggests that the anaphase spindle midzone microtubules are a principal regulator of furrow formation (reviewed in Glotzer, 2004). Interestingly many regulators of mitosis localise to the central spindle, as discussed in section 1.2.2.2. Currently no consensus has been reached as to the mechanisms behind cleavage plane specification. It has been suggested that multiple, overlapping mechanisms function within the cell, but the relative contributions of each mechanism vary between cell type (Burgess and Chang, 2005).

1.2.2.2 Contractile ring assembly

The contractile ring generates the force required for membrane deformation, resulting in ingression of the cleavage furrow. Once the position of the cleavage furrow has been determined, the components of the contractile ring assemble in anaphase. The contractile ring is composed primarily of actin and the motor protein myosin II (Eggert *et al.*, 2006). Actin forms two-stranded helical polymers beneath the plasma membrane. Myosin II is a dimer of two heavy chains. Each of these is associated with two proteins, namely the essential light

chain (ELC) and regulatory light chain (rMLC). Each myosin heavy chain has a globular head domain at the N-terminus which interacts with actin and also binds to and hydrolyses ATP (Matsumura, 2005). The activity of myosin II generates the force required for constriction of the actomyosin ring, but the arrangement of actin filaments and myosin II in the contractile ring is unknown. The generally accepted model for furrow ingression is the 'purse string' model (Wang, 2005). Myosin II forms long bipolar filaments via interaction of the tail regions of their heavy chains. Myosin II filaments cross link anti-parallel actin filaments into contractile bundles around the equator. Upon hydrolysis of ATP by myosin II, oppositely opposed actin filaments slide past each other, causing the actin filaments to overlap and as a result the bundles shorten (Wang, 2005). This causes the associated membrane to ingress, forming a cleave furrow.

1.2.2.3 Molecular mechanisms of furrow ingression

Actin and myosin II activity reshapes the cell during cytokinesis; this process is regulated by a network of molecular mechanisms. The main regulators of actin dynamics are the Rho family of small GTPases (Piekny *et al.*, 2005). In animal cells, the role of RhoA is central to cytokinesis (Glotzer, 2005). RhoA accumulates at the future site of furrowing (Yüce *et al.*, 2005; Bement *et al.*, 2005). Upon activation, RhoA interacts with and regulates a collection of specific effector proteins (Piekny *et al.*, 2005). These in turn regulate the actomyosin contractile network. A schematic diagram of the molecular mechanisms of furrow ingression is provided in figure 1.2.

Like other small GTPases, RhoA cycles between a GDP-bound inactive form and a GTP-bound active form. This cycle is regulated by various proteins, which are delivered to the correct region of the cortex by the central spindle. ECT2 is the guanine nucleotide exchange factor (GEF) primarily responsible for activation of RhoA. CYK-4 is the GTPase-activating protein (GAP) responsible for inactivation of RhoA. Centralspindlin is a heterotetrameric protein assembly consisting of parallel homodimers of both the kinesin-6 microtubule motor MKLP1 (mitotic kinesin-like protein) and CYK-4. At anaphase the centralspindlin complex interacts with ECT2, via CYK-4, and MKLP1 restricts this ternary complex to the central spindle (Yüce *et al.*, 2005). Interaction of ECT2 with centralspindlin results in the release of ECT2 from its autoinhibitory state (Kim *et al.*, 2005).

ECT2 then promotes the accumulation of RhoA in the regions of the cortex surrounding the central spindle, thus inducing the recruitment of actin and myosin II and assembly of the contractile ring (Werner and Glotzer, 2008).

RhoA regulates contractile ring formation both directly and indirectly, by binding and regulating specific effector proteins. RhoA effectors include members of the formin family and Rho-associated kinase (ROCK) (Piekny *et al.*, 2005). RhoA activates the actin assembly factor formin, thus promoting formation of the contractile ring (Glotzer, 2005). Myosin II is activated by phosphorylation of its regulatory light chain (rMLC) at a highly conserved serine residue at position 19. Upon phosphorylation of Ser19, myosin II assembles into filaments, interacts with actin and the actin-dependent ATPase activity of the motor domain is activated (Matsumura, 2005). RhoA activation results in the activation of ROCK, which phosphorylates rMLC at Ser19, thus activating myosin and furrow formation (Piekny *et al.*, 2005). ROCK also phosphorylates and inhibits the myosin-binding subunit (MBS) of a phosphatase which dephosphorylates Ser19 of rMLC, thus activating myosin phosphorylation (Piekny *et al.*, 2005).

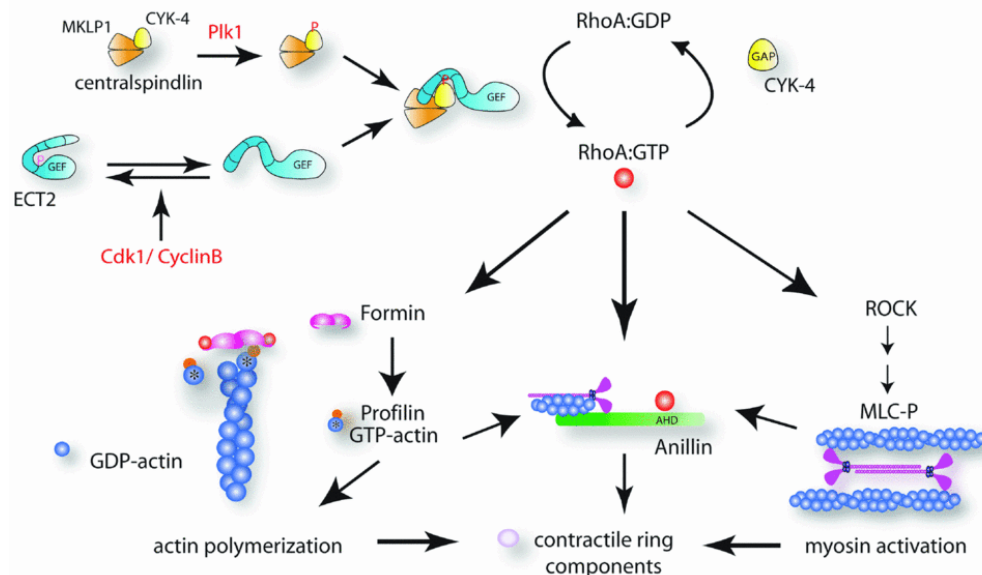


Figure 1-2 Schematic diagram of the molecular mechanisms of furrow ingression (modified from Werner and Glotzer, 2008)

Centralspindlin is a heterotetrameric protein assembly consisting of both the microtubule motor MKLP1 and the RhoA GAP CYK-4. At anaphase the centralspindlin complex interacts with the RhoGEF ECT2, via CYK-4. MKLP1 restricts this ternary complex to the central spindle. Interaction of ECT2 with centralspindlin results in the release of ECT2 from its autoinhibitory state. ECT2 then promotes the accumulation of RhoA in the regions of the cortex surrounding the central spindle. RhoA activates the actin assembly factor formin, thus promoting formation of the contractile ring. RhoA activates ROCK, which phosphorylates rMLC at Ser19, thus activating myosin II. As a result, the actomyosin contractile ring constricts and the cleavage furrow is formed.

1.2.2.4 The midbody

In the later stages of telophase, the spindle midzone is compressed by the ingressing cleavage furrow to the point at which the furrow cannot ingress any further. As a result, the cytoplasm of the two daughter cells is connected by a narrow intracellular bridge. The spindle microtubules form tightly packed antiparallel bundles, which overlap at the central region of the intracellular bridge. This is known as the midbody, a compact electron-dense matrix of proteins from the spindle midzone and cleavage furrow, covering the overlapping microtubule bundles of the central spindle (Steigemann and Gerlich, 2009). The midbody is also known as the Flemming body, stembody or midbody-ring. This structure can persist for some time as a tether between the two daughter cells, before resolution of the bridge (Steigemann and Gerlich, 2009). An electron micrograph of the intracellular bridge is shown in figure 1.5A of section 1.5.7.

The function of the midbody is largely unknown and is currently being intensely researched. Skop and co-workers used a proteomic approach to analyse the protein complement of the midbody, using midbodies purified from Chinese hamster ovary (CHO) cells (Skop *et al.*, 2004). This study identified 160 candidate midbody proteins and these were categorised into five groups. The largest class of proteins (33%) were involved in secretory or membrane-trafficking; 29% were actin-associated proteins; 11% were microtubule-associated proteins; and another 11% were protein kinases. The remaining 16% of the midbody proteins were not classified as they fell into multiple groups. Thus a host of proteins are found within the midbody and could potentially regulate cytokinesis.

Interestingly, the largest class of proteins (33%) identified were involved in secretory or membrane trafficking pathways (Skop *et al.*, 2004). This suggests that membrane trafficking may not only be involved in cytokinesis, but plays an essential role in it. As discussed in section 1.2.1.2, higher plant cells do not employ an actomyosin-contractile ring to drive cytokinesis. In plant cells, the phragmoplast created between divided nuclei, via vesicle trafficking, forms a membrane partition and a new cell wall, resulting in abscission (Jürgens, 2005). It is suggested that in that aspect, the midbody might be analogous to the

phragmoplast and that membrane delivery to the furrow plays a critical role in cytokinesis (Otegui *et al.*, 2005).

1.2.2.5 Completion of cytokinesis

Cytokinesis reaches completion upon abscission of the intracellular bridge, forming two separate daughter cells (Steigemann and Gerlich, 2009). The cellular dynamics at the midbody resulting in abscission are the subject of intense research. Cytokinesis is a multi-step process: the intracellular bridge must be stabilised to prevent regression, following cleavage furrow ingression the contractile ring must be disassembled and the membrane must be remodeled for abscission of the two daughter cells (Schweitzer and D'Souza-Schorey, 2004).

Current research has placed membrane trafficking at the heart of cytokinesis. Daughter cells separate via a more complicated process than a mechanical 'ripping' of the cell in two. Membrane fusion events are thought to play a key role during abscission, when the intracellular bridge is resolved and the two daughter cells finally divide and seal (Barr and Gruneberg, 2007). The involvement of membrane trafficking in cytokinesis will be covered in depth, in section 1.4.

1.3 Membrane trafficking

1.3.1 Intracellular membrane-trafficking pathways

Eukaryotic cells contain various distinct membrane-bound intracellular compartments, called organelles. These include the nucleus, endoplasmic reticulum (ER), Golgi apparatus, mitochondria, endosomes and lysosomes (van Vliet *et al.*, 2003). This high degree of organisation allows biochemically discrete processes to be carried out in isolation, under the correct cellular conditions. There are two main vesicular trafficking pathways within the cell, the secretory pathway and the endocytic pathway, which communicate via vesicle trafficking. Membrane bound vesicles bud-off from the donor compartment membrane, translocate to their target compartment, tether with this compartment and finally dock and fuse with the target organelle membrane (Bonifacino and Glick, 2004).

Depending on their role in the cell, proteins within the secretory pathway can be secreted from the cell, become plasma membrane bound, trafficked to the lysosomes or retained within any of the organelles (reviewed in van Vliet *et al.*, 2003). For secretion, protein must traffic through various distinct organelles within the secretory pathway. Proteins are synthesised, folded and quality controlled within the ER. They are packaged into vesicles and trafficked to the Golgi apparatus. Secretory proteins are then transported through the Golgi cisternae, where they are processed and sorted before traffic to the *trans*-Golgi network (TGN). At the TGN proteins are sorted according to their final destinations and secretory proteins are packaged into vesicles which are transported to the cell surface prior to exocytosis and secretion (van Vliet *et al.*, 2003).

Within the endocytic pathway, proteins on the plasma membrane can be internalised through the inward budding of endocytic vesicles (reviewed in Maxfield and McGraw, 2004; Grant and Donaldson, 2009). Following endocytosis, vesicles are incorporated into early endosomes where sorting occurs. Cargo can be directed to the recycling endosomes which subsequently directs vesicles back to the plasma membrane. From the early endosomes, cargo can also be targeted to the late endosomes and lysosomes for degradation or to the TGN.

A host of proteins regulate intracellular membrane trafficking, including Rab GTPases, ARF GTPases, a variety of vesicle-tethering factors and SNARE proteins (Bonifacino and Glick, 2004).

1.3.2 Rab GTPase family

The Rab family of proteins is the largest group in the Ras superfamily of small GTPases; it comprises of approximately 60 family members in humans (Stenmark, 2009). Specific Rabs are localised to the cytosolic side of specific intracellular membrane compartments, where they regulate distinct steps in vesicular membrane traffic pathways and Rabs are considered to regulate specificity of membrane trafficking (reviewed in Zerial and McBride, 2001). Rab proteins exist in two distinct conformations: in the GTP-bound form, the Rab protein is active, enabling it to interact with downstream effectors; in the GDP-bound form the protein is inactive. Rab proteins switch between these two

conformations, under the influence of two classes of protein: the guanine nucleotide exchange factors (GEFs) catalyse nucleotide exchange from the GDP- to the GTP-bound state, thus activating the Rab protein; the GTPase activating proteins (GAPs) catalyse GTP hydrolysis from the GTP- to the GDP-bound state, thus inactivating the Rab protein (Lee *et al.*, 2009).

1.3.3 The ADP-ribosylation factor (ARF) family

The ADP-ribosylation factor (ARF) family of proteins belongs to the Ras superfamily of small GTPases. They cycle between an active GTP-bound and an inactive GDP-bound conformation, a process which is mediated by GAPs and GEFs, as discussed in section 1.3.2 (D'Souza-Schorey and Chavrier, 2006). Six mammalian ARFs have been identified, and based on amino-acid sequence they can be categorised into three classes: Class I includes ARF1, ARF2 and ARF3; Class II includes ARF4 and ARF5; Class III has only one member, ARF6. However, this classification has been disputed (Kahn *et al.*, 2006). The ARF family of proteins is involved in regulating membrane trafficking by recruiting coat proteins, influencing phospholipid metabolism and actin dynamics (D'Souza-Schorey and Chavrier, 2006).

1.3.4 SNARE proteins

SNARE (soluble *N*-ethylmaleimide-sensitive factor attachment protein receptor) proteins were first characterised during the late 1980s. Since then it has been revealed that SNARE proteins form a superfamily which is conserved from yeast to humans. There are 25 members in *S. cerevisiae*, 36 members in humans and 54 members in *Arabidopsis thaliana* (Jahn and Scheller, 2006). SNARE proteins are the key constituents of membrane fusion. Studies using reconstituted lipid vesicles show that purified SNARE proteins are the minimal machinery required for membrane fusion (Weber *et al.*, 1998). SNAREs can be classified with regards to their function. The donor compartment, which gives rise to the vesicle, hosts the v-SNARE (vesicle-membrane SNARE); the acceptor, or target, compartment contains the t-SNARE (target-membrane SNARE) (Sollner *et al.*, 1993). SNAREs play a central role in the final stages of vesicle trafficking; they are responsible for docking and fusion of vesicles in a wide array of vesicle-mediated transport

pathways and also help to achieve compartmentalisation specificity. For fusion to occur the v-SNARE must interact specifically with its cognate t-SNARE. On interaction of the v-SNARE with the appropriate t-SNARE, the two opposing membranes are brought together, resulting in membrane fusion (Sollner *et al.*, 1993). This is known as the SNARE hypothesis.

1.3.5 Vesicle-tethering factors

In eukaryotic cells, membranes are often initially attached by tethering factors, which brings donor and target membranes into close enough proximity to allow SNARE proteins to fuse the opposing membranes (Pfeffer, 1999).

One protein family which function as membrane tethers is the Exocyst family (Munson and Novick, 2006). The Exocyst is a large octameric complex that contains subunits Sec3, Sec5, Sec6, Sec8, Sec10, Sec15 and Exo70 and Exo84. The Exocyst functions to tether transport vesicles to the docking site on the plasma membrane, enabling SNARE assembly to occur. Members of the Exocyst family have been implicated in cytokinesis (Gromley *et al.*, 2005;Fielding *et al.*, 2005).

1.4 Membrane trafficking in cytokinesis

1.4.1 The role of membrane trafficking in cytokinesis

As discussed in section 1.2.1.2, membrane trafficking has long been known to be central to plant cell cytokinesis (Jürgens, 2005). Mammalian cell cytokinesis was considered to be driven solely by constriction of the actomyosin-contractile ring. However, recent research has placed membrane traffic at the heart of mammalian cytokinesis (Albertson *et al.*, 2005;Glotzer, 2005;Barr and Gruneberg, 2007;Prekeris and Gould, 2008).

Membrane delivery to the cleavage furrow accommodates for the changes in surface area required to produce two daughter cells. Research using sea urchin embryos and *Xenopus* eggs has shown that membrane delivery is targeted to the cleavage furrow (Shuster and Burgess, 2002;Danilchik *et al.*, 2003). This additional membrane is not derived from expansion of pre-existing plasma

membrane, but is delivered to the plasma membrane from internal stores (Bluemink and de Laat, 1973). *D. melanogaster* embryogenesis requires a large amount of new membrane to be synthesised and delivered to the ingressing furrow canals to allow for cellularisation (Strickland and Burgess, 2004). Secretory and endocytic vesicles have been found to accumulate adjacent to the midbody in mammalian cells (Gromley *et al.*, 2005; Goss and Toomre, 2008).

Various RNAi screens and proteomic analyses have revealed that a significant number of membrane trafficking proteins are essential for cytokinesis (Skop *et al.*, 2004; Echard *et al.*, 2004; Eggert *et al.*, 2004). Skop and co-workers used a proteomic approach to analyse the protein complement of the midbody, using midbodies purified from CHO cells (Skop *et al.*, 2004). Interestingly, the largest class of proteins (33%) identified were involved in secretory or membrane trafficking, suggesting that membrane trafficking may be involved in cytokinesis. Various protein families known for their roles in membrane trafficking pathways have been implicated in cytokinesis. For example, studies have demonstrated roles for SNARE proteins (Low *et al.*, 2003) and the Rab GTPase family (Skop *et al.*, 2001).

The importance of membrane dynamics may impinge on a variety of processes involved in cytokinesis. Membrane delivery to the cleavage furrow accommodates for the change in cell shape required to produce two daughter cells. Studies have shown that the lipid and protein composition of the membrane at furrow is distinct (Ng *et al.*, 2005). Proteins required for cytokinesis, such as structural and signalling proteins, may be delivered to the cleavage furrow in conjunction with the delivery of new membrane (Strickland and Burgess, 2004). Membrane dynamics are thought to play a key role when the intracellular bridge is resolved and the two daughter cells finally divide and seal. Vesicles are thought to accumulate at the furrow and eventually fuse with the plasma membrane, resulting in the abscission of the two daughter cells (Steigemann and Gerlich, 2009).

1.4.2 Origin of the membrane delivered to the cleavage furrow

The origins of the membrane delivered to the cleavage furrow have been intensely studied and both the secretory and recycling endosomal pathways have been implicated (Albertson *et al.*, 2005).

1.4.2.1 The secretory pathway

One model for the origin of the membrane delivered to the plasma membrane during cytokinesis suggests that the secretory pathway is involved. A variety of evidence suggests that the delivery of Golgi-derived membrane to the furrow and midbody is a requirement during cytokinesis (Albertson *et al.*, 2005). In a variety of cell types the Golgi apparatus is disassembled as the cell enters mitosis (Colanzi *et al.*, 2003) and it has been suggested that the Golgi not only provides membrane for the invagination of the cleavage furrow, but also releases protein required for cytokinesis into the cytoplasm (Altan-Bonnet *et al.*, 2003).

In plant cytokinesis, Golgi-derived vesicles are known to be the major source of membrane in the cell plate (Jürgens, 2005). In animal cytokinesis, it has been demonstrated that Golgi-derived vesicles are essential for the terminal stages of cytokinesis. Brefeldin A (BFA) is an inhibitor of ARF GTPases and disrupts the secretory pathway by inhibiting the budding of vesicles from the Golgi apparatus, thus preventing anterograde transport from the ER to the plasma membrane. BFA was observed to inhibit *D. melanogaster* cellularisation (Sisson *et al.*, 2000) and cytokinesis in *C. elegans* embryonic blastomeres (Skop *et al.*, 2001). Using time-lapse microscopy, secretory vesicles have been found to accumulate adjacent to the midbody in mammalian cells (Gromley *et al.*, 2005; Goss and Toomre, 2008).

Research has uncovered a variety of Golgi-associated proteins which are essential for cytokinesis. One quarter of the proteins identified by Skop *et al.* in midbodies was Golgi-associated proteins. RNAi-based function analysis in *C. elegans* embryos found that many of these proteins are essential in early and late stages of cytokinesis (Skop *et al.*, 2004). A host of Golgi-associated proteins has been identified as required for cytokinesis in *D. melanogaster*. For example,

on injection of embryos with antibodies directed against the *D. melanogaster* Golgi-associated protein, Lava Lamp, it was revealed that, in addition to disruption of Golgi morphology, furrow formation during cellularisation was also inhibited (Sisson *et al.*, 2000). Mutations in the *D. melanogaster* Syntaxin 5 homologue, a Golgi-localised SNARE, resulted in male sterility due to a failure in cytokinesis (Xu *et al.*, 2002).

1.4.2.2 The endosomal pathway

One model for the origin of the membrane delivered to the plasma membrane during cytokinesis suggests that the endocytic pathway also plays a role in this process (Prekeris and Gould, 2008; Montagnac *et al.*, 2008; Fürthauer and González-Gaitán, 2009; Ai and Skop, 2009). As discussed in section 1.3.1, proteins on the plasma membrane can be internalised through the inward budding of endocytic vesicles and incorporated into early endosomes where sorting occurs. Cargo can be directed to the recycling endosomes which subsequently directs vesicles back to the plasma membrane (Maxfield and McGraw, 2004; Grant and Donaldson, 2009). Studies have highlighted the potential importance of the endocytic recycling pathway in cytokinesis. Membrane delivery to the cleavage furrow originates from internal stores (Shuster and Burgess, 2002; Danilchik *et al.*, 2003) and it has been suggested that endosomes are involved (Albertson *et al.*, 2005). Also, it is considered that perhaps the endosomal pathway may deliver lipids and proteins required for cytokinesis progression to the furrow; studies have shown that the lipid and protein composition of the membrane at furrow is distinct (Ng *et al.*, 2005). Additionally, the recycling endosome is microtubule associated and localises to the microtubule-organising centre (MTOC), which is key to positioning of the contractile ring (Albertson *et al.*, 2005).

A variety of evidence supports the model for the involvement of endosomal-derived membranes in cytokinesis. Research has shown that furrow-specific endocytosis is crucial for the completion of cytokinesis. Endocytosis has been observed to occur specifically at the furrow during terminal cytokinesis in zebrafish embryos (Feng *et al.*, 2002). Previously it was thought that endocytosis stopped during mitosis and only resumed after cell division, but two recent studies have shed new light on the changes which occur in endocytic recycling

during mitosis. Studies in cultured mammalian cells have shown that at the start of mitosis, as the cell rounds up, endocytic recycling of internalised membranes back to the cell surface slows significantly. Yet, clathrin-based endocytosis carries on as normal throughout cell division (Boucrot and Kirchhausen, 2007). Thus, there is a decrease in plasma membrane surface area and an accumulation of cell surface-derived membrane in the endosomal system at the beginning of mitosis. Following this, the contractile ring forms and furrow ingresses. As anaphase begins, endocytic recycling resumes and a massive fusion of endosomes with the plasma membrane has been observed. Consequently, the cell surface area recovers before abscission. These changes in endocytic recycling rates and cell surface area appear to be required for cytokinesis (Boucrot and Kirchhausen, 2007). Another study using cultured HeLa cells shows that during furrow ingression, membrane is endocytosed from the plasma membrane at the polar regions of dividing HeLa cells, during furrow ingression in anaphase, and from the midbody during late telophase. Vesicles endocytosed from the polar region during ingression are trafficked to the midbody during late cytokinesis, perhaps delivering cargo required for abscission (Schweitzer *et al.*, 2005).

A variety of endocytic proteins have been shown to be important for the final events of animal cytokinesis. Inhibition of the GTPase dynamin, a protein involved in clathrin-dependent endocytosis, inhibits cleavage furrow ingression in *C. elegans* embryos (Thompson *et al.*, 2002). Inhibition of cytokinesis is observed when clathrin-dependent endocytosis is blocked via expression of a dominant negative form of Eps15, an accessory protein of clathrin-mediated endocytosis (Schweitzer *et al.*, 2005). An endocytic SNARE, VAMP8, has been shown to localise to the cleavage furrow and is required for cytokinesis (Low *et al.*, 2003).

The Rab GTPase family of proteins is essential for cytokinesis. As discussed in section 1.3.2, Rab proteins cycle between the GTP-active and GDP-inactive bound forms, recruiting different effector proteins which control targeting and fusion events (Zerial and McBride, 2001). Rab11 is localised to the recycling endosomes and is required for organisation and vesicular budding from this compartment to the plasma membrane (Ullrich *et al.*, 1996; Chen *et al.*, 1999; Dollar *et al.*, 2002). Several studies have uncovered a role for Rab11 in furrow ingression and cytokinesis. RNAi-induced depletion of Rab11 in *C. elegans*

embryos caused furrow regression during late cytokinesis (Skop *et al.*, 2001). Rab11 is essential for furrow ingression during *D. melanogaster* cellularisation (Pelissier *et al.*, 2003; Riggs *et al.*, 2003). In HeLa cells, Rab11 plays a role in the delivery of recycling endosome derived membrane to the cleavage furrow during late telophase, and this is essential for cytokinesis completion (Wilson *et al.*, 2005; Fielding *et al.*, 2005). Using a systematic RNAi approach, each of the 29 *Rab* genes were downregulated in *D. melanogaster* S2-cultured cells (Kouranti *et al.*, 2006) and downregulation of Rab35 resulted in cytokinesis defects which were attributed to de-stabilisation of the intracellular bridge. Rab35 was found to localise to the plasma membrane and the recycling endosomal pathway (Kouranti *et al.*, 2006).

The ARF family of small GTPases, discussed in section 1.3.3, is involved in regulating membrane trafficking by recruiting coat proteins, influencing phospholipid metabolism and regulating actin dynamics (D'Souza-Schorey and Chavrier, 2006). ARF6 regulates membrane trafficking in the endosomal pathway (D'Souza-Schorey *et al.*, 1995). ARF6-GTP is upregulated during cytokinesis in animal cells and has been observed to accumulate at the cleavage furrow and midbody (Schweitzer and D'Souza-Schorey, 2002). Depletion of ARF6 with RNAi inhibited the final stages of cytokinesis in HeLa cells, resulting in an increased number of binuclear cells (Schweitzer and D'Souza-Schorey, 2005). Contrastingly, Yu *et al.* demonstrated that ARF6 depletion using RNAi did not result in a significant level of cytokinesis failure. However, simultaneous knockdown of Rab11 and ARF6 resulted in a binuclear count greater than the sum of the counts from knockdown of Rab11 or ARF6 alone, suggesting that these proteins act synergistically as the cell moves from furrowing into abscission (Yu *et al.*, 2007). Recent data has shown that ARF6 is required for cytokinesis in the *D. melanogaster* male germ line (Dyer *et al.*, 2007). ARF6 localises to recycling endosomes associated with the central spindle, but does not target them to this location. However, ARF6 is required for the rapid membrane addition during furrowing (Dyer *et al.*, 2007).

Another recycling endosomal protein family shown to play a role in cytokinesis is the Rab11-family interacting proteins (Rab11-FIPs or FIPs) (Horgan and McCaffrey, 2009). One member of this family is Rab11-FIP3 (more commonly referred to as FIP3), which forms a ternary complex with Rab11 and ARF6

(Fielding *et al.*, 2005). Knockdown of FIP3 with RNAi results in an inhibition of abscission (Wilson *et al.*, 2005). FIP3 in complex with Rab11 has been proposed to regulate the delivery and targeting of recycling endosomes to the cleavage furrow and midbody; this is essential for abscission (Hickson *et al.*, 2003; Wilson *et al.*, 2005; Fielding *et al.*, 2005). FIP3 is discussed in section 1.5, along with a current working model for the role in membrane traffic in cytokinesis.

1.5 Rab11-FIP3

1.5.1 Rab11-family interacting proteins (Rab11-FIPs)

Rab11-family interacting proteins (Rab11-FIPs or FIPs) are an evolutionary conserved protein family which are effector molecules for the Rab and ARF GTPases (Horgan and McCaffrey, 2009). FIP proteins are encoded by five genes, and, based on primary structure, they can be placed into two categories: class I FIPs include Rip11 (Rab11-FIP5), Rab11-FIP2 and RCP (Rab-coupling protein or Rab11-FIP1); class II FIPs include Rab11-FIP3 and Rab11-FIP4. A schematic representation of the FIP protein family is provided in figure 1.3 (Simon and Prekeris, 2008).

Rab11-FIP3 (FIP3) was identified by several groups and thus has several aliases (Shin *et al.*, 1999; Prekeris *et al.*, 2001; Hales *et al.*, 2001). Rab11-FIP3 was initially characterised by one group as an ARF5-binding protein and was called arfophilin (Shin *et al.*, 1999; Shin *et al.*, 2001). Other groups identified Rab11-FIP3 as a Rab11-binding protein and referred to it as Eferin (Prekeris *et al.*, 2001). Rab11-FIP3 will be referred to as FIP3 in this thesis. Between them, FIPs display low sequence homology (14 to 34% amino acid identity) (Wallace *et al.*, 2002). However, FIPs share one distinguishing feature with which they were characterised. FIPs bind Rab11 via a conserved C-terminal twenty amino acid motif, called the Rab11-binding domain (RBD) (Prekeris *et al.*, 2001; Meyers and Prekeris, 2002). In addition to the RBD, class I FIPs have a phospholipid-binding C2-domain, whereas Class II FIPs have calcium binding EF-hand domains. Further research has shown that Class II FIPs also possess binding domains for ARF proteins and CYK-4, as discussed in sections 1.5.6.2 and 1.5.6.3, respectively (Horgan and McCaffrey, 2009). FIPs are key proteins in the regulation of multiple

distinct membrane trafficking processes including recycling of cargo to the cell surface, delivery of membrane to the cleavage furrow and midbody, and linker proteins between Rab11 and motor proteins (Horgan and McCaffrey, 2009).

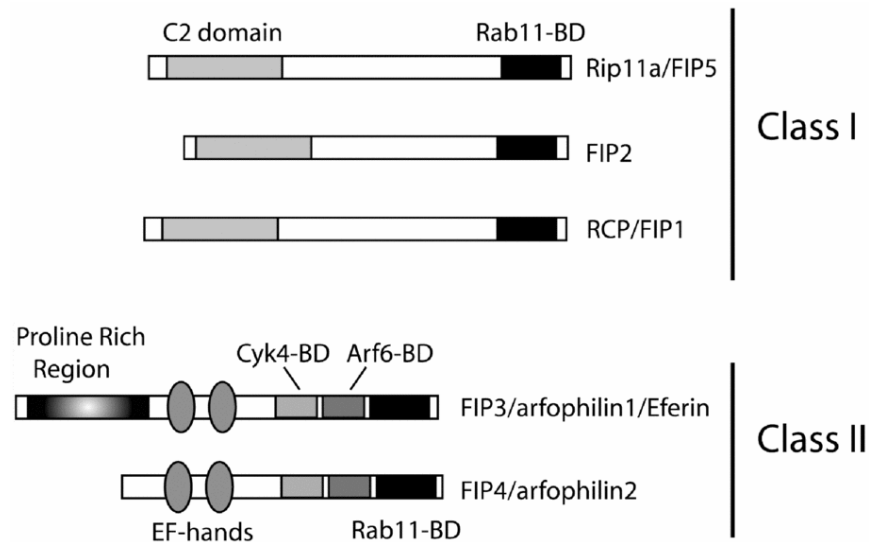


Figure 1-3 Schematic representation of predicted domains and classification of the FIPs (modified from Simon and Prekeris, 2008)

1.5.2 Nuf protein is a *D. melanogaster* homologue of FIP3

As discussed in section 1.2.1.5, *D. melanogaster* cellularisation is a specialised form of cytokinesis. In *D. melanogaster*, *nuclear fallout* (*nuf*) is an essential maternal-effect gene, the product of which is required for cellularisation (Rothwell *et al.*, 1998). *Nuf* is concentrated at the centrosomes during cellularisation and is essential for furrow formation by remodelling and recruiting actin to the cleavage furrow (Rothwell *et al.*, 1998). *Nuf* has also been implicated in membrane recruitment to the furrow (Rothwell *et al.*, 1999). *Nuf* and Rab11 colocalise at the centrosome during cellularisation (Riggs *et al.*, 2003), and since Rab11 is associated with the recycling endosome (Ullrich *et al.*, 1996), this suggests that *Nuf* is localised to the recycling endosomes during cellularisation. GST pull-downs show that Rab11 and *Nuf* interact and are mutually dependent upon each other for localisation to the recycling endosome, since disruption of either causes the other to mis-localise (Riggs *et al.*, 2003). The association of *Nuf* and Rab11 is essential for cellularisation as both Rab11- and *nuf*-derived embryos display similar defects in actin and membrane recruitment to the furrow site, resulting in defects in furrowing (Riggs *et al.*,

2003). Recent work has suggested that Rab11 and Nuf are involved in the delivery of F-actin-associated endosomal vesicles to the cellularisation furrow, via the microtubules (Albertson *et al.*, 2008) and that Nuf promotes local actin polymerisation at the furrow (Cao *et al.*, 2008).

Bioinformatic analysis of protein sequences reveals that Nuf exhibits a degree of homology to the mammalian proteins FIP3 and FIP4. In particular their C-terminal 300 amino acids share homology with Nuf in regions predicted to form coiled-coils (Riggs *et al.*, 2003; Hickson *et al.*, 2003). This region encompasses the RBD (Prekeris *et al.*, 2001; Meyers and Prekeris, 2002). The N-termini are more divergent. In HeLa cells, FIP3 and FIP4 both localise to centrosomes in interphase cells (Hickson *et al.*, 2003; Wilson *et al.*, 2005; Fielding *et al.*, 2005). In interphase HeLa cells, over-expressed GFP-Nuf and GFP-FIP4 alters the morphology of the recycling endosomes by confining them to a pericentrosomal region, suggesting that Nuf and FIP4 are functionally related (Hickson *et al.*, 2003). Thus Nuf and FIP3 are considered functional homologues in *D. melanogaster* and mammalian cells.

1.5.3 Cellular functions of FIP3

FIP3 was shown to regulate the late stage of cytokinesis. HeLa cells transfected with FIP3 RNAi for 48 and 72 hours produced in the order of 20 to 30% binuclear cells, indicating a failure of cytokinesis (Wilson *et al.*, 2005). Phase-contrast time-lapse imaging of FIP3 RNAi treated HeLa cells revealed that FIP3 is required for a late stage of cytokinesis (Wilson *et al.*, 2005). Cleavage furrows formed, but were not resolved; daughter cells remained connected by a long cytoplasmic bridge for an extended period of time. Frequently, daughter cells did not undergo cytokinesis, but appeared to detach and apoptose. The intracellular bridges of some cells appeared to break under the strain of pulling from the two daughter cells, which does not count as cytokinesis. Thus FIP3 is required for abscission, at the very end of telophase. FIP3 functions downstream of Rab11, and it has been proposed that the FIP3-Rab11 complex plays a key role in cytokinesis by delivering membrane derived from the recycling endosomes to the cleavage furrow and midbody (Wilson *et al.*, 2005; Fielding *et al.*, 2005), which is essential for abscission. A current working model for membrane traffic to the

furrow during cytokinesis was created by A.R. Skop and is reproduced in this thesis, in section 1.5.7, figure 1.5. As mentioned in section 1.5.2, the *D. melanogaster* homologue of FIP3, Nuf, regulates actin polymerisation at, and delivery of recycling endosomal material to, the cleavage furrow of *D. melanogaster* embryos (Rothwell *et al.*, 1998). Recently FIP3 was also found to modulate the actin cytoskeleton (Jing *et al.*, 2009). Knockdown of FIP3 by RNAi inhibits the motility of MDA-MB-231 breast carcinoma cells. Data suggests that FIP3 regulates polarised Rac1 activation by mediating the targeting of ARF6 to the leading edge of motile cells. Thus, FIP3 is at the centre of two processes: membrane traffic from the recycling endosome, via a Rab11 interaction, and plasma membrane and actin remodelling via an ARF6 interaction.

1.5.4 Subcellular localisation of FIP3

Time-lapse microscopy of HeLa cells expressing GFP-FIP3 has shown that FIP3 undergoes spatial and temporal dynamics during mitosis (Wilson *et al.*, 2005). During metaphase and early anaphase FIP3 is diffuse and localised to endosomal membrane structures in the cytosol. During early anaphase, following furrow initiation, FIP3 localises to membranes at the centrosome. At late cytokinesis, FIP3 rapidly relocates to the cleavage furrow and midbody. On separation of the daughter cells, FIP3 relocates to the centrosome. This is shown in figure 1.4. Immunofluorescence studies have shown that a proportion of FIP3 associates with the centrosome throughout the cell cycle (Wilson *et al.*, 2005).

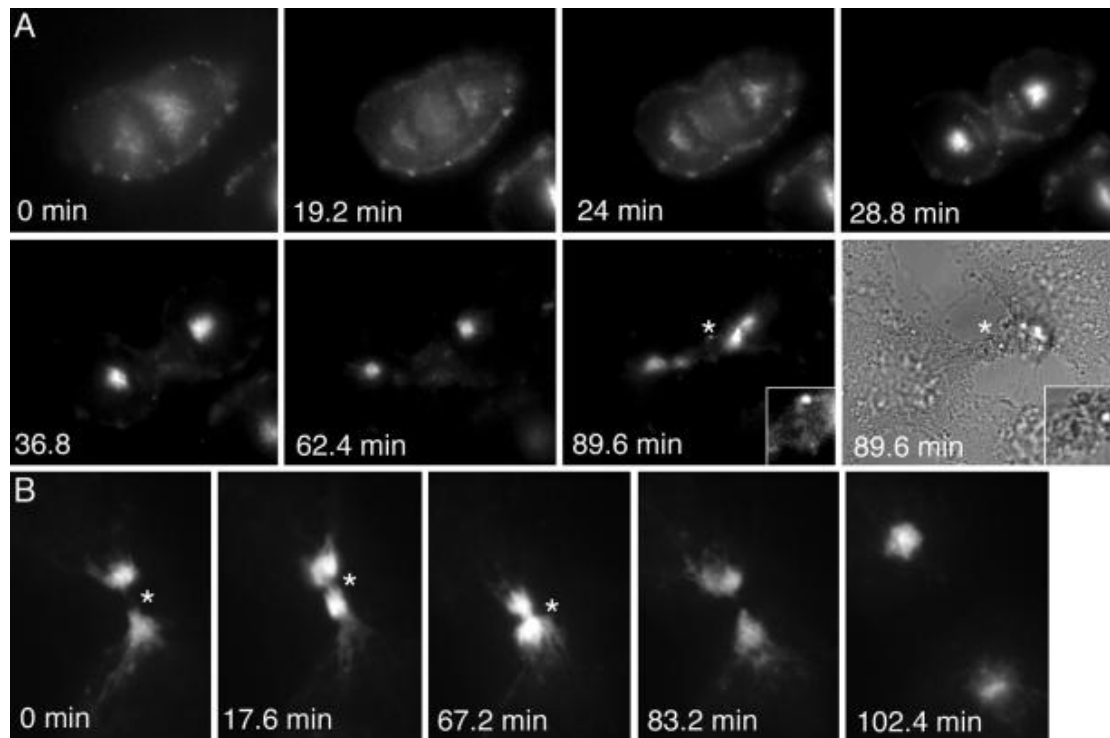


Figure 1-4 Temporal and spatial dynamics of GFP-FIP3 during mitosis (Wilson *et al.*, 2005). HeLa cells stably expressing GFP-FIP3 were imaged using time-lapse microscopy. (A) A cell in metaphase with an asterisk labelling the midbody. (B) A cell in the late phase of cytokinesis.

1.5.5 Structure of FIP3

FIPs display low sequence homology with the exception being a conserved C-terminal twenty amino acid motif, called the Rab11-binding domain (RBD) (Prekeris *et al.*, 2001), the minimal area of which encompasses residues 733 to 756 of FIP3 (Shiba *et al.*, 2006). Analysis of the amino acid sequence reveals that FIP3 also contains two putative EF-hand domains (Prekeris *et al.*, 2001) at approximately 202 to 237 and 234 to 269 amino acids (The UniProt Consortium, 2009). EF-hand domains are involved in calcium binding (Grabarek, 2006). Only the class II FIPs possess EF-hand domains; Class I FIPs possess phospholipid binding C2 domains. Also important to note is the proline rich region found at the N-terminus of FIP3 (Prekeris *et al.*, 2001), encompassing amino acids 5 to 197 (The UniProt Consortium, 2009). This type of region is known to mediate a large number of protein to protein interactions (Kay *et al.*, 2000). Prediction software has shown that FIP3 has an extensive α -helical coiled-coil region between residues 463 and 692 (Wallace *et al.*, 2002; Horgan *et al.*, 2007). Interestingly, the C-termini of FIPs mediate homodimerisation *in vitro* and

interact with two Rab11 proteins to form heterotetrameric complexes (Wallace *et al.*, 2002; Junutula *et al.*, 2004). A schematic representation of the domains of the FIP family is provided in figure 1.3 (Simon and Prekeris, 2008).

The 3D crystal structure of FIP3 in its entirety is not yet known. The crystal structure of the FIP3-RBD (695 to 756 amino acids) in complex with Rab11 reveals that the RBD of FIP3 mediates homodimerisation of the FIP molecules. Amphiphillic helices from two FIP3-RBDs form a parallel coiled-coil homodimer. This creates two symmetrical interfaces for binding the switch regions of two Rab11 molecules, thus forming a heterotetrameric complex between two FIPs and two Rab11s, with the FIPs forming the central α -helical coiled-coil (Eathiraj *et al.*, 2006; Shiba *et al.*, 2006). Resolution of the crystal structure of Rab11 in complex with the Class I FIP, FIP2, is similar, suggesting that this mode of binding is a feature of the FIP family (Jagoe *et al.*, 2006). However, it is important to note that points of contact between the two FIP3 proteins may exist out with the RBD, since prediction software has shown that FIP3 has an extensive α -helical coiled-coil region between residues 463 and 692 (Wallace *et al.*, 2002; Horgan *et al.*, 2007).

1.5.6 Interacting partners of FIP3

1.5.6.1 FIP3 interacts with members of the Rab GTPase family

FIP3 has been shown to directly interact with Rab11. The family of FIP proteins is characterised by a highly conserved RBD of 20 amino acids, located at the C-terminus of the protein (Prekeris *et al.*, 2001). A schematic representation of the protein binding domains of FIP3 is provided in figure 1.3 (Simon and Prekeris, 2008). The crystal structure of the FIP3-RBD in complex with Rab11 shows a heterotetrameric complex between two FIPs and two Rab11s (Eathiraj *et al.*, 2006; Shiba *et al.*, 2006). Work from our lab has shown that FIP3 has the binding preference of Rab11 > ARF6 >> ARF5 (Fielding *et al.*, 2005). Significantly, FIP3 binds to Rab11 and ARF6 at distinct and non-overlapping sites in its C-terminal domain, suggesting the FIP3 may interact with the two GTPases simultaneously, forming a ternary complex (Fielding *et al.*, 2005).

During interphase, Rab11 is predominantly associated with recycling endosomes in the pericentrosomal region (Ullrich *et al.*, 1996). Rab11-containing recycling endosomes become highly concentrated around the cleavage furrow and in the midbody in telophase (Wilson *et al.*, 2005). FIP3 displays a similar cell-cycle distribution (Wilson *et al.*, 2005). Rab11 knock-down with RNAi results in translocation of FIP3 from the membranes to the cytosol, suggesting that Rab11 mediates the association of FIP3 with endosomes (Wilson *et al.*, 2005). A Rab11-binding deficient mutant of FIP3 (FIP3-I737E) is predominantly cytosolic. Interestingly, FIP3 association with the midbody is Rab11-independent, since expression of a Rab11-binding deficient mutant (FIP3-I737E) does still appear to localise to the midbody in cytokinesis (Wilson *et al.*, 2005). However, Rab11 and FIP3 complex formation is required for abscission, since GFP-FIP3-I737E expression in HeLa cells resulted in cytokinesis defects and produced a binuclear count in the order of 35% (Wilson *et al.*, 2005). It has been proposed that the FIP3-Rab11 complex plays a key role in cytokinesis, by delivering and targeting recycling endosomes to the cleavage furrow and midbody (Wilson *et al.*, 2005; Fielding *et al.*, 2005).

1.5.6.2 FIP3 interacts with members of the ARF GTPase family

As discussed in section 1.3.3, the ADP-ribosylation factor (ARF) family of proteins belong to the Ras superfamily of small GTPases. They cycle between and active GTP-bound and inactive GDP-bound conformations and are involved in regulating membrane trafficking by recruiting coat proteins, influencing phospholipid metabolism and actin dynamics (D'Souza-Schorey and Chavrier, 2006).

FIP3 has been found to interact with members of the ARF GTPase family through its C-terminal domain. FIP3 was initially identified by one group as an ARF5-binding protein (Shin *et al.*, 1999). ARF5 is a class II ARF GTPase. Subsequently, FIP3 was also found to interact with the sole member of the class III ARF GTPases, ARF6 (Shin *et al.*, 2001). Later, work from our group showed that FIP3 preferentially binds to Rab11>ARF6>>ARF5 (Fielding *et al.*, 2005). Significantly, FIP3 binds to Rab11 and ARF6 at distinct and non-overlapping sites in its C-terminal domain, suggesting that FIP3 may interact with the two GTPases simultaneously, forming a ternary complex (Fielding *et al.*, 2005). Directly N-terminal to the RBD is the ARF binding domain (ABD), which involves amino acids

650 to 695 (Fielding *et al.*, 2005; Shiba *et al.*, 2006; Schonteich *et al.*, 2007). This is illustrated in figure 1.3 (Simon and Prekeris, 2008).

ARF6 regulates membrane trafficking in the endosomal pathway (D'Souza-Schorey *et al.*, 1995). ARF6-GTP accumulates at the central spindle and midbody (Schweitzer and D'Souza-Schorey, 2002), and depletion of ARF6 with RNAi inhibits the final stages of cytokinesis in HeLa cells (Schweitzer and D'Souza-Schorey, 2005). FIP3 association with the midbody is Rab11-independent, since expression of Rab11-binding deficient mutant (FIP3-I737E) did still appear to localise to the midbody in cytokinesis (Wilson *et al.*, 2005). However, ARF6 appears to mediate recruitment of FIP3 to the cleavage furrow, since FIP3 association with the furrow and midbody is blocked on expression of GDP-restricted ARF6-T27N (Fielding *et al.*, 2005). ARF6 has been shown to bind to FIP3 prior to their arrival at midbody; thus ARF6 is not considered to be an endosome tethering factor (Schonteich *et al.*, 2007). Recent work in *D. melanogaster* spermatocyte cytokinesis may shed light on this (Dyer *et al.*, 2007). ARF6 localises to recycling endosomes associated with the central spindle, but does not target them to this location. However, ARF6 is required for the rapid membrane addition during furrowing (Dyer *et al.*, 2007). Recently FIP3 was also found to modulate the actin cytoskeleton (Jing *et al.*, 2009). Knockdown of FIP3 by RNAi inhibits the motility of MDA-MB-231 breast carcinoma cells, suggesting that FIP3 regulates polarised Rac1 activation by mediating the targeting of ARF6 to the leading edge of motile cells.

1.5.6.3 FIP3 interacts with CYK-4

As discussed in section 1.2.2.2, the role of RhoA is central to cytokinesis, by regulating actin dynamics at the furrow (Piekny *et al.*, 2005). Centralspindlin is a protein assembly comprised of MKLP1 and CYK-4 (RhoA GAP). MKLP1 restricts this complex to the central spindle. CYK-4 recruits ECT2 (RhoA GEF) to the central spindle, where ECT2 activates RhoA, resulting in contractile ring function (Werner and Glotzer, 2008).

The combined approach of immunopurification of FIP3 from HeLa cells and proteomics revealed that FIP3 interacts with CYK-4 (Simon *et al.*, 2008). CYK-4 binds to FIP3, N-terminal to the ARF binding domain (ABD), encompassing amino

acids 441 to 610 (Simon *et al.*, 2008). This is illustrated in figure 1.3 (Simon and Prekeris, 2008). During anaphase, centralspindlin is located in the mid-zone, and by late telophase CYK-4 is highly concentrated at the midbody. CYK-4 co-localises with FIP3 in the midbody at late telophase; the two proteins only interact at this stage (Simon *et al.*, 2008). The binding regions for ECT2 and FIP3 on CYK-4 overlap, thus they form mutually exclusive complexes with CYK-4. At late telophase, ECT2 dissociation from centralspindlin allows CYK-4 to recruit FIP3 and recycling endosomes to the midbody (Simon and Prekeris, 2008).

1.5.6.4 FIP3 interacts with ASAP1

ASAP1 is an ARF GTPase Activating Protein (GAP). The function of this protein family is discussed in section 1.3.3. A two-hybrid screen revealed that FIP3 interacts with ASAP1 within the coiled-coil domain of the C-terminus of FIP3, including amino acids 565 to 650 (Inoue *et al.*, 2008). ASAP1 forms a ternary complex with Rab11, via FIP3. It was shown that FIP3 binding activated ASAP1 activity to ARF1, but not ARF6. Interestingly, ASAP1 and FIP3 co-localise in the pericentrosomal endocytic recycling compartment, where they function in endocytic recycling, since knockdown of ASAP1 or FIP3 disrupted localisation of the transferrin receptor to this compartment (Inoue *et al.*, 2008).

1.5.6.5 FIP3 interacts with molecular motor proteins

Recent research has uncovered the ability of FIPs to couple to the molecular motor protein machinery of the cell. An RNAi screen of kinesin molecular motors identified kinesin I as the microtubule motor which directs transport of recycling endosomes during mitosis (Simon and Prekeris, 2008). Kinesin also co-immunoprecipitated with the Rab11-FIP3 complex and depletion of kinesin I inhibits delivery of FIP3 to the furrow and inhibits cytokinesis (Simon and Prekeris, 2008). However, it has not been shown if this is a direct interaction between FIP3 and kinesin I. FIP3 has been suggested to interact with cytoplasmic dynein 1, a protein which is necessary for FIP3-dependent pericentrosomal accumulation of the ERC (Horgan and McCaffrey, 2009). However, this work is unpublished. Interestingly, Rip11 (Rab11-FIP5) has been shown to bind directly to kinesin II, a microtubule motor complex (Schonteich *et al.*, 2008). Thus there

is scope for the role of microtubule motor proteins in directing FIP3-Rab11 recycling endosomes to the furrow for cytokinesis.

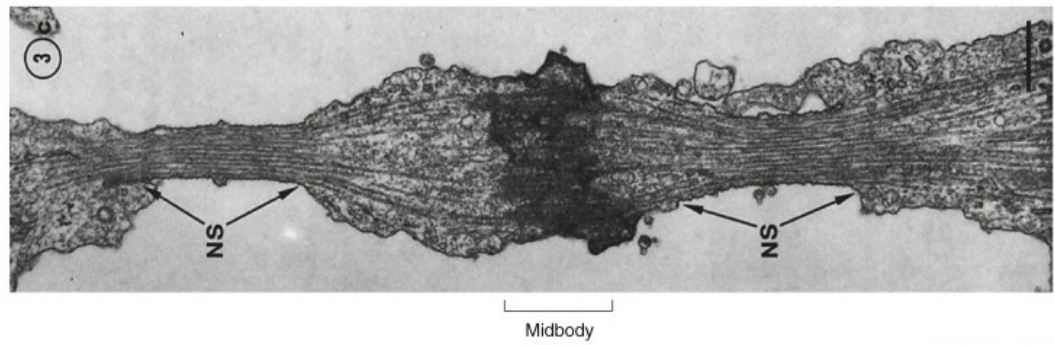
1.5.7 Model for membrane traffic during cytokinesis

The exact mechanism of abscission is still to be resolved. Various studies implicate the accumulation and simultaneous fusion of multiple vesicles on one, or either side, of the midbody in the resolution the intracellular bridge (Gromley *et al.*, 2005;Goss and Toomre, 2008). One model for the origin of the membrane delivered to the plasma membrane during cytokinesis suggests involvement of the endocytic pathway (Prekeris and Gould, 2008;Montagnac *et al.*, 2008;Fürthauer and González-Gaitán, 2009;Ai and Skop, 2009). It is thought that vesicles derived from the recycling endosome are tethered to microtubules at the centrosomes. Subsequently, they traffic to the furrow and midbody where they deliver the membrane and cargo essential for abscission (Gould and Lippincott-Schwartz, 2009). It has been proposed that FIP3 in complex with Rab11 plays a key role in the delivery and targeting of recycling endosomes to the furrow; this is essential for completion of cytokinesis (Wilson *et al.*, 2005;Fielding *et al.*, 2005).

A current working model for membrane traffic to the furrow during cytokinesis was created by A.R. Skop and is reproduced in figure 1.5. During prophase and metaphase, while clathrin-based endocytosis carries on as normal, endocytic recycling of internalised membranes back to the cell surface slows significantly. However, during early telophase endosomal recycling resumes and recycling endosomes are trafficked to the furrow. Rab11 recruits FIP3 onto recycling endosome-derived vesicles at the centrosome. In telophase, FIP3-Rab11 vesicles traffic to the furrow and at later stages the midbody. These vesicles are directed along the microtubules of the mitotic spindle, possibly via the motor protein kinesin I. A ternary complex is formed between ARF6-FIP3-Rab11. FIP3 delivers ARF6 to the furrow and midbody where it may regulate actin dynamics or co-ordinate membrane insertion with furrow ingression. Additionally ARF6 and Rab11 may tether FIP3-containing vesicles to the Exocyst machinery, thus anchoring FIP3-containing vesicles to the midbody prior to abscission. FIP3 also interacts with CYK-4 of the centralspindlin complex at the late stages of

telophase, serving to tether FIP3-vesicles to the midbody. These vesicles may serve as an organisation platform for the assembly of the abscission machinery or they may deliver the cargo required for abscission. FIP3-Rab11 vesicles may also be involved in a compound fusion event which seals the intracellular bridge, thus resolving the two daughter cells.

A.



B.

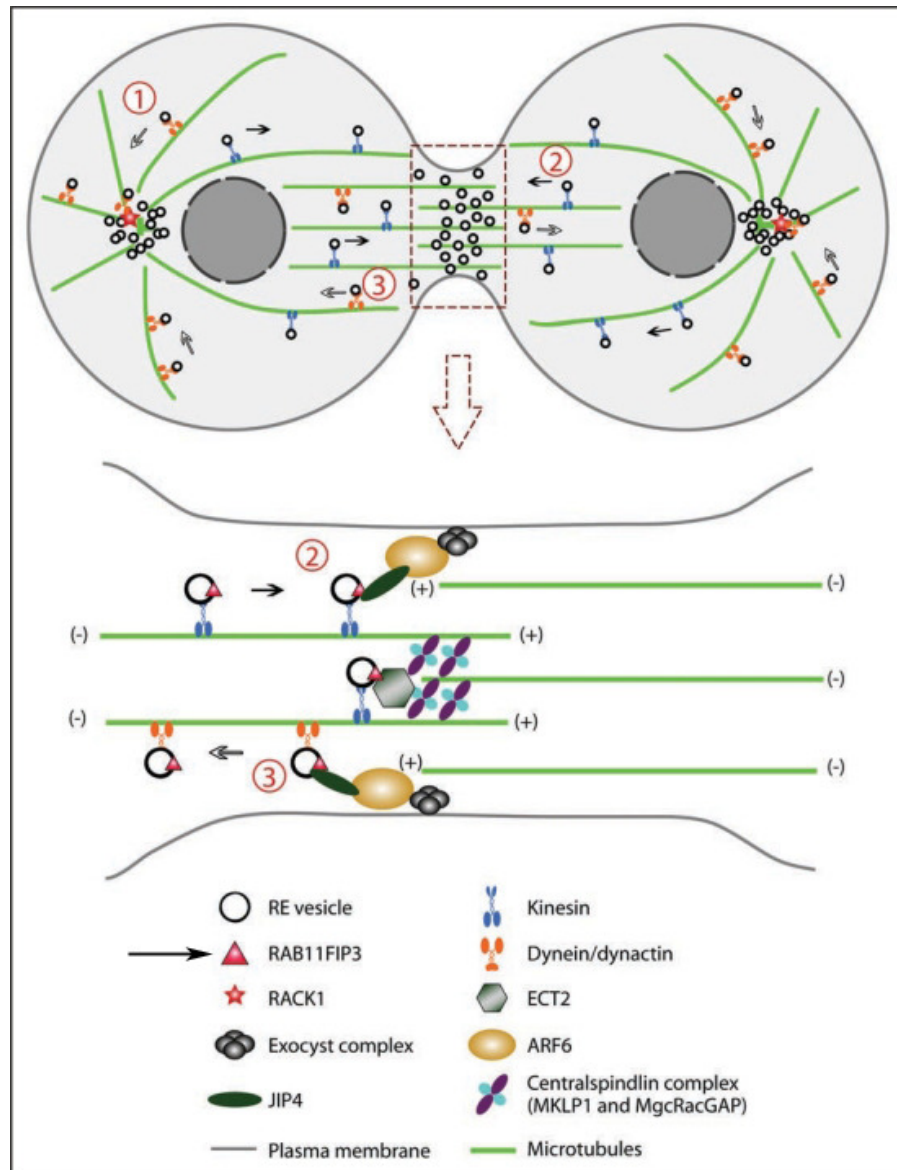


Figure 1-5 Model for membrane traffic during cytokinesis

A. Electron micrograph of an intracellular bridge in the late stages in telophase. Lateral constriction zones (NS) containing bundled microtubules are found either side of the central electron-dense midbody composed of overlapping ends of microtubules and a vast array of proteins (modified from Steigemann and Gerlich, 2009).

B. Model of recycling endosome (RE) trafficking during cytokinesis (modified from Ai and Skop, 2009). An arrow points to FIP3 (RAB11FIP3) in the key. (1) REs are concentrated at the MTOC. RE vesicles traffic along the microtubules under the influence of dynein/dynactin motors. RACK1 is thought to interact with dynactin, thus targeting REs to the centrosomes. (2) Rab11 recruits FIP3 onto recycling endosome-derived vesicles at the centrosome which then traffic along both spindle and midzone microtubules, under the influence of kinesin motors, to the furrow and at later stages the midbody. At the furrow they interact with ARF6 and members of the Exocyst family. A ternary complex is formed between ARF6-FIP3-Rab11. The centralspindlin complex also mediates the accumulation of RE vesicles at the midbody, via the interaction CYK-4 with FIP3. RE vesicles may serve as an organisation platform for the assembly of the abscission machinery or they may deliver the cargo required for abscission or they may be involved in a compound fusion event which seals the intracellular bridge, thus resolving the two daughter cells. (3) RE vesicles are thought to traffic from the site of cleavage via dynein/dynactin motors. The interaction between ARF6 and the scaffolding protein c-Jun-N-terminal-kinase interacting protein 4 (JIP4) is thought to control the bidirectional movement of endosomes, via association with kinesin or dynein/dynactin motors.

1.5.8 Regulation of FIP3

Time-lapse microscopy of HeLa cells expressing GFP-FIP3 has shown that FIP3 undergoes spatial and temporal dynamics during mitosis (Wilson et al., 2005). A potential candidate for the spatial and temporal regulation of FIP3 is phosphorylation, since reversible phosphorylation is a commonly used control mechanism in mitotic regulation (Morgan, 2007) and can regulate the activity, localisation and half-life of a protein, as well as its interaction with other proteins (Cohen, 2000).

Several lines of evidence suggest that FIP3 is a potential phospho-protein. As discussed in section 1.5.2, Nuf is a *D. melanogaster* homologue of FIP3 (Riggs et al., 2003; Hickson et al., 2003). Nuf is a highly phosphorylated protein (Rothwell et al., 1998). Interestingly, Nuf localisation alters during the cell-cycle (Rothwell et al., 1998). During early *Drosophila* development, the embryo undergoes thirteen rapid nuclear divisions, which occur without cytokinesis. During this development, Nuf is concentrated at the centrosomes during prophase, but is predominantly cytoplasmic through the rest of the nuclear cycle and remains so in interphase. During nuclear cycle 14 the embryo undergoes cellularisation (the equivalent of mammalian cytokinesis). Nuf is centrosomal throughout

cellularisation (Rothwell *et al.*, 1998). Since Nuf is highly phosphorylated, it has been suggested that localisation may be regulated by cell-cycle-dependent kinases (Riggs *et al.*, 2003). The activity of Class I FIPs is known to be regulated by phosphorylation. Prekeris *et al.*, showed that phosphorylation of Rip11 results in its dissociation from apical recycling endosomes to the cytosol (Prekeris *et al.*, 2000). The cell-cycle is rigorously regulated by a network of kinases. Thus, phosphorylation of FIP3 by cell-cycle-dependent kinases may play a key role in role in cytokinesis.

1.6 Cell-cycle kinases

1.6.1 Cell-cycle overview

As discussed in section 1.2.2, cytokinesis involves co-ordination of a number of stages and a multitude of proteins (Eggert *et al.*, 2006). These proteins undergo spatial and temporal regulation to ensure progression through the cell-cycle is error free. The two main regulators of the cell-cycle are protein phosphorylation and degradation. The cell-cycle is governed by a network of protein kinases which control the activity, localisation and interactions of proteins involved in cell-cycle progression (Nigg, 2001). The major mitotic regulators are CDK1, Plk1, Aurora A and Aurora B. Although the role of mitotic kinases in cytokinesis remains to be clearly defined, recent research points to these kinases playing a critical role in the regulation of events which control cytokinesis. A summary of some of the processes involved in cytokinesis and their regulation by cell-cycle kinases is provided in figure 1.6 (Barr and Gruneberg, 2007).

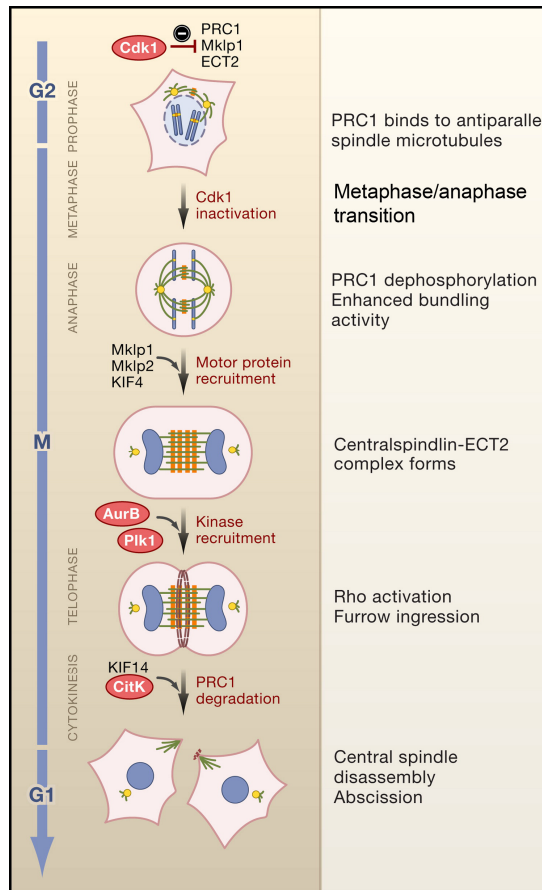


Figure 1-6 Cell-cycle regulation of the central spindle (modified from Barr and Gruneberg, 2007)

In the early stages of mitosis, CDK1 activity peaks and the kinase inhibits PRC1, MKLP1 and ECT2. CDK1 is inactivated at the onset of anaphase and its substrates become dephosphorylated. PRC1 bundles the microtubules of the central spindle and recruits MKLP1 (of the centralspindlin complex) and MKLP2. PRC1 also recruits PLK1 to the spindle for its role in cytokinesis. MKLP2 is involved in Aurora B localisation to the central spindle. Aurora B then phosphorylates centralspindlin, promoting its assembly with ECT2 and therefore influencing furrow formation via RhoA.

1.6.2 Cyclin-dependent kinase 1 (CDK1)

Pioneering cell-cycle studies in fission yeast defined cell division control protein 2 (*cdc2*) as the master regulator of cell-cycle progression (Nurse, 2000). *Cdc2* drives entry into mitosis and is conserved from yeast to mammalian cells, where it is known as cyclin-dependent kinase 1 (CDK1). CDK1 is a serine/threonine protein kinase which controls mitosis by phosphorylating a network of proteins involved in controlling the various mitotic stages (Morgan, 2007). It is a member of a large family of CDKs (CDK1 - CDK13), but only CDK1 drives mitosis (Malumbres and Barbacid, 2009). CDK substrates are serine or threonine residues

in a specific sequence context ([S/T*]PX[K/R]) which is recognised by the active site of the kinase. The target residue (S/T*) is usually followed by a proline residue (P) and often has a basic amino acid (K/R) two positions C-terminal to the target (Shetty *et al.*, 1993; Brown *et al.*, 1999; Ubersax and Ferrell Jr, 2007).

CDKs are activated by binding to their regulatory subunits, known as cyclins, which induces a conformational change, thus activating the kinase (Morgan, 2007). There are ten cyclins, in four different classes (the A-, B-, D- and E-type cyclins) involved in different stages of the cell-cycle, but only the A- and B-type cyclins are involved in mitosis (Malumbres and Barbacid, 2009). Cyclins are synthesised and destroyed at specific times during the cell cycle, thus controlling the temporal activation of their bound kinases (Fung and Poon, 2005). Cyclins also direct their bound CDKs to the appropriate subcellular location, thus controlling the spatial activation of their bound kinases (Fung and Poon, 2005).

The cyclin B1-CDK1 complex drives mitosis. In vertebrate cells, the concentration of cyclin B increases as the cell approaches mitosis and peaks in prophase/metaphase and associated CDK activity increases dramatically in prophase (Morgan, 2007). Cyclin B is destroyed in metaphase, which switches off CDK1 activity (Pines, 2006). There are two main types of cyclin B: B1 and B2 (Fung and Poon, 2005). Cyclin B1-CDK1 co-localises with microtubules; cyclin B2-CDK1 associates with the Golgi apparatus and stimulates phosphorylation of proteins which cause Golgi fragmentation during mitosis (Jackman *et al.*, 1995). Mice lacking the cyclin B2 gene develop normally and are fertile, but mice lacking the cyclin B1 gene are not viable (Brandeis *et al.*, 1998). Thus CDK1, in complex with cyclin B1, is chiefly responsible for the orchestration of mitosis (Nigg, 2001).

Following cyclin binding, CDK1 must be phosphorylated at threonine 161 (T161) in the T loop, by a CDK-activating kinase (CAK), for full kinase activity. CDKs are also negatively regulated by phosphorylation. Phosphorylation of threonine 14 (T14) and tyrosine 15 (Y15) in the ATP-binding site of CDK1 inhibits kinase activity. Wee1 is a kinase which is soluble and predominantly nuclear, although it also localises to the centrosomes; it inhibits CDK1 by phosphorylating Y15. In vertebrates, Myt1 is associated with Golgi and endoplasmic reticulum

membranes and is related to Wee1; it phosphorylates T14 and Y15 of CDK1, thus inhibiting the kinase. The dual-specificity phosphatase Cdc25C activates CDK1 by de-phosphorylating T14 and Y15. This regulation is referred to as the inner feedback loop of CDK1 activation (reviewed in Lindqvist *et al.*, 2009).

CDK1 activity undergoes a rapid 'switch-like' activation via a positive feedback loop (Morgan, 2007). CDK1 concentration is high during the cell-cycle, but its activity is low due to high Wee1 activity and low Cdc25C activity (Lindqvist *et al.*, 2009). CDK1 affinity for cyclins is high, ensuring that as soon as cyclin B expression increases, CDK1 immediately binds to cyclin B. This causes the cell to accumulate a stockpile of cyclin B1-CDK1 complexes, which are inactive due to Wee1 phosphorylation. A positive feedback loop results from CDK1 itself. At the beginning of mitosis, CDK1 phosphorylates and inhibits its own inhibitor (Wee1) and activates its own activator (Cdc25C), thus removing the inhibitory phosphate groups of CDK1. This results in the rapid 'switch-like' activation of the cyclin B1-CDK1 complex stockpile (Lindqvist *et al.*, 2009).

On activation of cyclin B1-CDK1, the cell enters mitosis (Nigg, 2001). CDK1 phosphorylates a host of substrates. One of the principal targets of cyclin B1-CDK1 is nuclear lamins, the cytoskeletal network that lies underneath the nuclear envelope. Before mitosis, cyclin B1-CDK1 is cytoplasmic, preventing its access to targets in the nucleus. In early prophase, when cyclin B1-CDK1 is first activated, the complex is found on duplicated centrosomes as they begin to separate. At late prophase it is rapidly translocated into the nucleus (Clute and Pines, 1999) where CDK1 phosphorylates nuclear lamin, thus stimulating nuclear envelope breakdown. Following nuclear envelope breakdown, the complex is once again located throughout the cell. CDK1 also functions in centrosome separation, disassembly of the Golgi apparatus, spindle assembly, chromosome condensation, Golgi fragmentation and anaphase promoting complex/cyclosome (APC/C) regulation (Nigg, 2001). Interestingly, phosphorylation by CDK1 can affect the membrane and cytosol distribution of proteins involved in mitosis: cyclin B1-CDK1 phosphorylation of the microtubule motor cytoplasmic dynein releases the protein from membranes, *in vitro* (Addinall *et al.*, 2001).

All B type cyclins have a short sequence (destruction box or D-box) which is a target of the APC/C, triggering their destruction and thereby inactivating CDK1

(Fung and Poon, 2005). APC/C is an E3 ubiquitin protein ligase which poly-ubiquitinates proteins, thus marking them for degradation by the proteasome (Morgan, 2007). Degradation of cyclin B by the APC/C begins as the last chromosome lines up on the metaphase plate, just after inactivation of the spindle-assembly checkpoint (Clute and Pines, 1999). On destruction of cyclin B, CDK1 becomes inactivated allowing mitotic exit and cytokinesis (Pines, 2006; Sullivan and Morgan, 2007).

Cyclin B1-CDK1 negatively regulates many of the protein complexes required for cytokinesis, until anaphase onset, when the sister chromatids have successfully separated and CDK1 is inactivated (Barr and Gruneberg, 2007). Indeed, inhibition of CDK1 with BMI-1026 results in initiation of cytokinesis before chromosome segregation (Niiya *et al.*, 2005). CDK1 regulation of events involved in cytokinesis is summarised in figure 1.6.

Cyclin B1-CDK1 has been implicated in the regulation of centralspindlin assembly (Niiya *et al.*, 2005; Glotzer, 2009). Cyclin B1-CDK1 phosphorylates the motor domain of MKLP1, reducing its affinity for, and ability to move along, the microtubules (Mishima *et al.*, 2004). In metaphase, cyclin B1-CDK1 phosphorylates ECT2, which adopts an autoinhibited conformation, preventing its interaction with CYK-4 (Yüce *et al.*, 2005). Reports also suggest that CDK1 phosphorylates CYK-4, *in vitro* (Touré *et al.*, 2008). Regulation of the centralspindlin complex by CDK1 ensures that RhoA localisation to the equatorial cortex by ECT2 and subsequent furrow formation does not occur until the chromosomes have segregated (Barr and Gruneberg, 2007). Cyclin B1-CDK1 has been implicated in the regulation of the chromosomal passenger complex (CPC), which is composed of Aurora B kinase, inner centromere protein INCENP, survivin and borealin (Glotzer, 2009). This complex will be discussed in more detail in section 1.6.5. The mitotic kinesin MKLP2 recruits the CPC to the spindle midzone; the association between these two proteins is negatively regulated by CDK1, suggesting that, following CDK1 inactivation at the metaphase/anaphase transition, the CPC and MKLP2 interact, targeting this complex to the spindle midzone (Hümmer and Mayer, 2009). Microtubule-associated proteins (MAPs) are involved in central spindle assembly and MAP protein regulator of cytokinesis 1 (PRC1) is involved in microtubule bundling (Glotzer, 2009). CDK1 phosphorylation of PRC1 in early mitosis keeps PRC1 in an inactive monomeric state, but on

dephosphorylation at anaphase onset, PRC1 is dephosphorylated, promoting PRC1 oligomerisation. This allows PRC1 to bundle microtubules, forming the spindle midzone which is necessary for cytokinesis (Mollinari *et al.*, 2002;Zhu *et al.*, 2006). Thus, on inactivation of CDK1 at anaphase onset various inhibitory phosphorylations are removed and the central spindle can assemble, driving cytokinesis (Barr and Gruneberg, 2007).

1.6.3 Polo-like kinase 1 (Plk1)

Polo-like kinase 1 (Plk1) is another key regulator of mitosis and has been implicated in the regulation of cytokinesis (Barr *et al.*, 2004;Petronczki *et al.*, 2008). Plk1 is activated in early mitosis and is degraded in anaphase, via APC/C mediated proteolysis; this is necessary for mitotic exit (Lindon and Pines, 2004).

The N-terminal region of Plk1 contains the serine/threonine kinase domain, followed by a central destruction motif (D-box) (Lindon and Pines, 2004). Towards the C-terminus is a conserved regulatory domain containing two motifs, classed as the polo-box domain (PBD) (Elia *et al.*, 2003a;Elia *et al.*, 2003b). The PBD is a phospho-peptide binding domain, which has a higher affinity for proteins which are phosphorylated at serine/threonine residues, within a certain sequence context, S-pS/pT-P/X. The PBD is thought to target Plk1 to specific substrates and subcellular localisations, thus conferring spatial regulation on Plk1 activity. The interaction of Plk1 with its substrates via the PBD requires prior phosphorylation (priming); this confers temporal regulation on Plk1 activity. It is thought that priming by cyclin B1-CDK1 may promote interaction between Plk1 and certain substrates, since the consensus for PBD binding fulfils the requirements of the proline directed CDK1 (Ubersax and Ferrell Jr, 2007;Lindqvist *et al.*, 2009).

Plk1 may be negatively regulated by its C-terminal domain (Barr *et al.*, 2004). In the absence of a phosphorylated substrate, the PBD is thought to interact with the kinase domain, thus preventing Plk1 function. The catalytic domain is only released on interaction of the PBD with a phosphorylated substrate. The catalytic domain can then be phosphorylated on the T-loop (Thr210), which is necessary for Plk1 activation (Barr *et al.*, 2004).

Plk1 displays dynamic cell-cycle dependent localisation (Petronczki *et al.*, 2008). Plk1 localises to the centrosomes in prophase and becomes concentrated at the centrosomes and kinetochores in prometaphase and metaphase. At late anaphase Plk1 redistributes to the midzone of the mitotic spindle and midbody during telophase (Barr *et al.*, 2004; Petronczki *et al.*, 2008).

Plk1 has been found to influence processes at its various cellular locations. In early mitosis Plk1 is localised at the centrosomes and is involved in centrosome separation and bipolar spindle formation (Petronczki *et al.*, 2008). In the absence of functional Polo in animal cells, assembly of bipolar spindles fails and instead the mitotic chromosomes arrange in a circular array around the monopolar spindle (Sunkel and Glover, 1988). Plk1 may be involved in the attachment of microtubules to kinetochores in prometaphase, thus regulating chromosome congression (Petronczki *et al.*, 2008). At the spindle poles, where cyclin B1-CDK1 is initially activated, Plk1 is thought to be involved in mitotic entry. Plk1 has been found to interact, via its PBD, with CDK1-primed Cdc25C at the centrosomes, thus activating it (Elia *et al.*, 2003a). In addition, Plk1 can bind, phosphorylate and inhibit CDK1-primed Wee1 and Myt1 and this creates an outer feed back loop of cyclin B1-CDK1 activation (Lindqvist *et al.*, 2009). Plk1 is also involved in mitotic exit since Plk1 phosphorylates subunits of the APC/C and is therefore involved in protein destruction in late mitosis (Barr *et al.*, 2004).

Plk1 relocates to the spindle midzone and then to the midbody in anaphase and telophase (Petronczki *et al.*, 2008). PRC1 and MKLP2 have both been implicated in the targeting of Plk1 to the spindle midzone. In anaphase PRC1 binds to Plk1, targeting it to the central spindle (Neef *et al.*, 2007). In metaphase, CDK1 phosphorylates PRC1, thus preventing binding of Plk1. At anaphase onset, on inactivation of CDK1, the inhibitory phosphorylation is removed and Plk1 creates its own docking site (self-primed) on PRC1. This recruits Plk1 to the spindle, which is required for cytokinesis (Neef *et al.*, 2007). Plk1 also interacts with and phosphorylates the mitotic kinesin MKLP2, which is necessary for MKLP2 function and the localisation of Plk1 to the central spindle in late anaphase/telophase (Neef *et al.*, 2003). This is necessary for cytokinesis.

The function of Plk1 in the regulation of the early stages of the cell cycle has meant that only relatively recently its role in the later stages of mitosis has been

revealed, owing to the development of inhibitors which can be used to block Plk1 activity at anaphase onset. Research has revealed that Plk1 controls initiation of cytokinesis via the ECT2-RhoA pathway (Petronczki *et al.*, 2008). Use of the Plk1 inhibitor ZK-Thiazolidinone (TAL), in anaphase HeLa cells, showed that cleavage furrow formation and ingression failed on inhibition of Plk1, resulting in an increased population of multinucleate cells (Santamaria *et al.*, 2007). TAL prevented RhoA accumulation at the equatorial cell cortex and ECT2 recruitment to the central spindle (Santamaria *et al.*, 2007). Similarly, the Plk1 inhibitor BI 2536 resulted in failure of furrow formation in anaphase HeLa cells due to a lack of RhoA localisation at the equatorial cortex (Petronczki *et al.*, 2007). Via ECT2 immunoprecipitation of synchronized HeLa lysates, BI 2536 was found to abolish the anaphase interaction between ECT2 and CYK-4, thus preventing ECT2 localisation to the central spindle (Petronczki *et al.*, 2007). Using tandem mass spectrometry and phosphospecific antibodies, Burkard *et al.*, revealed that Plk1 binds and directly phosphorylates the CYK-4 at the midzone, creating a docking site for ECT2 (Burkard *et al.*, 2009), which is essential for cleavage furrow formation. Thus, through data from these groups and others, it has been suggested that late mitotic activity of Plk1 is an upstream regulator of ECT2-RhoA cascade by promoting recruitment of ECT2 to the central spindle by CYK-4; this is essential for the initiation of cytokinesis.

1.6.4 Aurora A kinase

The mitotic kinase Aurora A is a member of the Aurora family serine/threonine protein kinases (Morgan, 2007). Aurora A is active in the early stages of mitosis, but is degraded via the APC/C when the spindle microtubules have elongated to their maximum in anaphase B (Lindon and Pines, 2004). Interestingly, degradation of Aurora A is only complete by G1 phase (Lindon and Pines, 2004). Aurora A is concentrated at the centrosomes and also localises to the spindle microtubules during mitosis (Marumoto *et al.*, 2003; Lindon and Pines, 2004; Barr and Gergely, 2007). The consensus phosphorylation site for Aurora A was defined in budding yeast as [KR]X[TS][ILV] (Cheeseman *et al.*, 2002) and later confirmed in higher eukaryotes in proteins such as Cdc25B (Dutertre *et al.*, 2004). Aurora A is activated via autophosphorylation of Thr288 in its T loop and for full activity,

Aurora A also requires co-factors, including Bora, Ajuba, PAK1 and Tpx2 (reviewed in Barr and Gergely, 2007).

Aurora A regulates mitotic centrosomes and bipolar spindle assembly (Barr and Gergely, 2007). Aurora A has been identified as a key regulator of centrosome separation and maturation, spindle pole organisation, microtubule stability and accurate completion of chromosome segregation (reviewed in Barr and Gergely, 2007). Depletion of Aurora A or addition of inactive kinase results in the formation of monopolar spindles (Liu and Ruderman, 2006). Aurora A has been implicated in regulation of the G2/M transition via the outer feed back loop of cyclin B-CDK1 activation (Lindqvist *et al.*, 2009). In *Xenopus* egg extracts, depletion of Aurora A or addition of inactive kinase resulted in a delay of mitotic entry, but not a block (Liu and Ruderman, 2006). This could be explained by the fact that Aurora A directly phosphorylates and activates Cdc25B, thus stimulating cyclin B-CDK1 activity at the centrosomes further and promoting mitotic entry (Dutertre *et al.*, 2004).

Interestingly, Aurora A activity may impinge on cytokinesis. Microinjection of anti-Aurora A antibodies into metaphase HeLa cells prevented cells from completing cytokinesis, resulting in the formation of binucleate cells (Marumoto *et al.*, 2003). This perhaps suggests that Aurora A functions in late mitosis, which is supported by the fact that Aurora A becomes localised on the spindle midzone towards the end of mitosis (Marumoto *et al.*, 2003;Lindon and Pines, 2004;Barr and Gergely, 2007) and while degradation of Aurora A commences in anaphase B, it is only complete by G1 phase (Lindon and Pines, 2004).

1.6.5 Aurora B kinase

The mitotic kinase Aurora B is a member of the Aurora family serine/threonine protein kinases (Morgan, 2007). Aurora B forms the chromosomal passenger complex (CPC) with inner centromere protein INCENP, survivin and borealin (Vagnarelli and Earnshaw, 2004;Vader *et al.*, 2006;Ruchaud *et al.*, 2007). These proteins are necessary for Aurora B activity and are required for its targeting to the correct compartments of the cell (Sessa *et al.*, 2005;Jeyaprakash *et al.*, 2007).

Aurora B displays dynamic cell-cycle localisation, where it functions to control different aspects of mitosis (Vader *et al.*, 2006). In early mitosis the CPC localises to the arms of condensing chromosomes and concentrates at the centromeres and kinetochores during prometaphase and metaphase (Vagnarelli and Earnshaw, 2004;Vader *et al.*, 2006). At this point Aurora B regulates processes including chromosome condensation and orientation, spindle assembly, microtubule-kinetochore interactions and the spindle assembly checkpoint (Vagnarelli and Earnshaw, 2004;Vader *et al.*, 2006;Ruchaud *et al.*, 2007).

Following separation of the sister chromatids in anaphase, Aurora B localises to the spindle midzone microtubules and later in telophase, Aurora B relocates to the intracellular bridge, either side of the midbody (Vagnarelli and Earnshaw, 2004;Vader *et al.*, 2006). Using RNAi to MKLP2 it was shown that at anaphase onset, the CPC is transferred from centromeres to the spindle midzone via the mitotic kinesin MKLP2 (Gruneberg *et al.*, 2004). Aurora B has been found to regulate cytokinesis (Barr and Gruneberg, 2007). RNAi knockdown of Aurora B in *C. elegans* embryos causes furrow regression, resulting in multinucleate cells (Kaitna *et al.*, 2000). Anaphase substrates of Aurora B include components of the centralspindlin complex, MKLP1 and CYK-4 (Minoshima *et al.*, 2003;Guse *et al.*, 2005;Neef *et al.*, 2006) and phosphorylation of these proteins by Aurora B is necessary for cytokinesis completion. Interestingly, Aurora B depletion prevented accumulation of FIP3 at the midbody of HeLa cells (Simon *et al.*, 2008).

A study has recently shown that Aurora B phosphorylates tumour suppressor RASSF1A on serine 203 during late mitosis (Song *et al.*, 2009). During late mitosis RASSF1A recruits syntaxin 16 to the midzone and midbody; Aurora B activity is a requirement for this interaction and completion of cytokinesis. As discussed in section 1.5.7, membrane traffic is at the heart of cytokinesis and Song *et al.*, have revealed that this key process is regulated by another important facet of the cell-cycle, namely regulation by the cell-cycle dependent kinases.

1.7 Aims

Time-lapse microscopy of HeLa cells expressing GFP-FIP3 has shown that FIP3 undergoes spatial and temporal dynamics during mitosis (Wilson *et al.*, 2005). It has been proposed that FIP3 in complex with Rab11 plays a key role in the delivery and targeting of recycling endosomes to the furrow; this is essential for completion of cytokinesis (Wilson *et al.*, 2005;Fielding *et al.*, 2005).

The regulatory mechanisms underlying the spatial and temporal dynamics of FIP3 during mitosis are unknown. The cell-cycle is governed by a network of protein kinases which control the activity, localisation and interactions of proteins involved in cell-cycle progression (Nigg, 2001). This work aims to determine if FIP3 can be phosphorylated by the mitotic kinases and whether this has an impact on its spatial and temporal dynamics.

2 Materials and Methods

2.1 Materials

2.1.1 General reagents

Avanti polar lipids, Alabaster, USA

1,2-dioleoyl phosphatidylserine (DOPS)

1-palmitoyl-2-oleoyl phosphatidylcholine (POPC)

Applied Biosystems, Warrington, UK

Nuclease-free water (not DEPC-treated)

Bio-Rad Laboratories Ltd., Hemel Hempstead, Hertfordshire, UK

Biobeads

Quick Start Bradford 1x Dye Reagent

Carl Zeiss Ltd., Welwyn Garden City, Hertfordshire, UK

Immersol™ 518F

Clontech, St-Germain-en-Laye, France

Advantage® GC Genomic LA Polymerase

Dundee Cell Products, Dundee, UK

HeLa cytoplasmic extract (S100 fraction)

Dutscher Scientific UK, Essex, UK

Ethidium Bromide Dropper Bottle (0.5µg/ml)

Fisher Scientific UK Ltd., Loughborough, Leicestershire, UK

Calcium chloride
Pierce Immunopure Affinity-Purified Polyclonal Rabbit Anti-Sheep IgG (H + L) HRP-linked
Dimethyl sulphoxide (DMSO)
Ethanol
Glycine
N-(2-Hydroxyethyl)piperazine-N'-2-ethanesulphonic acid (HEPES)
Shandon Immu-Mount™
Sucrose
Trichloroacetic acid (TCA)
Tris base

Formedium Ltd., Hunstanton, Norfolk, United Kingdom

Agar
Tryptone enzymatic digest of casein
Yeast Extract, Powder

GE Healthcare Global Headquarters, Chalfont, St Giles, Buckinghamshire

Amersham ECL Mouse IgG, HRP-Linked Whole Ab (from sheep)
Amersham ECL Rabbit IgG, HRP-Linked Whole Ab (from donkey)
Amersham ECL Rat IgG, HRP-Linked Whole Antibody (from goat)
Protein G Sepharose 4 Fast Flow
Protein A Sepharose Fast Flow

Invitrogen Ltd., Paisley, UK

Albumin from bovine serum (BSA)
Alexa Fluor® 568 goat anti-rat IgG (H + L)
Alexa Fluor® 488 donkey anti-rat IgG (H + L)
Alexa Fluor® 647 goat anti-rat IgG (H + L)
10mM dNTP Mix
Lipofectamine™ 2000 Transfection Reagent

Myelin Basic Protein (MBP) from bovine brain
NuPAGE® Sample Reducing Agent (10x)
NuPAGE® Antioxidant
NuPAGE® SDS Sample Buffer
NuPAGE® MOPS SDS Running Buffer (20x)
NuPAGE® NOVEX 10% Bis-Tris Gel 1.0mm, 10 well
One Shot® TOP10 Chemically competent *E.coli*
Plk1 kinase (PV3501)
SOC medium

New England Biolabs (UK) Ltd., Hitchin, Hertfordshire

1 kb DNA Ladder
Prestained Protein Marker, Broad Range (7-175 kDa)
T4 DNA Ligase

Kodak, Hemel Hempstead, Hertfordshire, UK

X-ray film

Melford Laboratories Ltd., Chelworth, Ipswich, Suffolk, UK

Dithiothreitol (DTT)

Millipore (UK) Ltd., Watford, Hertfordshire, UK

Aurora A kinase, active (14-511)
Aurora B kinase, active (14-489)
Cyclin B-CDK1, active (14-450)

Premier Foods, Long Sutton, Spalding, Lincolnshire, UK

Marvel

Promega, Southampton, UK

Alkaline Phosphatase (Shrimp)
Dpnl
EcoRI
KpnI
Wizard® Plus SV Minipreps DNA Purification System
XhoI

QIAGEN Ltd., Crawley, West Sussex, UK

Nickel-NTA Agarose (Ni-NTA Agarose)
QIAfilter™ Plasmid Maxi Kit
QIAquick Gel Extraction Kit

Roche Diagnostics Ltd., Burgess Hill, UK

Agarose MP
Complete™ Protease Inhibitor Cocktail Tablets
Complete™, EDTA-free Protease Inhibitor Cocktail Tablets

Severn Biotech Ltd., Kidderminster, Worcestershire, UK

30% (w/v) Acrylamide [Acrylamide to Bis-Acrylamide
ratio 37.5:1]

Sigma-Aldrich Ltd., Gillingham, Dorset, UK

Adenosine 5'-triphosphate magnesium salt (ATP.Mg²⁺)
Ammonium persulphate (APS)
Brilliant Blue R
Brilliant Blue G-Colloidal Concentrate
p-Coumaric acid
4',6-Diamidino-2-phenylindole, dilactate (DAPI, dilactate)
Ethylenediaminetetraacetic acid disodium salt dehydrate (EDTA)
Ethylene glycol-bis(2-aminoethylether)-N,N',N'-tetraacetic acid (EGTA)

Ficoll® PM 400
Gelatin from cold water fish skin
Glycerol
Goat serum
Hygromycin B solution from *Streptomyces hygroscopicus*
Kanamycin sulfate from *Streptomyces kanamyceticus*
Luminol
2-(N-Morpholino)ethanesulphonic acid (MES)
MG132 (Z-Leu-Leu-Leu-al)
3-(N-Morpholino)propanesulphonic acid (MOPS)
Methanol
Nocodazole
Nonidet™ P 40 Substitute
5-(N-2,3-Dihydroxypropylacetamido)-2,4,6-triiodo-N,N'-bis(2,3-dihydroxypropyl)isophthalamide (Nycodenz®)
OptiPrep® Density Gradient Medium
Paraformaldehyde
Sodium dodecyl sulphate (SDS)
Sodium fluoride
Sodium orthovanadate (Na₃VO₄)
Sodium phosphate monobasic dihydrate (NaH₂PO₄ · 2H₂O)
Thymidine
N,N,N',N'-Tetramethylethylenediamine (TEMED)
Triton® X-100
TWEEN® 20
Urea

Spectrum laboratories

Float-a-lyzer, 3 ml 10000 kDa MWCO

VWR International Ltd., Lutterworth, Leicestershire, UK

Acetic acid (glacial) 100%
Hydrogen peroxide
Magnesium Chloride-6-Hydrate (MgCl₂·6H₂O)

Di-Potassium hydrogen phosphate (K_2HPO_4)
Propan-2-ol
Sodium chloride
di-Sodium hydrogen orthophosphate anhydrous (Na_2HPO_4)
tetra-Sodium pyrophosphate ($Na_4P_2O_7 \cdot 10H_2O$)

2.1.2 Cell culture reagents

All cell culture reagents were purchased from Invitrogen Ltd., Paisley, UK.

Dulbecco's Modified Eagle Medium (D-MEM) (1x) liquid (High Glucose). (With L-Glutamine, with 4500mg/L, D-Glucose, without Sodium Pyruvate)
Opti-MEM® I Reduced Serum Media
Foetal Bovine Serum (Heat Inactivated), EU Approved
L-Glutamine 200mM (100x) liquid
Penicillin - Streptomycin
Trypsin, 0.05% (1x) with EDTA 4Na, liquid

Nutrient Mixture F-12 Ham, with L-glutamine and sodium bicarbonate (liquid, sterile-filtered, cell culture tested) was purchased from Sigma-Aldrich Ltd., UK.

2.1.3 Primary antibodies

Anti-FIP3 (sheep) was produced by The Scottish Blood Transfusion Service using baculovirus Sf9 insect cell expressed human His-tagged FIP3 as an antigen. Whole serum was purified using a FIP3 column.

Phospho-specific antibodies were raised against the phospho-peptides detailed in section 2.1.7. This was carried out by The Scottish Blood Transfusion Service. Whole serum was obtained and purified against a Protein A Sepharose column.

All other antibodies were purchased from the following suppliers:

Abcam plc., Cambridge, UK

Mouse monoclonal anti-GAPDH antibody

2.1.6 Primers

All primers were purchased from Yorkshire Bioscience Ltd., Heslington, York, UK.

Site directed mutagenesis primers:

The sites of mutagenesis have been underlined.

FIP3 S102A Forward	GGGCAGCTTGCG <u>GCCCC</u> GACGCCCC
FIP3 S102A Reverse	GGGGCGTCGGGG <u>GCCG</u> CAAGCTGCCC
FIP3 S102D Forward	GGGCAGCTTGCG <u>GACCCC</u> GACGCCCC
FIP3 S102D Reverse	GGGGCGTCGGGG <u>TCCG</u> CAAGCTGCCC
FIP3 S281A Forward	CTACGGTGGTGTGCGCT <u>GCTG</u> CCCAAGATGAGGG
FIP3 S281A Reverse	CCCTCATCTTGGGC <u>AGCAG</u> CGACACCACCGTAG
FIP3 S281D Forward	GCTACGGTGGTGTGCGCT <u>GATG</u> CCCAAGATGAGGAGC
FIP3 S281D Reverse	GCTCCTCATCTTGGGC <u>ATCAG</u> CGACACCACCGTAGC
FIP3 S348A Forward	GACAGTGCCGGCGG <u>GCGG</u> CCGTGCCCTCTGAG
FIP3 S348A Reverse	CTCAGAGGGCACGG <u>CCGCG</u> CCGCCGCGGCACTGTC
FIP3 S348D Forward	CAGTGCCGGCGG <u>GACG</u> CCGTGCCCTCTGAG
FIP3 S348D Reverse	CTCAGAGGGCACGG <u>CGTCG</u> CCGCCGCGGCACTG
FIP3 S451A Forward	GAGGCCCTGGAGGACCCT <u>GCCCC</u> GAGCTCATGGAGGGC
FIP3 S451A Reverse	GCCCTCCATGAGCTCGGGG <u>GCA</u> GGTCCCTCCAGGGCCTC
FIP3 S451D Forward	GAGGCCCTGGAGGACCCT <u>GACCCC</u> GAGCTCATGGAGGGC

FIP3 S451D Reverse GCCCTCCATGAGCTCGGGGTCAGGGTCCTCCAGGGCCTC

Sequencing primers:

The pEGFP-N1 forward and reverse primers were designed to bind to sequences approximately 100bp upstream and downstream of the multiple cloning site of pEGFP-N1, respectively. The numbers in each FIP3 primer detail the base pair from which the primer starts within the human FIP3 sequence.

pEGFP-N1 Forward CCAAATGTCGTAACAACCTCCGCC

pEGFP-N1 Reverse GTGGTGCAGATGAACTTCAGGGTCAG

FIP3 432 Reverse GCGGAAAGGCGCGCTCTCCGGGC

FIP3 691 Forward GCTACGGTCTACGGGGCAGAGCAG

FIP3 1161 Reverse CTCGCCCCGATCACCGTGATGAC

FIP3 1225 Forward GGCAGCTGGGCTGCAGTGAC

FIP3 1509 Reverse GGCGTTTGCTCTGTGCACCAGCTG

2.1.7 Rab11-FIP3 phospho-peptides

Phosphorylated and non-phosphorylated peptides to Rab11-FIP3 serines 102, 281, 348 and 451, were purchased from Quality Controlled Biochemicals, Hopkinton, Mass, USA. The sequences of the peptides were as follows:

Rab11-FIP3 Serine 102 GQLA(p)SPDAP

Rab11-FIP3 Serine 281 GGVA(p)SAQDE

Rab11-FIP3 Serine 348 SAGG(p)SAVPS

Rab11-FIP3 Serine 451 LEDP(p)SPLEM

2.1.8 Radiochemicals

Adenosine 5' triphosphate, ATP, [γ - ^{32}P]-3000Ci/mmol (10mCi/ml) was purchased from PerkinElmer Life and Analytical Sciences, Monza (Milano), Italy

2.1.9 Kinase Inhibitors

BMI-1026 (CDK1 inhibitor) was a kind gift from Dr K.S. Lee, Laboratory of Metabolism, Centre for Cancer Research, National Cancer Institute, NIH. Bethesda, Maryland 20892, USA.

Plk1 inhibitors U19479/72/1 (Plk1a) and U20723/56/1 (Plk1b) were gifted by Timothy J. Lansing, GlaxoSmithKline R&D

All other kinase inhibitors were purchased from the following suppliers:

MERCK CHEMICALS LTD., Beeston, Nottingham, UK

PD 98059 (2'-Amino-3'-methoxyflavone) (Inhibitor of MAP kinase kinase, MEK)

SB 203580 (4-(4-Fluorophenyl)-2-(4-methylsulfinylphenyl)-5-(4-pyridyl)1H-imidazole) (inhibitor of p38 MAP kinase)

Sigma-Aldrich Ltd., Gillingham, Dorset, UK

Y-27632 dihydrochloride monohydrate [(R)-(+)-trans-4-(1-Aminoethyl)-N-(4-Pyridyl)cyclohexanecarboxamide dihydrochloride monohydrate] (ROCK inhibitor)

Tocris Bioscience, Avonmouth, Bristol, UK

ZM 447439 (Aurora B Inhibitor)

2.1.10 General solutions

Buffer A200	25mM Hepes pH 7.4, 200mM KCl, 10% (w/v) glycerol, 2mM β -mercaptoethanol
Coomassie blue stain solution	0.25% Coomassie Brilliant Blue R in 90ml methanol:water at a ratio of 1:1 and 10ml glacial acetic acid. This was thoroughly mixed and filtered through Whatman No. 2 filter paper.
Coomassie blue destain solution	10% (v/v) methanol and 10% (v/v) acetic acid
DNA loading buffer (6x)	0.25% (w/v) Bromophenol Blue, 15% (w/v) Ficoll® PM 400
ECL Solution A	100mM Tris-HCl, pH 8.5, 2.25mM Luminol, 0.4mM p-coumaric acid, 1.44% (v/v) DMSO.
ECL Solution B	100mM Tris-HCl, pH 8.5, 0.018% (v/v) H ₂ O ₂
4% p-formaldehyde	4% p-formaldehyde, 1mM CaCl ₂ , 1mM MgCl ₂ in PBS. p-formaldehyde was dissolved in PBS using a microwave. The remaining components were added and then the solution filtered through a 0.2 μ m Nalgene vacuum filter.
HES buffer	20mM Hepes, pH 7.4, 1mM EDTA, 225mM sucrose, protease inhibitor tablet
His-tag buffer	50mM sodium phosphate, 150mM NaCl, pH 7.4, 0.02% (v/v) Triton X-100

HPFEV buffer	50mM Hepes pH 7.4, 10mM sodium pyrophosphate, 100mM sodium fluoride, 2mM EDTA, 2mM activated sodium orthovanadate, protease inhibitor tablet
Immunofluorescence (IF) buffer	PBS containing 0.2% (w/v) fish skin gelatin and 0.1% (v/v) goat serum (different species to the one in which the secondary antibodies were raised). This was made on the day and filtered through a Nalgene 0.2µm vacuum filter.
Kinase assay buffer	50mM Hepes pH 7.5, 10mM MgCl ₂ , 2mM MnCl ₂ , 0.2mM DTT, 50µM ATP.Mg ²⁺
Cell lysis buffer	50mM Hepes pH 7.2, 100mM KCl, 5mM NaCl, 1mM MgCl ₂ , 0.5mM EGTA, 1mM EDTA, 1X protease inhibitor tablet (added immediately before use), 0.1% (v/v) Triton X100, 1mM DTT (added immediately before use)
Phosphate buffered saline (PBS)	136mM NaCl, 2.5mM KCl, 10mM Na ₂ HPO ₄ , 1.8mM KH ₂ PO ₄ , pH 7.4
PBS-T	PBS, 0.01% (v/v) Tween-20
SDS-PAGE electrode buffer	25mM Tris base, 190mM glycine, 0.1% (w/v) SDS
SDS-PAGE sample buffer (4x)	200mM Tris-HCl pH 6.8, 400mM DTT (added immediately before use), 8% (w/v) SDS, 0.4% (w/v) bromophenol blue, 40% (w/v) glycerol
TAE	40mM Tris-acetate, 1mM EDTA, pH 7.8
Transfer buffer	25mM Tris base, 192mM glycine, 20% (v/v) ethanol

2 YT medium	1.6% (w/v) tryptone, 1% (w/v) yeast extract, 0.5% (w/v) NaCl
2 YT agar	1.6% (w/v) tryptone, 1% (w/v) yeast extract, 0.5% (w/v) NaCl, 2% (w/v) agar

2.2 General laboratory procedures

2.2.1 Protein assays

The protein concentration of purified protein fractions was measured using Bio-Rad Bradford protein assay reagent. Bovine serum albumin (1-20 μ g) was used as the standard. The amount of sample assayed was selected in order to ensure the absorbance fell within the linear range of the standard. Assays were set up in triplicate in a 96 well plate, according to the manufacturer's instructions. Absorbance was measured at 595nm using a FLUOstar Optima plate reader. Protein concentrations were calculated using a curve derived from the BSA standard values.

2.2.2 SDS-polyacrylamide gel electrophoresis (SDS-PAGE)

SDS-PAGE was used to separate proteins on the basis of size. SDS-PAGE was performed using Bio-Rad Mini-PROTEAN 3 apparatus. Proteins were separated using tris-HCl gels. The percentage of acrylamide in the resolving gel ranged from 8 to 15% depending on the molecular weight of the protein of interest.

Samples were solubilised in SDS-PAGE sample buffer and incubated in a heat block at 95°C for 5 minutes. Electrophoresis was carried out using SDS-PAGE electrode buffer. Gels were run at a constant voltage of 80 volts, until the protein sample had passed through the stacking gel; this was increased to 120 volts through the resolving gel. Electrophoresis continued until the pre-stained broad range markers had separated adequately and the dye front had reached the bottom of the gel.

2.2.3 Western blotting

Following SDS-PAGE, proteins were transferred onto a nitrocellulose membrane for immunodetection. Gels were removed from the glass plates and the stacking gel removed. Transfer components were pre-soaked in transfer buffer. The transfer system was assembled as follows, from cathode to anode: sponge pad, Whatman 3mm chromatography paper, nitrocellulose membrane (0.45µm pore size), polyacryamide gel (containing electrophoresed proteins, as outlined in section 2.2.2), Whatman 3mm chromatography paper and a sponge pad. This sandwich was assembled in a cassette and inserted into a Bio-Rad mini Trans-Blot cell, filled with transfer buffer. Proteins were transferred onto nitrocellulose at room temperature for two hours at a constant current of 200mA or overnight at 40mA.

2.2.4 Immunodetection of proteins

Following Western Blotting, as detailed in section 2.2.3, proteins were visualised by Enhanced Chemical Luminescence (ECL). Nitrocellulose membranes were removed from the transfer cassette and washed with PBS-T. To block non-specific binding sites, membranes were incubated in 5% (w/v) dried non-fat milk made up in PBS-T, for 30 minutes at room temperature. Primary antibodies were diluted in 1% (w/v) dried non-fat milk/PBS-T at an appropriate dilution. Membranes were incubated, with shaking, in primary antibody for a minimum of 1 hour at room temperature or overnight at 4°C, if required. Membranes were washed three times with PBS-T over a 30 minute period. Secondary IgG horseradish peroxidase-conjugated antibodies (HRP-linked IgG) were diluted in 5% (w/v) dried non-fat milk/PBS-T to an appropriate dilution. Membranes were exposed to HRP-linked IgG for one hour at room temperature, with shaking. Membranes were washed three times with PBS-T over a 30 minute period.

HRP-Immunolabelled proteins were visualised using the ECL system. ECL reagents 1 and 2 were mixed in a 1:1 ratio. The nitrocellulose membrane was immersed in ECL reagent for 1 minute then removed immediately. The membrane was exposed to Kodak X-ray film in a light-proof cassette and developed using an X-Omat Processor.

2.2.5 Stripping of nitrocellulose membranes

To strip nitrocellulose membranes of bound antibodies, membranes were incubated in stripping buffer (50mM glycine, pH 2.5) for 20 minutes at room temperature under agitation. Blots were then washed with PBS-T and then blocked with 5% (w/v) dried non-fat milk/PBS-T for 1 hour. Blots were checked for effectiveness of stripping via ECL and then further incubated in primary antibody, as required.

2.2.6 Coomassie blue staining of SDS polyacrylamide gels

To detect protein in a SDS-PAGE gel, gels were immersed in Coomassie blue stain solution for one hour (minimum), with agitation. Coomassie blue stain was then removed and gels were destained overnight, under agitation in Coomassie blue destain solution.

2.2.7 Brilliant Blue G-Colloidal Coomassie

Brilliant Blue G-Colloidal Coomassie staining is used to stain for proteins destined for proteomic analysis, owing to the reversible binding of the Coomassie. Gels were stained according to the manufacturer's instructions. All solutions, except the Brilliant Blue G-Colloidal Coomassie itself, were filtered prior to use. Manipulation of the gel was carried out in the fume hood to minimise contamination by keratin. Briefly, following eletrophoresis, proteins were fixed for one hour in a solution of 7% (v/v) glacial acetic acid in 40% (v/v) methanol. 800 ml of deionised water was added to the bottle of Brilliant Blue G-Colloidal Concentrate, and this was mixed by inversion. This formed the 1x working solution, which was not filtered. Immediately before staining, 4 parts of the 1x working solution were combined with 1 part methanol. This was mixed well by vortexing for 30 seconds. The gel was placed in staining suspension for 1 to 2 hours. Gels were destained with 10% (v/v) acetic acid in 25% (v/v) methanol for 60 seconds with shaking. Gels were rinsed with 25% (v/v) methanol. This was discarded and then gels were destained in 25% (v/v) methanol for up to 24 hours.

2.3 General molecular biology

2.3.1 Site directed mutagenesis

Site-directed mutagenesis was carried out according to the QuickChange® method (Stratagene). Owing to the high GC content of Rab11-FIP3, Advantage® GC Genomic LA Polymerase Mix was purchased from Clontech. The exchange of one amino acid to another was performed using synthetic oligonucleotides which were designed with the desired mutation in the middle of the primer (refer to section 2.1.6 for primer details). The template was purified using QIAfilter™ Plasmid Maxi Kit.

The reaction mixture used for site directed mutagenesis was as follows.

2X Advantage GC-Melt LA Buffer	12.5µl
dNTPs (10mM each dCTP, dGTP, dATP, dTTP)	1µl
Forward primer	0.1 - 0.5µM
Reverse primer	0.1 - 0.5µM
Template DNA	10-100ng
Polymerase mix	0.25µl
Nuclease free water	to 25µl

Tubes were flick mixed and briefly spun in a microcentrifuge.

The thermocycling conditions used for site directed mutagenesis were as follows.

<u>94° C 1 min</u>	} 16 to 30 cycles
94° C 30 sec	
60° C 30 sec	
<u>72° C 2min/kb</u>	
72° C 5 min	
4° C Hold	

To remove the parental plasmid DNA, mixtures were incubated for 1 hour at 37° C in the presence of 1µl DpnI. 5µl of the mixture was used to transform

TOP10 chemical competent cells, as detailed in section 2.3.2. Plasmids were isolated from single colonies as outlined in 2.3.3. Mutations were confirmed by DNA sequencing, as detailed in section 2.3.10.

2.3.2 Transformation of *Escherichia coli*

Chemically competent TOP10 cells were transformed according to the manufacturer's instructions. Briefly, cells were thawed on ice for 15 minutes. 5µl of SDM reaction/miniprep or 1µl maxiprep was added to the cells. These were incubated on ice for 30 minutes. The cells were then subject to heat shock at 42°C for 45 seconds, then chilled on ice for 1 minute. 250µl SOC medium was added to each vial of cells, which was then incubated at 37°C, with shaking, for 1 hour. Cells were plated on warmed 2 YT selection plates, containing the required antibiotic. For pEGFP-N1 plasmid, containing human FIP3, Kanamycin at a concentration of 50µg/ml was used. For the pCR3.1 vector, Ampicillin at a concentration of 100µg/ml was used. Plates were inverted and grown at 37°C overnight.

2.3.3 Small scale DNA preparations (miniprep)

Small scale DNA preparations were carried out using Promega Wizard® Plus SV Minipreps DNA Purification System, following the manufacturer's instructions. Briefly, individual bacterial colonies from 2 YT selective plates were picked and transferred to 5ml 2 YT media containing the appropriate antibiotic. For pEGFP-N1 plasmid, containing human FIP3, Kanamycin at a concentration of 50µg/ml was used. For the pCR3.1 vector, Ampicillin at a concentration of 100µg/ml was used. These were grown overnight at 37°C with shaking. Cells were collected via centrifugation at 3273 g in a refrigerated bench top centrifuge and resuspended in 250µl cell resuspension buffer. Cells were transferred to 1.5ml eppendorf tubes. 250µl cell lysis buffer was added and the tubes were mixed by inverting four times. 5µl alkaline protease solution was added and the tubes were mixed by inverting four times. These were incubated at room temperature for 5 minutes. 350µl neutralisation solution was added and the tubes were mixed by inverting four times. Microcentrifuge tubes were centrifuged for 10 minutes at full speed in a microcentrifuge and supernatants were decanted into spin

columns. These were then spun at full speed for 1 minute in a microcentrifuge. The flow through was discarded and 750 μ l column wash buffer (containing ethanol) was applied. This was spun at full speed for 1 minute in a microcentrifuge and the flow-through discarded. This was repeated using 250 μ l column wash buffer. Flow through was discarded and the tubes were spun for a further minute to remove any residual column wash solution. Columns were placed in fresh sterile 1.5ml microcentrifuge tubes. 100 μ l nuclease free water was pipetted into the centre of the column. DNA was collected by centrifugation for 1 minute.

2.3.4 Large-scale DNA preparation (maxiprep)

Large-scale DNA preparations were performed using QIAfilter™ Plasmid Maxi Kit, according to the manufacturer's instructions. Briefly, individual bacterial colonies from 2 YT selection plates were picked and transferred to 5ml 2 YT media containing the appropriate antibiotic. For pEGFP-N1 plasmid, containing human FIP3, Kanamycin at a concentration of 50 μ g/ml was used. For the pCR3.1 vector, Ampicillin at a concentration of 100 μ g/ml was used. Several hours later the 5ml culture was added to 50ml 2 YT (including antibiotic) in a sterile 250ml conical flask. This was incubated at 37°C overnight, with shaking. Cells were harvested in 50ml centrifuge tubes at 3273 g in a refrigerated benchtop centrifuge for 30 minutes at 4°C. Bacterial pellets were resuspended in 10ml Buffer P1 (containing RNase A). 10ml Buffer P2 was then added and mixed thoroughly by vigorously inverting the sealed tube 4-6 times. This was left to incubate at room temperature for 5 minutes. The reaction was neutralised on addition of 10ml pre-chilled Buffer P3. This was mixed immediately by vigorously inverting 4-6 times. The cap onto the outlet nozzle of the QIAfilter Maxi Cartridge was attached and placed in a 50ml centrifuge tube. The lysate was poured into the barrel of the QIAfilter Maxi Cartridge and incubated at room temperature for 10 minutes. The QIAGEN-tip 500 was equilibrated by applying 10 ml QBT Buffer and allowed to empty by gravity flow. The cell lysate was filtered into the equilibrated tip and the cleared lysate entered the resin by gravity. The tip was then washed twice with 30ml Buffer QC (containing ethanol). DNA was eluted into a 50ml centrifuge tube with 15ml Buffer QF. DNA was precipitated by adding 10.5ml room temperature isopropanol. This was mixed and centrifuged

immediately at 3273 g for 1 hour in a refrigerated benchtop centrifuge. The supernatant was decanted and the pellet washed with 5ml room temperature 70% (v/v) ethanol. This was centrifuged at 3273 g for 30 minutes. The supernatant was removed and the pellet air-dried for 5 to 10 minutes. The pellet was resuspended in 150 to 250µl nuclease-free water.

2.3.5 DNA restriction digests

Restriction digests were carried out according to manufacturer's instructions. For digests using two restriction enzymes, the digest buffer used was selected on the basis that both enzymes retained 75-100% activity in the buffer. A general outline for a restriction digest using Promega enzymes is provided below.

Restriction digests were set up as follows:

DNA (1µg/µl)	1µl
RE 10X Buffer	2µl
Acetylated BSA (10µg/µl)	0.2µl
Restriction enzyme 1 (10u/µl)	1µl
Restriction enzyme 2 (10u/µl)	1µl
Sterile nuclease-free water	to 20µl

The tubes were flick mixed and briefly centrifuged in a microcentrifuge, prior to incubation at 37°C for 2 hours. The digestion products were prepared for agarose gel electrophoresis with the addition of 4µl 6x DNA loading buffer and electrophoresis was performed as outlined in section 2.3.7.

2.3.6 Ligation

Restriction digests of the destination vector and the vector containing insert were prepared separately using the same buffer and appropriate enzymes. The digests were then separated using agarose gel electrophoresis, as outlined in section 2.3.7, and the digested bands of the appropriate size were excised using a clean scalpel. The gel slices were purified, as outlined in section 2.3.8. The vector and insert were mixed at a ratio of 1:1 and 1:5. The final reaction volume was 10µl and this included 1µl of 10X T4 DNA ligase buffer and 1µl of T4 DNA

ligase. Controls were set up with vector only, insert only and vector with insert (minus T4 DNA ligase). Ligations were incubated at 16°C overnight to allow the complimentary ends to anneal. The following morning, the entire ligation mixture was used to transform Top10 cells, as outlined in section 2.3.2.

2.3.7 Agarose gel electrophoresis

1% (w/v) agarose gels were prepared in TAE buffer, using a microwave oven. Once cooled slightly, ethidium bromide from a dropper bottle (0.5µg/ml) was added. One drop was sufficient for 50ml of agarose solution. This was mixed and poured into a horizontal electrophoresis gel tray, within a casting tray, using the appropriate comb. Once set at room temperature, the gel was transferred to a submerged horizontal electrophoresis tank containing TAE buffer. All electrophoresis equipment was purchased from BioRad. DNA samples, prepared in 6x DNA loading buffer, were applied to the wells. 0.5µg of 1kb DNA ladder (500µg/ml) was applied to an adjacent lane. Electrophoresis was carried out at 100 volts until the dye front had migrated far enough to have allowed the resolution of DNA fragments. Gels were visualized and recorded using a Molecular Imager ChemiDoc XRS+ System from BioRad.

2.3.8 Gel extraction of DNA

DNA products were separated via agarose gel electrophoresis as described in section 2.3.7 and the product of the correct size identified under UV light. Bands of interest were excised using a clean scalpel blade and placed in clean 1.5ml microcentrifuge tubes. The size of the gel slice was minimised by removing excess agarose. DNA of interest was then purified using the QIAquick Gel Extraction Kit following the manufacturer's instructions. Briefly, 600µl of solubilisation buffer QC was added to the gel slice. This was incubated at 50°C for 10 minutes or until the agarose had completely dissolved. The sample was vortexed at regular intervals to aid this process. Once dissolved, 200µl of isopropanol was added. This was transferred to a QIAspin column and centrifuged at full speed in a microcentrifuge for 1 minute. Eluate was discarded. The column was then washed with 750µl of Buffer PE and the eluate discarded. The column was then centrifuged for 1 minute, eluate discarded, and

any traces of ethanol removed by a final spin for 2 minutes. The DNA was eluted in a final volume of 20µl of nuclease-free water, which was added to the centre of the column and incubated for 1 minute prior to centrifugation for 1 minute at full speed in a microcentrifuge.

2.3.9 Alkaline phosphatase treatment of linearised plasmid DNA

Shrimp Alkaline Phosphatase prevents the re-ligation of linearised plasmid DNA by catalyzing the dephosphorylation of phosphate groups from both 5' termini. SAP (1 unit/µg DNA) was incubated with gel purified restriction-digested vector at 37°C for 30 minutes in 1x SAP reaction buffer in a final volume of 20µl. SAP was inactivated by heating at 65°C for 15 minutes. The reaction mix was centrifuged in a microcentrifuge and used in subsequent ligation reactions, as detailed in section 2.3.6.

2.3.10 DNA sequencing

The University of Dundee Sequencing Service performed all DNA sequencing. For each sequencing run, 600ng DNA was provided in 30µl; primers were provided at a concentration of 3.2µM in 10µl. FIP3 sequencing primers are detailed in section 2.1.6. Sequencing was analysed using Vector NTi version 11 from Invitrogen.

2.4 Mammalian cell culture

2.4.1 Cell culture conditions

Human cervical carcinoma HeLa cells were cultured in Dulbecco's Modified Eagle Medium (D-MEM), supplemented with 10% (v/v) Foetal Calf Serum EU, 2mM Glutamine, 100Units/ml Penicillin and 100µg/ml Streptomycin. This is referred to as HeLa complete growth media.

HeLa cells stably expressing GFP-FIP3 were obtained from Rytis Prekeris, University of Colorado. These were maintained in D-MEM supplemented with 10% (v/v) Foetal Calf Serum EU, 2mM Glutamine and 100µg/ml Hygromycin B. This is referred to as GFP-FIP3 selection media.

Chinese hamster ovary (CHO) cells were cultured in Nutrient Mixture F-12 Ham, supplemented with 10% (v/v) Foetal Calf Serum EU, 2mM Glutamine and 100Units/ml Penicillin and 100µg/ml Streptomycin. This is referred to as CHO complete growth media.

Cells were grown at 37°C in 5% (v/v) CO₂. Cells were cultured in 75cm² flasks.

2.4.2 Passage of cells

Cells were passaged at approximately 70% confluency. Media was aspirated and cells rinsed with 2ml of trypsin/EDTA, which had been warmed to 37°C. This was aspirated and replaced with 3ml of trypsin/EDTA, evenly distributed over the monolayer of cells. Cells were incubated for several minutes at 37°C and gently dislodged by tapping the flask. Media was added to the cells to give the appropriate dilution. Cells were transferred to fresh flasks or culture dishes, containing the desired volume of complete growth media. For confocal microscopy, cells were plated onto 13mm diameter glass coverslips that had been immersed in 100% ethanol, air dried in the cell culture hood and then exposed to UV for a minimum of one hour.

2.4.3 Cryopreservation of cells

Cells were cultured as normal to achieve a confluent 75cm² flask 24 hours later. Cells trypsinised, as detailed in section 2.4.2, were added to 12ml of complete growth media. Cells were centrifuged at 1000 rpm for 5 minutes. Media was removed, the pellet dislodged, and the cells resuspended in 5ml complete growth media. Cells were centrifuged at 1000 rpm for 5 minutes and the media removed. Cells were resuspended in 1 ml freezing media per flask of cells. Freezing media contained Foetal Calf Serum EU supplemented with 10% (v/v) DMSO. These were transferred to 1 ml to 1.8ml polypropylene cryo-vials on ice. These were stored in 5100 Cryo 1°C Freezing Container from Nalgene, containing isoropropanol for four hours at -80°C. Cells were then transferred to a liquid nitrogen storage vat.

2.4.4 Resurrecting cells

To resurrect cells from liquid nitrogen storage, vials were rapidly thawed in a 37°C water bath. Cells were then transferred to 15ml warmed complete growth media in 75cm² flask. 24 hours later the media was changed to remove DMSO.

2.4.5 HeLa cell synchronisation

2.4.5.1 Thymidine, nocodazole block

HeLa cells were synchronised using a thymidine, nocodazole block (Harper, 2005). Cells were passaged into flasks to achieve approximately 50 to 60% confluency by the following day. In the evening of day two, thymidine was added to the cells at a concentration of 5mM. Cells were incubated for 16 hours at 37°C in 5% (v/v) CO₂. On the morning of day three, flasks were washed twice in cold sterile PBS and twice in warm media. Cells were incubated for approximately 8 hours. Cells were then incubated in 100ng/ml of nocodazole for 16 hours at 37°C in 5% (v/v) CO₂. On the morning of day four, metaphase arrested cells were harvested. Flasks were gently transported to the cell culture hood and media removed. Flasks were tapped gently on the cell culture hood bench and dislodged cells were washed off from the growth surface with sterile PBS. Cells were collected in 15ml centrifuge tubes, washed twice in sterile PBS, three times in warm media, then plated as required. In our hands, plated HeLa cells tend to divide at 45 (metaphase) and 90-110 minutes (telophase).

2.4.5.2 Thymidine, nocodazole and MG132 block

HeLa cells were synchronised using a thymidine, nocodazole and MG132 block (Petronczki *et al.*, 2007). Cells were passaged into flasks to achieve approximately 50 to 60% confluency by the following day. Cells were incubated overnight at 37°C in 5% (v/v) CO₂. Thymidine (prepared in water) was added to the cells at a concentration of 2mM for 24 hours. Cells were then washed twice in cold sterile PBS and twice in warm media. Cells were released for approximately six hours. Following this 50ng/ml nocodazole (prepared in DMSO) was added for four hours. Next, media was removed gently and replaced with media containing 10µM MG132 (prepared in DMSO) for two hours. Cells were

gently transported to the cell culture hood and media removed. Cells were tapped gently on the cell culture hood bench and dislodged cells were washed off the growth surface with sterile PBS. Cells were collected in 15ml centrifuge tubes and washed twice in warm media. Cells were plated as desired. This treatment arrested cells in metaphase and on release cells entered anaphase. At approximately 60 minutes cells entered telophase.

2.4.6 Plasmid DNA transfection

Cells were transfected with plasmid DNA, using Lipofectamine™ 2000, following the manufacturer's instructions. The following instructions detail how to transfect DNA into mammalian cells in a 24-well format. For other formats, the volumes used were scaled up or down, as directed by the manufacturer. All amounts and volumes are on a per well basis. Briefly, cells were passaged in 500µl antibiotic free growth media per well of a 24-well cell culture plate, to achieve 90-95% confluency for the following day. For cells destined for immunofluorescence, cells were passaged onto ethanol sterilised 13mm diameter glass coverslips and the confluency was lowered to 60-70%. The following day complexes were prepared as follows. Firstly, 0.8µg DNA was diluted in 50µl of Opti-MEM® I Reduced Serum Medium and mixed. Secondly, Lipofectamine™ 2000 was mixed gently before use and 2µl was diluted in 50 µl of Opti-MEM® I Medium. This was incubated for 5 minutes at room temperature. Next, the diluted DNA was combined with the diluted Lipofectamine™ 2000 (total volume of 100µl). This was mixed gently and incubated for 20 minutes at room temperature. The DNA/Lipofectamine™ 2000 complex was added to the well containing cells and 500µl of fresh antibiotic-free growth media. This was mixed gently by rocking the plate back and forth. Cells were incubated at 37°C in 5% (v/v) CO₂. The antibiotic-free growth media was changed after 4-6 hours. Cells were processed for transgene expression 24 to 72 hours post-transfection.

2.4.7 Cell lysis

For crude analysis of protein expression in cells, lysis buffer containing 0.1% (v/v) Triton X100 was used, as detailed in section 2.1.10. On day of harvest, cells were placed on ice, media was removed and cells washed three times in ice

cold PBS. All PBS was removed and 50 μ l (12 well plate), 100 μ l (6 well plate), 500 μ l (10cm plate) of cell lysis buffer was added per well. Cells were scraped off and placed in microcentrifuge tubes. Cells were then subject to ten passes through a 26G needle and allowed to rest on ice for 20 minutes, before repeating the needle homogenisation. Cells were then spun at 23,880 g in a refrigerated benchtop centrifuge. The supernatant was retained and prepared for electrophoresis in 4x SDS-PAGE sample buffer.

2.4.8 Membrane and cytosol fractionation

Cells were collected in 15 ml centrifuge tubes via centrifugation at 3273 g for 5 minutes in a refrigerated benchtop centrifuge. Cells were resuspended in 1.5 ml HPFEV buffer. Cells were passed ten times through a ball-bearing homogeniser, with a 14 μ m clearance, from Isobiotec, Germany. 75 μ l of the homogenate was retained and diluted in 4x SDS-PAGE sample buffer for analysis. Cell homogenate was then transferred to Beckman Thinwall Polyallomer 11x34mm tubes and centrifuged in a bench top ultracentrifuge at 35,000 g for 1 hour at 4°C in a Beckman TLS.55 rotor.

Cytosolic proteins in the supernatant fraction were precipitated by the addition of TCA to a final concentration of 10% (w/v). After incubation on ice for 15 minutes, the sample was centrifuged at 23,880 g in a refrigerated benchtop centrifuge for 15 minutes at 4°C. The pellet, containing cytosolic proteins, was resuspended in 80 μ l 2x SDS-PAGE sample buffer. 5 μ l saturated Tris solution was added.

The cell pellet from the first spin, containing cell membranes, was washed by resuspending in 2 ml of HES buffer and centrifuged in a bench top ultracentrifuge at 35,000 g for 1 hour 4°C. For the purposes of SDS-PAGE, membrane bound proteins were released from the membrane fraction. Membrane proteins within the pellet were resuspended in 1ml of HES buffer, containing 1% Triton X100, using a 26G needle. This was left on ice for 10 minutes and centrifuged in a bench top ultracentrifuge at 214,200 g for 1 hour. The supernatant was removed and solubilised membrane proteins were precipitated using TCA, as before. The pellet, containing membrane proteins,

was resuspended in 80µl 2x SDS-PAGE sample buffer. 5µl saturated Tris solution was added.

Cytosolic and membrane fractions were analysed for proteins of interest using immunoblotting. Syntaxin 6 and GAPDH were used as markers for membrane and cytosol fractions, respectively.

2.4.9 Density gradient fractionation

Recombinant baculovirus Sf9 cell expressed FIP3 was incubated with either HeLa membranes or protein-free liposomes. These membranes (or vesicles) were then floated up through an Optiprep gradient. Fractions were collected and the distribution of proteins within the gradients was assayed by immunoblotting.

HeLa membranes were prepared by homogenising HeLa cells in HES buffer via ten passes through a ball-bearing homogeniser with a 14µm clearance, from Isobiotec, Germany. The homogenate was centrifuged in a refrigerated benchtop centrifuge at 3000 g to pellet nuclei and heavy debris. The supernatant was transferred to Beckman Ultra-Clear 13x51mm tubes in a Beckman TLA 100.3 rotor. Membranes were collected by sedimentation using a benchtop ultracentrifuge at 100,000 g for 60 minutes. Membrane pellets were re-suspended in HES buffer to approximately 2mg/ml.

Protein-free liposomes were first prepared (Brandie *et al.*, 2008). In brief, lipid stocks were prepared in chloroform and stored at -80°C under nitrogen. A 15mM lipid stock was prepared in chloroform containing 85 mol% Palmitoyl oleoyl phosphatidyl choline (POPC) and 15 mol% dioleoylphosphatidylserine (DOPS). 100µl of 15mM lipid stock was placed at the bottom of a 12x75 mm glass test tube. The chloroform was then evaporated using a stream of nitrogen for 15 minutes in a fume hood. To ensure that the lipid films were completely dry the samples were then dried for 30 minutes under vacuum. The lipid film was then resuspended, in A200 buffer containing 1% (w/v) octyl glucoside, by vortexing for 15 minutes. After the lipid film was completely resuspended, the detergent was diluted below its critical micellar concentration via the addition of 1 ml of Buffer A200 containing 1mM DTT, drop-wise, while the sample was continuously vortexed. To remove any remaining detergent, the samples were placed into

pre-equilibrated 3ml Float-a-Lyzers with a molecular weight cut off of 10,000 and dialysed against 4 L of Buffer A200, containing 1mM DTT and 4g of Bio-Beads, with stirring at 4°C overnight. Samples were recovered the following day and placed at the bottom of an SW60 tube on ice for subsequent separation using gradient centrifugation. Liposomes were recovered by floatation on a Nycodenz (Histodenz™) gradient. An equal volume of 80% (v/v) Nycodenz in buffer A200 containing 1mM DTT was mixed with the recovered dialysate to produce a 40% (v/v) Nycodenz mixture. This was overlaid with 1.5ml of 30% (v/v) Nycodenz in buffer A200 containing 1mM DTT. This layer was then overlaid with 250µl of glycerol-free A200 and centrifuged at 65,000 g for 4 hours at 4°C. Liposomes were recovered by removal of 400µl from the top of the gradient, snap frozen and stored at -80°C.

30µl of HeLa membranes were mixed with or without 10µM recombinant FIP3 in HES buffer and incubated on ice for 90 minutes with occasional mixing. In parallel, 30µl of protein-free liposomes were also incubated with 10µM recombinant FIP3 in HES buffer on ice for 90 minutes. After this incubation, samples were mixed with OptiPrep® Density Gradient Medium such that the final concentration was 40% (v/v), and overlaid with 1ml of 20% (v/v) and 1ml of 5% (v/v) OptiPrep® Density Gradient Medium. These were prepared in Beckman Ultra-Clear 13x51mm tubes. These were centrifuged in a bench top ultracentrifuge, using a Beckman TLA 100.3 rotor at 85,000 g for 4 hours at 4°C. Under these conditions, membranes and liposomes float to the top of the gradient, whereas soluble proteins remain in the dense, lower layer. Samples were collected by tube puncture and subjected to TCA precipitation. TCA was added to a final concentration of 10% (w/v), the samples vortexed and incubated on ice for 20 min. After this, samples were centrifuged at 23,880 g in a refrigerated bench top centrifuge for ten minutes. The supernatant was discarded and the protein precipitate re-suspended in 4x SDS-PAGE sample buffer containing 20mM DTT and 1M Urea. Thereafter the distribution of proteins within the gradients was assayed by immunoblotting.

2.5 Immunofluorescence

2.5.1 Immunofluorescence

Cells were passaged in 12-well plates containing ethanol sterilised 13 mm diameter glass coverslips. Cells were grown on coverslips for 24 hours prior to processing. The exposure of coverslips to light was minimised throughout the procedure to help prevent photo-bleaching. Media was aspirated and cells washed gently three times in room temperature PBS. Cells were fixed with 1 ml 4% (w/v) ρ -formaldehyde per well and incubated at room temperature for 20 minutes. Coverslips were washed three times with PBS and then incubated in 1 ml of 30mM NH_4Cl for 10 minutes. Coverslips were washed three times with PBS.

If all that was required was to verify the presence of a GFP-FIP3 plasmid, coverslips were mounted onto glass slides using a drop of Immunomount and stored overnight in the dark to dry.

For immunofluorescence, following the PBS washes, 0.1% (v/v) Triton (in PBS) was added to permeabilise the cells for 4 minutes. Cells were washed three times in PBS. Cells were then left to block in immunofluorescence (IF) buffer, which was prepared freshly on the day and filtered through a Nalgene 0.2 μm vacuum filter. Primary antibody was diluted to the appropriate concentration in IF buffer. 100 μl of primary antibody was then applied to a sheet of nescofilm and the coverslip placed cell-side down onto the antibody. After 1 hour incubation at room temperature, the cells were washed again three times in IF buffer. Alexa Fluor® Dyes were used to fluorescently label the primary antibodies. Alexa Fluor® 568 goat anti-rat IgG (H + L) emits fluorescence in the red-orange part of the spectra. The secondary antibodies were diluted in IF buffer at 1:400. 100 μl secondary antibody solution was applied to each coverslip as before and incubated for 1 hour in the dark. The coverslips were again washed three times in IF buffer. For nuclear staining, DAPI (4',6-Diamidino-2-phenylindole, dilactate) was diluted in IF buffer to a final concentration of 1 $\mu\text{g}/\text{ml}$. 1ml of the DAPI solution was added to each well and incubated for 5 minutes in the dark, before a final three washes with IF buffer. Coverslips were

then mounted onto glass slides using a drop of Immunomount and stored overnight in the dark to dry.

2.5.2 Confocal microscopy

Mounted coverslips were analysed using a 63X Zeiss oil immersion objective, on a Zeiss confocal microscope (Carl Zeiss, Germany) equipped with a Zeiss LSM5 Pascal instrument. An argon laser was used to excite 488nm Alexa Fluor® Dyes and GFP fusion proteins. Helium neon lasers were used to excite 568nm Alexa Fluor® Dyes. Zeiss Pascal software was used to collect images, which were saved as .mdb files.

2.6 In vitro phosphorylation assays

Recombinant Aurora A, Aurora B and cyclin B-CDK1 were purchased from Upstate; Plk1 was purchased from Invitrogen. FIP3 was expressed and purified by the University of York Biocentre using the baculovirus Sf9 insect cell system. The construct used to express this protein was made by a previous student of the Gould lab and has a tag of six histidine residues at the C-terminus.

Reactions were set up in screw capped microcentrifuge tubes, as follows. Firstly, 50ng kinase was added to appropriate tubes, followed by kinase assay buffer (containing 50µM ATP.Mg²⁺) to produce a final volume of 50µl. Then 2µg or 5µg recombinant FIP3 was added to appropriate tubes. 2µg myelin basic protein (MBP) was used as a positive control for kinase activity. To start the reaction, 6µCi adenosine 5'-triphosphate [γ -³²P] (ATP- γ -³²P) was added to each tube and reactions were incubated in a water bath at 30°C for 30 minutes. 20µl of 4x SDS-PAGE sample buffer (with 80mM DTT) was added to each tube to stop the reaction. Samples were separated by SDS-PAGE, as detailed in section 2.2.2, using an 8% gel for FIP3 samples and a 15% gel for MBP samples. Gels were stained with Coomassie blue stain (as detailed in section 2.2.6). Gels were dried using cellophane and exposed to Kodak X-ray film in a cassette with no intensifying screen at room temperature for 24 to 96 hours.

2.7 Proteomics

2.7.1 Phosphorylation site mapping of Rab11-FIP3

Phosphorylation site mapping of kinase phosphorylated FIP3 was carried out commercially by the FingerPrints Proteomic Facility at the University of Dundee.

A summary of the sample preparation process and techniques used to map the sites of phosphorylation are provided below. Importantly, measures were taken to minimise dust contamination (specifically, keratin). All gel manipulation was carried out in a laminar flow cabinet; buffers were filtered; ultrapure SDS-PAGE reagents were purchased from Invitrogen.

In vitro phosphorylation assays were performed on recombinant FIP3 using the kinases Aurora A, cyclin B-CDK1 and Plk1. FIP3 which had not been kinase - phosphorylated was included as a control. The ability of the recombinant FIP3 sample to autophosphorylate was abolished by heat treatment of FIP3 at 60°C for 30 minutes. For more details, refer to section 3.3.4 where this is discussed fully. *In vitro* phosphorylation assays were performed, as detailed in section 2.6, with some modifications to ensure a band corresponding to FIP3 was present at good intensity by colloidal Coomassie staining. Reactions were set up in screw capped microcentrifuge tubes, as follows. Firstly, 200ng recombinant kinase was added to appropriate tubes, followed by kinase assay buffer (supplemented with 100µM ATP.Mg²⁺) to produce a final volume of 100µl. Next, 50µg recombinant heat treated FIP3 was added. This was incubated at 30°C for 60 minutes. Protein was TCA precipitated, on ice for 15 minutes. This was centrifuged at 23,880 g in a refrigerated benchtop centrifuge for 15 minutes at 4°C.

Samples were separated via SDS-PAGE using NuPAGE® reagents from Invitrogen, following the manufacturer's instructions. TCA precipitated protein pellets were resuspended in 20µl NuPAGE® SDS Sample Buffer, with NuPAGE® Sample Reducing Agent (10x). 5µl saturated-Tris solution was added. Samples were separated using NuPAGE® NOVEX 10% Bis-Tris, with NuPAGE® MOPS SDS Running Buffer (20x) containing NuPAGE® Antioxidant. The gel was removed from the plastic casing and stained with colloidal Coomassie, as detailed in section 2.2.7,

following the manufacturer's instructions. Following destaining, bands according to FIP3 were excised, placed in sterile microcentrifuge tubes and shipped on dry ice to the FingerPrints Proteomics Facility at the University of Dundee.

This service uses a technique known as parent ion scanning (also known as Parents of -79) to detect phosphorylated peptides (Loyet *et al.*, 2005;Paradela and Albar, 2008), in conjunction with the generation of tandem MS data to identify the protein(s) in the solution (www.matrixscience.com) (Perkins *et al.*, 1999). Together these are used to determine the sites of phosphorylation in the protein.

2.7.2 Proteomic analysis of recombinant Rab11-FIP3

The FIP3 sample used in this thesis was expressed and purified by the University of York Biocentre using the baculovirus Sf9 insect cell system and has a tag of six histidine residues at the C-terminus. Via an *in vitro* phosphorylation assay discussed in section 3.3.4, the FIP3 sample was shown to possess kinase activity. To identify any potential kinases contaminating the purified FIP3 sample, a proteomic approach was used. Two attempts were made at this. Firstly using the Sir Henry Wellcome Functional Genomics Facility (SHWFGF) at the University of Glasgow and secondly using Aberdeen Proteomics at the University of Aberdeen. Sample preparation for the two proteomic facilities are described below.

Measures were taken to minimise dust contamination (specifically, keratin). All gel manipulation was carried out in a laminar flow cabinet; buffers were filtered; SDS-PAGE NuPAGE® reagents were purchased from Invitrogen.

Two different sample preparations were analysed by the SHWFGF at the University of Glasgow. Firstly, 15µg of the recombinant FIP3 solution was analysed by the facility to identify proteins in the sample solution. This was achieved using nanoflow HPLC Electrospray Tandem Mass Spectrometry (nLC-ESI-MS/MS), searching *Mammalia* and *Drosophila* databases (Bridges *et al.*, 2008).

Concern was raised over the overexpressed FIP3 protein masking the presence of less well expressed kinases. To that end the FIP3 sample was separated by SDS-PAGE and gel slices were analysed individually, allowing proteins to be analysed

in the absence of FIP3. The FIP3 sample was separated using SDS-PAGE, using NuPAGE® reagents from Invitrogen, following the manufacturer's instructions. In brief, 5µg FIP3 was made up in NuPAGE® SDS Sample Buffer, with NuPAGE® Sample Reducing Agent (10x). Samples were separated using NuPAGE® NOVEX 10% Bis-Tris, with NuPAGE® MOPS SDS Running Buffer (20x) containing NuPAGE® Antioxidant. The gel was removed from the plastic casing and stained with colloidal Coomassie, as detailed in section 2.2.7. The FIP3 lane was cut into 5 slices which were placed in sterile Eppendorfs and analysed using nLC-ESI-MS/MS searching *Mammalia* and *Drosophila* databases. Data was exported to the Mascot (Matrix Science) search engine for protein identification (www.matrixscience.com) (Perkins *et al.*, 1999). Only proteins with a probability based MASCOT score greater than the cut off score that indicates homology or identity, were included in the list of proteins.

In a further attempt to identify contaminating kinases, 5µg FIP3 was separated by SDS-PAGE, as described above, and cut into 16 gel slices which were analysed by Aberdeen Proteomics at the University of Aberdeen. Protein identification of gel bands was achieved by LC-MS/MS searching Human and *Spodoptera Frugiperda* databases.

2.8 Phospho-specific antibody production

2.8.1 Phospho-specific antibody generation

We sought to produce a panel of antibodies generated against phosphorylated serines 102, 281, 348 and 451 of FIP3. Phospho-peptides, according to the four sites, were synthesised by Quality Controlled Biochemicals, Hopkinton, Mass, USA. Both phospho-specific and non-phosphorylated peptides were generated, the amino acid sequences of which are listed in section 2.1.7. The phospho-specific peptides were immunised in rabbits by The Scottish Blood Transfusion Service. Whole serum was obtained.

2.8.2 Phospho-specific antibody purification

The IgG fraction for each antibody was affinity purified from whole serum, against a protein A sepharose column. The purification of the antibodies was carried out by Mrs M.C. Millar.

To prepare the column, 4ml of protein A sepharose slurry was re-suspended in PBS, applied to a 2ml column and washed three times with 10ml of PBS. Prior to use, the column was washed with 30ml PBS. A vial of serum was thawed and 10X PBS was added to bring the concentration to 1x. 5ml of the serum was applied to the column. The flow through was collected and re-applied. This was repeated so that the serum had passed through the column three times. Following this, the column was washed with 30-40ml PBS. 20ml 0.05M sodium acetate, pH 3.0 was then applied to the column. 1ml fractions were collected and 25 μ l saturated Tris solution added to each. The column was stripped by applying 20ml 1M sodium acetate, pH 2.5. The column was then re-equilibrated in PBS with sodium azide and stored at 4°C for re-use. The protein concentration of each fraction was calculated by measuring the optical density at 280nm (OD₂₈₀). Fractions spanning the peak protein concentration were pooled and dialysed against PBS. Following dialysis, the protein concentration was determined and the purified phospho-specific antibodies stored at -80°C.

2.8.3 Peptide competition assay (PCA)

To validate the specificity of a phospho-specific antibody, we performed a peptide competition assay (PCA). The protocol used was obtained from Rockland Immunochemicals, a brief outline of which is provided. This procedure describes a PCA using phosphorylated and non-phosphorylated peptides.

We first separated various FIP3 samples by SDS-PAGE, as described in section 2.2.2. These were 200ng baculovirus sf9 insect cell expressed FIP3; 1 μ g CDK1 phosphorylated heat-treated FIP3 (prepared according to section 2.6); HeLa lysate stably expressing GFP-FIP3; mitotic HeLa lysate. FIP3 proteins were transferred onto nitrocellulose, as described in section 2.2.3, and blocked in PBS-T containing 5% (w/v) dried non-fat milk overnight. This was done in triplicate to produce three identical test samples for analysis by PCA.

Affinity purified phospho-specific primary antibodies, described in section 2.8.2, were diluted to 1:500 in PBS-T containing 1% (w/v) dried non-fat milk. For each blot a 3ml solution of primary antibody was prepared, thus 9ml was prepared in total.

Lyophilised peptides (both the phosphorylated and non-phosphorylated forms of the immunising peptide) were reconstituted to a concentration of 100 μ M using nuclease-free water, at room temperature. The peptides were allowed to dissolve at room temperature, and then gently triturated several times using a pipette. The introduction of air bubbles was avoided.

Three test samples were labelled as follows. Sample A: water only (no peptide control); sample B: phosphorylated peptide; sample C: non-phosphorylated peptide. Next, peptide stock solutions of 2.66 μ M and water control were prepared by pipetting the following. Sample A, the no peptide control, contained 973 μ l PBS-T containing 1% (w/v) dried non-fat milk plus 27 μ l water. Sample B, the phosphorylated peptide incubation, contained 973 μ l PBS-T containing 1% (w/v) dried non-fat milk plus 27 μ l reconstituted (100 μ M) phosphorylated peptide. Sample C, the non-phosphorylated peptide incubation, contained 973 μ l PBS-T containing 1% (w/v) dried non-fat milk plus 27 μ l reconstituted (100 μ M) non-phosphorylated peptide.

3ml of the phospho-specific antibody was added into each of the samples marked A, B or C. The tubes were incubated for 2 hours at room temperature with gentle rocking. Samples were centrifuged at 3273 g in a refrigerated benchtop centrifuge for 15 minutes at 4°C to pellet any immune complexes. The supernatant was removed and the pellet discarded. The pre-incubated antibody was added to one of the three identical nitrocellulose membranes for immunoblotting. These were incubated overnight at 4°C. These were processed for immunodetection using an Amersham ECL Rabbit IgG, HRP-Linked Whole Ab, as described in section 2.2.4. The signals obtained with antibody incubated with sample A (water only, no peptide control) represent the maximum signal. Signals obtained with sample B (phosphorylated peptide) and sample C (non-phosphorylated peptide) are compared to the signal from sample A to determine if the peptide(s) compete for FIP3 binding.

3 *In vitro* phosphorylation of Rab11-FIP3

3.1 Introduction

Rab11-FIP3 (FIP3) undergoes spatial and temporal regulation during mitosis (Wilson *et al.*, 2005). During metaphase and early anaphase FIP3 is largely cytosolic with some localised to endosomal membrane structures. During late anaphase, following furrow initiation, FIP3 localises to the centrosome. At late cytokinesis, FIP3 relocates to the cleavage furrow and midbody. On separation of the daughter cells, FIP3 returns to the centrosome. This is shown in figure 1.4 (section 1.5.4) of the introduction.

A potential candidate for the spatial and temporal regulation of FIP3 is phosphorylation, since reversible phosphorylation is a commonly used control mechanism in mitotic regulation and can regulate the activity, localisation and half-life of a protein, as well as its and interaction with other proteins (Cohen, 2000).

Several lines of evidence suggest that FIP3 is a potential phospho-protein. Firstly, Nuclear fallout (Nuf), a *D. melanogaster* protein identified as a homologue of FIP3 (Riggs *et al.*, 2003; Hickson *et al.*, 2003), is a highly phosphorylated protein (Rothwell *et al.*, 1998). Interestingly, Nuf localisation alters during the cell-cycle (Rothwell *et al.*, 1998; Riggs *et al.*, 2003). During early *D. melanogaster* development, the embryo undergoes thirteen rapid nuclear divisions, which occur without cytokinesis. During this development, Nuf is concentrated at the centrosomes during prophase, but is predominantly cytoplasmic through the rest of the nuclear cycle. During nuclear cycle 14, the embryo undergoes cellularisation (the equivalent of mammalian cytokinesis). Nuf is centrosomal throughout cellularisation (Rothwell *et al.*, 1998). Since Nuf is highly phosphorylated, it has been suggested that its localisation may be regulated by cell-cycle dependent kinases (Riggs *et al.*, 2003).

In addition, work from a collaborating lab proposes that FIP3 phosphorylation and dephosphorylation may be a regulator of FIP3 localisation (R. Prekeris, personal communication). Figure 3.1 illustrates mass spectrometry data from

this lab. Briefly, lysates from synchronised cells at metaphase were separated by 2D gel electrophoresis and probed for FIP3, as detailed in figure 3.1A. Four forms of FIP3 are observed (top panel); on phosphatase treatment three of these disappear (bottom panel). This suggests that FIP3 is a phospho-protein, which can exist in different, reversible phosphorylation states. FIP3 was immunoprecipitated from metaphase cells and subject to proteomic analysis to identify the phosphorylation sites. The experiment was repeated three times and the sites found in all three repeats are serines 102, 281, 348 and 451, as shown in figure 3.1B.

3.2 Aims

This work aims to understand the mechanism of controlling FIP3 localisation during cytokinesis. It is considered likely that phosphorylation or dephosphorylation of FIP3 may be involved in the regulation of FIP3 localisation to the centrosome and midbody during cytokinesis. In order to prevent aberrant cell division, the cell-cycle is tightly regulated via a network of kinases, which phosphorylate a vast number of protein substrates (Morgan, 2007). A variety of mitotic kinases are active during the cell-cycle, including Aurora A, Aurora B, Plk1 and CDK1. This work aims to determine whether candidate cell-cycle kinases can phosphorylate FIP3 *in vitro*.

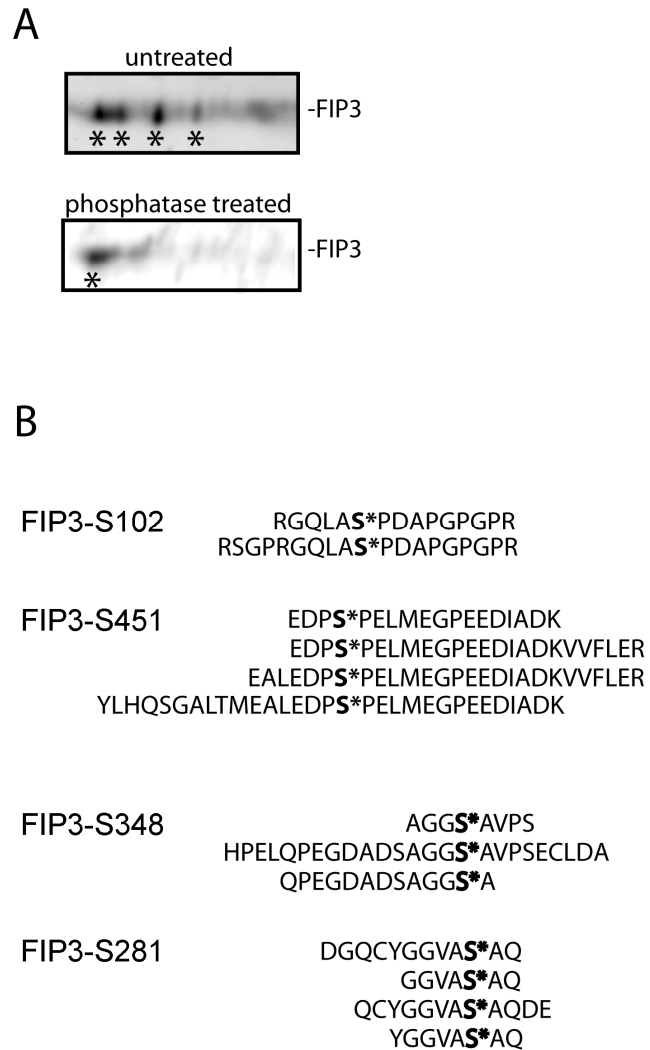


Figure 3-1 Identification of FIP3 phosphosites from metaphase HeLa lysates (R. Prekeris, personal communication)

HeLa cells were synchronised and arrested in metaphase using a thymidine-nocodazole block. (A) Lysates from synchronised cells at metaphase were separated by 2D gel electrophoresis and probed for FIP3. Four forms of FIP3 are observed (top panel); on phosphatase treatment, three of these disappear (bottom panel). This suggests that FIP3 can exist in different, reversible phosphorylation states. (B) FIP3 was immunoprecipitated from metaphase cells and subject to proteomic analysis to identify the phosphorylation sites. The experiment was repeated three times and the sites found in all three repeats are shown. These results suggest that FIP3 can be phosphorylated at serines 102, 281, 348 and 451.

3.3 Results

3.3.1 *Generic (non kinase specific) phosphorylation predictions*

Firstly, we sought to map potential phosphorylation sites in the sequence of human Rab11-FIP3. This was achieved using the NetPhos 2.0 server (Technical University of Denmark) which uses an artificial neural network (ANN) method to predict serine, threonine and tyrosine phosphorylation sites in eukaryotic protein sequences (Blom *et al.*, 1999). The prediction server is available at <http://www.cbs.dtu.dk/services/NetPhos/>.

For Rab11-FIP3, 42 serine residues, 7 threonine residues and 4 tyrosine residues were predicted to be potentially phosphorylated. Table 3.1 details the output from NetPhos for serine residues. The output score is provided as a value in the range 0.000 - 1.000, with a threshold of 0.500. Below this threshold the residue is predicted not to be phosphorylated; scores above the threshold of 0.500 are predicted to be potential phosphosites. In general, the higher the score, the higher the confidence of the prediction and the higher the similarity to one or more of the phosphorylation sites used in development of the NetPhos 2.0 method. From the 42 serine residues predicted to be phosphorylated, three of these were mapped by the Prekeris lab. Serines 102, 281 and 451 have scores of 0.522, 0.814 and 0.983, respectively. Serine 348 was not identified as a phosphosite, with a score just short of the threshold of 0.428.

Pos	Context	Score	Pred
3	--MA <u>S</u> APPA	0.002	.
8	APPA <u>S</u> PPGS	0.982	*S*
12	SPPG <u>S</u> EPPG	0.768	*S*
52	PDQ <u>S</u> PGLD	0.908	*S*
71	GARW <u>S</u> AGPA	0.750	*S*
88	DPG <u>S</u> APPP	0.654	*S*
94	PPR <u>S</u> GRPG	0.593	*S*
102	GQLA <u>S</u> PDAP	0.522	*S*
112	PGPR <u>S</u> EAPL	0.415	.
124	DPL <u>S</u> WTEE	0.967	*S*
136	CGPA <u>S</u> CPES	0.699	*S*
140	SCPE <u>S</u> APFR	0.028	.
148	RLQ <u>S</u> SSSH	0.823	*S*
149	LQ <u>S</u> SSSHR	0.142	.
150	QG <u>S</u> SSSHRA	0.961	*S*
151	G <u>S</u> SSSHRAR	0.555	*S*
162	VDV <u>S</u> PFPA	0.798	*S*
180	QGP <u>S</u> PPQP	0.927	*S*
185	PPQ <u>S</u> DLSQ	0.222	.
188	PSD <u>S</u> QTHP	0.279	.
195	HPL <u>S</u> EPVG	0.337	.
200	EPV <u>S</u> QEDG	0.997	*S*
249	YLD <u>S</u> PGLGV	0.041	.
255	LGVI <u>S</u> FEDF	0.981	*S*
281	GGVA <u>S</u> AQDE	0.814	*S*
308	EVTD <u>S</u> AYMG	0.506	*S*
313	AYMG <u>S</u> ESTY	0.005	.
315	MGSE <u>S</u> TYSE	0.824	*S*
318	ESTY <u>S</u> ECET	0.995	*S*
329	DEDT <u>S</u> TLVH	0.940	*S*
344	GDAD <u>S</u> AGGS	0.740	*S*
348	SAGG <u>S</u> AVPS	0.428	.

Pos	Context	Score	Pred
352	SAVP <u>S</u> ECLD	0.117	.
379	PHGQ <u>S</u> VITV	0.004	.
397	YGEG <u>S</u> EAEL	0.842	*S*
402	EAEL <u>S</u> PETL	0.987	*S*
414	QLGC <u>S</u> DPAF	0.011	.
422	FLTP <u>S</u> PTKR	0.073	.
428	TKRL <u>S</u> SKKV	0.996	*S*
429	KRL <u>S</u> SKKVA	0.998	*S*
439	YLHQ <u>S</u> GALT	0.018	.
451	LED <u>S</u> PPELM	0.983	*S*
488	GEQH <u>S</u> RRLQ	0.987	*S*
538	EREK <u>S</u> IEIE	0.979	*S*
556	DEEN <u>S</u> ELRS	0.368	.
560	SELR <u>S</u> CTPC	0.011	.
585	DEIE <u>S</u> LTLR	0.004	.
591	TLRL <u>S</u> EEQE	0.976	*S*
605	GDRL <u>S</u> SHERH	0.997	*S*
646	RRGR <u>S</u> SSMG	0.971	*S*
647	RGR <u>S</u> SSMGL	0.985	*S*
648	GR <u>S</u> SSMGLQ	0.990	*S*
656	QEYH <u>S</u> RARE	0.834	*S*
661	RARE <u>S</u> ELEQ	0.997	*S*
692	IITL <u>S</u> IQGA	0.016	.
698	QGA <u>S</u> LFST	0.960	*S*
701	KSLF <u>S</u> TAFS	0.729	*S*
705	STAF <u>S</u> ESLA	0.625	*S*
707	AFSE <u>S</u> LAAE	0.140	.
713	AAEI <u>S</u> SVSR	0.009	.
714	AEI <u>S</u> SVSRD	0.898	*S*
716	ISSV <u>S</u> RDEL	0.972	*S*
751	ETNP <u>S</u> ILEV	0.639	*S*

Table 3.1 Generic (non kinase specific) phosphorylation predictions for serine residues of human Rab11-FIP3.

Potential phosphorylation sites of human Rab11-FIP3 were mapped using the NetPhos 2.0 server (Technical University of Denmark). Overall for Rab11-FIP3, 42 serine residues were predicted to be potentially phosphorylated. Column 1 details the position of the residue being analysed (pos); column 2 provides the sequence context shown as a 9-residue sequence centred on the residue being analysed (context); column 3 gives the output score as a value in the range 0.000-1.000 (score); column 4 details the assignment (pred). Prediction scores above the threshold of 0.500 are potential phosphosites and are assigned as '*S*'. If the residue is predicted not to be phosphorylated then the position is marked by a dot (.). Serine residues shown to be phosphorylated by Prekeris *et al.*, are highlighted in red.

3.3.2 Kinase specific phosphorylation predictions

Next we sought to map the kinase specific phosphorylation sites of human Rab11-FIP3. A range of prediction programmes are available (Amanchy *et al.*, 2007). We chose to use the NetPhosK 1.0 server (Technical University of Denmark), available at <http://www.cbs.dtu.dk/services/NetPhosK/>. This server uses an ANN method to predict kinase specific protein phosphorylation sites in eukaryotic protein sequences, based on a data set of known phosphorylation sites (Blom *et al.*, 2004). To date, NetPhosK covers the following kinases: protein kinase A (cyclic-AMP dependent protein kinase, PKA), protein kinase C (PKC), protein kinase G (cyclic-GMP dependent protein kinase, PKG), casein kinase-II (CK2), cdc2 (cell division cycle 2 kinase, CDK1), Ca²⁺/calmodulin-dependent protein kinase-II (CaM-II), ataxia-telangiectasia mutated kinase (ATM), DNA-dependent protein kinase (DNA-PK), CDK5, p38 mitogen-activated protein kinase (p38 MAPK), glycogen synthase kinase 3 (GSK-3), casein kinase-I (CK-I), protein kinase B (PKB), p90 ribosomal S6 kinase (RSK), insulin receptor (INSR), epidermal growth factor receptor (EGFR) and Src. As for the generic phosphorylation predictions in section 3.3.1, scores are produced that range from 0.000-1.000. Above the threshold of 0.500, phosphorylation by the specific kinase is likely.

Many potential kinase specific phosphorylation sites were identified, but the focus was directed to those sites mapped by the Prekeris lab. For serine 102, p38 MAPK was found to be a potential kinase, with a score of 0.57. This site is also potentially phosphorylated by CDK5, with a score of 0.55. CDK5 is a member of the CDK family (Malumbres and Barbacid, 2009). Although CDK5 is ubiquitously expressed, neuronal cells demonstrate maximum expression and activity of this

kinase (Dhariwala and Rajadhyaksha, 2008), where it regulates pathways unrelated to the cell-cycle. CDK5 phosphorylates serine and threonine residues that have a proline residue at position +1 (Dhariwala and Rajadhyaksha, 2008). This consensus phosphorylation site is common to all CDKs as they are proline directed kinases (Shetty *et al.*, 1993; Brown *et al.*, 1999; Ubersax and Ferrell Jr, 2007). Perhaps other CDK family members could phosphorylate this site, including CDK1. For serine 281, CKII was identified as a potential kinase, with a score of 0.51. There was no potential kinase for serine 348, as expected, since this residue was not predicted to be a phospho-site in section 3.3.1. For serine 451, ATM produced a score of 0.55 and GSK3 a score of 0.50. The highest score produced was 0.89 for PKC at position 429.

3.3.3 In vitro phosphorylation of FIP3 by mitotic kinases

To address the question of whether FIP3 is a direct substrate of the mitotic kinases, *in vitro* phosphorylation assays were performed, using baculovirus Sf9 insect cell expressed FIP3 and a selection of mitotic kinases. We hypothesise that dephosphorylation of FIP3 is occurring in the later stages of mitosis, so kinases which show activity in the earlier stages of mitosis were selected. Aurora A, Aurora B, CDK1 (in complex with cyclin B) and Plk1 were selected as a starting point.

In vitro phosphorylation assays were performed, as detailed in section 2.6. Briefly, 50ng kinase was incubated with 2µg or 5µg recombinant FIP3 at 30°C for 30 minutes, in the presence of 6µCi ATP-γ-³²P. 2µg myelin basic protein (MBP) was used as a positive control for kinase activity. Further kinase only or substrate only controls were included. Samples were separated by SDS-PAGE and autoradiography was performed.

Figure 3.2 presents the autoradiographs for each kinase. As a control for kinase activity, myelin basic protein (MBP) was incubated with ATP-γ-³²P, in the presence and absence of kinase. Figures 3.2E-H show that MBP was phosphorylated in the presence of Aurora A, Aurora B, cyclin B-CDK1 and Plk1, thus confirming that all kinases were active. Autoradiographs 3.2A-D show that in the absence of kinase, FIP3 becomes phosphorylated, suggesting the presence of a contaminating kinase in the baculovirus Sf9 insect cell expressed FIP3

sample. FIP3 phosphorylation increases on addition of kinases Aurora A (Figure 3.2A), Aurora B (Figure 3.2B), cyclin B-CDK1 (Figure 3.2C) and Plk1 (Figure 3.2D). This work suggests that, *in vitro*, FIP3 is potentially phosphorylated by various mitotic kinases.

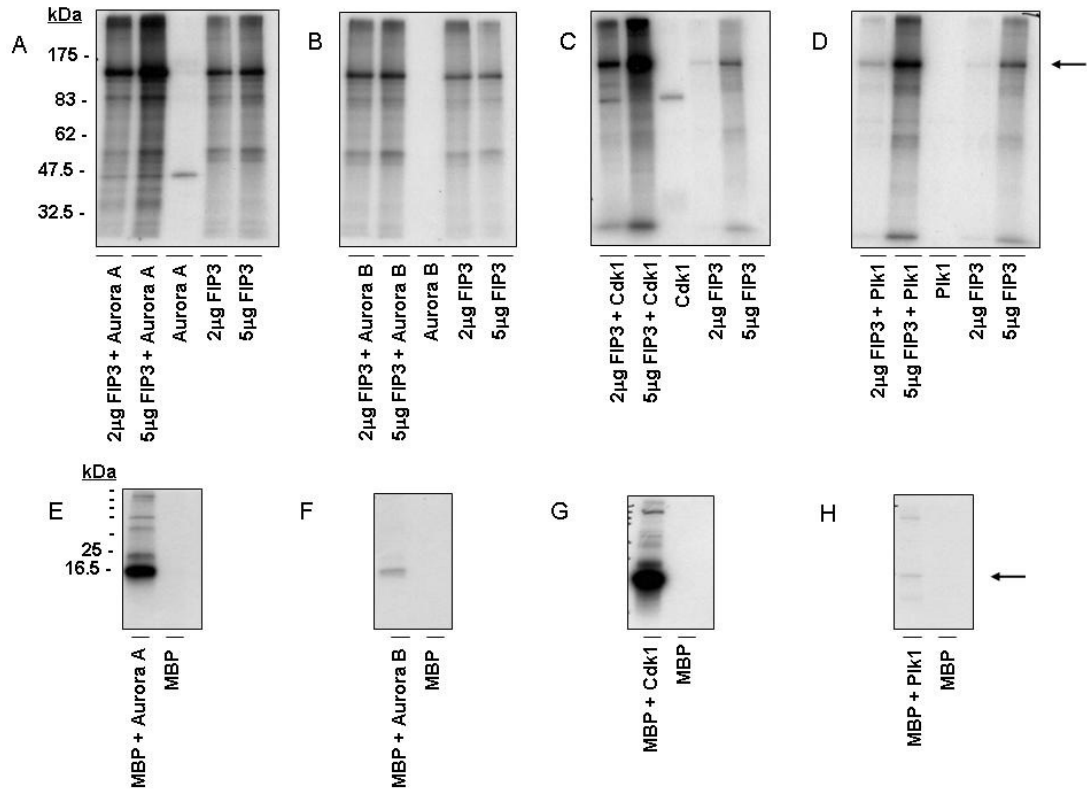


Figure 3-2 *In vitro* phosphorylation of FIP3 by mitotic kinases

In vitro phosphorylation assays were performed as detailed in section 2.6. Briefly, 50ng kinase was incubated with 2μg or 5μg recombinant FIP3 at 30°C for 30 minutes, in the presence of 6μCi ATP-γ-³²P (top panel). Figure legends are as follows: Lane 1, 2μg recombinant FIP3 incubated with kinase; Lane 2, 5μg recombinant FIP3 incubated with kinase; Lane 3, kinase only; Lane 4, 2μg recombinant FIP3 only; Lane 5, 5μg recombinant FIP3 only. The position of the Broad Range Prestained Protein Marker is illustrated. 2μg myelin basic protein (MBP) was used as a positive control for kinase activity (bottom panel). Figure legends are as follows: Lane 1, 2μg MBP incubated with kinase; Lane 2, 2μg MBP only. The position of the Broad Range Prestained Protein Marker is illustrated, with markers 175, 83, 62, 47.5 and 32.5 omitted due to space constraints. Samples were separated by SDS-PAGE as detailed in section 2.2.2 and autoradiography was performed. The positions of FIP3 and MBP on the autoradiographs are marked by arrows. Autoradiographs show that in the absence of kinase, FIP3 becomes phosphorylated. FIP3 phosphorylation increases on addition of kinases Aurora A (A), Aurora B (B), cyclin B-CDK1 (C) and Plk1 (D). Figures 3.2E-F show that all kinases are active since they phosphorylate MBP. Representative autoradiographs from an experiment performed in duplicate are presented.

3.3.4 Analysis of recombinant FIP3's capacity to autophosphorylate

Results from the *in vitro* phosphorylation assays performed in section 3.3.3 show that in the absence of kinase, FIP3 is phosphorylated in the presence of ATP- γ - ^{32}P . This suggests that either FIP3 is capable of autophosphorylation or that there may be a contaminating kinase in the sample. Since FIP3 is not a kinase, the latter was investigated.

An *in vitro* phosphorylation assay was performed, as detailed in section 2.6, using MBP as the substrate and FIP3 as the 'kinase'. 2 μg MBP was incubated for 30 minutes at 30°C in the presence of 2 μg FIP3 and 6 μCi ATP- γ - ^{32}P . Samples were separated by SDS-PAGE and autoradiography was performed. Interestingly, the Baculovirus Sf9 insect cell expressed human FIP3 sample is capable of phosphorylating MBP, as shown in figure 3.3A.

To study whether FIP3 can be phosphorylated by mitotic kinases, the autophosphorylating capacity of the FIP3 sample must first be removed. This was achieved through the incubation of FIP3 for 30 minutes at 60 or 80°C. Following this treatment, the FIP3 sample was tested in an *in vitro* phosphorylation assay. 2 μg FIP3 was incubated for 30 minutes at 60 or 80°C and then subject to an *in vitro* phosphorylation assay for 30 minutes at 30°C in the presence of 6 μCi ATP- γ - ^{32}P . Samples were separated by SDS-PAGE and autoradiography was performed. Figure 3.3B shows that the capacity of the FIP3 sample to autophosphorylate is lost on pre-incubation of FIP3 at 60 and 80°C.

Following this, the ability of FIP3 which had been incubated at 60°C (referred to heat-treated FIP3 from now on) to phosphorylate MBP was tested. Figure 3.3A shows that heat-treated FIP3 cannot phosphorylate MBP. Thus recombinant FIP3 was heat-treated in subsequent *in vitro* phosphorylation assays.

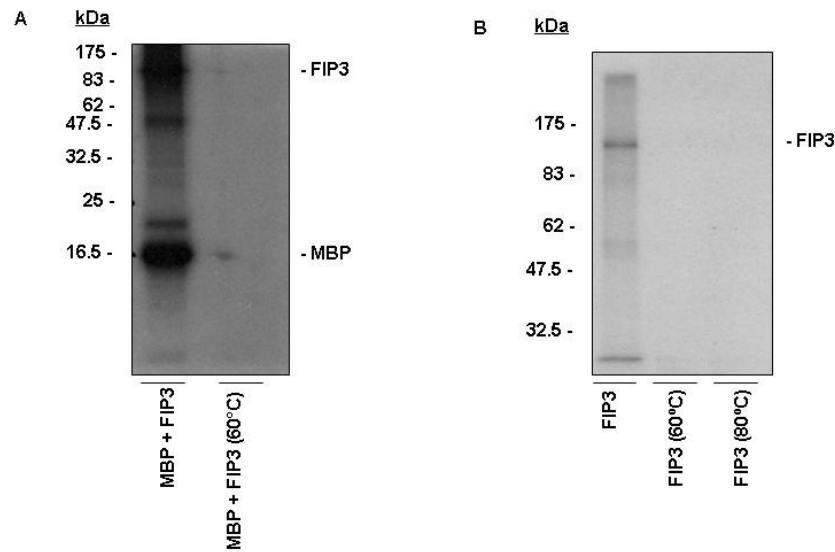


Figure 3-3 Analysis of recombinant FIP3's capacity to autophosphorylate

The capacity of the Baculovirus Sf9 insect cell expressed FIP3 sample to autophosphorylate was investigated via an *in vitro* phosphorylation assay, as detailed in section 2.6. (A) 2 μ g MBP was incubated for 30 minutes at 30 $^{\circ}$ C in the presence of 2 μ g FIP3 (with or without heat-treatment at 60 $^{\circ}$ C for 30 minutes) and 6 μ Ci ATP- γ - 32 P. Samples were separated by SDS-PAGE (section 2.2.2) and autoradiography was performed. Figure legends are as follows: Lane 1, 2 μ g MBP incubated with 2 μ g recombinant FIP3; Lane 2, 2 μ g MBP incubated with 2 μ g heat-treated recombinant FIP3. The position of the Broad Range Prestained Protein Marker is illustrated. Baculovirus expressed recombinant FIP3 is capable of phosphorylating MBP, but on heat-treatment this ability is lost. (B) 2 μ g recombinant FIP3 was incubated for 30 minutes at 60 $^{\circ}$ C or 80 $^{\circ}$ C and then subject to an *in vitro* phosphorylation assay for 30 minutes at 30 $^{\circ}$ C in the presence of 6 μ Ci ATP- γ - 32 P. Samples were separated by SDS-PAGE and autoradiography was performed. Figure legends are as follows: Lane 1, 2 μ g recombinant FIP3 only; Lane 2, 2 μ g recombinant FIP3 incubated at 60 $^{\circ}$ C; Lane 3, 2 μ g recombinant FIP3 incubated at 80 $^{\circ}$ C. The position of the Broad Range Prestained Protein Marker is illustrated. Baculovirus expressed recombinant FIP3 which has not been heat-treated is capable of autophosphorylation, but when heat treated, this kinase activity is lost. Data from a single experiment is presented.

3.3.5 *In vitro* phosphorylation of heat-treated FIP3 by mitotic kinases

To address the question of whether FIP3 is a direct substrate of the mitotic kinases, *in vitro* phosphorylation assays have been performed using Baculovirus Sf9 insect cell expressed human FIP3 (which had been subject to heat-treatment) and a selection of mitotic kinases. Kinase assays were performed as detailed in section 2.6. Firstly, recombinant FIP3 was subject to heat-treatment at 60°C for 30 minutes to abolish the autophosphorylating capacity of the sample. 50ng kinase was incubated with 2µg or 5µg recombinant FIP3 at 30°C for 30 minutes, in the presence of 6µCi ATP-γ-³²P. 2µg myelin basic protein (MBP) was used as a positive control for kinase activity. Further kinase only or substrate only controls were included. Samples were separated by SDS-PAGE and autoradiography was performed.

Figure 3.4 presents the autoradiographs for each kinase. It appears that FIP3 can be phosphorylated by cyclin B-CDK1 (Figure 3.4C), Plk1 (Figure 3.4D) and Aurora A (Figure 3.4A). Aurora B (Figure 3.4B) phosphorylates FIP3 to a lesser extent. Myelin basic protein (MBP) was phosphorylated only in the presence of kinase (Figures 3.4E-H). This work suggests that, *in vitro*, FIP3 is potentially phosphorylated by various mitotic kinases.

To examine this further, the stoichiometry of ATP-γ-³²P incorporation into 5µg FIP3 was calculated, for each kinase. Phosphorylation of 5µg FIP3 by Aurora A, Aurora B, CDK1 and Plk1 incorporated 0.0094 (0.94%), 0.0008 (0.08%), 0.072 (7.2%) and 0.02 (2%) pmol ATP/pmol FIP3, respectively. Whilst FIP3 can be phosphorylated by all kinases tested, as shown in figure 3.4, CDK1 phosphorylates FIP3 to the greatest extent. This may, however, reflect the fact that CDK1 appears to be the most active kinase against MBP, as shown in figure 3.4G.

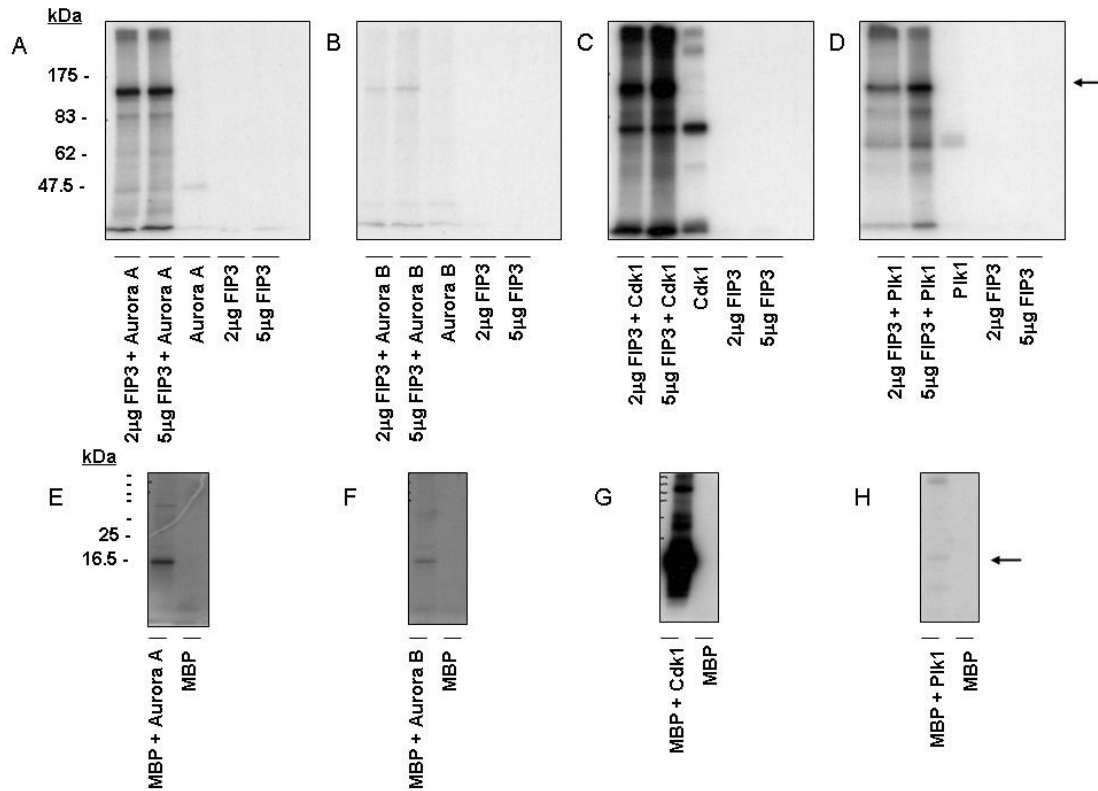


Figure 3-4 *In vitro* phosphorylation of heat-treated FIP3 by mitotic kinases
In vitro phosphorylation assays were performed as detailed in section 2.6. Firstly, Baculovirus Sf9 insect cell expressed FIP3 was subject to heat treatment at 60°C for 30 minutes to abolish the autophosphorylating capacity of the sample. 50ng kinase was incubated with 2µg or 5µg recombinant FIP3 at 30°C for 30 minutes, in the presence of 6µCi ATP-γ-³²P (top panel). Figure legends are as follows: Lane 1, 2µg recombinant FIP3 incubated with kinase; Lane 2, 5µg recombinant FIP3 incubated with kinase; Lane 3, kinase only; Lane 4, 2µg recombinant FIP3 only; Lane 5, 5µg recombinant FIP3 only. Samples were separated by SDS-PAGE as detailed in section 2.2.2 and autoradiography was performed. The position of the Broad Range Prestained Protein Marker is illustrated. The position of FIP3 on the autoradiograph is marked by an arrow. Autoradiographs show that FIP3 can be phosphorylated by cyclin B-CDK1 (C), Plk1 (D) and Aurora A (A). Aurora B (B) phosphorylates FIP3 to a lesser extent. 2µg myelin basic protein (MBP) was used as a positive control for kinase activity (bottom panel). Figure legends are as follows: Lane 1, 2µg MBP incubated with kinase; Lane 2, 2µg MBP only. The position of the Broad Range Prestained Protein Marker is illustrated, with markers 175, 83, 62, 47.5 and 32.5 omitted due to space constraints. The position of MBP on the autoradiograph is marked by an arrow. Figure E-F show that all kinases are active since they phosphorylate MBP. Representative autoradiographs from an experiment performed in triplicate are presented.

3.3.6 Phosphorylation site mapping of FIP3

Next we sought to map the phosphorylation sites of Aurora A, cyclin B-CDK1 and Plk1 in FIP3. This was carried out commercially by the FingerPrints Proteomic Facility at the University of Dundee.

A summary of the sample preparation process and techniques used to map the sites of phosphorylation are provided in section 2.7.1. In brief, *in vitro* phosphorylation assays were performed on recombinant heat-treated FIP3 using the kinases Aurora A, cyclin B-CDK1 and Plk1. A control was included in which FIP3 was not treated with any kinases. 200ng kinase was incubated with 50µg Baculovirus Sf9 insect cell expressed FIP3 (heat-treated) in a volume of 100µl kinase assay buffer, supplemented with 100µM ATP.Mg²⁺. This was incubated at 30°C for 60 minutes and protein was TCA precipitated. Proteins were separated by SDS-PAGE and the bands corresponding to FIP3 were excised. These were shipped on dry ice to the FingerPrints Proteomic Facility where nano-liquid chromatography-tandem mass spectrometry (nLC-MS/MS) and a technique known as parent ion scanning (Parents of -79) were used to detect phosphorylated peptides (Loyet *et al.*, 2005;Paradela and Albar, 2008). From this a mascot report was generated of the identified phosphorylation sites (www.matrixscience.com) (Perkins *et al.*, 1999).

Mascot reports of kinase phosphorylated FIP3 peptides are shown in figure 3.5. E-values of less than 1 denote significant FIP3 phosphorylation. No significant phosphorylation was detected in non-phosphorylated FIP3 (Figure 3.5A), or Plk1 phosphorylated FIP3 (Figure 3.5D). Significant phosphorylation was identified in CDK1-phosphorylated FIP3 (Figure 3.5C) at Serine 102 (GQLASPDAPGPGPR), with an E-value of 0.19. Potentially CDK1 phosphorylates FIP3 at serine 52 (LGAPVGGPDPQSPGLDEPAPGAAADGGAR), with an E-value of 0.69. Interestingly serine 102 was identified by collaborators as a potential phosphorylation site, from the proteomic analysis of FIP3 immunoprecipitated from metaphase HeLa cells (R. Prekeris, personal communication). Weak phosphorylation was detected at Serine 71 (WSAGPAPGLEGGPR) with an E-value of 0.31, in Aurora A phosphorylated FIP3 (Figure 3.5B). In conclusion, this work shows that cyclin B-CDK1 phosphorylates FIP3 at serine 102, *in vitro*.

No significant hits to report

Peptide matches not assigned to protein hits: (no details means no match)

Query	Observed	Mr(expt)	Mr(calc)	Delta	Miss	Score	Expect	Rank	Peptide
<input checked="" type="checkbox"/> 8	970.607131	1939.199710	1936.775299	2.424411	0	36	1.8e+02	1	VTTFIPYMTNTGLCK + Dioxidation (M); Phospho (ST); Phospho (Y)
<input checked="" type="checkbox"/> 9	647.407354	1939.200234	1938.888336	0.311898	2	34	2.7e+02	1	NLMHRRAPFSGSADLR + Dioxidation (M); Phospho (ST)
<input checked="" type="checkbox"/> 1	588.466191	1174.917830	1172.478424	2.439406	0	32	2.9e+02	1	ADTEALTNMK + Phospho (ST)
<input checked="" type="checkbox"/> 5	386.307421	1541.200580	1540.641510	0.559070	0	32	3.8e+02	1	GVDVALEASMGPCR + Phospho (ST)
<input checked="" type="checkbox"/> 7	458.796771	1831.157980	1830.924042	0.233938	2	29	7.8e+02	1	KVATALTHGQKVEAEK + Acetyl (N-term); Phospho (ST)
<input checked="" type="checkbox"/> 10	1057.808078	2113.601604	2113.943771	-0.342167	2	29	8.9e+02	1	MKSPYEAAHERALMVNR + Dioxidation (M); Phospho (ST)
<input checked="" type="checkbox"/> 6	611.393095	1831.157457	1830.727676	0.429781	0	27	1.3e+03	1	DGSMLEGLTITLGLR + Oxidation (M); 3 Phospho (ST)
<input checked="" type="checkbox"/> 11	705.541319	2113.602129	2111.944199	1.657930	0	27	1.6e+03	1	SAPTPTPAPTGSRPALAYR + Acetyl (N-term); 2 Phospho (ST)
<input checked="" type="checkbox"/> 4	514.740628	1541.200056	1539.736740	1.463316	2	25	1.9e+03	1	MSAEAKLGAGVERK + Acetyl (N-term); Phospho (ST)
<input checked="" type="checkbox"/> 2	591.674753	1181.334954	1180.607742	0.727212	2	25	1.4e+03	1	AQSVLGKRSR + Phospho (ST)
<input checked="" type="checkbox"/> 12	529.407939	2113.602652	2112.928223	0.674429	0	23	3.4e+03	1	GHAAIYSAPVADAASATGPK + Phospho (ST); Phospho (Y)
<input checked="" type="checkbox"/> 3	394.785768	1181.335476	1180.448776	0.886700	0	22	2.4e+03	1	MSSIITPSK + Acetyl (N-term); Oxidation (M); 2 Phospho (ST)

Figure 3-5A Phosphorylation site mapping of non-phosphorylated FIP3

Mascot report of non-phosphorylated FIP3 peptides, performed by the FingerPrints Proteomic Facility, University of Dundee. An *in vitro* phosphorylation assay was performed on 50µg recombinant heat-treated FIP3, in the presence of 100µM ATP.Mg²⁺, at 30°C for 60 minutes. The sample was TCA precipitated and separated by SDS-PAGE (section 2.2.2). The band corresponding to FIP3 was excised and subjected to nLC-MS/MS and parent ion scanning. Sites of significant phosphorylation (with E-values (expect) less than 1) are marked with a star. No significant phosphorylation was detected in non-phosphorylated FIP3.

No significant hits to report

Peptide matches not assigned to protein hits: (no details means no match)

Query	Observed	Mr (expt)	Mr (calc)	Delta	Miss	Score	Expect	Rank	Peptide
★ <input checked="" type="checkbox"/> 1	716.448100	1430.881648	1430.634369	0.247279	0	62	0.31	1	WSAGPAPGLEGGPR + Phospho (ST)
<input checked="" type="checkbox"/> 5	601.434667	1801.282173	1798.840668	2.441505	1	52	4.3	1	MAYTEEQIENIKTR + Acetyl (N-term); Dioxidation (M)
<input checked="" type="checkbox"/> 6	451.327950	1801.282696	1801.659058	-0.376362	1	42	38	1	MLIGSRSDSGSSETR + Dioxidation (M); 2 Phospho (ST)
<input checked="" type="checkbox"/> 15	517.551343	2066.176268	2066.020126	0.156142	2	39	1e+02	1	LGSDLEMRDADTVVNATKK + Dioxidation (M)
<input checked="" type="checkbox"/> 20	834.969399	2501.886369	2499.468338	2.418031	1	37	1.7e+02	1	IILLMLSIILVLIIRYLK + Oxidation (M); Phospho (ST); Phospho (Y)
<input checked="" type="checkbox"/> 14	689.732524	2066.175744	2065.940353	0.235391	0	36	1.9e+02	1	QPQTRPGILLAAASYALR + 2 Phospho (ST); Phospho (Y)
<input checked="" type="checkbox"/> 9	456.767700	1823.041696	1822.830734	0.210962	2	36	1.8e+02	1	QKISTQAYLPKEFK + Gln->pyro-Glu (N-term Q); Phospho (ST); Phospho (Y)
<input checked="" type="checkbox"/> 4	901.648100	1801.281648	1800.794617	0.487031	0	35	2e+02	1	AFYNLWVYGALGGMK + Dioxidation (M); Phospho (Y)
<input checked="" type="checkbox"/> 18	794.706333	2381.097171	2380.152237	0.944934	1	35	2.6e+02	1	EVEERKLASSAQALSQAQTQLK + Acetyl (N-term); Phospho (ST)
<input checked="" type="checkbox"/> 21	626.478999	2501.886892	2499.986618	1.900274	0	34	3.9e+02	1	VVDVNNYNIATGSGTDIIDMR + Acetyl (N-term); Oxidation (M); 2 Phospho (ST)
<input checked="" type="checkbox"/> 13	1034.094886	2066.175220	2063.927475	2.247745	1	33	3.8e+02	1	QYKEDVALGAMSLLEYR + Gln->pyro-Glu (N-term Q); Oxidation (M); Phospho (Y)
<input checked="" type="checkbox"/> 12	479.797143	1915.159468	1914.823761	0.335707	1	33	3.6e+02	1	GADLLDSAPQTEQVRR + 2 Phospho (ST)
<input checked="" type="checkbox"/> 7	912.527600	1823.040648	1822.741745	0.298903	1	32	3.9e+02	1	DMNRTLHDTNNAQR + Acetyl (N-term); Oxidation (M); Phospho (ST)
<input checked="" type="checkbox"/> 8	608.687667	1823.041173	1822.931259	0.109914	1	32	4e+02	1	GSSAVGLTAYITKDPDTK
<input checked="" type="checkbox"/> 22	928.563782	2782.669518	2782.232117	0.437401	0	31	7e+02	1	APDLILLDIMMPGMDGYEVASVLK + 2 Oxidation (M); Phospho (ST); Phospho (Y)
<input checked="" type="checkbox"/> 3	593.635699	1777.885269	1777.716431	0.168838	0	31	5.5e+02	1	LMQAAMSYGSEHGLR + Dioxidation (M); Oxidation (M); Phospho (ST)
<input checked="" type="checkbox"/> 17	1191.555600	2381.096648	2380.032776	1.063872	1	31	7.4e+02	1	ETFGTSPMTRKMATANQVSDVK + Acetyl (N-term); Oxidation (M); Phospho (ST)
<input checked="" type="checkbox"/> 24	1005.129454	4016.488712	4016.695404	-0.206692	1	30	1e+03	1	LMRAGDVTGGTTIFDAMTASFTMADGNLINOQLAMK + 2 Dioxidation (M); Oxidation (M); 2 Phospho (ST)
<input checked="" type="checkbox"/> 19	596.281700	2381.097696	2381.051392	0.046304	1	28	1.3e+03	1	IATIIKQVPMIDLEEYR + Acetyl (N-term); Dioxidation (M); Phospho (ST); Phospho (Y)
<input checked="" type="checkbox"/> 16	584.301787	2333.178044	2332.047592	1.130452	2	28	1.4e+03	1	SAPPVMALANRYHEKFATK + Acetyl (N-term); Phospho (ST); Phospho (Y)
<input checked="" type="checkbox"/> 23	696.674786	2782.670040	2783.098160	-0.428120	2	27	2e+03	1	LGQRSHYKTLTITGSSWPEMR + Oxidation (M); 4 Phospho (ST)
<input checked="" type="checkbox"/> 10	958.586486	1915.158420	1912.823380	2.335040	1	26	1.6e+03	1	RNSPDLGLGSPPSFGPR + 2 Phospho (ST)
<input checked="" type="checkbox"/> 2	477.968000	1430.882172	1430.697617	0.184555	0	26	1.3e+03	1	MAAFGALPAGGEPAR + Oxidation (M)
<input checked="" type="checkbox"/> 11	639.393591	1915.158945	1912.873749	2.285196	1	23	3.4e+03	1	NTDDNIQSFMGAFQRK + Acetyl (N-term)

Figure 3-5B Phosphorylation site mapping of Aurora A phosphorylated FIP3

Mascot report of Aurora A phosphorylated FIP3 peptides, performed by the FingerPrints Proteomic Facility, University of Dundee. An *in vitro* phosphorylation assay was performed on 50µg recombinant heat-treated FIP3 using 200ng Aurora A, in the presence of 100µM ATP.Mg²⁺, at 30°C for 60 minutes. The samples was TCA precipitated and separated by SDS-PAGE (section 2.2.2). The band corresponding to FIP3 was excised and subjected to nLC-MS/MS and parent ion scanning. Sites of significant phosphorylation (with E-values (expect) less than 1) are marked with a star. Weak phosphorylation was found in Aurora A phosphorylated FIP3 at Serine 71 (WSAGPAPGLEGGPR).

1. [UniRef100_075154](#) Mass: 83073 Score: 364 Queries matched: 15
 Rab11 family-interacting protein 3 n=1 Tax=Homo sapiens RepID=RFIP3_HUMAN
 Check to include this hit in error tolerant search or archive report

Query	Observed	Mr (expt)	Mr (calc)	Delta	Miss	Score	Expect	Rank	Peptide
★ <input checked="" type="checkbox"/> 15	700.361247	1398.707942	1398.629288	0.078654	0	64	0.19	1	R.GQLASPDAPGGPR.S + Phospho (ST)
<input checked="" type="checkbox"/> 16	467.243431	1398.708465	1398.629288	0.079177	0	(51)	4.2	1	R.GQLASPDAPGGPR.S + Phospho (ST)
<input checked="" type="checkbox"/> 23	730.430906	1458.847260	1458.767776	0.079484	1	(47)	11	1	R.EKSIEIENLQTR.L
<input checked="" type="checkbox"/> 24	487.289871	1458.847785	1458.767776	0.080009	1	55	1.9	1	R.EKSIEIENLQTR.L
<input checked="" type="checkbox"/> 25	737.437545	1472.860538	1472.710663	0.149875	0	(32)	4e+02	2	R.LQQLDEENSELR.S
<input checked="" type="checkbox"/> 26	491.960964	1472.861064	1472.710663	0.150401	0	73	0.031	1	R.LQQLDEENSELR.S
<input checked="" type="checkbox"/> 38	893.565405	1785.116258	1784.995743	0.120515	0	(72)	0.046	1	R.IIVAIMETNPSILEVK.- + Oxidation (M)
<input checked="" type="checkbox"/> 39	596.046203	1785.116781	1784.995743	0.121038	0	73	0.03	1	R.IIVAIMETNPSILEVK.- + Oxidation (M)
<input checked="" type="checkbox"/> 52	1043.069217	2084.123882	2084.074921	0.048961	0	(31)	6.1e+02	1	K.EQNEELNGQIITLSIQGAK.S
<input checked="" type="checkbox"/> 53	695.715411	2084.124405	2084.074921	0.049484	0	34	3.3e+02	1	K.EQNEELNGQIITLSIQGAK.S
★ <input checked="" type="checkbox"/> 62	1339.189299	2676.364046	2676.218094	0.145952	0	(61)	0.69	1	R.LGAPVGGPDPQSPGLDEPAPGAAADGGAR.W + Phospho (ST)
<input checked="" type="checkbox"/> 63	893.128799	2676.364569	2676.218094	0.146475	0	78	0.015	1	R.LGAPVGGPDPQSPGLDEPAPGAAADGGAR.W + Phospho (ST)
<input checked="" type="checkbox"/> 64	670.098549	2676.365092	2676.218094	0.146998	0	(45)	27	1	R.LGAPVGGPDPQSPGLDEPAPGAAADGGAR.W + Phospho (ST)
<input checked="" type="checkbox"/> 68	907.117475	2718.330597	2718.228653	0.101944	0	(29)	1.2e+03	3	R.LGAPVGGPDPQSPGLDEPAPGAAADGGAR.W + Acetyl (N-term); Phospho (ST)
<input checked="" type="checkbox"/> 70	1360.203746	2718.392940	2718.228653	0.164287	0	(34)	4e+02	1	R.LGAPVGGPDPQSPGLDEPAPGAAADGGAR.W + Acetyl (N-term); Phospho (ST)

Figure 3-5C Phosphorylation site mapping of CDK1 phosphorylated FIP3

Mascot report of CDK1 phosphorylated FIP3 peptides, performed by the FingerPrints Proteomic Facility, University of Dundee. An *in vitro* phosphorylation assay was performed on 50µg recombinant heat-treated FIP3 using 200ng CDK1/cyclin B, in the presence of 100µM ATP.Mg²⁺, at 30°C for 60 minutes. The sample was TCA precipitated and separated by SDS-PAGE (section 2.2.2). The band corresponding to FIP3 was excised and subjected to nLC-MS/MS and parent ion scanning. Sites of significant phosphorylation (with E-values (expect) less than 1) are marked with a star. Significant phosphorylation was identified in CDK1 phosphorylated FIP3, at Serine 102 (GQLASPDAPGGPR) and Serine 52 (LGAPVGGPDPQSPGLDEPAPGAAADGGAR).

1. [tr|BOQYI8|BOQYI8_HUMAN](#) Mass: 76667 Score: 126 Queries matched: 2
 RAB11 family interacting protein 3 (Class II) (Fragment) OS=Homo sapiens GN=RAB11FIP3 PE=4 SV=1
 Check to include this hit in error tolerant search or archive report

Query	Observed	Mr(expt)	Mr(calc)	Delta	Miss	Score	Expect	Rank	Peptide
<input checked="" type="checkbox"/> 7	651.491686	1300.968820	1300.723801	0.245019	0	71	0.041	1	K.LLDEIESLTLR.L
<input checked="" type="checkbox"/> 14	590.849325	1769.526147	1769.000824	0.525323	0	60	0.65	1	R.IIVAIMETNPSILEVK.-

Figure 3-5D Phosphorylation site mapping of Plk1 phosphorylated FIP3

Mascot report of Plk1 phosphorylated FIP3 peptides performed by the FingerPrints Proteomic Facility, University of Dundee. An *in vitro* phosphorylation assay was performed on 50µg recombinant heat-treated FIP3 using 200ng Plk1, in the presence of 100µM ATP.Mg²⁺, at 30°C for 60 minutes. The sample was TCA precipitated and separated by SDS-PAGE (section 2.2.2). The band corresponding to FIP3 was excised and subjected to nLC-MS/MS and parent ion scanning. Sites of significant phosphorylation (with E-values (expect) less than 1) are marked with a star. No significant phosphorylation was detected in Plk1 phosphorylated FIP3.

3.3.7 In vitro phosphorylation of FIP3 by Aurora B (co-expressed with INCENP and survivin)

For full activity of Aurora B, as tested via *in vitro* phosphorylation assays, the kinase must be co-expressed and purified with the chromosomal passenger proteins INCENP and survivin (AIS complex) (Sessa *et al.*, 2005). Figure 3.4B shows that FIP3 is weakly phosphorylated by Aurora B, when tested in an *in vitro* phosphorylation assay. Aurora B used in the assay of section 3.3.5 was obtained from Upstate (now known as Millipore (UK) Ltd, as detailed in section 2.1.1), and the methods of expressing and purifying Aurora B were not described. Thus, to examine Aurora B phosphorylation further, Aurora B co-expressed and purified with INCENP and survivin was obtained from Dr. Sandrine Ruchaud at the University of Edinburgh.

In vitro phosphorylation assays were repeated with Aurora B (purchased from Upstate) as used in section 3.3.5 and elution 1 and elution 2 of the AIS complex. These were the fractions provided by Dr. Ruchaud which demonstrated the highest level of kinase activity, as tested by *in vitro* phosphorylation assays. 5µg heat-treated recombinant FIP3 was phosphorylated with 50ng Aurora B (purchased from Upstate), or with elution 1 and elution 2 of the AIS complex. Incubations were carried out at 30°C for 30 minutes, in the presence of 6µCi ATP-γ-³²P. 2µg myelin basic protein (MBP) was used as a control for kinase activity. Samples were separated by SDS-PAGE and autoradiography was performed.

Elution 1 and elution 2 of the AIS complex phosphorylates MBP control protein, but not FIP3 (data not shown). This suggests, in addition to the results presented in section 3.3.5, that Aurora B may not phosphorylate FIP3.

3.3.8 In vitro phosphorylation of CDK1 and Aurora A primed FIP3

For Plk1 to phosphorylate its substrate, the substrate first requires to be phosphorylated by another kinase, for example CDK1 (Petronczki *et al.*, 2008). This is known as phosphate priming. Plk1 can then bind to the substrate via its phosphopeptide binding domain, known as the Polo-box domain (PBD) (Elia *et*

al., 2003a; Elia *et al.*, 2003b). To that end, *in vitro* phosphorylation assays were performed on recombinant FIP3, primed with cyclin B-CDK1 and also Aurora A.

Firstly, FIP3 was primed with either cyclin B-CDK1 or Aurora A via *in vitro* phosphorylation assays, as detailed in section 2.6 (without the addition of ATP- γ - ^{32}P). 2 μg heat-treated recombinant FIP3 was pre-incubated with 50ng of cyclin B-CDK1 (Figure 3.6A) or Aurora A (Figure 3.6C) for 90 minutes at 30°C, in the presence of 50 μM ATP.Mg $^{2+}$. The control protein MBP was similarly pre-incubated with cyclin B-CDK1 and Aurora A (Figures 3.6B and 3.6D, respectively). *In vitro* phosphorylation assays were then performed on the phosphate primed FIP3 and MBP, in the presence of 6 μCi ATP- γ - ^{32}P and 50ng of Aurora A, Aurora B, Plk1 or cyclin B-CDK1, as described in section 2.6. Incubations were carried out in a water bath at 30°C for 60 minutes. Samples were separated by SDS-PAGE, as described in section 2.2.2, and autoradiography was performed.

The phosphorylation increase in CDK1 primed samples on addition of Aurora A, Aurora B or Plk1 is due to residual CDK1 activity in the presence of ATP- γ - ^{32}P , as shown in lane 1 of figure 3.6A. This is also seen in CDK1 primed MBP samples, shown in figure 3.6B. A similar effect can be seen on pre-incubation of FIP3 or MBP with Aurora A, as shown in figure 3.6C and figure 3.6D. Owing to the lack of conclusive data, this experiment was only performed once for each priming kinase and was not investigated further.

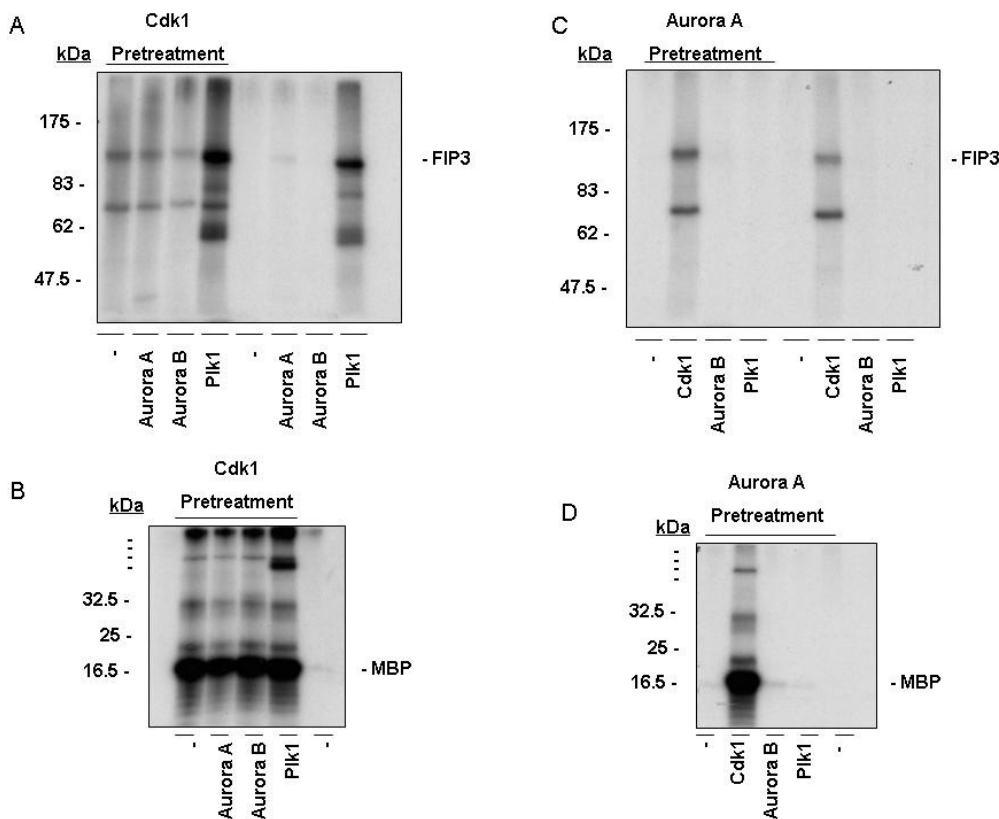


Figure 3-6 *In vitro* phosphorylation of CDK1 and Aurora A primed FIP3

(Top panel) 2µg heat-treated recombinant FIP3 was pre-incubated with 50ng of cyclin B-CDK1 (A) or Aurora A (C) for 90 minutes at 30°C, in the presence of 50µM ATP.Mg²⁺. Kinase assays were then performed on the phosphate primed FIP3, in the presence of 6µCi ATP-γ-³²P and 50ng of Aurora A, Aurora B, Plk1 or cyclin B-CDK1. Incubations were carried out in a water bath at 30°C for 60 minutes. Samples were separated by SDS-PAGE and autoradiography was performed. Figure legends for figure 3.6A are as follows: Lane 1, 2µg recombinant FIP3 pre-incubated with CDK1; Lane 2, 2µg recombinant FIP3 pre-incubated with CDK1 and phosphorylated by Aurora A; Lane 3, 2µg recombinant FIP3 pre-incubated with CDK1 and phosphorylated by Aurora B; Lane 4, 2µg recombinant FIP3 pre-incubated with CDK1 and phosphorylated by Plk1; Lane 5, 2µg recombinant FIP3; Lane 6, 2µg recombinant FIP3 phosphorylated by Aurora A; Lane 7, 2µg recombinant FIP3 phosphorylated by Aurora B; Lane 8, 2µg recombinant FIP3 phosphorylated by Plk1. The position of the Broad Range Prestained Protein Marker is illustrated. Data from a single experiment is presented.

(Bottom panel) This was repeated for the control protein, MBP which was pre-incubated with CDK1 (B) and Aurora A (D). Figure legends for figure 3.6B are as follows: Lane 1, 2µg MBP pre-incubated with CDK1; Lane 2, 2µg MBP pre-incubated with CDK1 and phosphorylated by Aurora A; Lane 3, 2µg MBP pre-incubated with CDK1 and phosphorylated by Aurora B; Lane 4, 2µg MBP pre-incubated with CDK1 and phosphorylated by Plk1; Lane 5, 2µg MBP. The position of the Broad Range Prestained Protein Marker is illustrated, with markers 175, 83, 62, 47.5 and 32.5 omitted due to space constraints. The positions of FIP3 and MBP on the autoradiograph are marked. Data from a single experiment is presented.

3.3.9 In vitro phosphorylation of Alkaline Phosphatase treated FIP3 by mitotic kinases

An attempt was made to improve kinase phosphorylation of FIP3 by dephosphorylating the protein, prior to performing the *in vitro* phosphorylation assays. This was achieved by treating FIP3 with alkaline phosphatase. Prior to this treatment, FIP3 was coupled to Ni-NTA agarose, allowing the removal of the alkaline phosphatase before performing the *in vitro* phosphorylation assays.

Firstly, recombinant FIP3 (2µg per reaction) was heat-treated. This FIP3 sample was then brought to a volume of 500µl with His-tag buffer. Next, 200µl of Ni-NTA agarose was washed three times with 1ml of His-tag buffer, before resuspending in 200µl of His-tag buffer. 160µl of the Ni-NTA agarose slurry was added to the FIP3 sample and this was incubated with end-over-end rotation at 4°C overnight. This was washed twice with His-tag buffer and re-suspended in 100µl Alkaline Phosphatase buffer from Promega. To half of this suspension, 10µl Alkaline Phosphatase was added for 30 minutes at room temperature. Three washes in His-tag buffer followed, in an attempt to remove the alkaline phosphatase. Both samples of Ni-NTA agarose immobilised FIP3 were then re-suspended in 100µl kinase assay buffer, and were then subject to kinase assays, as detailed in section 2.6. 20µl Ni-NTA agarose immobilised FIP3 (with or without alkaline phosphatase treatment) were incubated with 50ng kinase, at 30°C for 60 minutes, in the presence of 6µCi ATP-γ-³²P. A control was included where the kinase was omitted. Following this incubation, the reactions were washed twice in cold kinase assay buffer (without the ATP). Following the last wash, the Ni-NTA agarose immobilised FIP3 was re-suspended in 20µl SDS-PAGE sample buffer, boiled for 5 minutes and the supernatants separated by SDS-page and autoradiography was performed.

This experiment was carried out twice, with no significant results and the data is not presented. Interestingly, in one of the experimental repeats, Plk1 phosphorylation of phosphatase treated FIP3 may have been reduced. This may correlate with Plk1's requirement for substrate phosphate priming, however this result is preliminary and was not investigated further.

3.3.10 Proteomic analysis of recombinant FIP3

In vitro phosphorylation assays in section 3.3.4 suggest that the baculovirus Sf9 insect cell expressed FIP3 sample co-purified with a kinase. Indeed, when 2 μ g or 5 μ g recombinant FIP3 was separated by SDS-PAGE (as detailed in section 2.2.2) and stained with Coomassie brilliant blue (as detailed in section 2.2.6), FIP3 appears in addition to numerous other bands, as shown in figure 3.7. These were assumed to be FIP3 degradation products, however owing to the kinase activity of the FIP3 solution, it was thought that perhaps one of these bands could be an insect cell kinase. This could point to a mammalian kinase which could potentially phosphorylate FIP3.

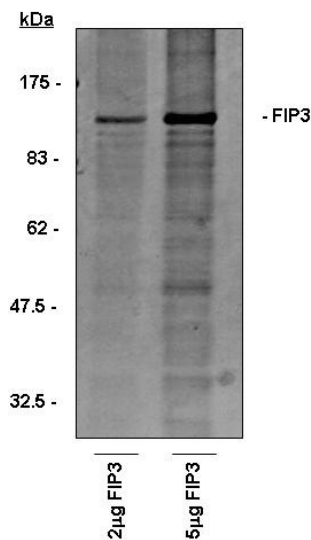


Figure 3-7 Recombinant FIP3 separated by SDS-PAGE and stained with Coomassie Blue Stain. 2 μ g (Lane 1) and 5 μ g (Lane 2) recombinant FIP3 were diluted in 4X SDS-PAGE loading buffer. Samples were separated by SDS-PAGE as detailed in section 2.2.2 and Coomassie Blue stained as outlined in section 2.2.6. The position of the Broad Range Prestained Protein Marker is illustrated. FIP3 appears as expected at approximately 100 kDa. Additional proteins bands are present. These may show degradation of the FIP3 sample or perhaps suggest the purification procedure resulted in contamination with insect cell proteins.

To identify any potential insect cell kinases contaminating the recombinant FIP3 sample, a proteomic approach was used. Two attempts were made at this. Firstly using the Sir Henry Wellcome Functional Genomics Facility (SHWFGF) at the University of Glasgow and secondly using Aberdeen Proteomics at the University of Aberdeen. Sample preparation and methods used by the two proteomic facilities are described in section 2.7.2.

Firstly 15µg of the recombinant FIP3 sample was analysed for protein content using nLC-ESI-MS/MS by the SHWFGF at the University of Glasgow (Bridges *et al.*, 2008). Data was exported to the Mascot (Matrix Science) search engine for protein identification (www.matrixscience.com) (Perkins *et al.*, 1999) and the results are presented in section 7.1.1 of the appendix. The scoring system measures the degree of similarity between the experimental MS/MS data and the theoretical spectra constructed for each database peptide (database parameters are set by the user). The significance threshold is set at 5% ($p < 0.05$) and above the MASCOT cut-off score, the match has less than 5% probability of being a random event and indicates homology or extensive identity. Candidate peptides are ranked according to the score and the highest scoring peptide is the best match. Multiple matches to peptides from the same protein produce the highest scores.

A search of the *Mammalia* (Table 7.1) or *Drosophila* (Table 7.2) databases did not reveal any kinases in the FIP3 sample. Both alpha and beta tubulin were detected. This could be a side effect of the purification procedure. However, the association of FIP3 and tubulin has been previously reported, as tubulin co-immunoprecipitated with FIP3 (J. Matheson, unpublished data). Whether this is a direct or indirect interaction is still in question. Two protein hits of interest in the FIP3 solution, searching the *Mammalia* database, were for protein phosphatase 2A (PP2A). However, these hits had scores of 58 and 50, just above the cut off score of 49. Another protein hit of interest in the FIP3 solution, searching the *Drosophila* database, was for kinesin heavy chain, with a score of 62 (the cut off score is 39). The kinesins are a superfamily of microtubule-based molecular motor proteins (Hirokawa *et al.*, 2009), members of which are known to have mitotic functions (Sharp *et al.*, 2000). As discussed in section 1.5.6.5, FIP3 may interact with members of the kinesin family.

Concern was raised over the overexpressed FIP3 protein masking the presence of less well expressed insect cell kinases in the solution. Thus 5µg FIP3 was separated by SDS-PAGE, the gel lane cut into 5 slices and analysed for protein content using nLC-ESI-MS/MS. Gel slice 1 contained the major FIP3 band. Data was exported to the Mascot (Matrix Science) search engine for protein identification, searching the *Mammalia* and *Drosophila* databases. The results are presented in the Appendix, section 7.1.2.

As expected, a search of the *Mammalia* databases shows that FIP3 is present in gel slice 1 (Table 7.3 of the appendix). Searches of the *Mammalia* databases for gel slices 2 (Table 7.5 of the appendix), 3 (Table 7.7 of the appendix), 4 (Table 7.9 of the appendix) and 5 (Table 7.11 of the appendix), show that FIP3 is present in all gel slices. This perhaps suggests that the protein bands observed in figure 3.7 could be FIP3 degradation products. Searches of the *Mammalia* and *Drosophila* databases for all gel slices again show the presence of alpha and beta tubulin in the FIP3 solution. One protein hit from gel slice 3 was a peptide similar to casein kinase-II (known as CK2) alpha 1 subunit. A search of the *Mammalia* database detects CK2 alpha 1 subunit isoform a, with a score of 121 and CK2 alpha 1 subunit isoform b, with a score of 98 (Table 7.7, cut off score of 48); a search of the *Drosophila* database detects CK2 with a score of 78 (Table 7.8, cut off score of 38). CK2 is a serine/threonine kinase thought to play a role in mitotic progression via maintenance of centrosome integrity, spindle formation, chromosomal segregation (St Denis *et al.*, 2009) and entry into mitosis by regulating Wee1 stability (Yde *et al.*, 2008). Interestingly, CK2 was predicted to potentially phosphorylate FIP3 at serine 281, as discussed in section 3.3.2. The presence of CK2 in the FIP3 sample was investigated further (see section 3.3.11).

Other potential kinase hits were for a peptide similar to ribosomal S6 kinase. This was detected in gel slice 3, searching the *Mammalia* database (Table 7.7 of the appendix). It produced a score of 54, which was marginally above the cut off score of 48. The 90kDa ribosomal S6 kinase (RSK) family of proteins are highly conserved serine/threonine kinases shown to regulate cell proliferation, survival, growth and motility (Anjum and Blenis, 2008). Other potential kinase hits were for a peptide similar to BMK1 alpha kinase. This was detected in gel slice 2, searching the *Mammalia* database (Table 7.5 of the appendix). It

produced a score of 68, which was marginally above the cut off score of 49. BMK1 is also known as extracellular-regulated protein kinase 5 (ERK5) and is a mitogen-activated protein kinase (MAPK) (Wang and Tournier, 2006). ERK5 is active during mitosis and has been implicated in the survival of dividing cells (Gírio *et al.*, 2007).

Next, 5µg FIP3 was separated by SDS-PAGE and the gel lane cut into 16 gel slices which were analysed by Aberdeen Proteomics at the University of Aberdeen. Protein identification of gel bands was achieved by LC-MS/MS searching Human and *Spodoptera Frugiperda* databases. The top of the gel was excised as gel slice 1; the bottom gel was excised as gel slice 16; the major FIP3 was excised in gel slice 4.

A summary of the results are presented in the Appendix, section 7.1.3, table 7.13. Searches of the human database showed that FIP3 was present in gel slice 4 as expected. FIP3 was also detected in slices 1, 3, 5, 6, 7, 9, 10 and 12. This suggests that the bands observed in figure 3.7 may be degradation products of FIP3. Also detected was beta-tubulin in gel slice 8 in both the human and *Spodoptera Frugiperda* databases. No kinases were detected in this analysis.

In summary, proteomic analysis of the recombinant FIP3 sample was carried out in the hope that a contaminating insect kinase would be revealed. The results suggest that the protein bands observed in figure 3.7, which run at a molecular weight lower than expected for FIP3, may be FIP3 degradation products. However, proteomic data suggests that CK2 may be present in the FIP3 sample. On discussion with others in the kinase field, it was revealed that the baculovirus Sf9 insect cell expression system is notorious for producing purified protein samples with contaminating kinases. In future, perhaps different expression systems may be used to produce FIP3.

3.3.11 *Immunoblot analysis of recombinant FIP3*

We next tested whether any contaminating kinase present in the FIP3 sample could be identified by immunoblotting. 2µg recombinant FIP3 sample was separated by SDS-PAGE as detailed in section 2.2.2. As a control, 10µg of a HeLa cytoplasmic extract (known as the S100 fraction) and a HeLa lysate (produced in our lab) were included on the gel. SDS-PAGE gels were then subject to Western Blotting, as detailed in section 2.2.3. Nitrocellulose membranes were then probed for a selection of mitotic kinases, as described in section 2.2.4. Kinases tested were CDK1, Aurora A, Aurora B, Plk1, ROCK, MLCK and CK2. The results for each kinase were similar, thus only the data for CDK1 is presented in figure 3.8. Kinases were only detected in the S100 fraction and homemade HeLa lysate. No kinases were detected in the recombinant FIP3 sample, even upon prolonged exposure of the immunoblots.

We then went on to perform immunoprecipitation experiments to determine if FIP3 immunoprecipitated from metaphase HeLa lysates interacted with any kinases from the HeLa lysate. Ten T150 flasks of HeLa cells were synchronised, as detailed in section 2.4.5.1. FIP3 was then immunoprecipitated from these cells. Samples were then separated by SDS-PAGE (section 2.2.2), western blotted (section 2.2.3) and subject to immunoblotting (section 2.2.4) with antibodies directed to FIP3 and the mitotic kinases mentioned previously. This was repeated several times, with attempts made to increase the starting volume of cells. FIP3 was successfully immunoprecipitated from metaphase lysates, but no kinases were detected, thus the data has not been presented.

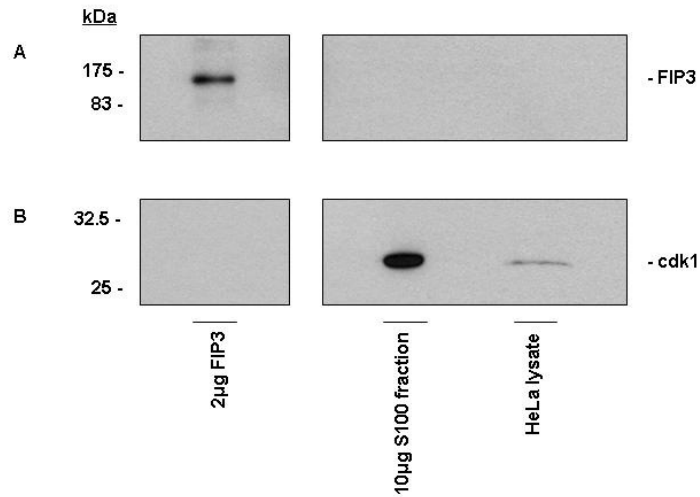


Figure 3-8 Immunoblot analysis of recombinant FIP3

2µg recombinant FIP3 sample was separated by SDS-PAGE, as detailed in section 2.2.2. As a control, 10µg of S100 fraction and a HeLa lysate were included on the gel. SDS-PAGE gels were then subject to western blotting, as detailed in section 2.2.3. Nitrocellulose membranes were then probed for a selection of mitotic kinases, as described in section 2.2.4. A representative blot is shown, depicting FIP3 (A) and CDK1 (B). Figure legends are as follows: Lane 1, 2µg FIP3; Lane 2, 10µg S100 fraction; Lane 3, homemade HeLa lysate. The position of the Broad Range Prestained Protein Marker is illustrated. Samples were run on the same SDS-PAGE gel, with the protein marker in a lane between 2µg FIP3 and the S100 fraction, but for presentation purposes the protein marker was removed from the above figure. Kinases were detected in the S100 fraction and homemade HeLa lysate. No kinases were detected in the recombinant FIP3 sample, even upon prolonged exposure of the immunoblots. Data from a single experiment is presented.

3.3.12 FIP3 autophosphorylation in the presence of kinase inhibitors

In another attempt to identify the kinase(s) potentially contaminating the recombinant FIP3 sample, we employed a range of kinase inhibitors in FIP3 autophosphorylation reactions, to ascertain whether any decrease in FIP3 phosphorylation could be observed.

Recombinant FIP3 which had not been heat-treated was used in an *in vitro* phosphorylation assay, as described in section 2.6. 2µg autophosphorylating FIP3 was incubated for 30 minutes at 30°C in the presence of 6µCi ATP-γ-³²P. Identical incubations were set up, but with kinase inhibitors which were added for the duration of the assay: 100µM ZM447439 (inhibitor of Aurora B and Aurora A); 100µM PD98059 (inhibitor of MEK1); 100µM SB203580 (inhibitor of p38-MAPK); 100µM Plk1a (Plk1 inhibitor supplied by GSK); 100µM Plk1b (Plk1 inhibitor supplied by GSK); 100µM Y-27632 (inhibitor of ROCK-I and ROCK-II); 5µM BMI 1026 (inhibitor of CDK1). Samples were separated by SDS-PAGE and autoradiography was performed. No significant change in FIP3 autophosphorylation was observed for any of the kinase inhibitors tested, as shown in figure 3.9A. To test the extent of CDK1 inhibition by BMI-1026, 2µg MBP and 50ng CDK1 were incubated for 30 minutes at 30°C with 6µCi ATP-γ-³²P. This was carried out in duplicate, with 5µM BMI-1026 added to one for the duration of the assay. 5µM BMI-1026 quantitatively inhibits CDK1 phosphorylation of MBP, as seen in figure 3.9B.

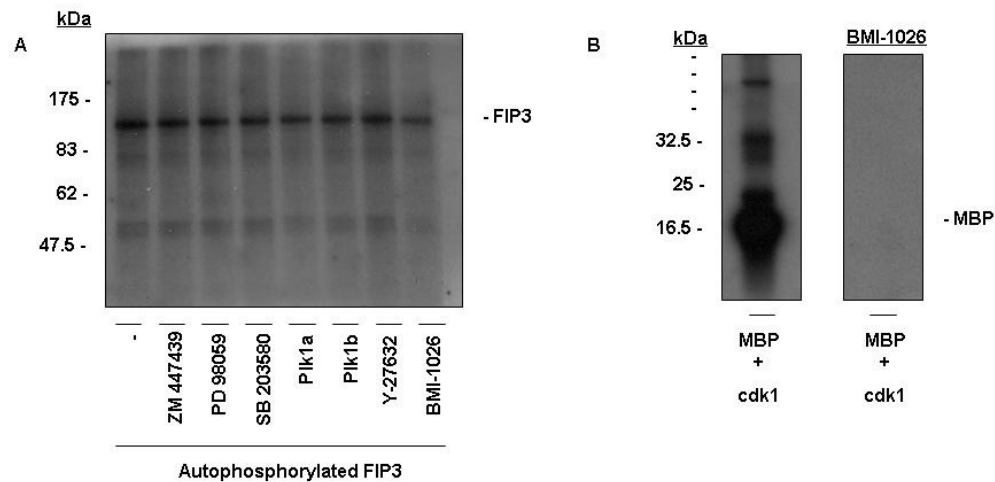


Figure 3-9 FIP3 autophosphorylation in the presence of kinase inhibitors
 (A) 2 μ g autophosphorylating FIP3 was incubated for 30 minutes at 30°C in the presence of 6 μ Ci ATP- γ - 32 P (Lane 1). Identical incubations were set up, but with kinase inhibitors which were added for the duration of the assay: 100 μ M ZM447439 (Lane 2), 100 μ M PD98059 (Lane 3), 100 μ M SB203580 (Lane 4), 100 μ M Plk1a (Lane 5), 100 μ M Plk1b (Lane 6), 100 μ M Y-27632 (Lane 7) and 5 μ M BMI-1026 (Lane 8). Samples were separated by SDS-PAGE (section 2.2.2) and autoradiography was performed. The position of the Broad Range Prestained Protein Marker is illustrated. No significant change in FIP3 autophosphorylation was observed for any of the kinase inhibitors tested. (B) To test the extent of CDK1 inhibition by BMI-1026, 2 μ g MBP and 50ng CDK1 were incubated for 30 minutes at 30°C with 6 μ Ci ATP- γ - 32 P (Lane 1). This was carried out in duplicate, with 5 μ M BMI-1026 added to one for the duration of the assay (Lane 2). 5 μ M BMI-1026 inhibits CDK1 phosphorylation of MBP. The positions of FIP3 and MBP on the autoradiographs are marked. Representative autoradiographs from an experiment performed in duplicate are presented.

3.3.13 *HeLa cytoplasmic S100 fraction phosphorylation of FIP3*

Next we tested whether kinases within a HeLa cytoplasmic extract could phosphorylate FIP3, as tested in an *in vitro* phosphorylation assay. HeLa cytoplasmic fraction S100 was purchased from Dundee Cell Products at the University of Dundee. An *in vitro* phosphorylation assay was carried out, as detailed in section 2.6, with several modifications.

Firstly, baculovirus Sf9 insect cell expressed FIP3 was subject to heat-treatment at 60°C for 30 minutes to abolish the autophosphorylating capacity of the sample. 50µg of S100 fraction was added to screw topped microcentrifuge tubes. Kinase assay buffer was added to a final volume of 50 µl and 20µg recombinant heat-treated FIP3 was added. The reaction was started on addition of 6µCi ATP- γ -³²P and carried out in a 30°C water bath. At 0, 30, 60 and 120 minutes, 12.5 µl of the reaction mixture was removed and added to screw topped microcentrifuge tubes containing 3µl 4x SDS-PAGE loading buffer. FIP3 only and S100 fraction only controls were set up, and, at 120 minutes, 20µl 4x SDS-PAGE loading buffer was added to each tube. Samples were separated by SDS-PAGE, as detailed in section 2.2.2, and autoradiography was performed. The resulting autorad is presented in figure 3.10.

A phospho-protein(s) band can be seen at the expected molecular weight for FIP3, suggesting that FIP3 may be phosphorylated by a kinase(s) contained within the HeLa cytoplasmic S100 fraction. However, a band is present in the S100 fraction only lane at the same molecular weight as FIP3. Thus, by using this method, proteins from the S100 fraction cannot be distinguished from FIP3. Various attempts were made to refine this experiment. Recombinant FIP3 protein (which contains an N-terminal hexa-His-tag) was bound to Ni-NTA agarose before incubating with S100 fraction in an *in vitro* phosphorylation assay. Following the assay, it was hoped that FIP3 could be separated from S100 proteins by washing the Ni-NTA agarose with buffer. The intention was to use kinase inhibitors to block potential phosphorylation of FIP3 in an attempt to identify any kinase(s) which might phosphorylate FIP3. However, FIP3 could not be separated from proteins in the HeLa cytoplasmic S100 fraction, or the contaminant proteins from the original baculovirus system (see figure 3.7). Thus it was decided not to pursue this further.

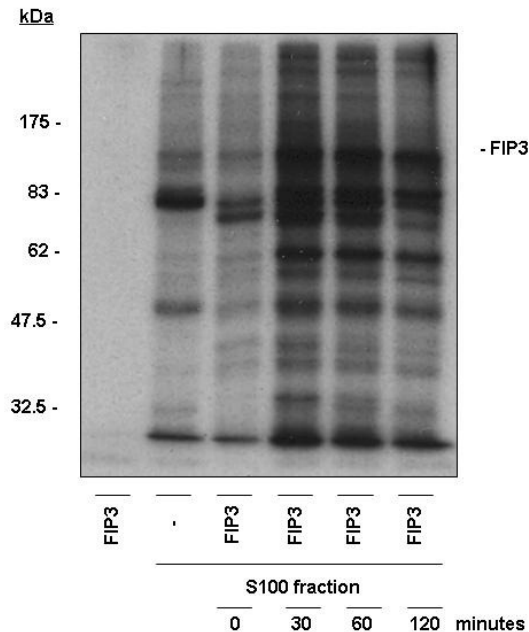


Figure 3-10 HeLa cytoplasmic S100 fraction phosphorylation of FIP3

Baculovirus Sf9 insect cell expressed FIP3 was subject to heat-treatment at 60°C for 30 minutes. 50µg of S100 fraction was added to screw topped eppendorfs. Kinase assay buffer was added to a final volume of 50µl followed by 20µg recombinant heat-treated FIP3. The reaction was started on addition of 6µCi ATP-γ-³²P and carried out in a 30°C water bath. At 0 (lane 3), 30 (lane 4), 60 (lane 5) and 120 (lane 6) minutes, 12.5µl of the reaction mixture was removed and added to screw topped eppendorfs containing 3µl 4x SDS-PAGE loading buffer. FIP3 only (lane 1) and S100 fraction only (lane 2) controls were set up, and, at 120 minutes, 20µl 4x SDS-PAGE loading buffer was added to each tube. Samples were separated by SDS-PAGE, as detailed in section 2.2.2, and autoradiography was performed. The position of the Broad Range Prestained Protein Marker is illustrated. The positions of FIP3 on the autoradiograph are marked. Data from a single experiment is presented.

3.4 Conclusions

The regulatory controls governing the spatial and temporal regulation of FIP3 during mitosis are unknown. A potential candidate is phosphorylation, since phosphorylation is a commonly used control mechanism in mitotic regulation (Cohen, 2000). FIP3 has been identified as a phospho-protein (R. Prekeris, personal communication) and four potential phosphosites have been mapped (serines 102, 281, 348 and 451). In order to prevent aberrant cell division, the cell-cycle is tightly regulated via a network of kinases, which phosphorylate a vast number of protein substrates (Morgan, 2007). A variety of mitotic kinases are active during the cell-cycle, including Aurora A, Aurora B, Plk1 and CDK1.

This work aimed to determine whether candidate cell-cycle kinases phosphorylate FIP3 *in vitro*.

First we sought to map the kinase specific phosphorylation sites of human FIP3 using a prediction programme, focusing on the sites identified by the Prekeris lab. FIP3 was not identified as a potential substrate of Aurora A, Aurora B or Plk1. Serine 102 (in the sequence context GQLAS*PDAPGPGPR) was identified as a potential target of the CDKs, owing to the presence of a proline residue immediately following the phospho-serine (Shetty *et al.*, 1993; Brown *et al.*, 1999; Ubersax and Ferrell Jr, 2007). CDK1 substrates typically have a basic residue at the +2 or +3 positions, which serine 102 lacks. However, other CDK1 sites are known to lack this basic residue (Yüce *et al.*, 2005).

We examined whether recombinant FIP3 is a substrate for mitotic kinases *in vitro* and found that FIP3 was phosphorylated by cyclin B-CDK1, Plk1, Aurora A and weakly by Aurora B. Cyclin B-CDK1 produced the most robust phosphorylation of FIP3, but this may be a result of the higher activity of this enzyme when compared to the other kinases, via *in vitro* phosphorylation of control protein MBP. Using a proteomic approach, the phosphorylation sites of Aurora A, cyclin B-CDK1 and Plk1 in FIP3 were mapped. Cyclin B-CDK1 phosphorylation of FIP3 was the only substrate/kinase pair to produce significant phosphorylation. This approach characterised serine 102 as a phosphorylation site of cyclin B-CDK1. Weak phosphorylation was detected at serine 71 in Aurora A-phosphorylated FIP3. Plk1 was found not to phosphorylate FIP3.

Serine 102 was predicted to be a potential CDK1 phospho-site and this was validated via *in vitro* phosphorylation assays, but the other kinases tested yielded no significant results. However, these kinases should not be discounted. Modification of the *in vitro* phosphorylation assay, such as buffer composition, amounts of protein used and incubation time may have yielded better results. As previously mentioned, cyclin B-CDK1 produced the most robust phosphorylation of FIP3, possibly due to the higher activity of this enzyme when compared to the other kinases via *in vitro* phosphorylation of control protein MBP. Perhaps Aurora A, Aurora B and Plk1 were not fully active. For full activity of Aurora B, as tested via *in vitro* phosphorylation assays, the kinase must be co-expressed and purified with the chromosomal passenger proteins INCENP and Survivin (AIS complex)

(Sessa *et al.*, 2005). We obtained AIS complex and tested its phosphorylation of FIP3 and MBP via *in vitro* phosphorylation assays, however FIP3 phosphorylation was not observed. Indeed, even phosphorylation of MBP was weak, leading us to question the activity of Aurora B in the purification. Perhaps a fresh purification of Aurora B would produce a higher level of phosphorylation. In addition, a kinase must recognise its substrate in a huge pool of potentially phosphorylatable residues. Specificity of phosphorylation results, among other factors, from the structure of the catalytic site and interactions between the substrate and kinase, local and distal to the phosphorylation site (Ubersax and Ferrell Jr, 2007). FIP3 used in the phospho-site mapping of kinase phosphorylated FIP3 was heat-treated at 60°C for 30 minutes to abolish the contaminating kinase activity in the FIP3 preparation. Perhaps this heat-treatment affected the structure of FIP3, thus inhibiting kinase recognition of the substrate. For Plk1 to phosphorylate its substrate, the substrate first requires to be phosphorylated by another kinase, for example CDK1 (Petronczki *et al.*, 2008). This was investigated via *in vitro* phosphorylation assays and an increase in phosphorylation by Plk1 of CDK1-primed FIP3 was observed. But it is likely that this was due to residual CDK1 activity in the assay. Perhaps CDK1 phosphorylated FIP3 could be heat-treated to denature CDK1, prior to *in vitro* phosphorylation with Plk1. It was questioned whether a lack of phosphorylation by Aurora A, Aurora B and Plk1 was due to FIP3 being already phosphorylated at the key phospho-sites. We carried out a study using alkaline phosphatase to remove phosphate groups from FIP3, but no significant improvement in phosphorylation was observed. Plk1 phosphorylation of phosphatase treated FIP3 may have been reduced, correlating with Plk1's requirement for substrate phosphate priming, but this was not a reproducible result and was not pursued further.

Surprisingly, the Baculovirus Sf9 insect cell expressed FIP3 sample had intrinsic kinase activity and work was carried out to identify the contaminating kinase(s). The hope was that any identified kinase may relate to a human kinase which phosphorylates FIP3 during the cell-cycle. Various different approaches were used. Firstly, various proteomic approaches were carried out to analyse the FIP3 solution and potentially CK2 may contaminate the solution. CK2 is a serine/threonine kinase thought to play a role in mitotic progression via

maintenance of centrosome integrity, spindle formation, chromosomal segregation (St Denis *et al.*, 2009) and entry into mitosis by regulating Wee1 stability (Yde *et al.*, 2008). Using a kinase specific phosphorylation prediction programme, CK2 was predicted to phosphorylate FIP3 as serine 281. However, the presence of CK2 in the FIP3 solution was not verified, nor was CDK1, Aurora A, Aurora B, Plk1, ROCK and MLCK, in the various immunoblot analyses of the recombinant FIP3 solution. FIP3 immunoprecipitated from metaphase HeLa lysates did not co-precipitate with the kinases mentioned above. In another attempt to identify the kinase(s) potentially contaminating the recombinant FIP3 sample, we performed *in vitro* phosphorylation assays on 'autophosphorylating' FIP3, using a range of kinase inhibitors, to ascertain whether any decrease in FIP3 phosphorylation could be observed. No significant change in FIP3 autophosphorylation was observed for any of the kinase inhibitors tested. On discussion with others in the kinase field, we learned that the baculovirus Sf9 insect cell expression system is notorious for producing purified protein samples with contaminating kinases. In future, perhaps different expression systems may be used to produce FIP3.

In summary, this work has shown that FIP3 can be phosphorylated at serine 102 by cyclin B-CDK1, *in vitro*. CDK1 in complex with its regulatory subunit, cyclin B1, is chiefly responsible for the orchestration of mitosis (Nigg, 2001). The activity of the cyclin B1-CDK1 complex peaks in prophase and prometaphase. Degradation of cyclin B1 by the APC/C begins as the last chromosome lines up on the metaphase plate, just after inactivation of the spindle-assembly checkpoint (Clute and Pines, 1999). On destruction of cyclin B, CDK1 becomes inactivated allowing mitotic exit and cytokinesis. FIP3 was found to be phosphorylated at serine 102 in metaphase HeLa lysates (R. Prekeris, personal communication), when the activity of CDK1 is at its peak and we have shown that CDK1 phosphorylates FIP3 at serine 102. Thus, a candidate for FIP3 regulation is CDK1. This will be investigated further in the following chapters.

4 Consequences of Rab11-FIP3 phosphorylation

4.1 Introduction

Rab11-FIP3 (FIP3) undergoes spatial and temporal regulation during mitosis (Wilson *et al.*, 2005). During metaphase and early anaphase, FIP3 is largely cytosolic with some localised to endosomal membrane structures. During late anaphase, following furrow initiation, FIP3 localises to the centrosome. At late cytokinesis, FIP3 relocates to the cleavage furrow and midbody. On separation of the daughter cells, FIP3 relocates to the centrosome. This is shown in figure 1.4 (section 1.5.4) of the introduction.

A potential candidate for the spatial and temporal regulation of FIP3 is phosphorylation, since reversible phosphorylation is a commonly used control mechanism in mitotic regulation and can regulate the activity, localisation and half-life of a protein, as well as its interaction with other proteins (Cohen, 2000).

Work from a collaborating lab proposes that FIP3 phosphorylation and dephosphorylation may be a regulator of FIP3 localisation (R. Prekeris, personal communication). FIP3 has been identified as a phospho-protein and four potential phospho-sites have been mapped (Serines 102, 281, 348 and 451), as described in chapter 3. Analysis of the role of phosphorylation in the membrane and cytosol distribution of FIP3 throughout the cell-cycle has shown that phosphorylation and dephosphorylation of FIP3 during mitosis may regulate FIP3 association with membranes. Synchronised HeLa cells fractionated at metaphase and telophase show that during prometaphase and metaphase, FIP3 is predominantly cytosolic. FIP3 is membrane associated in telophase cells, as detailed in figures 4.1A and B. This association is dependent upon dephosphorylation of FIP3, as phosphatase treatment of cell extracts from metaphase results in FIP3 associating with membranes; this is shown in figure 4.1D. Interestingly, FIP3 phosphorylation appears to decrease at telophase, as shown in figure 4.1C. Such data offer the hypothesis that FIP3 is phosphorylated during early stages of the cell-cycle, and that dephosphorylation of FIP3 is the trigger for the association of FIP3 with membranes.

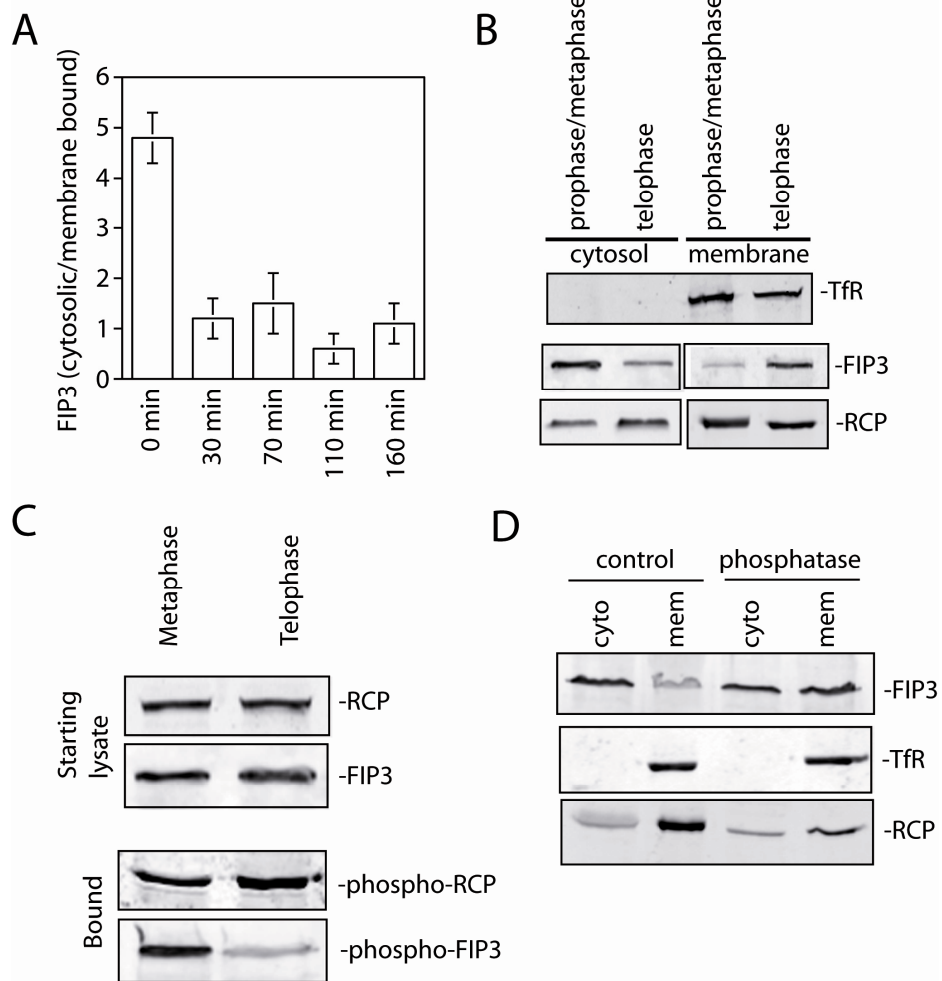


Figure 4-1 Analysis of the role of phosphorylation in the membrane and cytosol distribution of FIP3 throughout the cell-cycle (R. Prekeris, personal communication). HeLa cells were synchronised using a thymidine and nocodazole block. Cells were released into metaphase and fractionated at metaphase and telophase. **A.** Fractionation at various time points after release from nocodazole. Fractions were blotted for FIP3 and the ratio of FIP3 in the membrane and cytosol was determined. During prometaphase and metaphase, FIP3 is predominantly cytosolic; FIP3 is membrane associated in telophase cells. **B.** Examples of gels from experiment shown in A. Fractions were blotted for FIP3, transferrin receptor (TfR) and RCP (class I FIP). **C.** Qiagen phospho-binding column was used to isolate phosphorylated proteins from metaphase or telophase cells. FIP3 phosphorylation appears to decrease at telophase; there is no effect on RCP phosphorylation. **D.** Analysis of the effect of phosphorylation on FIP3 binding to membranes. Fractions from metaphase cells were isolated and treated with phosphatase, resulting in increased FIP3 association with membranes. There is no effect on RCP phosphorylation. In summary, phosphorylation and dephosphorylation of FIP3 during mitosis may regulate FIP3 association with membranes.

4.2 Aims

This work aimed to expand on the findings of Prekeris *et al.*, and further analyse the role of phosphorylation on the spatial and temporal regulation of FIP3. We aimed to recreate the fractionation of synchronised HeLa cells and analyse the membrane and cytosol distribution of FIP3 during the cell-cycle. We then aimed to make phospho-specific antibodies to FIP3 serines 102, 281, 348 and 451. Following their validation via peptide competition assays, we then screened a crude homogenate from synchronised HeLa cells in order to study the cell-cycle dependent distribution of the four phosphorylated forms of FIP3. We also aimed to perform initial studies of the effect of kinase inhibitors on the localisation of GFP-FIP3. This work aimed to expand our current understanding of the role of phosphorylation on the spatial and temporal regulation of FIP3.

4.3 Results

4.3.1 Membrane and cytosol fractionation of synchronised GFP-FIP3 expressing HeLa cells

Unpublished data from Prekeris *et al.*, has shown that the membrane and cytosol ratio of FIP3 alters during mitosis. During prometaphase and metaphase FIP3 is cytosolic, but in telophase FIP3 becomes membrane associated. We sought to replicate this work, with the intention of expanding the scope of the initial studies.

This work was initially performed in HeLa cells. However, detecting endogenous FIP3 with the available antibodies is a commonly encountered problem in the field. A stable HeLa cell line expressing FIP3 with a GFP tag at the C-terminus was obtained from Rytis Prekeris. These cells were grown in normal HeLa growth media, under the selection of Hygromycin, as described in section 2.4.1. These cells were first synchronised in either metaphase or telophase, then processed into membrane or cytosol fractions. These were then probed for FIP3 to analyse its membrane and cytosol distribution during the cell-cycle. Briefly, GFP-FIP3 expressing HeLa cells were synchronised at the G2/M transition using a thymidine/nocodazole block, as detailed in section 2.4.5.1. This blocked the

cells in the G2/M transition and on release, the cells entered metaphase as a synchronous population. In our hands, plated HeLa cells tend to divide at 45 (metaphase) and 90-110 minutes (telophase), as assessed by microscopy. Cells were fractionated, as described in section 2.4.8, using HPFEV buffer and a ball-bearing homogeniser at 45, 60, 90 and 110 minutes. Proteins were separated by SDS-PAGE, as detailed in section 2.2.2; transferred to nitrocellulose via western blotting, as detailed in section 2.2.3; detection of proteins was performed by immunodetection, as detailed in section 2.2.4. Antibodies to both FIP3 and GFP were used to detect the GFP-FIP3. Syntaxin 6 and GAPDH were used as markers for membrane and cytosol fractions, respectively. Immunoblot data is presented in figure 4.2.

Syntaxin 6 (Figure 4.2C) and GAPDH (Figure 4.2D) show consistent levels of protein in the input (crude homogenate), membrane and cytosol fractions. FIP3 levels are constant throughout the cell-cycle in the input (Figure 4.2A). However, in metaphase membrane extracts, FIP3 is present at low levels; these levels increase as the cell progresses through the cell-cycle and peak as the cell enters telophase. In contrast, levels of FIP3 peak in metaphase cytosol extracts, but decrease as the cell goes through the cell-cycle. This is replicated by GFP (Figure 4.2B). Figure 4.3 shows the quantification of GFP levels in the membrane and cytosol fractions of synchronised GFP-FIP3 expressing HeLa cells, from an experiment performed in duplicate. Thus in correlation with unpublished data from Prekeris *et al.*, during prometaphase and metaphase FIP3 is predominantly cytosolic, but in telophase FIP3 becomes membrane associated.

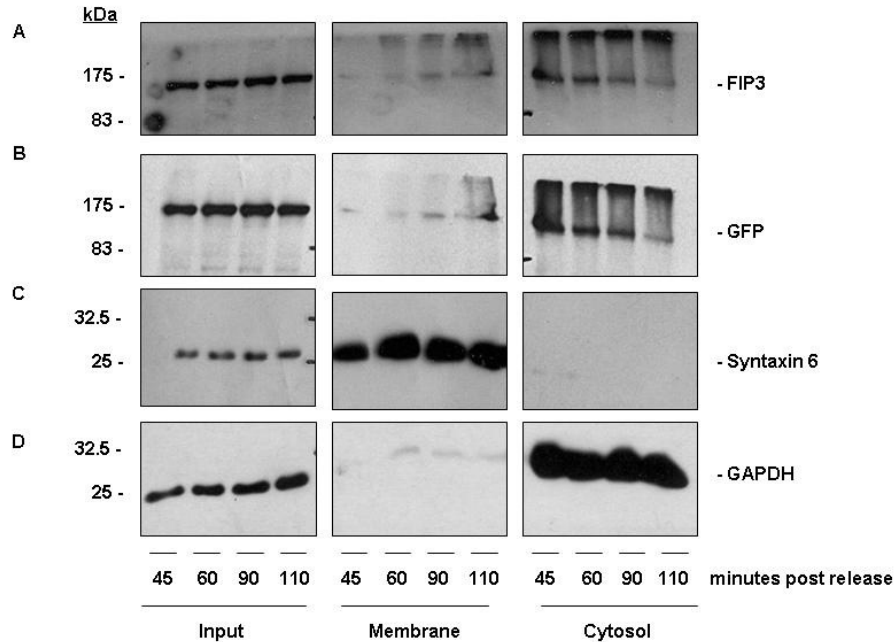


Figure 4-2 Membrane and cytosol fractionation of synchronised GFP-FIP3 expressing HeLa cells

HeLa cells stably expressing GFP-FIP3 were synchronised using a thymidine and nocodazole block, as detailed in section 2.4.5.1. Cells were fractionated using HPFEV buffer and a ball-bearing homogeniser at metaphase (45 minutes) and telophase (90 and 110 minutes), as detailed in section 2.4.8. Proteins were separated by SDS-PAGE, as detailed in section 2.2.2; transferred to nitrocellulose via western blotting, as detailed in section 2.2.3; detection of proteins was performed by immunodetection, as detailed in section 2.2.4. Crude homogenate (input), membrane and cytosol fraction were probed for FIP3, GFP, syntaxin 6 (membrane control) and GAPDH (cytosol control). The position of the Broad Range Prestained Protein Marker is illustrated. Samples were run on the same gel, with protein markers separating the input, membrane and cytosol fractions; these have been removed for the purpose of presentation. Data from a typical experiment is presented. Syntaxin 6 (Figure 4.2C) and GAPDH (Figure 4.2D) show consistent levels of protein in the input, membrane and cytosol fractions. FIP3 levels are constant throughout the cell-cycle in the input (Figure 4.2A). In metaphase FIP3 is predominantly cytosolic; in telophase FIP3 is predominantly membrane associated. Representative immunoblots from an experiment performed in duplicate are presented.

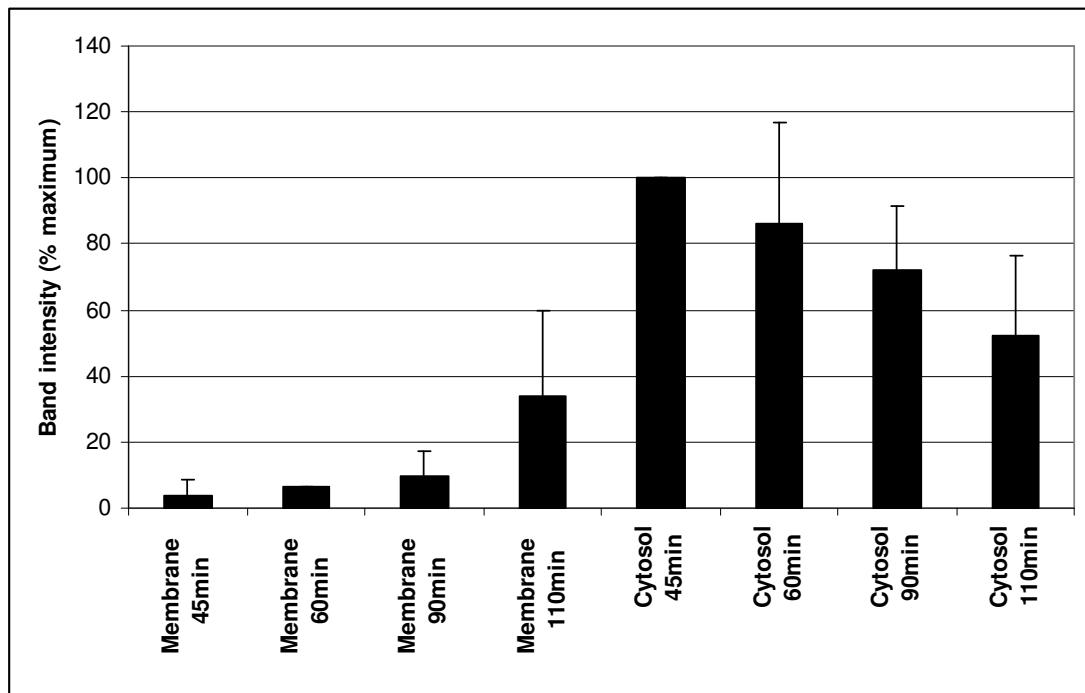


Figure 4-3 Quantification of GFP levels in the membrane and cytosol fractions of synchronised GFP-FIP3 expressing HeLa cells. Data from an experiment performed in duplicate are presented.

4.3.2 Phospho-specific antibody validation via peptide competition assays (PCAs)

In metaphase, we hypothesise that FIP3 is phosphorylated and cytosolic, but in telophase FIP3 is dephosphorylated and membrane bound (R. Prekeris, personal communication). FIP3 isolated from metaphase lysates has shown to be phosphorylated at serines 102, 281, 348 and 451. Next we sought to analyse these phospho-sites in more detail. Four phospho-specific antibodies to serines 102, 281, 348 and 451 were generated by The Scottish Blood Transfusion Service. Details are provided in section 2.8.1. In brief, phospho-specific peptides were generated, the amino acid sequences of which are listed in section 2.1.7. The phospho-specific peptides were immunised in rabbits and whole serum was obtained. IgG fractions were affinity purified from whole serum, against a protein A sepharose column, as detailed in section 2.8.2. The purification of the antibodies was carried out by Mrs M.C. Millar.

To validate the specificity of the phospho-specific antibodies, we performed peptide competition assays (PCAs). The protocol used is detailed in section

2.8.3. This procedure describes a PCA using phosphorylated and non-phosphorylated peptides.

In brief, various FIP3 samples were separated by SDS-PAGE, as described in section 2.2.2. These were 200ng baculovirus Sf9 insect cell expressed FIP3, 1µg CDK1 phosphorylated heat-treated FIP3 (prepared according to section 2.6), HeLa lysate stably expressing GFP-FIP3 and a wild type HeLa lysate. FIP3 proteins were transferred onto nitrocellulose, as described in section 2.2.3, and blocked in PBS-T containing 5% (w/v) non fat milk overnight. This was done in triplicate and identical membranes were incubated with either a no peptide control, phosphorylated peptide or non-phosphorylated peptide. These were processed for immunodetection using an Amersham ECL Rabbit IgG, HRP-Linked Whole Ab, as described in section 2.2.4.

The resulting immunoblots are presented in figures 4.4-4.7. The phospho-specific antibody to pS102 (from rabbit 2294) produced the most significant results to date, as shown in figure 4.4. pS102 (2294) antibody detects recombinant FIP3 and CDK1 phosphorylated FIP3. On incubation of the antibody with the phospho-specific peptide this avidity is all but lost. On incubation of the antibody with the non-phosphorylated peptide pS102 once again detects recombinant FIP3 and CDK1 phosphorylated FIP3. pS102 does not detect GFP-FIP3, which runs just below the 175 kDa marker. It is unclear whether pS102 detects FIP3 in the wild type HeLa lysate. Thus pS102 antibody from rabbit 2294 appears to be specific for pS102 and detects CDK1 phosphorylated FIP3.

The phospho-specific antibody to pS281 (from rabbit 2295) produced less striking results, as shown in figure 4.5. The pS281 antibody detects recombinant FIP3, but not CDK1 phosphorylated FIP3. On incubation of the antibody with the phospho-specific peptide there is a small decrease in signal. On incubation of the antibody with the non-phosphorylated peptide, pS281 again detects recombinant FIP3. However, the specificity of this interaction is not as convincing as for the pS102 antibody. pS281 does not detect GFP-FIP3, which runs just below the 175 kDa marker. It is unclear whether pS281 detects FIP3 in the wild type HeLa lysate. Thus pS281 antibody from rabbit 2295 does not appear to be specific for pS281.

The PCA for phospho-specific antibody to pS348 (from rabbit 2297) is shown in figure 4.6. The pS348 antibody detects recombinant FIP3, but not CDK1 phosphorylated FIP3. On incubation of the antibody with the phospho-specific peptide this is lost. On incubation of the antibody with the non-phosphorylated peptide, p348 again detects recombinant FIP3. pS348 does not appear to detect FIP3 in the GFP-FIP3 HeLa lysate or the wild type HeLa lysate. Thus pS348 antibody from rabbit 2297 could be specific for pS348.

The PCA for phospho-specific antibody to pS451 (from rabbit 2299) is shown in figure 4.7. The pS451 antibody detects recombinant FIP3, but not CDK1 phosphorylated FIP3. On incubation of the antibody with the phospho-specific peptide this reduced. On incubation of the antibody with the non-phosphorylated peptide, p451 again detects recombinant FIP3. pS451 does not appear to detect FIP3 in the GFP-FIP3 HeLa lysate or the wild type HeLa lysate. Thus pS451 antibody from rabbit 2299 could be specific for pS451.

In summary, pS102, pS348 and p451 detect baculovirus Sf9 insect cell expressed human FIP3, and are competed for by the peptides from which the antibodies were generated. pS281 detects FIP3, but the signal is not competed for with the phospho-peptide. These antibodies do not appear to detect phospho-FIP3 in endogenous HeLa lysates. However, it is important to note that our lab, and others, cannot readily detect FIP3 in endogenous HeLa lysates with various antibodies against FIP3. These experiments introduce an interesting result in that pS102 (2294) detects CDK1 phosphorylated FIP3, but pS281, p348 and pS451 do not. This may reflect on our previous findings (presented in section 3.3.6) that cyclin B-CDK1 phosphorylates baculovirus Sf9 insect cell expressed human FIP3 at serine 102, as tested *in vitro*.

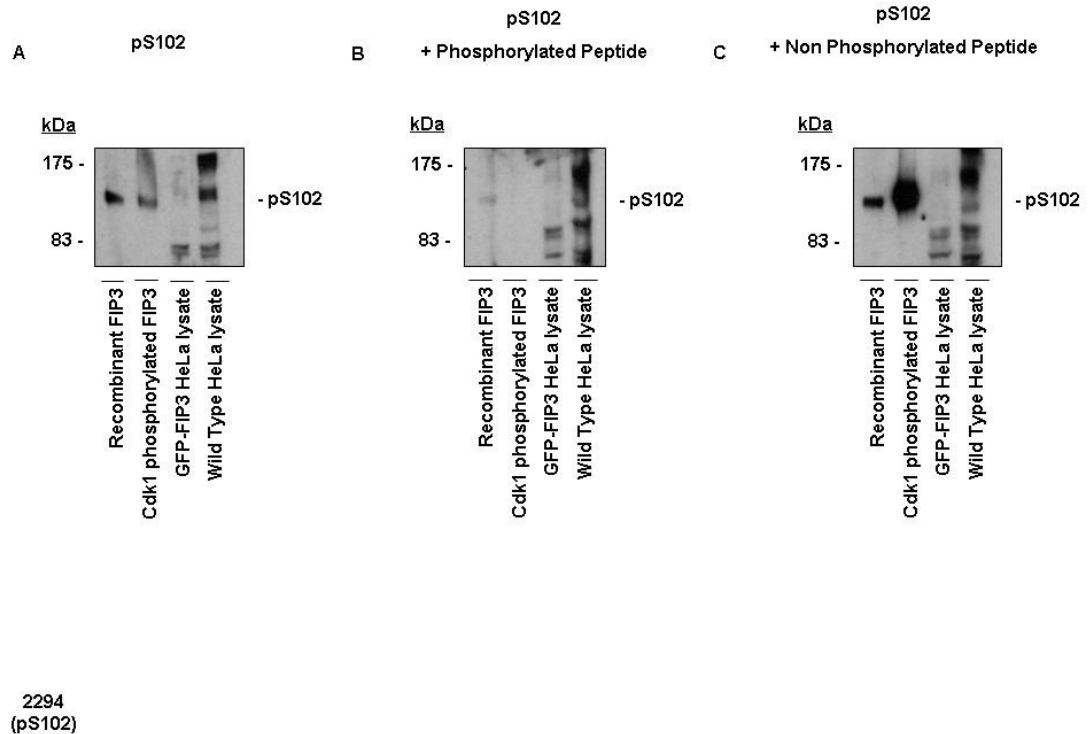


Figure 4-4 FIP3 pS102 peptide competition assay

To validate the specificity of the phospho-specific antibodies, we performed peptide competition assays (PCAs). The protocol used is detailed in section 2.8.3. In brief, various FIP3 samples were separated by SDS-PAGE, as described in section 2.2.2. These were 200ng baculovirus sf9 insect cell expressed FIP3 (Lane 1); 1 μ g CDK1 phosphorylated heat-treated FIP3 (Lane 2); HeLa lysate stably expressing GFP-FIP3 (Lane 3); HeLa lysate (Lane 4). FIP3 proteins were transferred onto nitrocellulose, as described in section 2.2.3, and blocked in PBS-T containing 5% (w/v) non fat milk overnight. This was done in triplicate to produce three identical test samples for analysis by PCA. Three test samples were prepared as follows. Sample A: water only (no peptide control) in a total volume of 1ml PBS-T containing 1% Marvel; sample B: 2.66 μ M phosphorylated peptide to serine 102 in a total volume of 1ml PBS-T containing 1% Marvel; sample C: 2.66 μ M non-phosphorylated peptide to serine 102 in a total volume of 1ml PBS-T containing 1% Marvel. 3ml of a 1:500 dilution of the phospho-specific antibody was added into each of the samples. The tubes were incubated for 2 hours at room temperature with gentle rocking. Samples were centrifuged at 3273 *g* in a refrigerated benchtop centrifuge for 15 minutes at 4 $^{\circ}$ C to pellet any immune complexes. The pre-incubated antibody was added to one of the three identical nitrocellulose membranes for immunoblotting. These were incubated overnight at 4 $^{\circ}$ C and processed for immunodetection using an Amersham ECL Rabbit IgG, HRP-Linked Whole Ab, as described in section 2.2.4. The position of the Broad Range Prestained Protein Marker is illustrated. Representative immunoblots from an experiment performed in duplicate are presented.

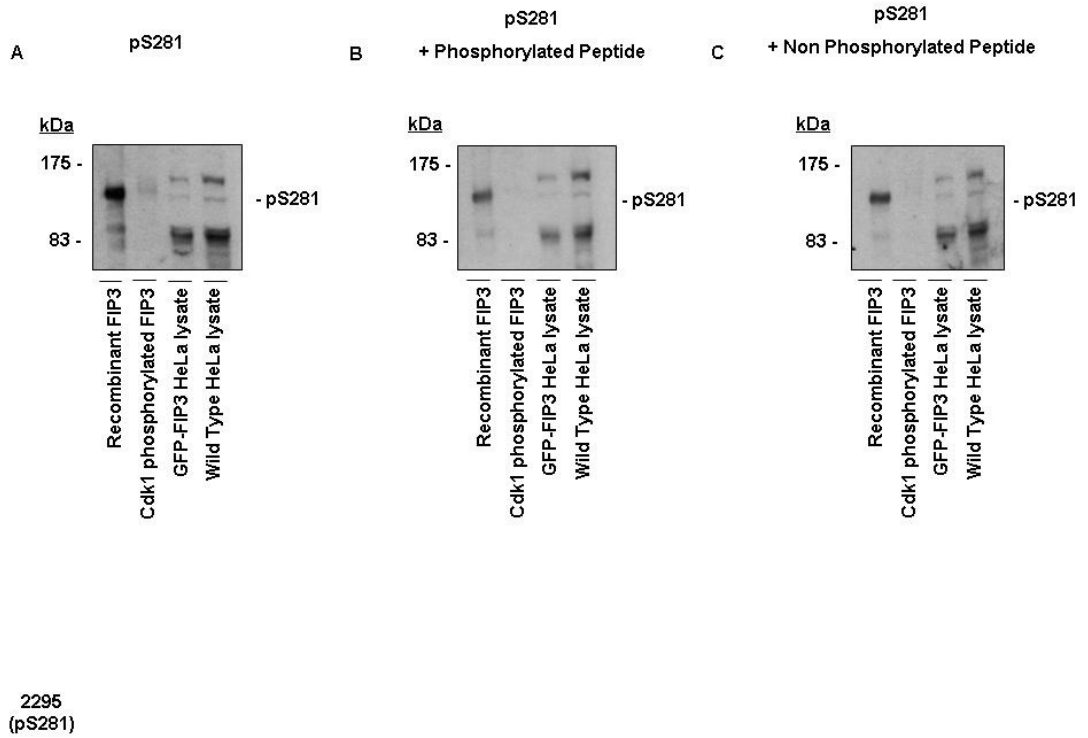


Figure 4-5 FIP3 pS281 peptide competition assay

To validate the specificity of the phospho-specific antibodies, we performed peptide competition assays (PCAs), details of which can be found in the figure legend of Figure 4.4. Representative immunoblots from an experiment performed in duplicate are presented.

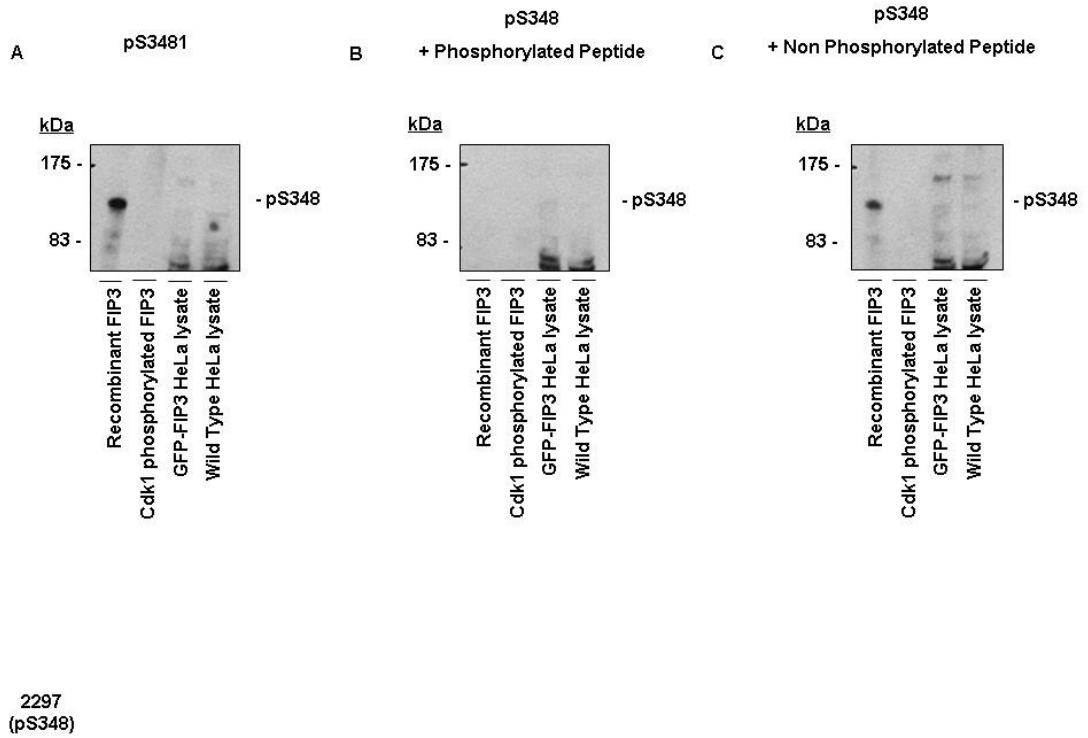


Figure 4-6 FIP3 pS348 peptide competition assay

To validate the specificity of the phospho-specific antibodies, we performed peptide competition assays (PCAs), details of which can be found in the figure legend of Figure 4.4. Representative immunoblots from an experiment performed in duplicate are presented.

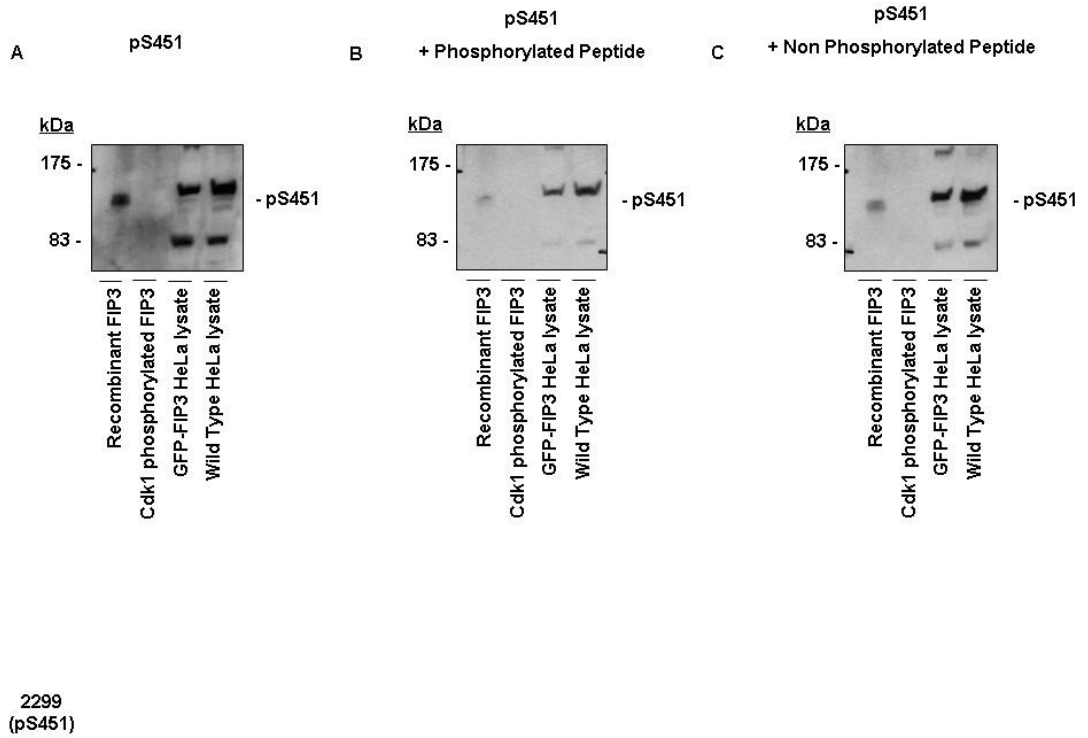


Figure 4-7 FIP3 pS451 peptide competition assay

To validate the specificity of the phospho-specific antibodies, we performed peptide competition assays (PCAs), details of which can be found in the figure legend of Figure 4.4. Representative immunoblots from an experiment performed in duplicate are presented.

4.3.3 Phospho-specific antibody analysis of membrane and cytosol fractions from synchronised GFP-FIP3 expressing HeLa cells

As shown in Figure 4.2, in prometaphase and metaphase FIP3 is cytosolic, but in telophase FIP3 becomes membrane associated. Work from Rytis Prekeris, shown in figure 4.1, has revealed that this association is dependent upon dephosphorylation of FIP3, as phosphatase treatment of cell extracts from metaphase results in FIP3 associating with membranes. Interestingly, FIP3 phosphorylation appears to decrease at telophase.

We have a panel of antibodies generated against phosphorylated serines 102, 281, 348 and 451. We have performed competition assays to validate their specificity. The pS102 antibody has produced the most significant results to date. The immunoblot presented in figure 4.2 was stripped of antibody (section 2.2.5) and reprobed for pS102. The data is presented in figure 4.8, along with the original FIP3 and GFP blots. Figure 4.9 shows the quantification of pS102 expression in the membrane and cytosol fractions of synchronised GFP-FIP3 expressing HeLa cells from figure 4.8. In addition, quantification of pS102 expression in the input fractions of synchronised GFP-FIP3 expressing HeLa cells from figure 4.8 and 4.10D is presented in figure 4.9. In the input, FIP3 levels remain constant throughout the cell-cycle. However, pS102 peaks in metaphase, but decreases towards telophase. pS102 is all but absent in the membrane fraction. In the cytosol fraction pS102 peaks in metaphase, but decreases as the cell progresses through the cell cycle and is present at very low levels in telophase. This adds a new level to the original understanding that FIP3 is phosphorylated in metaphase and dephosphorylated in telophase; serine 102 is likely to be involved.

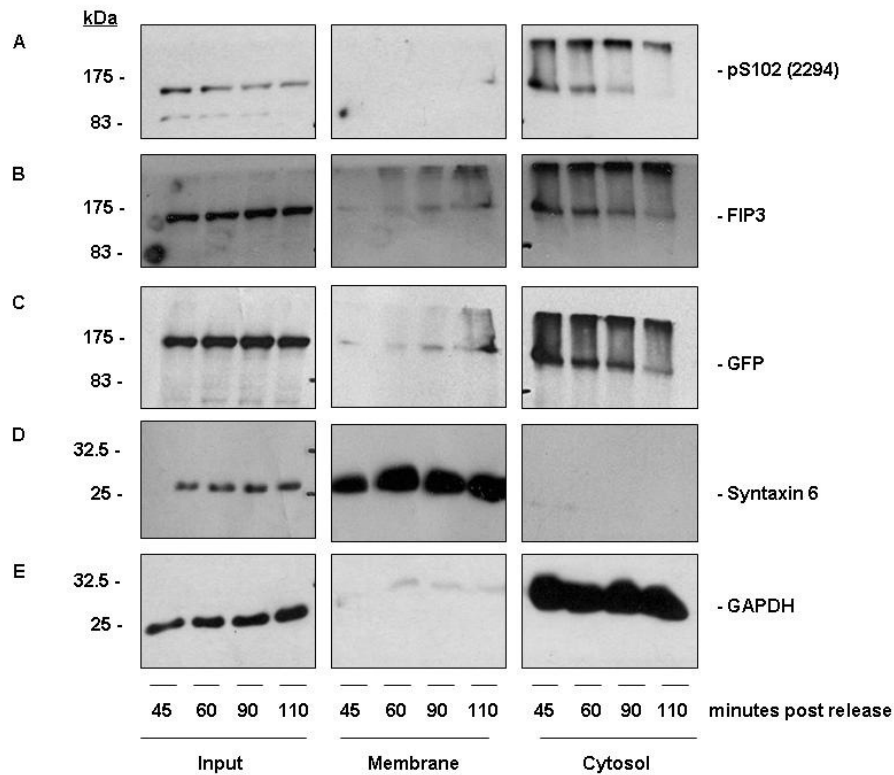


Figure 4-8 Analysis of phosphorylated serine 102 in membrane and cytosol fractionated synchronised GFP-FIP3 expressing HeLa cells

HeLa cells stably expressing GFP-FIP3 were synchronised using a thymidine and nocodazole block, as detailed in section 2.4.5.1. Cells were fractionated using HPFEV buffer and a ball-bearing homogeniser at metaphase (45 minutes) and telophase (90 and 110 minutes), as detailed in section 2.4.8. Proteins were separated by SDS-PAGE, as detailed in section 2.2.2; transferred to nitrocellulose via western blotting, as detailed in section 2.2.3; detection of proteins was performed by immunodetection, as detailed in section 2.2.4. Crude homogenate (input), membrane and cytosol fraction were probed for FIP3, GFP, syntaxin 6 (membrane control) and GAPDH (cytosol control). These immunoblots, previously presented in figure 4.2, were stripped of antibody (section 2.2.5) and reprobed for pS102 (Figure 4.8A). The position of the Broad Range Prestained Protein Marker is illustrated. Samples were run on the same gel, with protein markers separating the input, membrane and cytosol fractions; these have been removed for the purpose of presentation. In the input, FIP3 levels remain constant throughout the cell-cycle. However, pS102 peaks in metaphase, but decreases towards telophase. pS102 is all but absent in the membrane fraction. In the cytosol fraction pS102 peaks in metaphase, but decreases as the cell progresses through the cell-cycle and is present at very low levels in telophase. Data from a single experiment is presented.

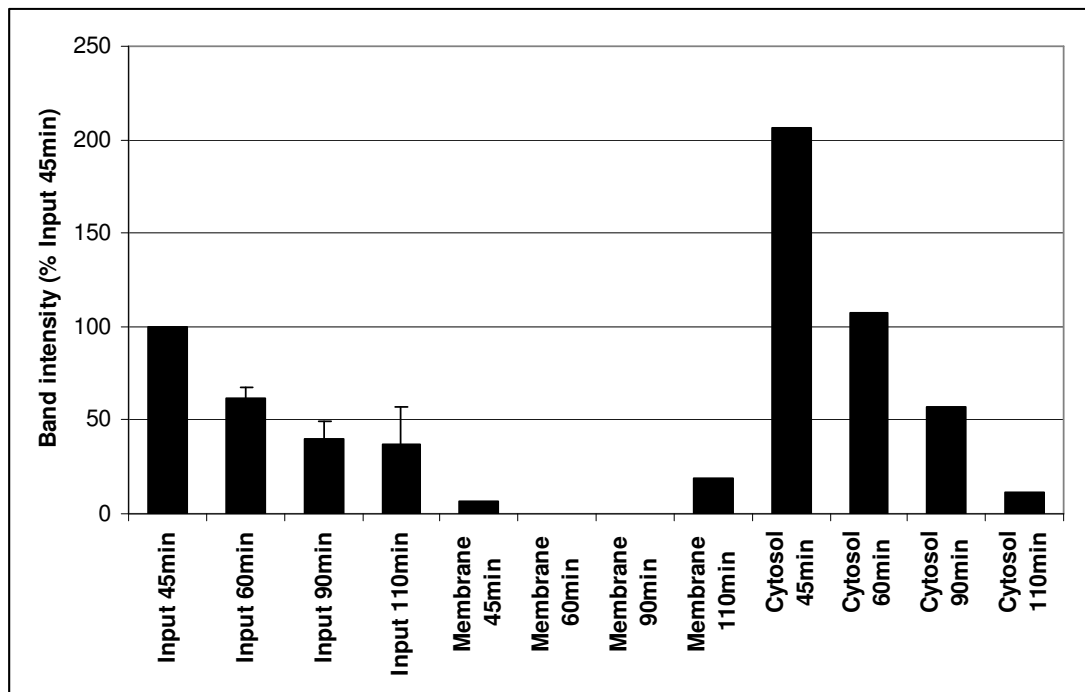


Figure 4-9 Quantification of pS102 expression in the input, membrane and cytosol fractions of synchronised GFP-FIP3 expressing HeLa cells. Input fractions are quantified from pS102 expression from figures 4.8 and 4.10D (data from an experiment performed in duplicate). Membrane and cytosol fractions are quantified from pS102 expression from figure 4.8 (data from a single experiment).

We performed a screen of all phospho-specific antibodies on just the crude homogenate from synchronised GFP-FIP3 expressing HeLa cells. This experiment was repeated in duplicate with consistently similar results; representative immunoblots are presented in figure 4.10. Immunoblots of GFP (Figure 4.10A) and GAPDH (Figure 4.10B) show equal loading of protein. Crude homogenate was also analysed for cyclin B1 expression (Figure 4.10C). Cyclin B1 is the regulatory subunit of CDK1; on activation of this complex the cell enters mitosis (Fung and Poon, 2005). Degradation of cyclin B1 by the APC begins as the last chromosome lines up on the metaphase plate, just after inactivation of the spindle-assembly checkpoint (Clute and Pines, 1999). On destruction of cyclin B1, CDK1 becomes inactivated allowing mitotic exit and cytokinesis. Thus levels of cyclin B1 should be observed to degrade at the metaphase/anaphase transition. Cyclin B1 expression is constant in the 45 and 60 minute fractions, when the cells are in early mitosis. However, as cells enter telophase at approximately 90 to 110 minutes, cyclin B1 expression decreases. As shown previously, pS102 detects GFP-FIP3, the levels of which decrease from 45 minutes to 110 minutes post

release (Figure 4.10D). It is unclear whether pS281 (Figure 4.10E), pS348 (Figure 4.10F) and pS451 (Figure 4.10G) detect the GFP-FIP3 band expected at the 175 kDa marker. However, they detect faint bands just below the 175 kDa marker, but it is unclear whether these relate to FIP3. The intensity of the bands detected by pS281, pS348 and pS451 do not alter during the cell-cycle. Thus, the pS102 antibody, which is specific for phosphorylated serine 102 (validated in section 4.3.2) detects phosphorylated GFP-FIP3, the levels of which are highest in metaphase cell lysates and decrease as the cell progresses through the cell-cycle towards telophase. This result is consistent in repeats of this experiment.

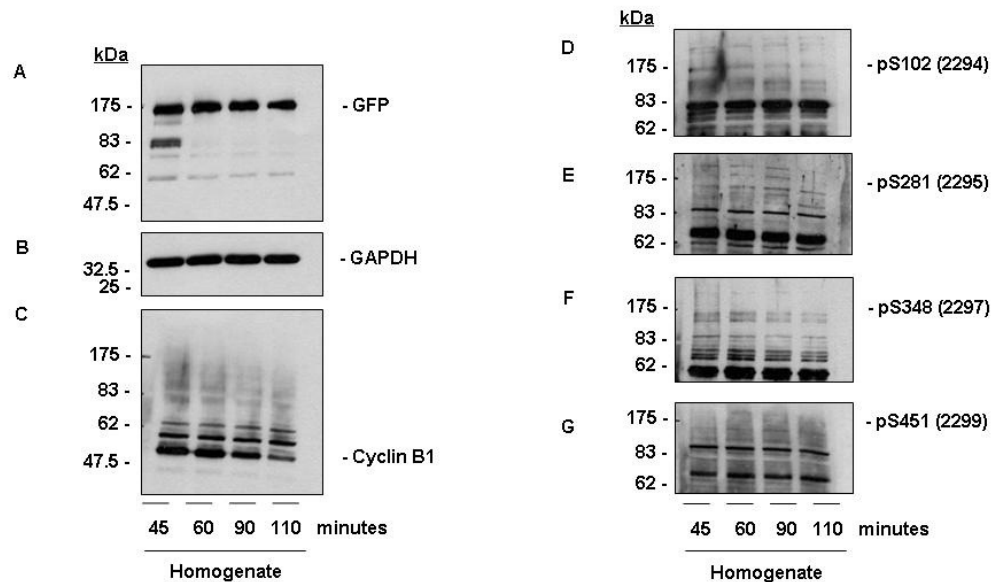


Figure 4-10 Phospho-specific antibody analysis of crude cell homogenate from synchronised GFP-FIP3 expressing HeLa cells

HeLa cells stably expressing GFP-FIP3 were synchronised using a thymidine and nocodazole block, as detailed in section 2.4.5.1. Cells were homogenised using HPFEV buffer and a ball bearing homogeniser at metaphase (45 minutes) and telophase (90 and 110 minutes), as detailed in section 2.4.8. Proteins were separated by SDS-PAGE, as detailed in section 2.2.2; transferred to nitrocellulose via western blotting, as detailed in section 2.2.3; detection of proteins was performed by immunodetection, as detailed in section 2.2.4. Crude homogenate was probed for pS102, pS281, pS348 and pS451. Data from a typical experiment is presented. The position of the Broad Range Prestained Protein Marker is illustrated. Immunoblots of GFP (Figure 4.10A) and GAPDH (Figure 4.10B) show equal loading of protein. Cyclin B1 expression (Figure 4.10C) is level in 45 and 60 minute fractions, but decreases as cells enter telophase. pS102 detects GFP-FIP3, the levels of which decrease from 45 minutes to 110 minutes post release (Figure 4.10D). It is unclear whether pS281 (Figure 4.10E), pS348 (Figure 4.10F) and pS451 (Figure 4.10G) detect GFP-FIP3. Representative immunoblots from an experiment performed in duplicate are presented.

4.3.4 Density gradient analysis of FIP3's association with HeLa membranes

We hypothesised that phosphorylation or dephosphorylation regulates the association of FIP3 with cell membranes. In particular, evidence points to dephosphorylation of FIP3 enabling the protein to interact with the cell membrane. We questioned whether dephosphorylation of FIP3 is simply allowing the protein to bind randomly to membranes or if it is coupled to a change in affinity of FIP3 for the membranes, perhaps by increasing its affinity for proteins such as Rab11.

Recombinant baculovirus Sf9 cell expressed human FIP3 was incubated with either HeLa membranes or protein-free liposomes. These membranes (or vesicles) were then floated up through an Optiprep gradient. Fractions were collected and the distribution of proteins within the gradients was assayed by immunoblotting. A detailed description of the methods used is provided in section 2.4.9 of the materials and methods. This work was carried out with Prof. G.W. Gould. Fractions were separated by SDS-PAGE, as detailed in section 2.2.2. Proteins were transferred to nitrocellulose via Western Blotting, as detailed in section 2.2.3 and immunoblotted for FIP3, as detailed in section 2.2.4. The FIP3 sample that had been incubated with HeLa membranes was blotted for Rab5, as a marker for the position of the membrane fraction in the gradient. Rab5 is a Rab GTPase found on early endosomes, phagosomes, caveosomes and the plasma membrane where it mediates various processes including endocytosis and endosome fusion of clathrin coated vesicles, macropinocytosis and maturation of early phagosomes (Stenmark, 2009).

The resulting immunoblot is presented in figure 4.11, with the bottom and top of the Optiprep density gradient detailed. The experiment was repeated and the same results were obtained. In both the HeLa membrane and the protein-free liposome incubations, FIP3 is found at the bottom of the gradient. However, in the HeLa membrane incubation, Rab5 floated up through the gradient. If FIP3 associated randomly with membranes, then we would expect it to bind to the membranes and float up the Optiprep density gradient and localise to the same fraction as Rab5. However FIP3 was not found in the same fraction as Rab5, thus

suggesting that FIP3 requires association with another protein (for example Rab11) to interact with membranes.

Additionally, recombinant baculovirus Sf9 cell expressed FIP3 is not phosphorylated, as determined by proteomic analysis of the sample, discussed in section 3.3.6. It is hypothesised that FIP3 is phosphorylated in metaphase and cytosolic; dephosphorylation allows FIP3 to associate with the membranes in telophase. This experiment shows that dephosphorylated FIP3 does not randomly associate with cell membranes. Thus we suggest that the dephosphorylation event required for membrane association must in some way be coupled to a change in affinity for membranes, perhaps affinity for another protein, such as Rab11.

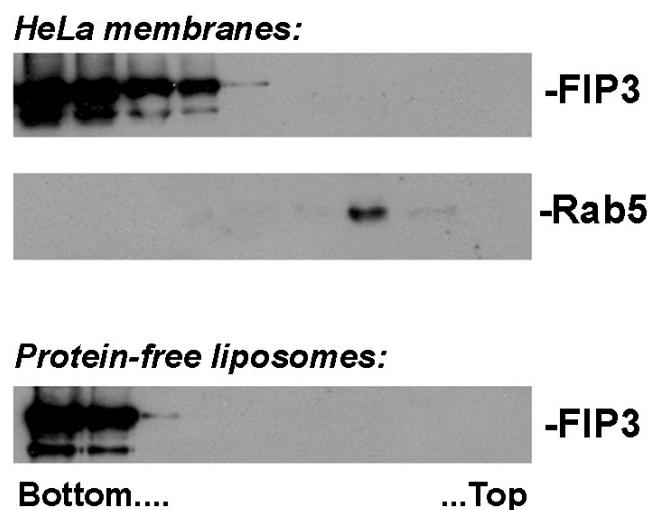


Figure 4-11 Density gradient analysis of FIP3's association with HeLa membranes
 Recombinant baculovirus Sf9 cell expressed FIP3 was incubated with either HeLa membranes or protein-free liposomes. These membranes (or vesicles) were then floated up through an Optiprep gradient. Fractions were collected and the distribution of proteins within the gradients was assayed by immunoblotting. A detailed description of the methods used is provided in section 2.4.9 of the materials and methods. Fractions were separated by SDS-PAGE, as detailed in section 2.2.2. Proteins were transferred to nitrocellulose via Western Blotting, as detailed in section 2.2.3 and immunoblotted for FIP3, as detailed in section 2.2.4. The FIP3 sample incubated with HeLa membranes was blotted for Rab5, as a marker for endocytic membranes. The bottom and top of the Optiprep density gradient is marked. Representative immunoblots from an experiment performed in duplicate are presented.

4.3.5 Effect of kinase inhibition on GFP-FIP3 localisation in HeLa cells

FIP3 has been identified as a phospho-protein (R. Prekeris, personal communication). We have shown that CDK1 phosphorylates recombinant FIP3 *in vitro* (discussed in section 3.3.6). We next sought to explore if CDK1 influences the localisation of FIP3. Initial studies have been performed, employing the use of kinase inhibitors to study the effect of kinase inhibition on the localisation of GFP-FIP3, stably expressed by HeLa cells.

First we incubated non-synchronised GFP-FIP3 expressing HeLa cells, overnight, with a range of kinase inhibitors. These were 100µM Y-27632 (Uehata *et al.*, 1997; Ishizaki *et al.*, 2000), 10µM PD 98059 (Dudley *et al.*, 1995; Alessi *et al.*, 1995), 200µM BMI-1026 (Seong *et al.*, 2003), 2µM ZM 447439 (Ditchfield *et al.*, 2003) and 0.15% (v/v) or 0.5% (v/v) DMSO. Details of inhibitors and their suppliers are listed in section 2.1.9. The concentrations were chosen from a review of the literature. Cells were plated onto ethanol sterilised glass coverslips and incubated for 24 hours in 5% (v/v) CO₂ at 37°C. Following this, media was replaced with fresh media containing the inhibitors. After incubating for 24 hours, cells were fixed with 4% (w/v) p-formaldehyde and stained for alpha-tubulin and DAPI, as described in section 2.5. This work was performed in conjunction with Dr. J. Matheson. It was noted that the localisation of GFP-FIP3 in telophase cells predominantly fell into one of two categories: early telophase (figure 4.12A) or late telophase (figure 4.12B). We sought to quantify the proportion of cells in each stage of telophase, for each inhibitor and DMSO control. The results are presented in figure 4.13. Treatment with DMSO resulted in 65 to 80% of telophase cells in late telophase. The Aurora B inhibitor, ZM 447439, produced a similar effect. Inhibiting ROCK (Y-27632) or MEK (PD 98059) resulted in an equal proportion of cells in early and late telophase. Interestingly, inhibiting CDK1 with BMI-1026 resulted in only 30% of cells reaching late telophase. This perhaps suggests that by inhibiting CDK1 there is a mis-localisation of GFP-FIP3 or a delay in cytokinesis.

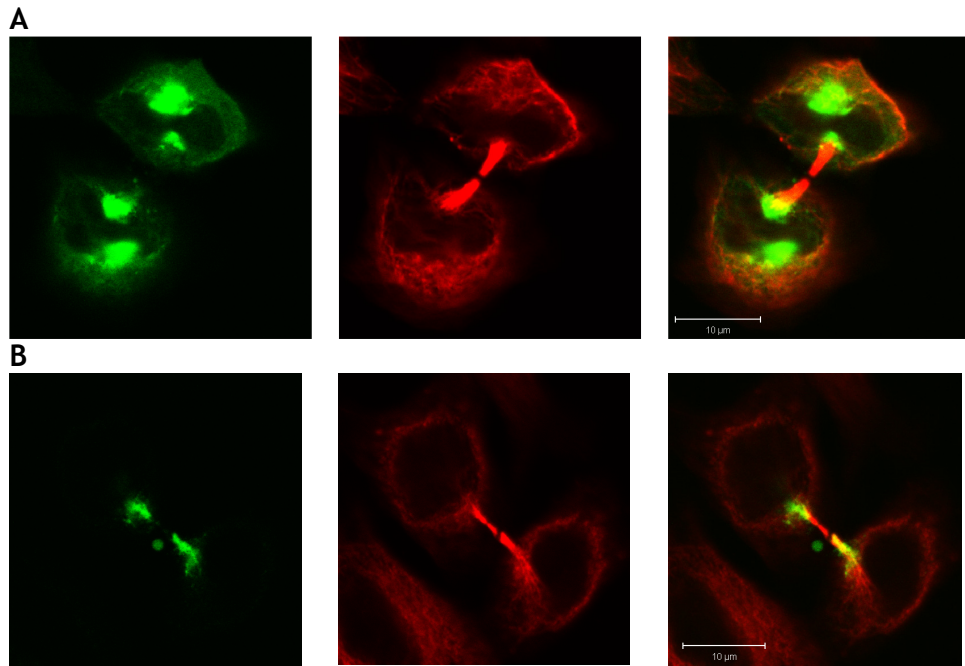


Figure 4-12 Telophase localisations of GFP-FIP3 in HeLa cells

HeLa cells were transfected with a GFP-FIP3 expressing plasmid (detailed in section 2.1.5), as described in section 2.4.6. Cells were fixed with 4% (w/v) ρ -formaldehyde and processed for immunofluorescence 48 hours after transfection (section 2.5). Cells were stained for microtubules using a rat monoclonal antibody to α -Tubulin, followed by Alexa Fluor® 568 (red channel). Mounted coverslips were analysed using a 63x Zeiss oil immersion objective on a Zeiss confocal microscope (Carl Zeiss, Germany) equipped with Zeiss LSM5 Pascal instrument. Zeiss Pascal software was used to collect and edit images. Panel A shows a GFP-FIP3 expressing HeLa cell in an early stage of telophase. Panel B shows a GFP-FIP3 expressing HeLa cell in a late stage of telophase.

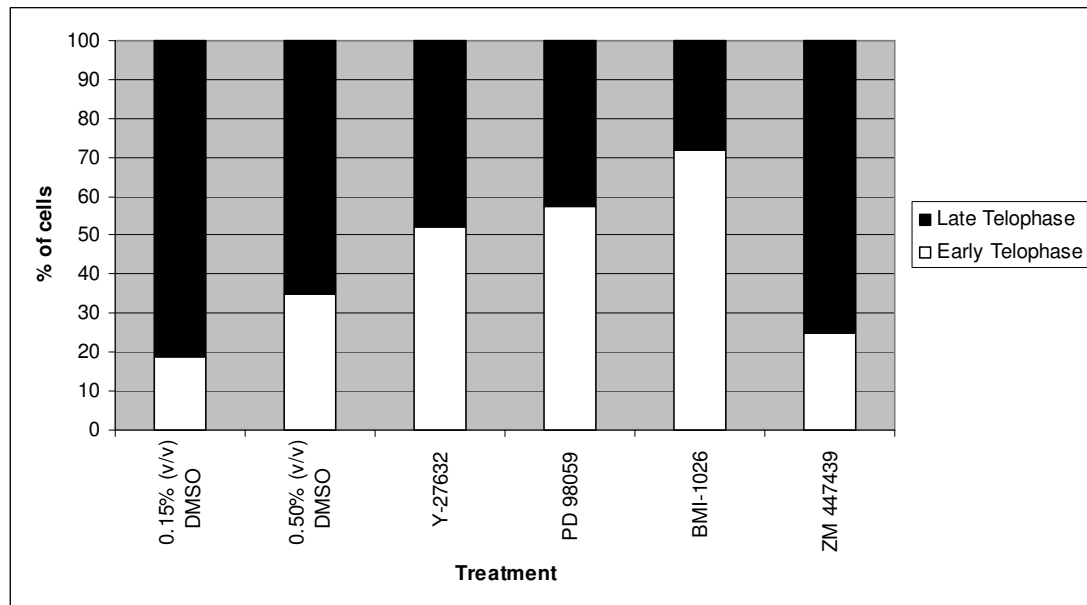


Figure 4-13 Effect of kinase inhibition on the localisation of GFP-FIP3 in non-synchronised HeLa cells

Non-synchronised GFP-FIP3 stably expressing HeLa cells were grown on coverslips for 24 hours, then incubated overnight with a range of kinase inhibitors. These were 100 μ M Y-27632, 10 μ M PD 98059, 200 μ M BMI-1026, 2 μ M ZM 447439 and 0.15% (v/v) or 0.5% (v/v) DMSO. Cells were fixed with 4% (w/v) ρ -formaldehyde and stained for alpha-tubulin and DAPI. The proportion of GFP-FIP3 expressing telophase cells in either early telophase or late telophase was quantified. Approximately 200 cells per condition were counted. Inhibiting CDK1 with BMI-1026 resulted in approximately 30% of cells in late telophase, compared to the DMSO controls of 65-80%. Data from a single experiment is presented.

We next sought to study the potential mis-localisation of GFP-FIP3 in CDK1-treated HeLa cells further. HeLa cell stably expressing GFP-FIP3 were synchronised using a thymidine, nocodazole and MG132 block, as described in section 2.4.5.2 of the materials and methods (Petronczki *et al.*, 2007). MG132, a reversible inhibitor of the proteasome, arrests cells in a metaphase-like state, and on release, cells enter a synchronous wave of anaphase. Following the two hour incubation with 10 μ M MG132 synchronised GFP-FIP3 expressing cells were harvested via shake off and washed with PBS, followed by warm media and plated onto ethanol sterilised glass coverslips. Cells were incubated for 10 minutes, before a selection of kinase inhibitors were added. We used 50nM BMI-1026, 50 μ M PD 98059 and a DMSO only control. Cells were incubated for 20, 30, 45, 60, 70, 80 and 90 minutes (including the 10 pre-inhibitor incubation) before cells were fixed with 4% (w/v) ρ -formaldehyde and stained for alpha-tubulin and DAPI, as described in section 2.5. Again we quantified the proportion of cells in early or late telophase. This work was carried out in conjunction with Dr. J. Matheson and the data is presented in figure 4.14. Cells released from the block

for less than 60 minutes were not captured as they may have been washed away during the fixation procedure. Approximately 60 to 70% of cells treated with DMSO and released for 60 to 90 minutes were in late telophase. This was similar to the previous experiment. In PD 98059 treated cells, this decreased marginally to 50 to 60% in late telophase, a result similar to the previous experiment. Interestingly, in BMI-1026 treated cells released for 60 to 70 minutes, approximately 20% of cells were in late telophase. At 80 to 90 minutes post release, this increased to 30 to 40% of cells in late telophase. This is again similar to the previous experiment.

These preliminary kinase inhibition studies have produced an interesting result. Our first experiment shows that an overnight incubation of non-synchronised GFP-FIP3 expressing HeLa cells with BMI-1026 (CDK1 inhibitor) resulted in approximately 30% cells in late telophase, in contrast to 65 to 80% of DMSO treated cells. Our next experiment developed this further by synchronising cells stably expressing GFP-FIP3 using a thymidine, nocodazole and MG-132 block. In approximately 20 to 40% of cells were in late telophase following BMI-1026 treatment. In contrast, 60 to 70% of DMSO cells were in late telophase. Such data suggests that CDK1 inhibition results in mis-localisation of GFP-FIP3 in HeLa cells or a delay in cytokinesis.

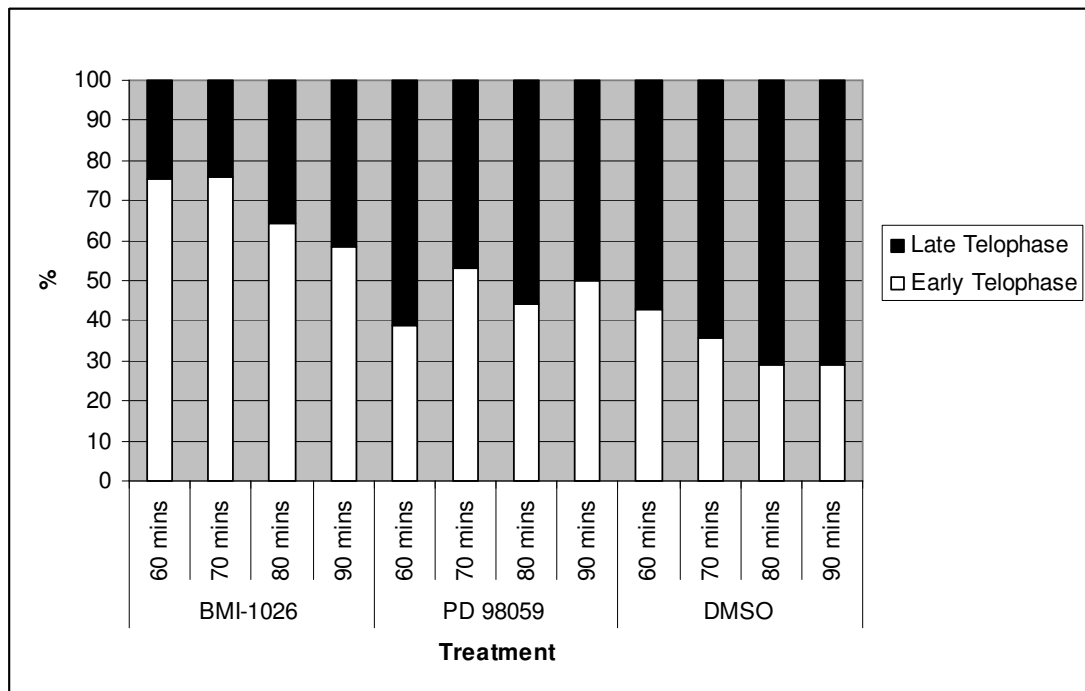


Figure 4-14 Effect of kinase inhibition on the localisation of GFP-FIP3 in synchronised HeLa cells

HeLa cells stably expressing GFP-FIP3 were synchronised using a thymidine, nocodazole and MG-132 block, as described in section 2.4.5.2 of the materials and methods. Synchronised cells were harvested via shake plated onto ethanol sterilised glass coverslips. Cells were incubated for 10 minutes, before a selection of kinase inhibitors were added: 50nM BMI-1026, 50 μ M PD 98059 and a DMSO only control. Cells were incubated for 60, 70, 80 and 90 minutes (including the 10 pre-inhibitor incubation) before coverslips were fixed with 4% (w/v) ρ -formaldehyde and stained for alpha-tubulin and DAPI, as described in section 2.5. The proportion of GFP-FIP3 expressing cells in early or late telophase was quantified. Approximately 200 cells per condition were counted. In BMI-1026 treated cells released for 60-70 minutes, approximately 20% of cells were in late telophase. At 80 to 90 minutes post release, this increased slightly to 30 to 40%. In contrast, 60 to 70% of cells treated with DMSO and released for 60 to 90 minutes were in late telophase. Data from a single experiment is presented.

4.4 Conclusions

The regulatory controls governing the spatial and temporal regulation of FIP3 during mitosis are unknown. A potential candidate is phosphorylation, since phosphorylation is a commonly used control mechanism in mitotic regulation (Morgan, 2007). FIP3 has been identified as a phospho-protein (R. Prekeris, personal communication) and four potential phosphosites have been mapped (serines 102, 281, 348 and 451). During prometaphase and metaphase, FIP3 is cytosolic, but in telophase FIP3 becomes membrane associated. This work was performed by Prekeris *et al.*, and subsequently replicated in this thesis. The association with membranes is dependent upon dephosphorylation of FIP3, as phosphatase treatment of cell extracts from metaphase results in FIP3 associating with membranes, and FIP3 phosphorylation appears to decrease at telophase (R. Prekeris, personal communication). Such data offer the hypothesis that FIP3 is phosphorylated during early stages of the cell-cycle, and that dephosphorylation of FIP3 is the trigger for the association of FIP3 with membranes. This may have implications for the regulation of FIP3's dynamics during the cell-cycle.

To explore the role of phosphorylation in the regulation of FIP3's dynamics, a panel of antibodies to serines 102, 281, 348 and 451 were generated. One antibody produced significant results. The antibody to pS102 detected baculovirus Sf9 insect cell expressed human FIP3 and CDK1 phosphorylated FIP3; this was competed for by the phospho-peptide from which the antibody was generated, thus signifying specificity. Interestingly, the antibody to pS102 detected CDK1 phosphorylated FIP3, but pS281, p348 and pS451 did not. This may reflect on our previous findings (presented in section 3.3.6) that cyclin B-CDK1 phosphorylates baculovirus Sf9 insect cell expressed human FIP3 at serine 102, as tested *in vitro*. This antibody was used in the analysis of crude homogenate from synchronised GFP-FIP3 expressing HeLa cells, showing that serine 102 is phosphorylated in metaphase and becomes dephosphorylated as the cell progresses through to telophase. Further analysis of membrane and cytosol fractions from these cells reveal that cytosolic levels of pS102 peak in metaphase and decrease towards telophase to negligible levels. pS102 is absent in the membrane fraction. This work suggests that FIP3 may be directly

phosphorylated by CDK1 at serine 102 in early mitosis. This may affect the membrane and cytosol distribution of FIP3 by preventing membrane association of FIP3 in metaphase. Cyclin B1-CDK1 is inactivated at the metaphase/anaphase transition (Fung and Poon, 2005), which is reflected in the dephosphorylation of pS102 that we observe in the crude cell homogenate of HeLa cells in telophase. The phospho-specific antibody for pS102 was used in an attempt to study the localisation of this phosphorylated form of FIP3 during the cell-cycle, via immunofluorescence. However, this antibody did not produce good quality immunofluorescence labelling, and this was not pursued further.

Preliminary kinase inhibition studies have produced an interesting result. Inhibition of CDK1 by the inhibitor BMI-1026 (Seong *et al.*, 2003) resulted in a mis-localisation of GFP-FIP3 in HeLa cells compared to a DMSO control. Inhibition of CDK1 appeared to result in fewer cells displaying the late telophase distribution of GFP-FIP3, where the protein is found in the intracellular bridge at either side of the midbody. Instead more cells were found with GFP-FIP3 at the centrosomes and at either side of the intracellular bridge, which is characteristic for cells in an earlier stage of telophase. While this finding is preliminary, it was observed in multiple experiments and perhaps suggests that CDK1 may influence the localisation of FIP3. Interestingly, work from our lab has produced similar results for another kinase. On knockdown of Aurora B with RNAi, a similar mis-localisation of GFP-FIP3 was observed (Simon *et al.*, 2008). This work contains one caveat. CDK1 is chiefly responsible for the orchestration of mitosis (Nigg, 2001) and perhaps by inhibiting the action of this kinase, other factors in the cell may have been disrupted, leading to mis-localisation of FIP3. Also important to note is that our work with CDK1 inhibition revealed a delay in mitosis, with more cells in the earlier stages of telophase. However, it is well documented that CDK1 inhibition by BMI-1026 forces cells to exit mitosis (Niiya *et al.*, 2005; Petronczki *et al.*, 2007).

This work does not reveal if the control of localisation of FIP3 by CDK1 is due to direct phosphorylation of FIP3 or an indirect one. Perhaps dephosphorylation alters the affinity of FIP3 for another protein such as Rab11. Significantly we found that dephosphorylated recombinant FIP3 does not interact randomly with HeLa membranes when subject to density gradient analysis. Thus we suggest that dephosphorylation required for membrane association must in some way be

coupled to a change in affinity for membranes, perhaps affinity for another protein, such as Rab11 (Prekeris *et al.*, 2001; Eathiraj *et al.*, 2006; Shiba *et al.*, 2006), ARF6 (Shin *et al.*, 2001; Fielding *et al.*, 2005), CYK-4 (Simon *et al.*, 2008) and ASAP1 (Inoue *et al.*, 2008) which have been found to interact with FIP3.

The effect of kinase inhibition on the localisation of GFP-FIP3 warrants further analysis. The inhibitors could be used at different concentrations to the ones used in this study. A study of the effects of the ROCK inhibitor Y-27632 on HeLa cells demonstrated a positive correlation between the number of binuclear cells and the concentration of the inhibitor (Ishizaki *et al.*, 2000). The concentration of BMI-1026 used in the first kinase inhibitor study may have been too high since we used BMI-1026 in the micromolar range, whereas other groups have used it in the nanomolar range (Seong *et al.*, 2003; Petronczki *et al.*, 2007). However, this was corrected in the second study. Further work should explore, via time lapse microscopy, of the effect of BMI-1026 on GFP-FIP3 localisation. Initial studies were made to analyse the effect of kinase inhibition on the membrane and cytosol ratio of GFP-FIP3. However, owing to time limitations this was not pursued further.

In summary, during prometaphase and metaphase, FIP3 is cytosolic, but in telophase FIP3 becomes membrane associated. The antibody to pS102 specifically detected baculovirus Sf9 insect cell expressed human FIP3 and CDK1 phosphorylated FIP3, but antibodies to pS281, p348 and pS451 did not. Serine 102 is phosphorylated in metaphase and becomes dephosphorylated as the cell progresses through to telophase. Cytosolic levels of pS102 peak in metaphase and decrease towards telophase to negligible levels. pS102 is absent in the membrane fraction. This work suggests that FIP3 may be directly phosphorylated by CDK1 at serine 102. Inhibition of CDK1 by the inhibitor BMI-1026 resulted in a mis-localisation of GFP-FIP3 in HeLa cells, as fewer cells displayed the late telophase distribution of GFP-FIP3, compared with the DMSO control. CDK1 inhibition appeared to delay cytokinesis, causing more cells to display an earlier telophase distribution of GFP-FIP3. Thus we have explored the role of phosphorylation in the distribution of FIP3 to the membrane and cytosol and have identified serine 102 of FIP3 as potentially an important residue in this system. This may impact on the spatial and temporal regulation of FIP3 during the cell-cycle. However, many questions remain unanswered. Importantly,

questions still remain as to the mode of interaction between FIP3 and the membrane, and the role of phosphorylation in the cycling of FIP3 on and off the membrane. Significantly, dephosphorylated recombinant FIP3 does not interact randomly with HeLa membranes, suggesting that dephosphorylation required for membrane association must in some way be coupled to a change in affinity for membranes, perhaps affinity for another protein, such as Rab11.

5 Analysis of Rab11-FIP3 phosphosites

5.1 Introduction

Rab11-FIP3 (FIP3) undergoes spatial and temporal regulation during mitosis (Wilson *et al.*, 2005). A potential candidate for the regulation of FIP3 is phosphorylation, since phosphorylation is a commonly used control mechanism in mitotic regulation (Morgan, 2007). As discussed in chapters 3 and 4, work from a collaborating lab proposes that FIP3 phosphorylation and dephosphorylation may be a regulator of FIP3 localisation (R. Prekeris, personal communication) and mass spectrometry analysis of FIP3 immunoprecipitated from metaphase cells has identified four phosphorylation sites: serines 102, 281, 348 and 451. The significance of these phosphosites in the spatial and temporal regulation of FIP3 during mitosis remains unknown.

5.2 Aims

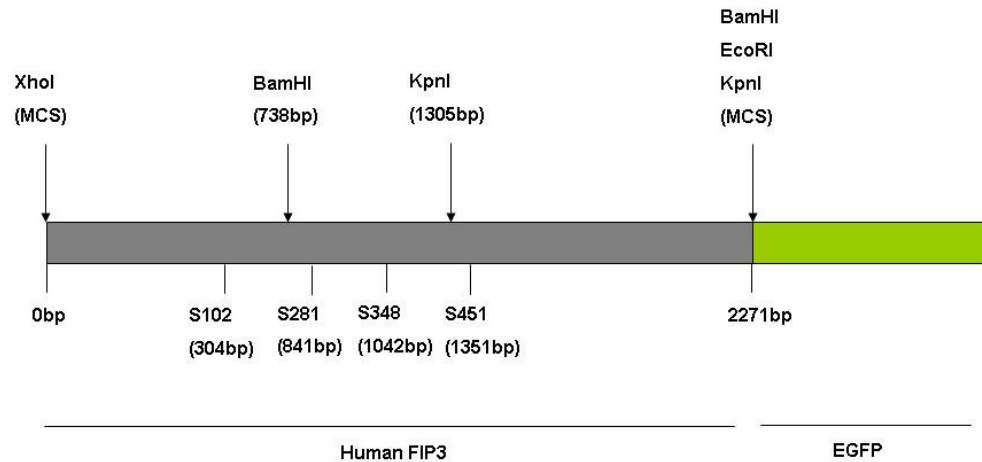
This chapter aims to analyse the role of FIP3 phosphorylation at serines 102, 281, 348 and 451 through the creation of phospho-null and phospho-mimetic mutants. Serines 102, 281, 348 and 451 were mutated to alanine (phospho-null) and aspartic acid (phospho-mimetic). These mutations were carried out in the pEGFP-N1 plasmid, containing the coding sequence for human FIP3. The aim was to study the role of the various phosphorylation sites of FIP3 through the analysis of the cell-cycle dependent subcellular localisation of each phospho-mutant protein. We also sought to determine whether mutation of any phosphosite had an effect on cytokinesis.

5.3 Methods

5.3.1 Site directed mutagenesis

Mutants were generated via site directed mutagenesis (SDM). This was carried out in the context of pEGFP-N1 plasmid, containing the coding sequence for human FIP3 which had been cloned into the multiple cloning site of the plasmid via XhoI (N-terminus of FIP3) and EcoRI (C-terminus of FIP3). This plasmid is

hereafter referred to as GFP-FIP3 and is detailed in section 2.1.5 of the materials and methods. A schematic figure of the GFP-FIP3 plasmid is provided in figure 5.1 and includes restriction sites used throughout this work.



pEGFP-N1 vector
4.7kb

Figure 5-1 Schematic figure of the GFP-FIP3 plasmid.

The coding sequence of human FIP3 was cloned into the multiple cloning site of the pEGFP-N1 plasmid via XhoI (N-terminus of FIP3) and EcoRI (C-terminus of FIP3). This plasmid is hereafter referred to as GFP-FIP3 and is detailed in section 2.1.5 of the materials and methods. Sites of digest by the restriction enzymes used in this work are detailed.

SDM was carried out according to the QuickChange® method from Stratagene. SDM was initially performed using Pfu DNA polymerase (Promega) and then PfuTurbo DNA polymerase (Stratagene). However, no mutants were generated. Analysis of the DNA sequence reveals that FIP3 is GC rich, particularly at the N-terminus where some of the potential phospho-sites are located. Addition of DMSO or glycerol into the SDM reaction mixture did not generate mutants. Next we investigated different polymerases. HotStarTaq DNA Polymerase (QIAGEN) yielded colonies on DpnI treated plates, but these proved to be wild-type. This is possibly due to this enzyme's lack of 3' to 5' exonuclease proofreading ability. Advantage® GC Genomic LA Polymerase Mix from Clontech has proofreading ability and was used in this project to successfully generate mutants. The basic

protocol is provided in section 2.3.1 of the materials and methods. However, this produced only some of the mutants required. Thus the modified protocols for phospho-mimetic and phospho-neutral mutants of serines 102, 281, 348 and 451 are provided in section 5.3.4.

5.3.2 Validation of mutant plasmids

Various problems were encountered during the generation of the mutants. Some mutants had insertions or deletions of DNA in their sequence. In addition, some mutants were generated which did not fluoresce when transfected into HeLa cells. Thus, measures were undertaken to ensure the mutant plasmid DNA produced a FIP3 protein of the correct molecular weight, which fluoresced on expression in HeLa cells.

Firstly, following mutagenesis, potential mutant DNA preparations were digested with XhoI and EcoRI to check for the presence of insertions or deletions in the DNA sequence. A protocol for digestion is detailed in section 2.3.5 of the materials and methods. DNA digestion products were separated by agarose gel electrophoresis, as detailed in section 2.3.7. Mutated GFP-FIP3 plasmids which contained a FIP3 insert of the correct length were transformed into HeLa cells, as outlined in section 2.4.6. Plasmids were transfected into cells grown on glass coverslips and processed for immunofluorescence by fixing with 4% (w/v) ρ -formaldehyde and mounting onto glass slides, as detailed in section 2.5.1. This ensured that all potential mutant plasmids produced a GFP-tagged protein which fluoresced. Plasmids were also transfected into HeLas and lysed, as detailed in section 2.4.7. Lysates were then separated by SDS-PAGE (2.2.2), transferred onto nitrocellulose via western blotting (2.2.3) and immunoblotted for GFP (2.2.4) to check the size of the expressed protein. If the plasmids were shown to produce a protein which expressed a fluorescent GFP tag and had the expected molecular weight, then one plasmid was sent for DNA sequencing (2.3.10) to ensure the generated plasmid was mutant.

5.3.3 Cloning of BamHI fragments into GFP-FIP3 or pCR3.1

For many of the mutants generated, insertions or deletions of DNA were present in the N-terminus of FIP3. These aberrations could be digested from the plasmid

by BamHI, which cuts the FIP3 sequence at position 738bp and is present in the MCS of pEGFP-N1, at the C-terminus of FIP3. This is detailed in figure 5.1. Thus the BamHI fragment containing the mutant could be ligated into wild type GFP-FIP3. In addition, some mutants were generated using a plasmid constructed from the BamHI fragment of GFP-FIP3 and BamHI digested pCR3.1. On generation of a mutant from this construct, the BamHI fragment containing the mutant was ligated into wild type GFP-FIP3. A brief outline of the protocol used is provided below.

The GFP-FIP3 plasmid containing the site of interest ('insert') and wild type GFP-FIP3 plasmid or pCR3.1 plasmid ('vector') were digested with BamHI, according to section 2.3.5. The products of digestion were separated by agarose gel electrophoresis, as detailed in section 2.3.7. The bands corresponding to the vector (minus its BamHI fragment) and the insert were excised and DNA was extracted according to section 2.3.8. To prevent the re-ligation of linearised plasmid DNA, gel purified 'vector' DNA was treated with Shrimp Alkaline Phosphatase (section 2.3.9). 'Insert' and 'vector' DNA were ligated (section 2.3.6) and the entire ligation transformed into Top10 cells (section 2.3.2). DNA was isolated from individual colonies via a small scale DNA preparation (section 2.3.3).

For the mutants which were constructed via ligation of BamHI fragments into fresh GFP-FIP3, the construct was digested with XhoI and EcoRI. This ensured that the modified FIP3 sequence did not contain any insertions or deletions of DNA. Plasmids of the correct length were digested with KpnI which cuts FIP3 at 1305bp and at the MCS of pEGFP-N1, towards the C-terminus of FIP3. This is detailed in figure 5.1. KpnI digestion verified that the FIP3 fragment had been cloned into the fresh vector in the correct orientation. Following this, mutants were validated according to section 5.3.2.

The plasmid constructed from the BamHI fragment of GFP-FIP3 and pCR3.1 was digested with BamHI to check for presence of the insert. This construct was then used in some SDM reactions and is hereafter referred to as BamHI-FIP3-pCR3.1.

5.3.4 Generation of phospho-mutant GFP-FIP3 plasmids

5.3.4.1 Generation of GFP-FIP3-S102A and GFP-FIP3-S102D plasmids

To generate GFP-FIP3-S102A we modified the basic SDM protocol provided in section 2.3.1 of the materials and methods: dNTPs were used at a concentration of 0.8mM each; primers were used at a concentration of 0.4µM each; 50ng of GFP-FIP3 was used as a template. The thermocycling conditions used for this SDM were as follows.

<u>94° C 3 min</u>	}	30 cycles
94° C 1 min		
55° C 30 sec		
<u>68° C 16 min</u>		
68° C 5 min		
4° C Hold		

Generation of GFP-FIP3-S102D proved to be challenging. Numerous attempts were made at modifying the basic SDM strategy, but this yielded no mutants. We next cloned XhoI/BstXI wild-type GFP-FIP3 fragment into XhoI/BstXI digested pCR3.1 and performed mutagenesis in this vector. BstXI digests GFP-FIP3 at 990 bp. However, creating this plasmid did not help since we believe the problems encountered during SDM of FIP3 occurred in the GC rich N-terminal domain. Next we tried to use GFP-FIP3-S102A as template for SDM, but this did not yield mutants. GFP-FIP3-S102D was therefore made using GFP-FIP3 as the template by Dundee Cell Products Ltd, Dundee, UK.

The mutated plasmids were verified, as detailed in section 5.3.2.

5.3.4.2 Generation of GFP-FIP3-S281A and GFP-FIP3-S281D plasmids

For GFP-FIP3-S281A we modified the basic SDM protocol provided in section 2.3.1 of the materials and methods: dNTPs were used at a concentration of 0.4mM each; primers were used at a concentration of 0.5µM each; 50ng GFP-FIP3 was used as template. The thermocycling conditions used for SDM were as follows.

95° C 5 min
95° C 1 min
60° C 30 sec
72° C 14 min } 30 cycles
72° C 5 min
4° C Hold

On verification of the mutant by DNA sequencing, we checked the DNA for any insertions or deletions. A double digest was performed using XhoI and EcoRI and the DNA products were separated by agarose gel electrophoresis, according to sections 2.3.5 and 2.3.7 of the materials and methods. This showed that there was a deletion of DNA as the XhoI/EcoRI fragment size was shorter than expected. A BamHI digest, which cuts the plasmid at 738bp of FIP3 and at the MCS, towards the C-terminus of FIP3, produced the expected insert. Thus the deletion of DNA had occurred N-terminal to 738bp. We cut out the BamHI fragment which contained the mutant and ligated it into fresh GFP-FIP3. This method is outlined in section 5.3.3.

For GFP-FIP3-S281D we modified the basic SDM protocol provided in section 2.3.1 of the materials and methods: dNTPs were used at a concentration of 0.8mM each; primers were used at a concentration of 0.8µM each; 50ng template was used. The thermocycling conditions used for site directed mutagenesis were as follows.

95° C 5 min
95° C 1 min
60° C 1 min
72° C 20 min } 30 cycles
72° C 5 min
4° C Hold

The mutated plasmids were verified, as detailed in section 5.3.2.

5.3.4.3 Generation of GFP-FIP3-S348A and GFP-FIP3-S348D plasmids

Various attempts were made at generating GFP-FIP3-S348A, each of which produced insertions of DNA towards the N-terminus of FIP3. To resolve this issue, we cloned a BamHI fragment from the wild-type GFP-FIP3 plasmid into BamHI digested pCR3.1 vector and performed mutagenesis in the absence of the N-terminus of FIP3. The methods used to produce the BamHI-FIP3-pCR3.1 construct are detailed in section 5.3.3. We modified the basic SDM protocol provided in section 2.3.1 of the materials and methods to the following: dNTPs were used at a concentration of 0.4mM each; primers were used at a concentration of 0.4 μ M each; 50ng BamHI-FIP3-pCR3.1 was used as a template.

The thermocycling conditions used for SDM were as follows.

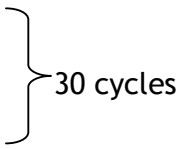
<u>94° C 1 min</u>	}	16 cycles
94° C 30 sec		
60° C 30 sec		
<u>72° C 6 min</u>		
72° C 5 min		
4° C Hold		

Once the mutagenesis was confirmed to have generated the S348A mutant, we digested out the BamHI fragment of the mutant and ligated it into fresh GFP-FIP3. The protocol for this is detailed in section 5.3.3.

To generate GFP-FIP3-S348D we modified the basic SDM protocol provided in section 2.3.1 of the materials and methods: dNTPs were used at a concentration of 0.4mM each; primers were used at a concentration of 0.4 μ M each; 50ng GFP-FIP3 template was used.

The thermocycling conditions used for SDM were as follows.

94° C 1 min
94° C 30 sec
60° C 30 sec
72° C 14 minutes
72° C 5 min
4° C Hold



The GFP-FIP3-S348D plasmid generated a FIP3 protein which had a smaller than expected molecular weight, as analysed by SDS-PAGE. On digestion of the plasmid with BamHI, it was shown that the deletion of DNA occurred in the N-terminus of FIP3. Thus we cut out the BamHI fragment of the mutant and ligated it into fresh GFP-FIP3, as described in section 5.3.3.

The mutated plasmids were verified, as detailed in section 5.3.2.

5.3.4.4 Generation of GFP-FIP3-S451A and GFP-FIP3-S451D plasmids

Generation of phospho-neutral and phospho-mimetic mutants of serine 451 from GFP-FIP3 proved challenging, since all mutants made contained insertions or deletions of DNA towards the N-terminus of FIP3. To resolve this issue, we cloned a BamHI fragment from the wild-type GFP-FIP3 plasmid into BamHI digested pCR3.1 vector and performed mutagenesis in the absence of the N-terminus of FIP3. The methods used to produce the BamHI-FIP3-pCR3.1 construct are detailed in section 5.3.3.

To generate GFP-FIP3-S451A we modified the basic SDM protocol provided in section 2.3.1 of the materials and methods to the following: dNTPs were used at a concentration of 0.4mM each; primers were used at a concentration of 0.25µM each; 25ng BamHI-FIP3-pCR3.1 was used as a template. The thermocycling conditions used for SDM were as follows.

<u>95° C 5 min</u>	}	16 cycles
95° C 1 min		
60° C 30 sec		
<u>68° C 12 min</u>		
68° C 10 min		
4° C Hold		

To generate GFP-FIP3-S451D we modified the basic SDM protocol provided in section 2.3.1 of the materials and methods to the following: dNTPs were used at a concentration of 0.4mM each; primers were used at a concentration of 0.25 μ M each; 25ng BamHI-FIP3-pCR3.1 was used as a template. The thermocycling conditions used for SDM were as follows.

<u>94° C 5 min</u>	}	30 cycles
94° C 1 min		
60° C 30 sec		
<u>72° C 12 min</u>		
72° C 10 min		
4° C Hold		

The mutated plasmids were verified, as detailed in section 5.3.2.

5.4 Results

5.4.1 Restriction digest analysis of phospho-mutant GFP-FIP3 plasmids

To ensure that the SDM protocol had not introduced unwanted insertions or deletions into the FIP3 sequence, the phospho-mutant GFP-FIP3 plasmids were subject to a restriction digest. The Prekeris lab cloned human FIP3 into the pEGFP-N1 plasmid using XhoI (at the N-terminus of FIP3) and EcoRI (at the C-terminus of FIP3), thus digestion with these enzymes should produce full length fragments of FIP3. Restriction digests were carried out according to section 2.3.5 of the materials and methods, using 1.5 μ g of plasmid DNA. For comparison, GFP-FIP3 and GFP-FIP3-I737E were also digested. In brief, plasmids were

incubated with XhoI and EcoRI for two hours at 37°C and DNA fragments separated and visualised via agarose gel electrophoresis (section 2.3.7).

Figure 5.2 shows the resulting DNA fragment pattern for GFP-FIP3-S102A and GFP-FIP3-S102D plasmids. In all DNA samples digested, FIP3 produced a fragment size between the 2 to 3kb markers, as expected, since the coding sequence of human FIP3 is approximately 2270bp. The pEGFP-N1 vector (4.7kb) appeared at the 5kb marker, as expected. The band of approximately 8kb is uncut plasmid. Thus, SDM did not introduce any insertions or deletions into the sequence of the GFP-FIP3-S102A and GFP-FIP3-S102D plasmids. The remaining mutant pairs produced identical DNA fragment patterns and are therefore not presented.

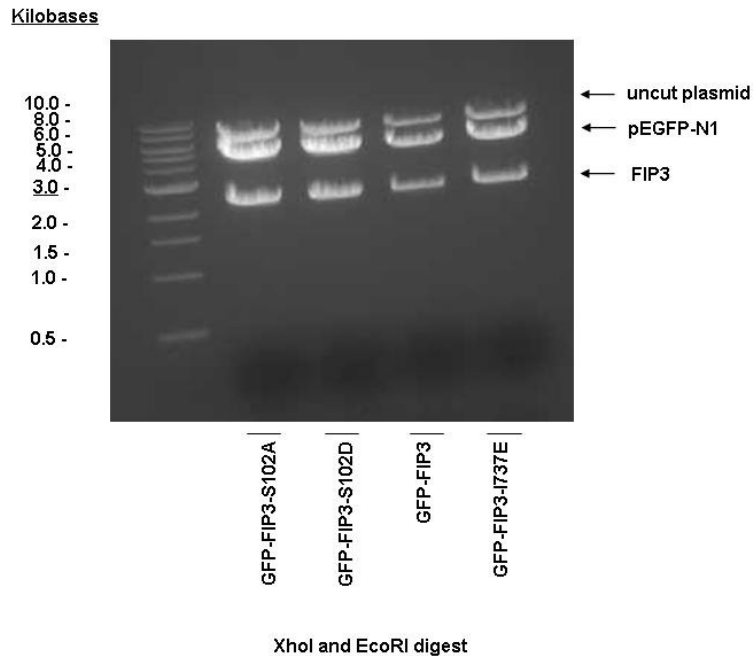


Figure 5-2 Restriction digest analysis of GFP-FIP3-S102A and GFP-FIP3-S102D plasmids
 GFP-FIP3-S102A and GFP-FIP3-S102D plasmids were subject to restriction digests to confirm FIP3 fragment size. Restriction digests were carried out according to section 2.3.5, using 1.5µg of plasmid. For comparison, GFP-FIP3 and GFP-FIP3-I737E were also digested. Plasmids were incubated with 10u XhoI and 10u EcoRI for two hours at 37°C and DNA fragments separated and visualised via agarose gel electrophoresis, according to section 2.5.7. Lane allocations are as follows: Lane 2, GFP-FIP3-S102A; Lane 3, GFP-FIP3-S102D; Lane 4, GFP-FIP3; Lane 5, GFP-FIP3-I737E. Lane 1 contains the 1kb DNA ladder, with the positions of the markers indicated. The position of FIP3 is marked. In all DNA samples digested FIP3 produces a fragment size between the 2-3kb markers, as expected, since the coding sequence of human FIP3 is 2270kb. Thus, SDM did not introduce any insertions or deletions into the FIP3 sequence of the mutants.

5.4.2 Immunoblot analysis of HeLa lysates from cells expressing phospho-mutant GFP-FIP3 plasmids

To check that the phospho-mutant GFP-FIP3 plasmids expressed their mutated FIP3 proteins at the correct molecular weight, the plasmids were transfected into HeLa cells, as outlined in section 2.4.6. In addition to the phospho-mutant GFP-FIP3 plasmids, wild type GFP-FIP3 and GFP-FIP3-I737E were transfected into HeLa cells. Two controls were set up: one with only the transfection reagent and one with untransfected cells. Cells were lysed following 24, 48 and 72 hours transfection (section 2.4.7). Samples were separated by SDS-PAGE (section 2.2.2), transferred onto nitrocellulose (section 2.2.3) and probed for GFP-FIP3 (section 2.2.4). As a loading control, the bottom half of the membrane, below the 47.5kDa marker, was probed for GAPDH.

The resulting immunoblots for the serine 102 phospho-mutant pair are shown in figure 5.3. GFP-FIP3-S102A and GFP-FIP3-S102D run at the same molecular weight as GFP-FIP3 and GFP-FIP3-I737E. Immunoblots for the serine 281 (figure 5.4) and serine 348 (figure 5.5) phospho-mutant pairs show that GFP-FIP3-S281A, GFP-FIP3-S281D, GFP-FIP3-S348A and GFP-FIP3-S348D run at the same molecular weight as GFP-FIP3 and GFP-FIP3-I737E.

Figure 5.6 presents the immunoblots from the serine 451 phospho-mutant pair. GFP-FIP3-S451A and GFP-FIP3-S451D run at the same molecular weight as GFP-FIP3 and GFP-FIP3-I737E. Interestingly, GFP-FIP3-S451A is expressed at much lower levels than the other GFP-FIP3 plasmids. This result was repeated in three separate transfections, using different preparations of DNA. Additionally, levels of GFP-FIP3-S451A decrease from the 24 hour transfection to the 72 hour transfection. GAPDH levels for the GFP-FIP3-S451A transfection are equal to that of the other plasmid transfections and show no decrease in signal from 24 to 72 hours.

Phospho-mutant GFP-FIP3 plasmids were also transfected into CHO cells and immunoblot analysis produced identical results as those from HeLa cells (data not shown).

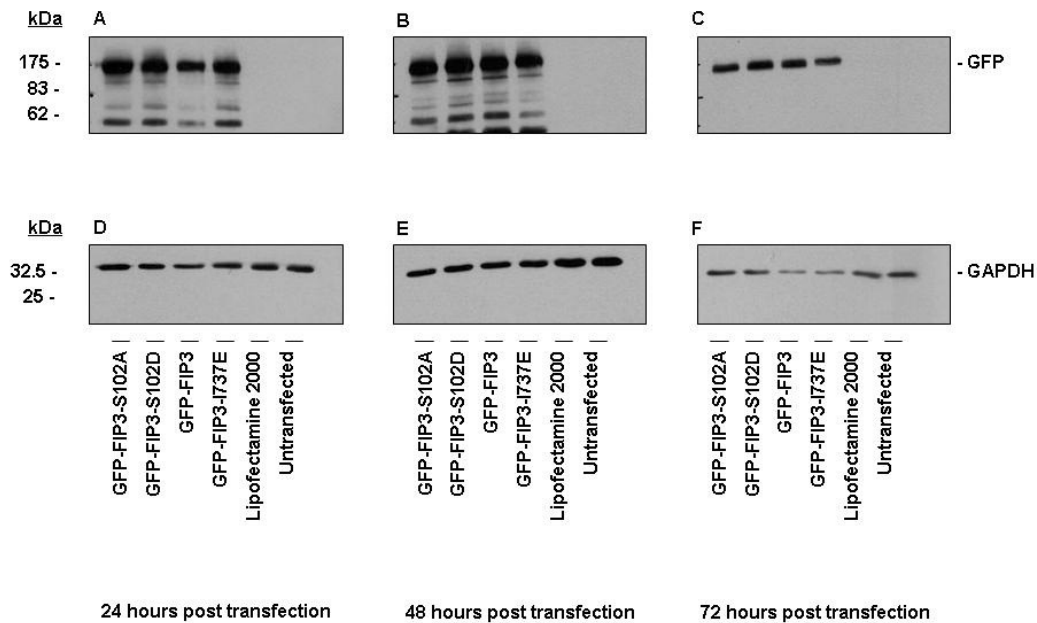


Figure 5-3 Immunoblot analysis of HeLa lysates from cells expressing GFP-FIP3-S102A and GFP-FIP3-S102D plasmids

To check that GFP-FIP3-S102A (Lane 1) and GFP-FIP3-S102D (Lane 2) plasmids expressed their mutated FIP3 proteins at the correct molecular weight, the plasmids were transfected into HeLa cells. Control transfections included GFP-FIP3 (Lane 3) and GFP-FIP3-I737E (Lane 4), Lipofectamine 2000 only (Lane 5) and untransfected cells (Lane 6). The protocol for which is detailed in section 2.4.6 of the materials and methods. Cells were lysed at 24 (Figures 5.3A and 5.3D), 48 (Figures 5.3B and 5.3E) and 72 (Figures 5.3C and 5.3F) hours after transfection. The protocol for which is detailed in section 2.4.7. Protein lysates were separated by SDS-PAGE, as detailed in section 2.2.2, and then transferred onto nitrocellulose via Western Blotting, as outlined in section 2.2.3. Following Western Blotting the membrane was cut in half at the 47.5kDa marker. The half of the membrane above 47.5kDa was probed for GFP (top panel). As a loading control, the half of the membrane below the 47.5kDa marker was probed for GAPDH (bottom panel). A protocol for this is provided in section 2.2.4. The resulting immunoblots are presented, with the positions of GFP and GAPDH labelled. The position of the Broad Range Prestained Protein Marker is illustrated. GFP-FIP3-S102A and GFP-FIP3-S102D run at the same molecular weight as GFP-FIP3 and GFP-FIP3-I737E. Representative immunoblots from an experiment performed in duplicate are presented.

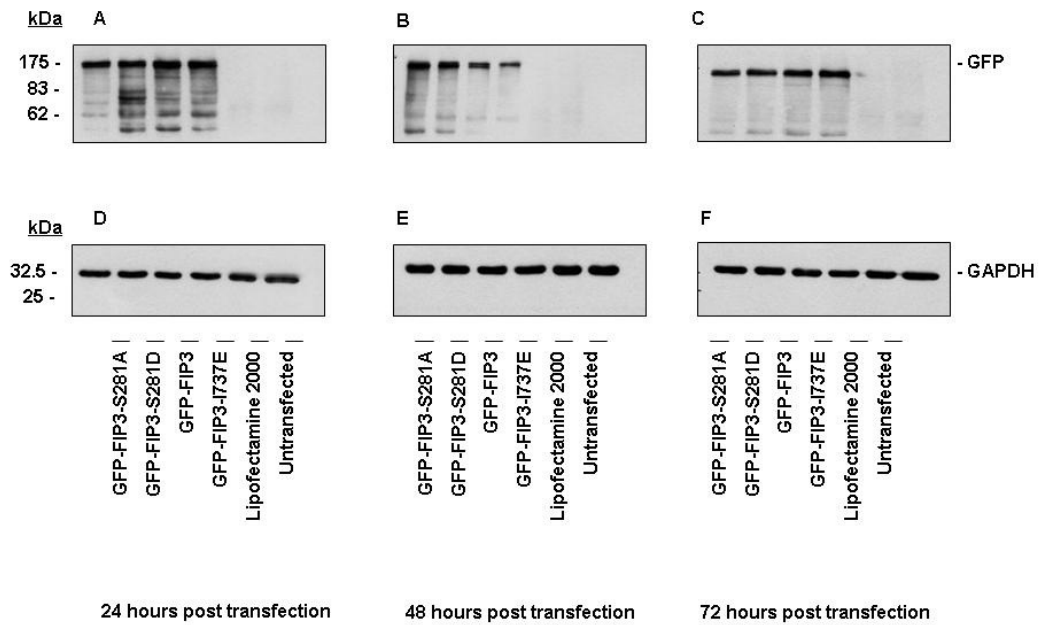


Figure 5-4 Immunoblot analysis of HeLa lysates from cells expressing GFP-FIP3-S281A and GFP-FIP3-S281D plasmids (figure legend as per figure 5.3). Representative immunoblots from an experiment performed in duplicate are presented.

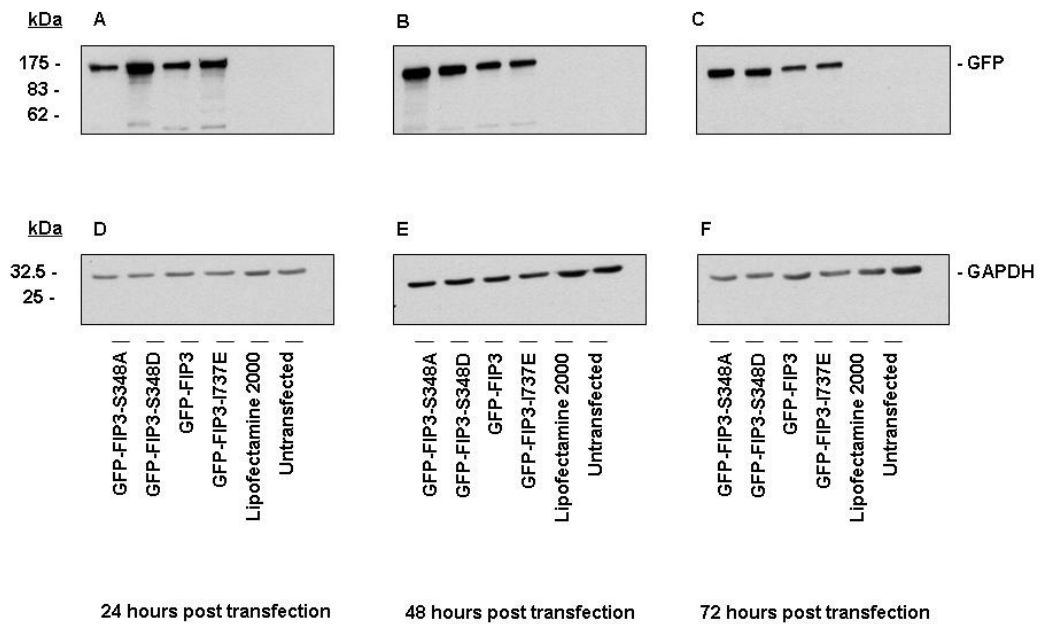


Figure 5-5 Immunoblot analysis of HeLa lysates from cells expressing GFP-FIP3-S348A and GFP-FIP3-S348D plasmids (figure legend as per figure 5.3). Representative immunoblots from an experiment performed in duplicate are presented.

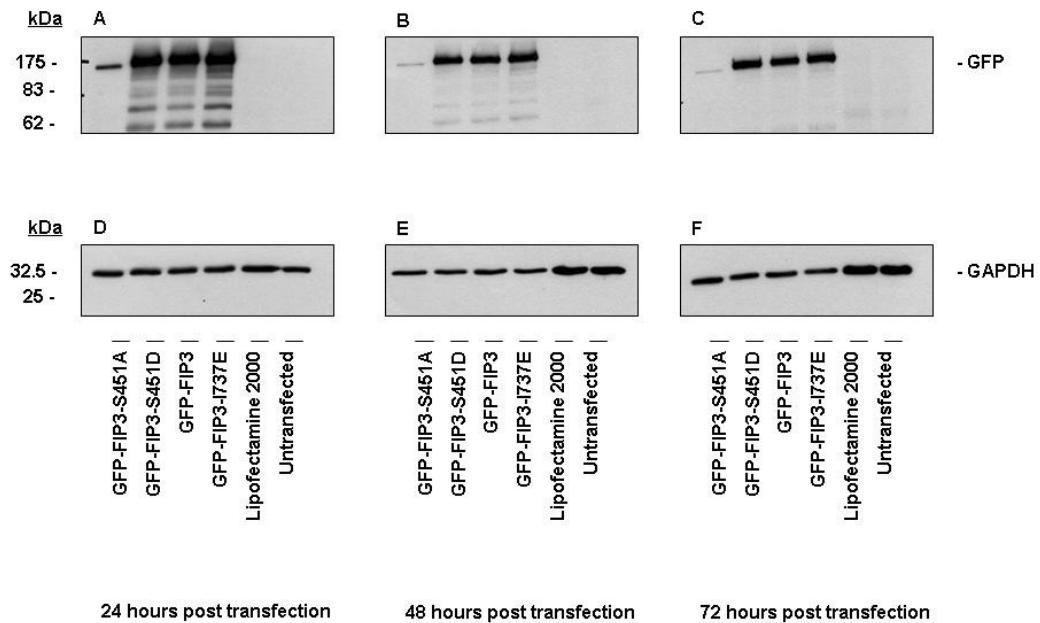


Figure 5-6 Immunoblot analysis of HeLa lysates from cells expressing GFP-FIP3-S451A and GFP-FIP3-S451D plasmids (figure legend as per figure 5.3). Representative immunoblots from an experiment performed in triplicate are presented.

5.4.3 Immunofluorescence analysis of HeLa cells expressing phospho-mutant GFP-FIP3 plasmids

To analyse the distribution of phospho-mutant GFP-FIP3, plasmids were transfected into HeLa cells, which allowed the analysis of the localisation of phospho-mutant proteins through the cell-cycle, owing to their GFP tags. HeLa cells were transfected with plasmid DNA (section 2.4.6). In addition to phospho-mutant GFP-FIP3 plasmids, wild type GFP-FIP3 and GFP-FIP3-I737E were also transfected into cells. Two controls were set up: one with the transfection reagent only and one with untransfected cells. Cells were fixed with 4% (w/v) ρ -formaldehyde and processed for immunofluorescence 24, 48 and 72 hours after transfection (section 2.5). Cells were stained for microtubules using a rat monoclonal antibody to α -Tubulin, followed by Alexa Fluor® 568. For nuclear staining, cells were stained with DAPI. Mounted coverslips were analysed using a 63x Zeiss oil immersion objective on a Zeiss confocal microscope (Carl Zeiss,

Germany) equipped with Zeiss LSM5 Pascal instrument. Zeiss Pascal software was used to collect and edit images.

The localisation of each phospho-mutant GFP-FIP3 was identical following 24, 48 and 72 hours expression, thus data for the 24 hour and 72 hour time points are not included, owing to space constraints. Images of HeLa cells expressing phospho-mutant GFP-FIP3 plasmids for 48 hours, along with the various controls, are presented at the end of this chapter in figures 5.11 to 5.28. Images were taken of cells in interphase (figures 5.11 to 5.13), metaphase (figures 5.14 to 5.16), anaphase (figures 5.17 to 5.19), early telophase (figures 5.20 to 5.22), and late telophase (figures 5.23 to 5.25). These images represent the majority of cells viewed.

GFP-FIP3 is found on membranes at the centrosome in interphase and the duplicated centrosomes in metaphase. In addition, GFP-FIP3 is located on endosomal membrane structures in the cytosol. By anaphase, the majority of GFP-FIP3 is concentrated at the centrosomes. In early telophase, GFP-FIP3 is found again at the centrosomes, but the beginnings of trafficking to the furrow are evident as GFP-FIP3 begins to concentrate in pools associated with the minus ends of the microtubules forming the spindle midzone. In late telophase GFP-FIP3 traffics into the intracellular bridge and is found on either side of the midbody. The Rab11 binding defective mutant of FIP3, GFP-FIP3-I737E, shows diffuse cytosolic staining throughout the cell-cycle, as expected. GFP-FIP3-S102A, GFP-FIP3-S102D, GFP-FIP3-S281A, GFP-FIP3-S281D, GFP-FIP3-S348A, GFP-FIP3-S348D and GFP-FIP3-S451D show the same localisation through the cell-cycle as the wild type GFP-FIP3 protein. They localise to the centrosomes in interphase and metaphase and then traffic into the intracellular bridge, on either side of the midbody, by late telophase.

While GFP-FIP3-S451D shows the same localisation through the cell-cycle as the wild type GFP-FIP3 protein, GFP-FIP3-S451A produced an interesting result. As shown in section 5.4.2, GFP-FIP3-S451A is expressed at much lower levels than the other GFP-FIP3 plasmids. Additionally, levels of GFP-FIP3-S451A decrease from the 24 hour transfection to the 72 hour transfection. However, GAPDH levels for the GFP-FIP3-S451A transfection are equal to that of the other plasmid transfections and show no decrease in signal from 24 to 72 hours. Coverslips

from these transfections were sparse and patches of cells rarely expressed GFP-FIP3-S451A. In the cells which did express GFP-FIP3-S451A, the cells appeared unhealthy and the protein did not accumulate in the same way as the wild type protein. Examples of average fields of view have been presented in figures 5.26 to 5.28 at the end of this chapter.

Phospho-mutant GFP-FIP3 plasmids were also transfected into CHO cells and immunofluorescence analysis produced similar results, however these are not presented owing to space constraints. Thus, on expression of phospho-mutant GFP-FIP3 plasmids for serines 102, 281 and 348 in HeLa and CHO cells, no apparent effect was observed on the cell-cycle dependent localisation of these mutated proteins. Expression of the phospho-mimetic form of serine 451 had no apparent effect on the cell-cycle dependent localisation of the protein. However, expression of the phospho-neutral form of serine 451 produced a dramatic effect as very few cells expressed the plasmid. The cells which did so were unhealthy and the protein did not accumulate in the same way as the wild type protein.

5.4.4 Binuclear cell count analysis of HeLa cells expressing phospho-mutant GFP-FIP3 plasmids

We next sought to determine the role of phosphorylation at serine 102, 281, 348 and 451 of FIP3 in cytokinesis. As a crude estimate of defects in cytokinesis, a binuclear cell count is widely used in the field. HeLa cells expressing phospho-mutant GFP-FIP3 plasmids from section 5.4.3 were used. The number of binuclear cells and total cells expressing GFP-FIP3 (or a mutant of) were counted in ten fields of view for each transfection condition. From this the average percentage of binuclear cells per field of view was calculated.

The binuclear cell count for serine 102 at the 48 hour time point is presented in figure 5.7. As expected, GFP-FIP3-I737E produced an increased binuclear phenotype in HeLa cells (approximately 4%). Binucleate counts for GFP-FIP3-S102A and GFP-FIP3-S102D plasmids were marginally higher (approximately 1.5%) to those of the controls (approximately 0.5 to 1%), but did not reach the levels observed for GFP-FIP3-I737E.

The binuclear cell count for serine 281 at 24 hours is presented in figure 5.8. As expected, GFP-FIP3-I737E produced an increased binuclear phenotype in HeLa cells (approximately 4.5%). Binucleate counts for GFP-FIP3-S281A and GFP-FIP3-S281D plasmids (approximately 2.5%) were marginally higher than those of the controls (between 1 and 1.5%).

The binuclear cell count for serine 348 at the 72 hour time point is presented in figure 5.9. As expected, GFP-FIP3-I737E produced an increased binuclear phenotype in HeLa cells (approximately 5%). Binucleate counts for GFP-FIP3-S348A and GFP-FIP3-S348D plasmids (between 0.5 to 1.0%) were similar to those of the controls (between 1.0 to 1.5%).

The binuclear cell count for serine 451 for 24 hours is presented in figure 5.10. Binuclear cells for GFP-FIP3-S451A could not be performed as very few cells expressing the plasmid were present on the coverslips and the ones which did express were often unhealthy. As expected, GFP-FIP3-I737E produced an increased binuclear phenotype in HeLa cells (approximately 4%). The binucleate count for the GFP-FIP3-S451D plasmid (2.5%) was similar to those of the controls (0.5 to 3%).

Phospho-mutant GFP-FIP3 plasmids were also transfected into CHO cells, which produced similar results and therefore data is not presented, owing to space constraints. In summary, on expression of phospho-mutant GFP-FIP3 plasmids of serines 102, 281 and 348, no discernible effect on cytokinesis was observed via a binuclear cell count. Expression of the phospho-mimetic form of serine 451 had no apparent effect on cytokinesis. However, expression of the phospho-neutral form of serine 451 produced a dramatic effect on the cell, as very few cells expressed the plasmid and the cells which did so were unhealthy. As a result, any effect on cytokinesis by GFP-FIP3-S451A could not be shown by this method.

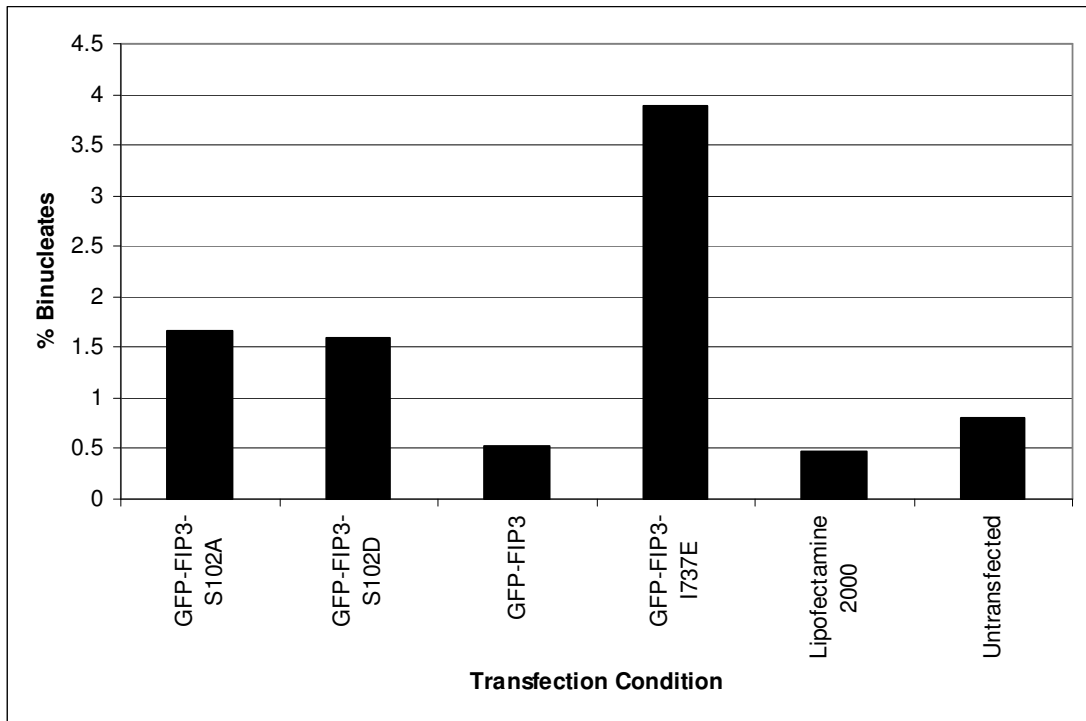


Figure 5-7 Binuclear cell count of HeLa cells expressing GFP-FIP3-S102A and GFP-FIP3-S102D plasmids for 48 hours. Approximately 500 cells per condition were counted. Data from a single experiment is presented.

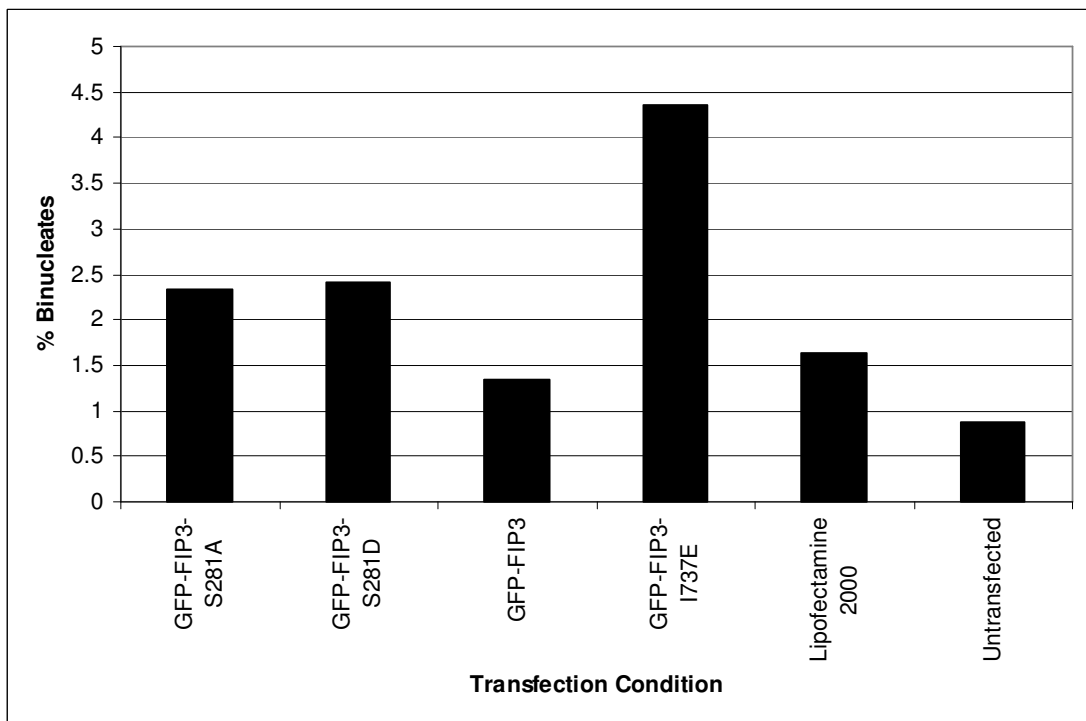


Figure 5-8 Binuclear cell count of HeLa cells expressing GFP-FIP3-S281A and GFP-FIP3-S281D plasmids for 24 hours. Approximately 500 cells per condition were counted. Data from a single experiment is presented.

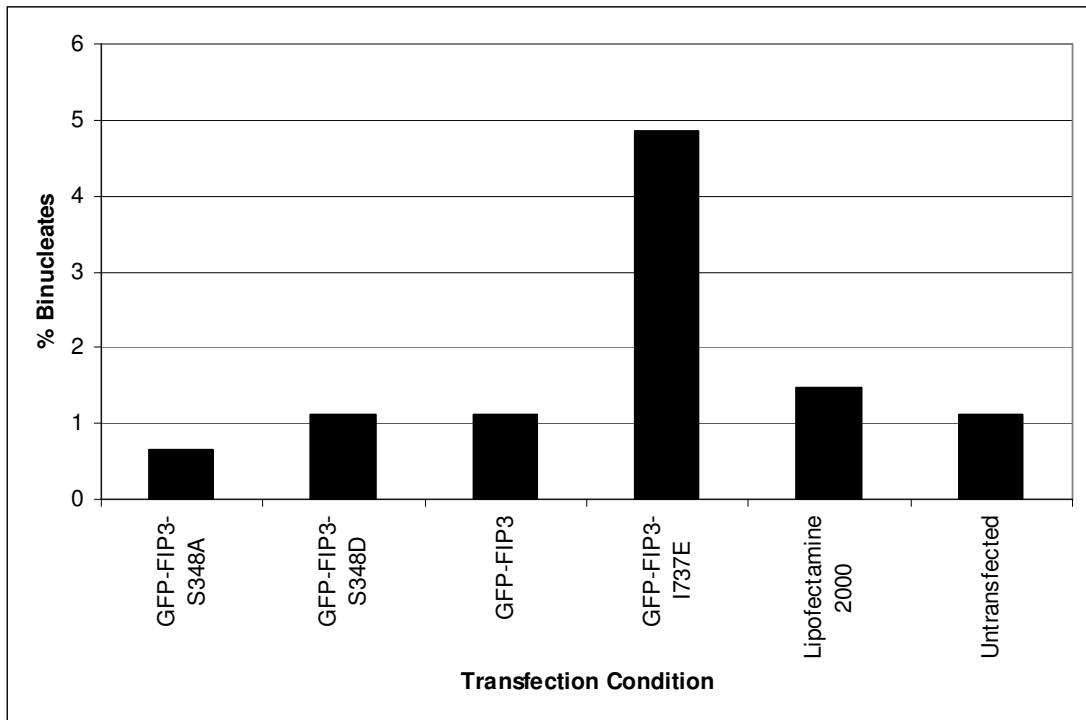


Figure 5-9 Binuclear cell count of HeLa cells expressing GFP-FIP3-S348A and GFP-FIP3-S348D plasmids for 72 hours. Approximately 500 cells per condition were counted. Data from a single experiment is presented.

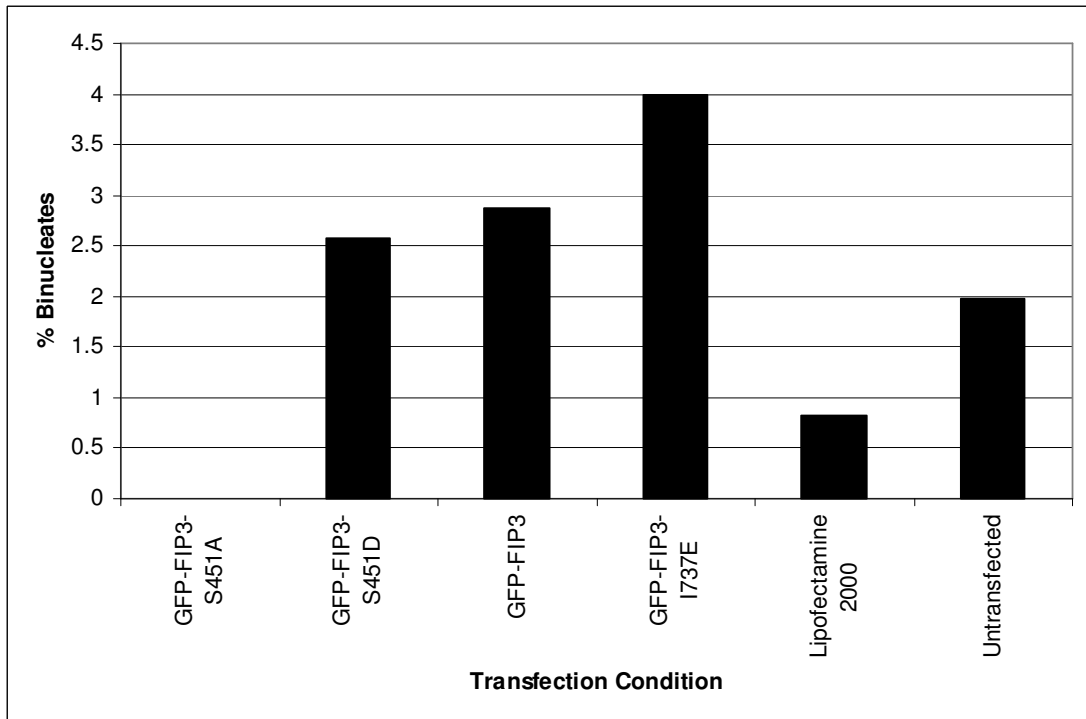


Figure 5-10 Binuclear cell count of HeLa cells expressing GFP-FIP3-S451A and GFP-FIP3-S451D plasmids for 24 hours. Approximately 500 cells per condition were counted. Data from a single experiment is presented.

5.5 Conclusions

FIP3 undergoes spatial and temporal regulation during mitosis (Wilson *et al.*, 2005). A potential candidate for the control of FIP3 dynamics is phosphorylation, since phosphorylation is a commonly used control mechanism in mitotic regulation (Morgan, 2007). As discussed in chapters 3 and 4, work from a collaborating lab proposes that FIP3 phosphorylation and dephosphorylation may be a regulator of FIP3 localisation (R. Prekeris, personal communication) and mass spectrometry analysis of FIP3 immunoprecipitated from metaphase cells has identified four phosphorylation sites: serines 102, 281, 348 and 451. The significance of these phosphosites in the spatial and temporal regulation of FIP3 during mitosis remains unknown. The aim of this chapter was to analyse the role of phosphorylation at serines 102, 281, 348 and 451 by creating alanine (phospho-null) and aspartic acid (phospho-mimetic) mutant FIP3. These mutations were carried out in the pEGFP-N1 plasmid, containing the coding sequence for human FIP3. The aim was to study the role of the various phosphorylation sites of FIP3 through the analysis of the cell-cycle dependent subcellular localisation of each phospho-mutant. We also performed binuclear cell counts to look for cytokinesis defects resulting from mutation of the various phosphosites. Ideally, we sought to analyse the membrane and cytosol ratios of these mutant proteins, but time constraints prevented this.

In considering the potential functions of phosphorylation at serines 102, 281, 348 and 451, it is important to explore where these sites are located within FIP3. The family of FIP proteins is characterised by a highly conserved Rab11-binding domain (RBD) of 20 amino acids located at the C-terminus of the protein (Prekeris *et al.*, 2001), the minimal area of which encompasses residues 733 to 756 of FIP3 (Shiba *et al.*, 2006). The structure of FIP3 in its entirety is not yet known. The crystal structure of the FIP3-RBD (695 to 756 amino acids) in complex with Rab11 reveals that amphiphilic helices from two FIP3-RBDs form a parallel coiled-coil homodimer. This creates two symmetrical interfaces for binding the switch regions of two Rab11 molecules, thus forming a heterotetrameric complex (Eathiraj *et al.*, 2006; Shiba *et al.*, 2006). Thus our phosphosites fall outside of the reported homodimerisation domain and RBDs. However, it is important to note that points of contact between the two FIP3

proteins may exist out with the RBD. Indeed, prediction software has shown that FIP3 has an extensive α -helical coiled-coil region between residues 463 and 692 (Wallace *et al.*, 2002;Horgan *et al.*, 2007). Perhaps future research may identify other points of dimerisation in the regions of the phosphosites investigated in this thesis. Analysis of the amino acid sequence reveals that FIP3 also contains two EF-hand domains (Prekeris *et al.*, 2001) at approximately 202 to 237 and 234 to 269 amino acids (The UniProt Consortium, 2009). EF-hand domains are involved in calcium binding (Grabarek, 2006). Also important to note is the proline rich region found at the N-terminus of FIP3 (Prekeris *et al.*, 2001), encompassing amino acids 5 to 197 (The UniProt Consortium, 2009). Interestingly serine 102 is located within this proline rich region; this type of region is known to mediate a large number of protein to protein interactions (Kay *et al.*, 2000).

It has been proposed that the FIP3-Rab11 complex plays a key role in cytokinesis by delivering and targeting recycling endosomes to the cleavage furrow and midbody (Wilson *et al.*, 2005;Fielding *et al.*, 2005). FIP3 may act as a scaffold in the recruitment of proteins to the recycling endosomes at the centrosome. An ever increasing list of proteins has been found to interact with FIP3. Directly N-terminal to the RBD is the Arf binding domain (ABD), which involves amino acids 650 to 695 (Fielding *et al.*, 2005;Shiba *et al.*, 2006;Schonteich *et al.*, 2007). N-terminal to this is the CYK-4 binding domain which is thought to encompass amino acids 441 to 610 (Simon *et al.*, 2008). Serine 451 lies just within this region. Recently, Kinesin I has been found to interact with FIP3, which is essential for cytokinesis (Simon and Prekeris, 2008). Also, Arf GTPase Activating Protein ASAP1 is thought to interact with amino acids 565 to 650 of FIP3, within the coiled-coil domain (Inoue *et al.*, 2008). Perhaps future research may identify proteins which interact with FIP3 in the regions of the phosphosites investigated in this thesis.

On transfection into HeLa cells, the cell-cycle dependent localisation of the wild type GFP-FIP3 plasmid was as expected. In interphase, metaphase and early anaphase, FIP3 localised to endosomal membrane structures in the cytosol (Wilson *et al.*, 2005). Data from this thesis shows that in addition to this, a pool of GFP-FIP3 is concentrated at endosomal membranes at the centrosome in interphase and metaphase. This has also been observed via immunofluorescence of fixed HeLa cells using an antibody for FIP3, where a pool of FIP3 associates

with the centrosome throughout the cell-cycle, in addition to the pool of FIP3 which is dynamic (Wilson *et al.*, 2005). Real-time microscopy shows a rapid redistribution of GFP-FIP3 to the centrosomes during late anaphase, following furrow initiation. We also observe a concentration of GFP-FIP3 at the centrosomes during anaphase. At late cytokinesis, FIP3 relocates to the cleavage furrow and midbody and on separation of the two daughter cells, FIP3 relocates to the centrosome (Wilson *et al.*, 2005). We have presented the dynamic localisation of GFP-FIP3 in stages: anaphase, where GFP-FIP3 is associated with the centrosomes; early telophase, where GFP-FIP3 associates with centrosomes, but begins to concentrate in pools associated with the minus ends of the microtubules forming the spindle midzone; late telophase, where GFP-FIP3 traffics into the intracellular bridge and can be found at either side of the midbody.

The majority of the plasmids constructed for this thesis localised in the same manner as wild type GFP-FIP3. The localisations of GFP-FIP3-S102A/D, GFP-FIP3-S281A/D, GFP-FIP3-S348A/D and GFP-FIP3-S451D mirrored that of the wild type protein. In addition, these plasmids did not demonstrate a disruption in cytokinesis as their binuclear counts in HeLa and CHO cells did not differ greatly to the binuclear counts produced by the wild type plasmid and the transfection controls. Thus it would appear that when mutated singly, the potential phospho-sites of serines 102, 281, 348 and 451 (aspartic acid mutation only) have no significant effect on the spatial and temporal regulation of FIP3 during mitosis.

However, before discounting these phospho-sites there is one note of caution which arises on consideration of the binuclear counts from the mutant of FIP3 defective in binding to Rab11, GFP-FIP3-I737E. On transfection of this plasmid into HeLa and CHO cells, GFP-FIP3-I737E showed diffuse cytosolic staining throughout the cell cycle, as expected (Wilson *et al.*, 2005). In this thesis, only a slightly higher binuclear phenotype to that of the controls was observed. Previously GFP-FIP3-I737E was reported to produce a binuclear cell count of 40% in HeLa cells (Wilson *et al.*, 2005). It was for that reason that transfections were repeated in CHO cells, but the binuclear counts were similar to those from HeLa cells. In addition, phospho-mutant proteins were expressed in HeLas, with a background of endogenous FIP3. Ongoing work in the lab aims to create a FIP3 knockdown system in HeLa cells.

A binuclear count is used widely in the field to quantify mitotic defects. However, it is in itself limited as it does not take into account cells which are connected by an intracellular bridge and appear normal, but will regress. Some research groups take into account cells attached by a midbody, in addition to the standard binuclear cell (Bajorek *et al.*, 2009). Thus, in addition to counting binuclear cells, we also counted separately cells in telophase. However, this did not reveal any difference between the mutants and the controls. Time lapse microscopy revealed the importance of FIP3 in cytokinesis as knockdown of FIP3 produced a delay in cytokinesis, leading to apoptosis (Wilson *et al.*, 2005). Thus to ensure that potential defects in mitosis are not overlooked, time lapse microscopy should be performed on cells transfected with these plasmids. Another potential reason for the lack of cytokinesis defects following mutation of these phosphosites is the fact that these sites were mutated singly. Multisite phosphorylation is a commonly recognised control of protein behaviour (Cohen, 2000). Further work to produce double/triple/quadruple mutants for these four sites would explore the role of these four phosphosites further.

The one plasmid which produced a phenotype different to that of the wild type plasmid was GFP-FIP3-S451A. GFP-FIP3-S451D shows the same localisation through the cell cycle as the wild type GFP-FIP3 protein. However, GFP-FIP3-S451A produced an interesting result. As shown in section 5.4.2, GFP-FIP3-S451A is expressed at much lower levels than the other GFP-FIP3 plasmids. Additionally, levels of GFP-FIP3-S451A decreased from the 24 hour transfection to the 72 hour transfection. However, GAPDH levels for the GFP-FIP3-S451A transfection are equal to that of the other plasmid transfections and show no decrease in signal from 24 to 72 hours. Coverslips from these transfections were sparse and patches of cells rarely expressed GFP-FIP3-S451A. In the cells which did express GFP-FIP3-S451A, the cells appeared unhealthy and the protein did not accumulate in the same way as the wild type plasmid. Very few cells which expressed GFP-FIP3-S451A were present on the coverslips to allow the cell-cycle localisation of this protein to be recorded. However, GFP-FIP3-S451A did not appear to concentrate at the centrosomes of interphase cells. It is important to note that GFP-FIP3-S451A did not produce the same phenotype as GFP-FIP3-I737E as it was not diffusely cytosolic.

The localisation of this protein should be studied in more depth. It would be interesting to determine if this mutation resulted in apoptosis of the cells. Mitotic catastrophe resulting from expression of phospho-mimetic mutations of CK2 has been previously reported (St Denis *et al.*, 2009). Again time lapse microscopy would potentially reveal more about this phospho-mutant. The only clues for the potential role of this site in the regulation of FIP3 come from the domain structure of FIP3, as a CYK-4 binding domain has been mapped to amino acids 441-610 (Simon *et al.*, 2008). FIP3 interacts with CYK-4 of the centralspindlin complex at the midbody, and is responsible for recruiting recycling endosomes to this area (Simon and Prekeris, 2008). Owing to time constraints GFP-FIP3-S451A was not investigated further, thus the significance of CYK-4 binding remains conjecture. Another possibility is that this mutation may have affected the processing of the protein.

In summary, the aim of this chapter was to analyse the role of FIP3 phosphorylation at serines 102, 281, 348 and 451 by creating phospho-null and phospho-mimetic mutants in the context of GFP-FIP3. The majority of the plasmids constructed for this thesis localised in the same way as wild type GFP-FIP3 and did not disrupt cytokinesis. This would suggest that phosphorylation at serines 102, 281, 348, 451 has no relevance in the spatial and temporal regulation of FIP3 during mitosis. However, these sites should not be discounted as perhaps the reality is more complex than this work accounts for; perhaps multisite phosphorylation is required in the regulation of FIP3's dynamics. However, mutation of serine 451 to alanine produced an interesting phenotype. Very few cells expressed this protein. The ones which did so were often unhealthy and the protein failed to localise as was expected. Therefore, mutation of serine 451 to alanine may not shed light on the role of phosphorylation in the spatial and temporal regulation of FIP3 during mitosis, but it does warrant further investigation as to the importance of this mutation in the expression of the protein and the survival of the cell.

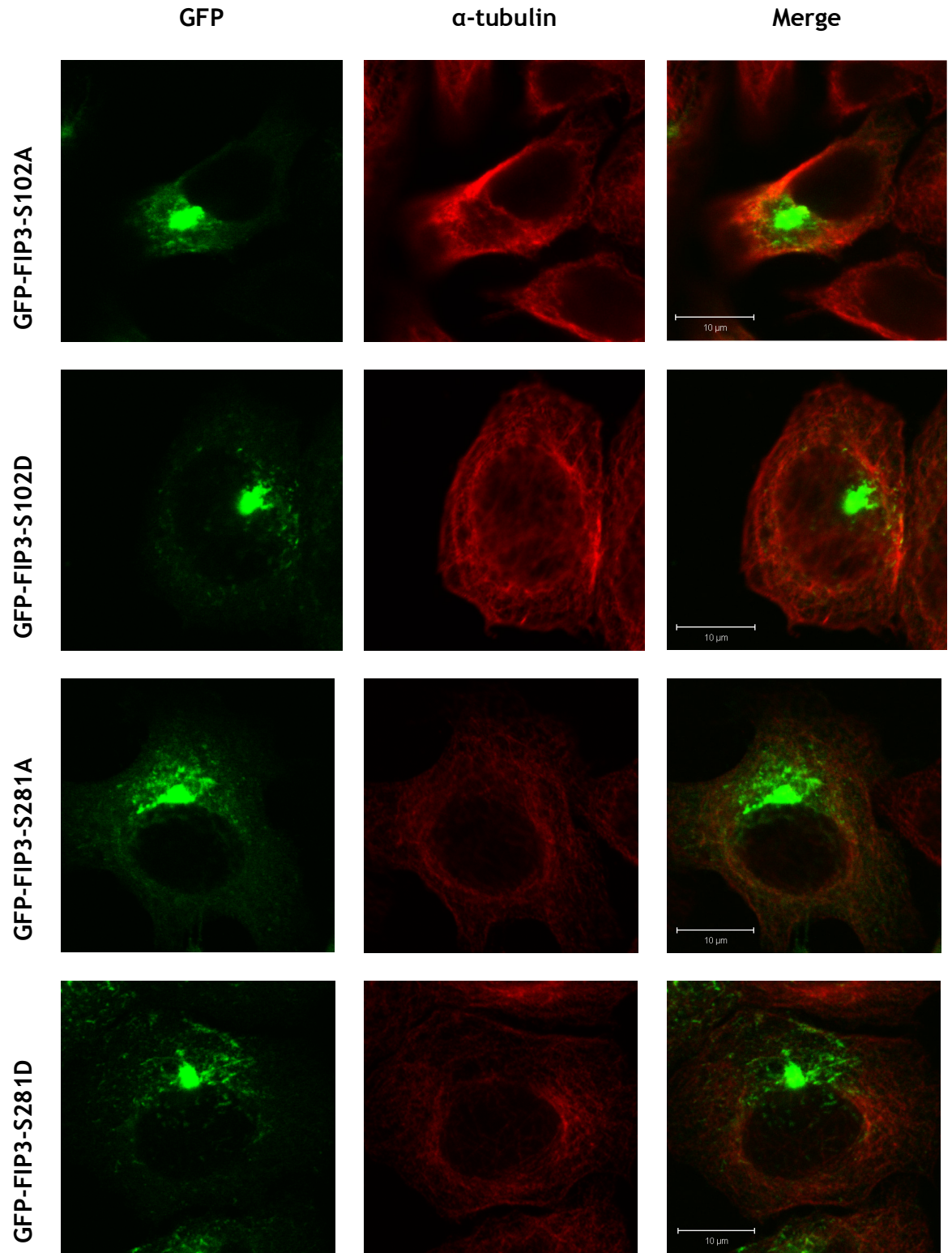


Figure 5-11 Immunofluorescence analysis of HeLa cells in interphase expressing GFP-FIP3-S102A/D and GFP-FIP3-S281A/D plasmids for 48 hours.

HeLa cells were transfected with plasmid DNA or the relevant controls (section 2.4.6). Cells were fixed with 4% (w/v) ρ -formaldehyde and processed for immunofluorescence 48 hours after transfection (section 2.5). Cells were stained for microtubules using a rat monoclonal antibody to α -Tubulin, followed by Alexa Fluor® 568 (red channel). This figure details HeLa cells in interphase expressing GFP-FIP3-S102A/D and GFP-FIP3-S281A/D plasmids for 48 hours. These images represent the majority of cells viewed.

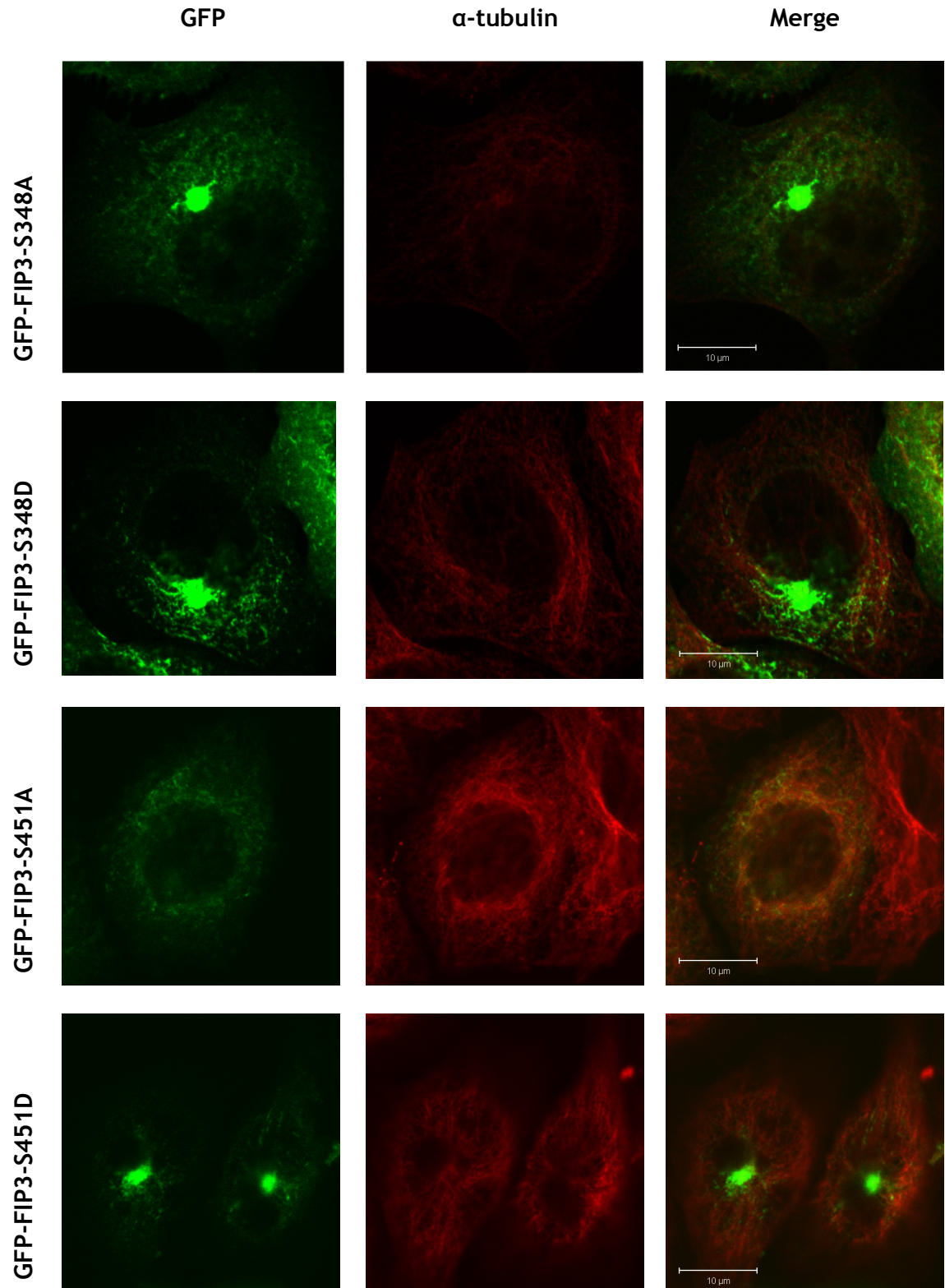


Figure 5-12 Immunofluorescence analysis of HeLa cells in interphase expressing GFP-FIP3-S348A/D and GFP-FIP3-S451A/D plasmids for 48 hours.

HeLa cells were transfected with plasmid DNA or the relevant controls (section 2.4.6). Cells were fixed with 4% (w/v) ρ -formaldehyde and processed for immunofluorescence 48 hours after transfection (section 2.5). Cells were stained for microtubules using a rat monoclonal antibody to α -Tubulin, followed by Alexa Fluor® 568 (red channel). This figure details HeLa cells in interphase expressing GFP-FIP3-S348A/D and GFP-FIP3-S451A/D plasmids for 48 hours. These images represent the majority of cells viewed.

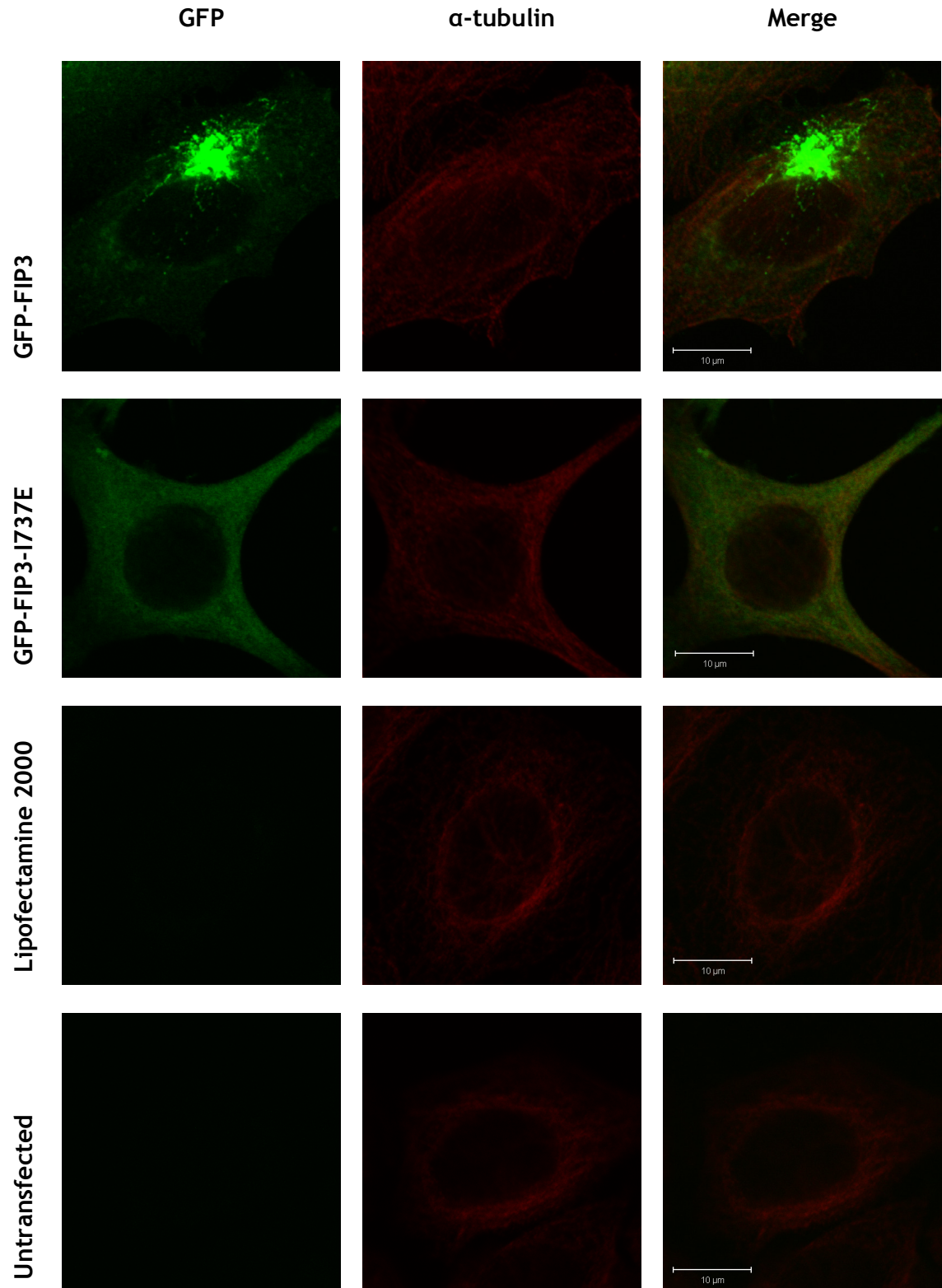


Figure 5-13 Immunofluorescence analysis of HeLa cells in interphase expressing wild-type GFP-FIP3 and GFP-FIP3-I737E plasmids, in addition to Lipofectamine 2000 only and untransfected controls, for 48 hours.

HeLa cells were transfected with plasmid DNA or the relevant controls (section 2.4.6). Cells were fixed with 4% (w/v) ρ -formaldehyde and processed for immunofluorescence 48 hours after transfection (section 2.5). Cells were stained for microtubules using a rat monoclonal antibody to α -Tubulin, followed by Alexa Fluor® 568 (red channel). This figure details HeLa cells in interphase expressing wild-type GFP-FIP3 and GFP-FIP3-I737E plasmids, in addition to control transfections, for 48 hours. These images represent the majority of cells viewed.

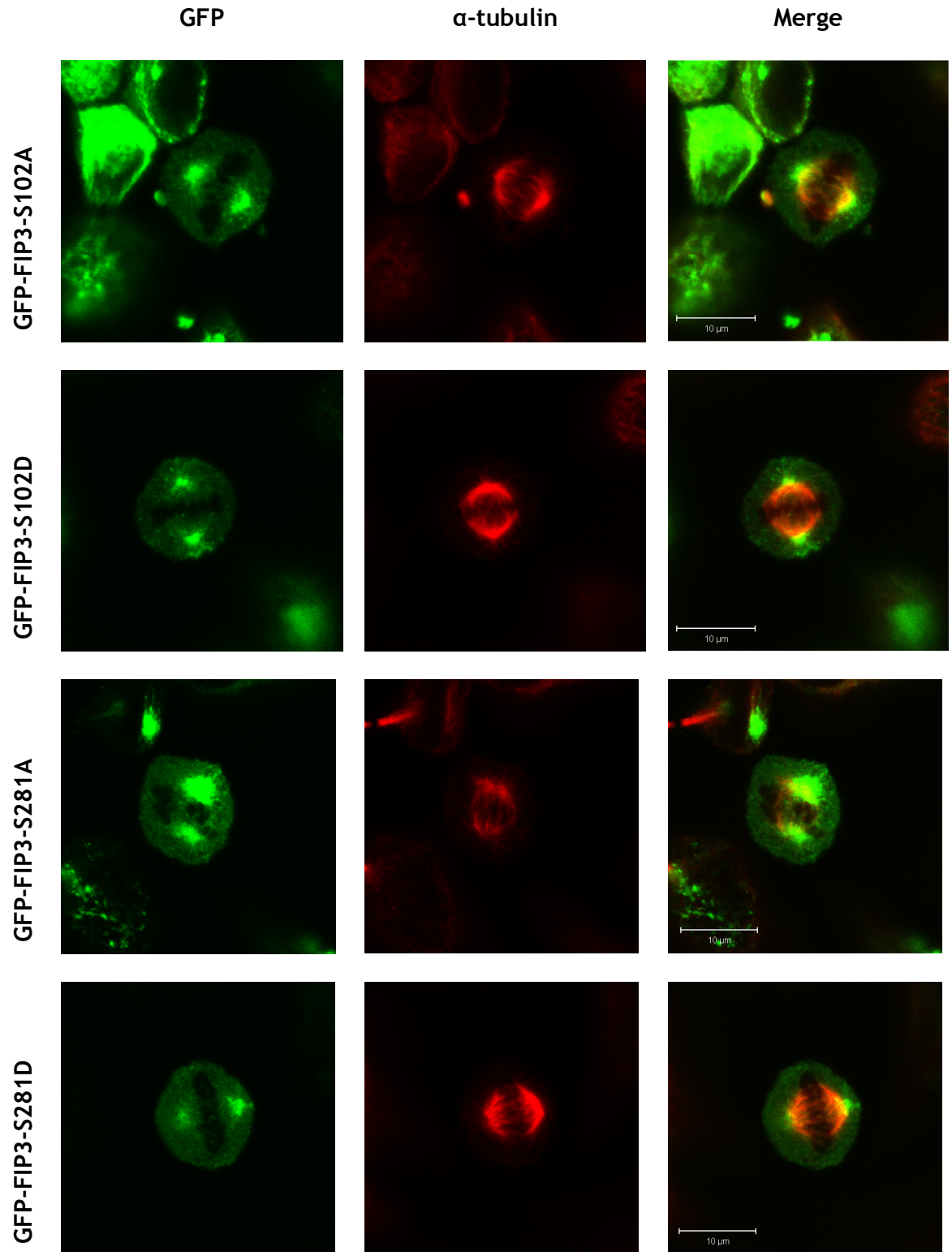


Figure 5-14 Immunofluorescence analysis of HeLa cells in metaphase expressing GFP-FIP3-S102A/D and GFP-FIP3-S281A/D plasmids for 48 hours.

HeLa cells were transfected with plasmid DNA or the relevant controls (section 2.4.6). Cells were fixed with 4% (w/v) ρ -formaldehyde and processed for immunofluorescence 48 hours after transfection (section 2.5). Cells were stained for microtubules using a rat monoclonal antibody to α -Tubulin, followed by Alexa Fluor® 568 (red channel). This figure details HeLa cells in metaphase expressing GFP-FIP3-S102A/D and GFP-FIP3-S281A/D plasmids for 48 hours. These images represent the majority of cells viewed.

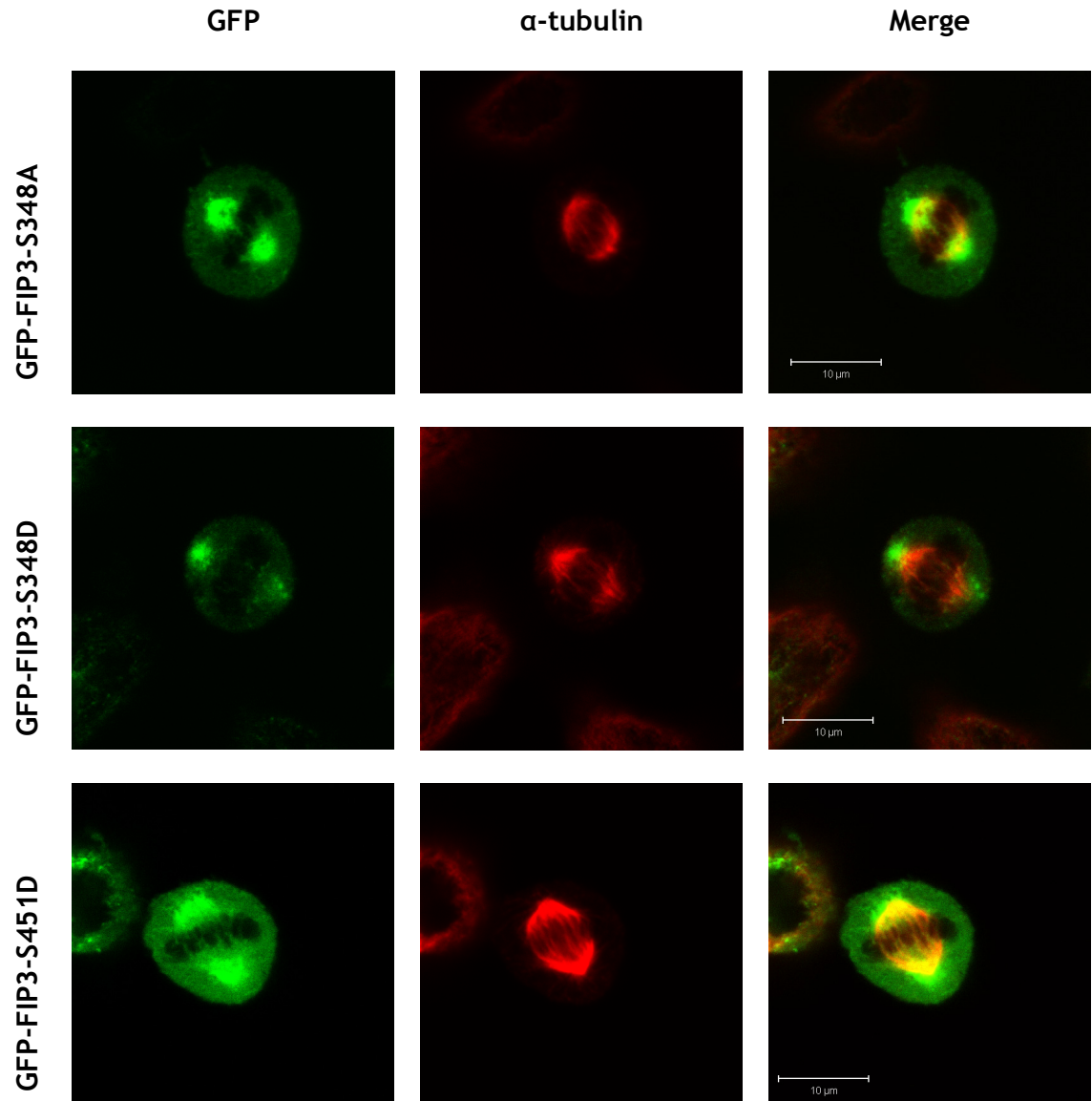


Figure 5-15 Immunofluorescence analysis of HeLa cells in metaphase expressing GFP-FIP3-S348A/D and GFP-FIP3-S451D plasmids for 48 hours.

HeLa cells were transfected with plasmid DNA or the relevant controls (section 2.4.6). Cells were fixed with 4% (w/v) ρ -formaldehyde and processed for immunofluorescence 48 hours after transfection (section 2.5). Cells were stained for microtubules using a rat monoclonal antibody to α -Tubulin, followed by Alexa Fluor® 568 (red channel). This figure details HeLa cells in metaphase expressing GFP-FIP3-S348A/D and GFP-FIP3-S451D plasmids for 48 hours. These images represent the majority of cells viewed.

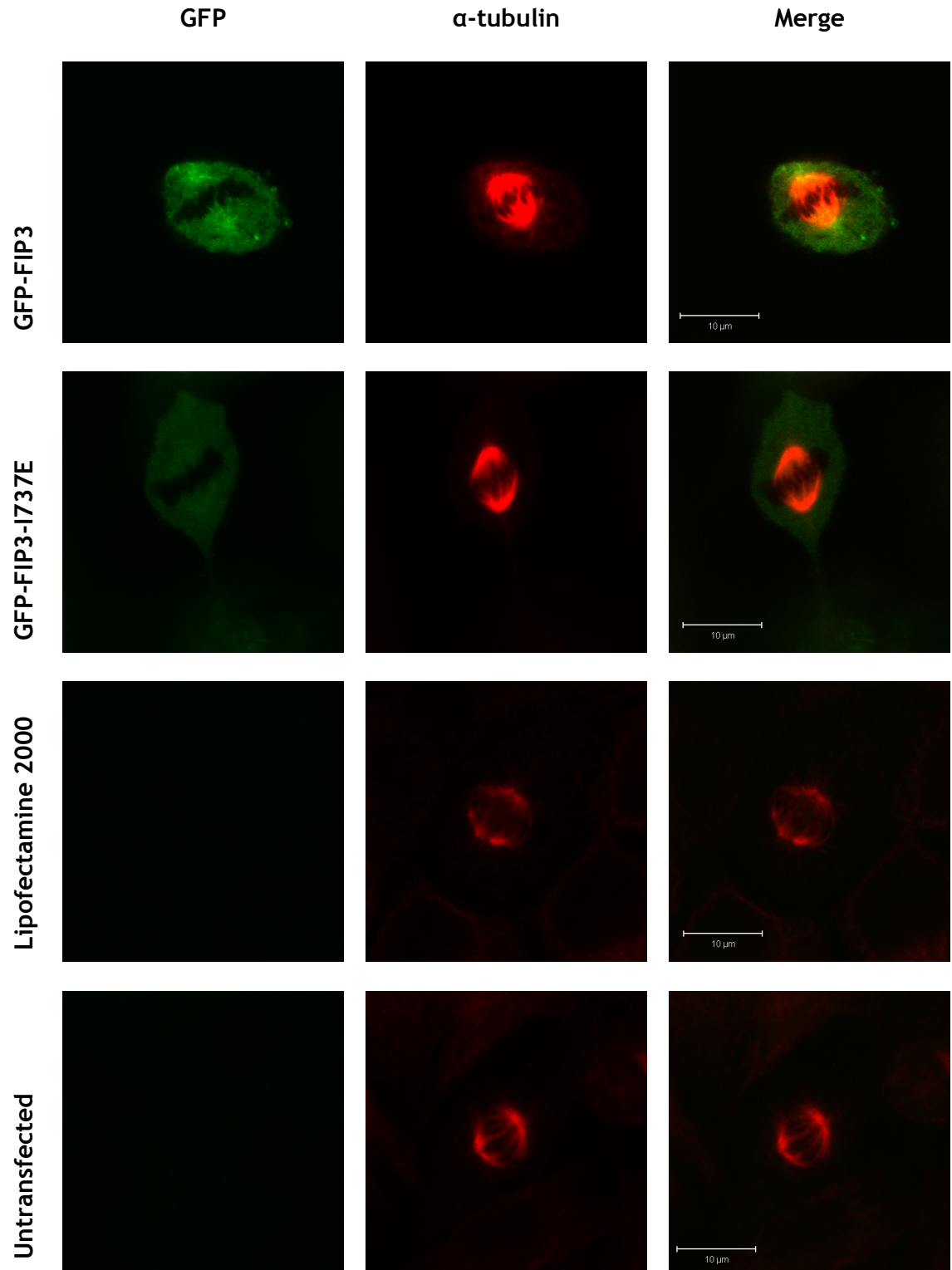


Figure 5-16 Immunofluorescence analysis of HeLa cells in metaphase expressing wild-type GFP-FIP3 and GFP-FIP3-I737E plasmids, in addition to Lipofectamine 2000 only and untransfected controls, for 48 hours.

HeLa cells were transfected with plasmid DNA or the relevant controls (section 2.4.6). Cells were fixed with 4% (w/v) ρ -formaldehyde and processed for immunofluorescence 48 hours after transfection (section 2.5). Cells were stained for microtubules using a rat monoclonal antibody to α -Tubulin, followed by Alexa Fluor® 568 (red channel). This figure details HeLa cells in metaphase expressing wild-type GFP-FIP3 and GFP-FIP3-I737E plasmids, in addition to control transfections, for 48 hours. These images represent the majority of cells viewed.

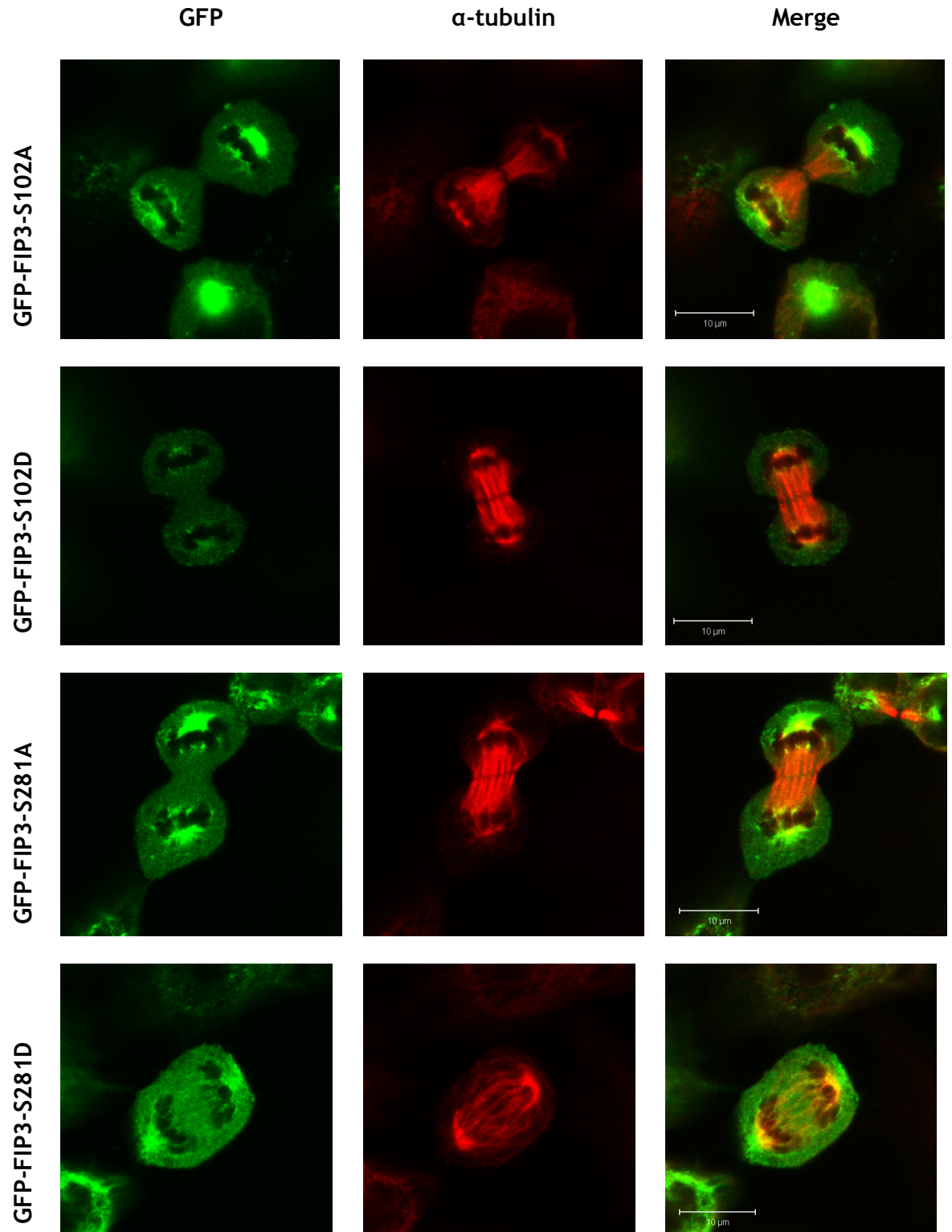


Figure 5-17 Immunofluorescence analysis of HeLa cells in anaphase expressing GFP-FIP3-S102A/D and GFP-FIP3-S281A/D plasmids for 48 hours.

HeLa cells were transfected with plasmid DNA or the relevant controls (section 2.4.6). Cells were fixed with 4% (w/v) ρ -formaldehyde and processed for immunofluorescence 48 hours after transfection (section 2.5). Cells were stained for microtubules using a rat monoclonal antibody to α -Tubulin, followed by Alexa Fluor® 568 (red channel). This figure details HeLa cells in anaphase expressing GFP-FIP3-S102A/D and GFP-FIP3-S281A/D plasmids for 48 hours. These images represent the majority of cells viewed.

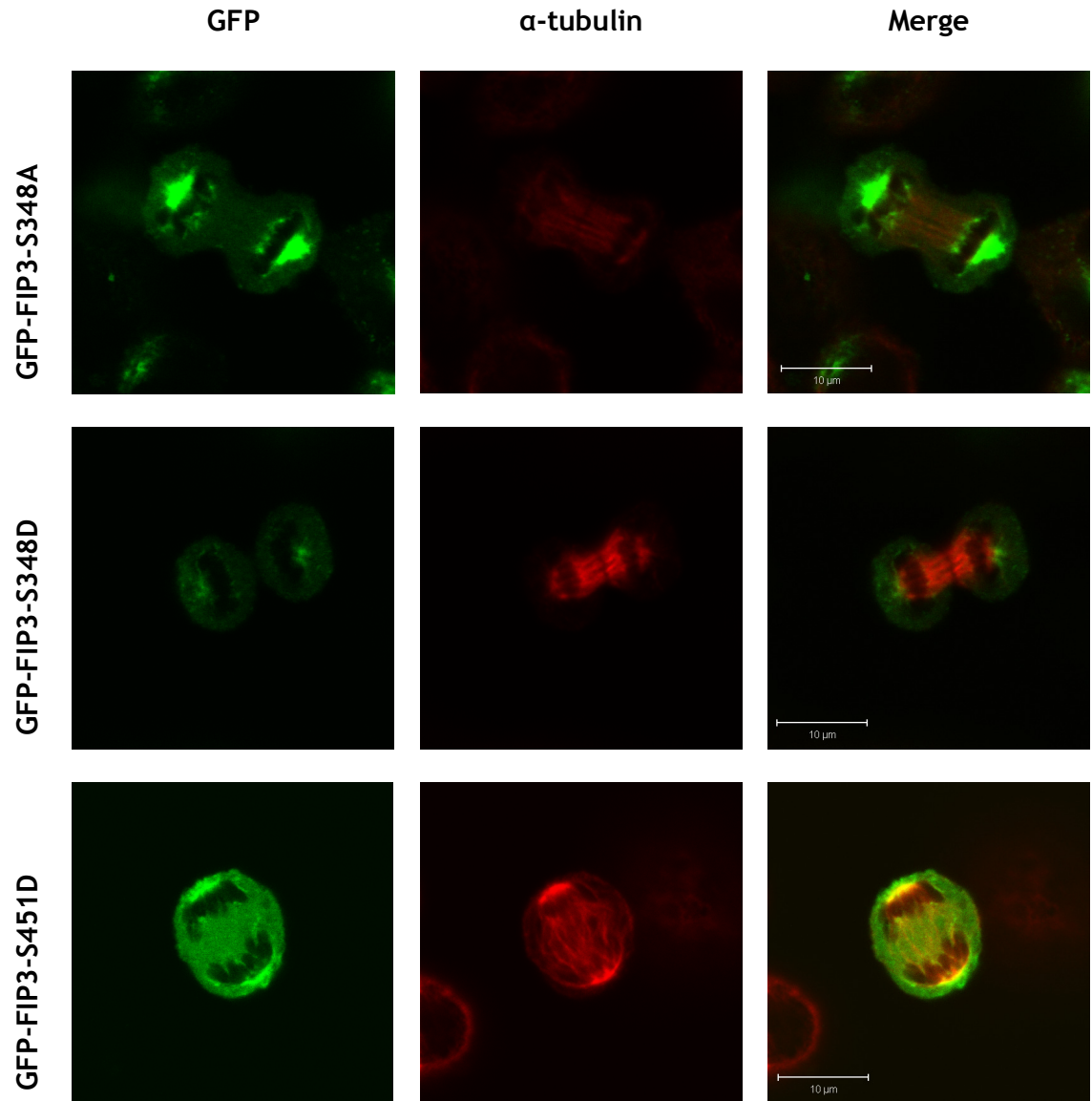


Figure 5-18 Immunofluorescence analysis of HeLa cells in anaphase expressing GFP-FIP3-S348A/D and GFP-FIP3-S451D plasmids for 48 hours.

HeLa cells were transfected with plasmid DNA or the relevant controls (section 2.4.6). Cells were fixed with 4% (w/v) ρ -formaldehyde and processed for immunofluorescence 48 hours after transfection (section 2.5). Cells were stained for microtubules using a rat monoclonal antibody to α -Tubulin, followed by Alexa Fluor® 568 (red channel). This figure details HeLa cells in anaphase expressing GFP-FIP3-S348A/D and GFP-FIP3-S451D plasmids for 48 hours. These images represent the majority of cells viewed.

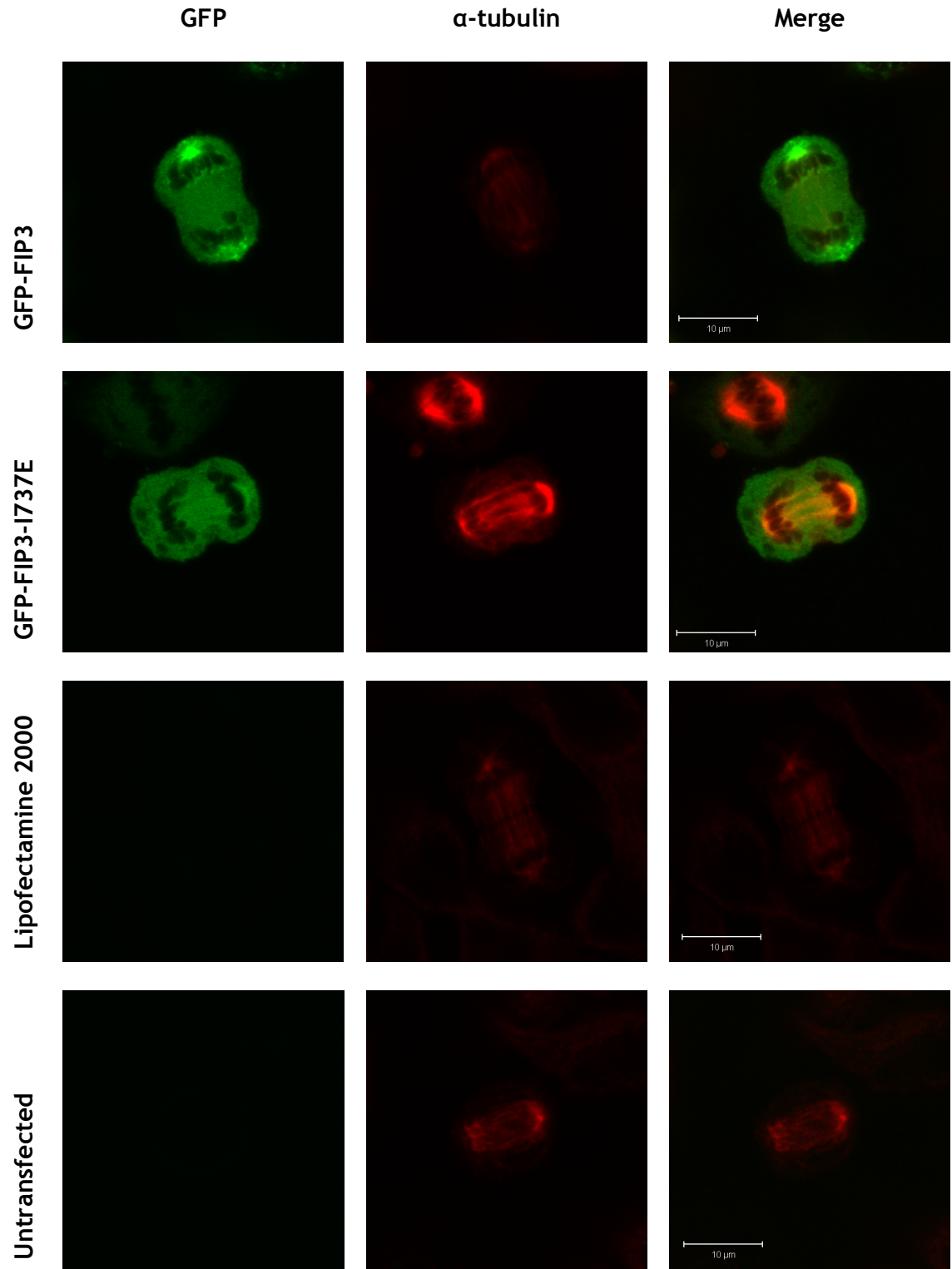


Figure 5-19 Immunofluorescence analysis of HeLa cells in anaphase expressing wild-type GFP-FIP3 and GFP-FIP3-I737E plasmids, in addition to Lipofectamine 2000 only and untransfected controls, for 48 hours.

HeLa cells were transfected with plasmid DNA or the relevant controls (section 2.4.6). Cells were fixed with 4% (w/v) ρ -formaldehyde and processed for immunofluorescence 48 hours after transfection (section 2.5). Cells were stained for microtubules using a rat monoclonal antibody to α -Tubulin, followed by Alexa Fluor® 568 (red channel). This figure details HeLa cells in anaphase expressing wild-type GFP-FIP3 and GFP-FIP3-I737E plasmids, in addition to control transfections, for 48 hours. These images represent the majority of cells viewed.

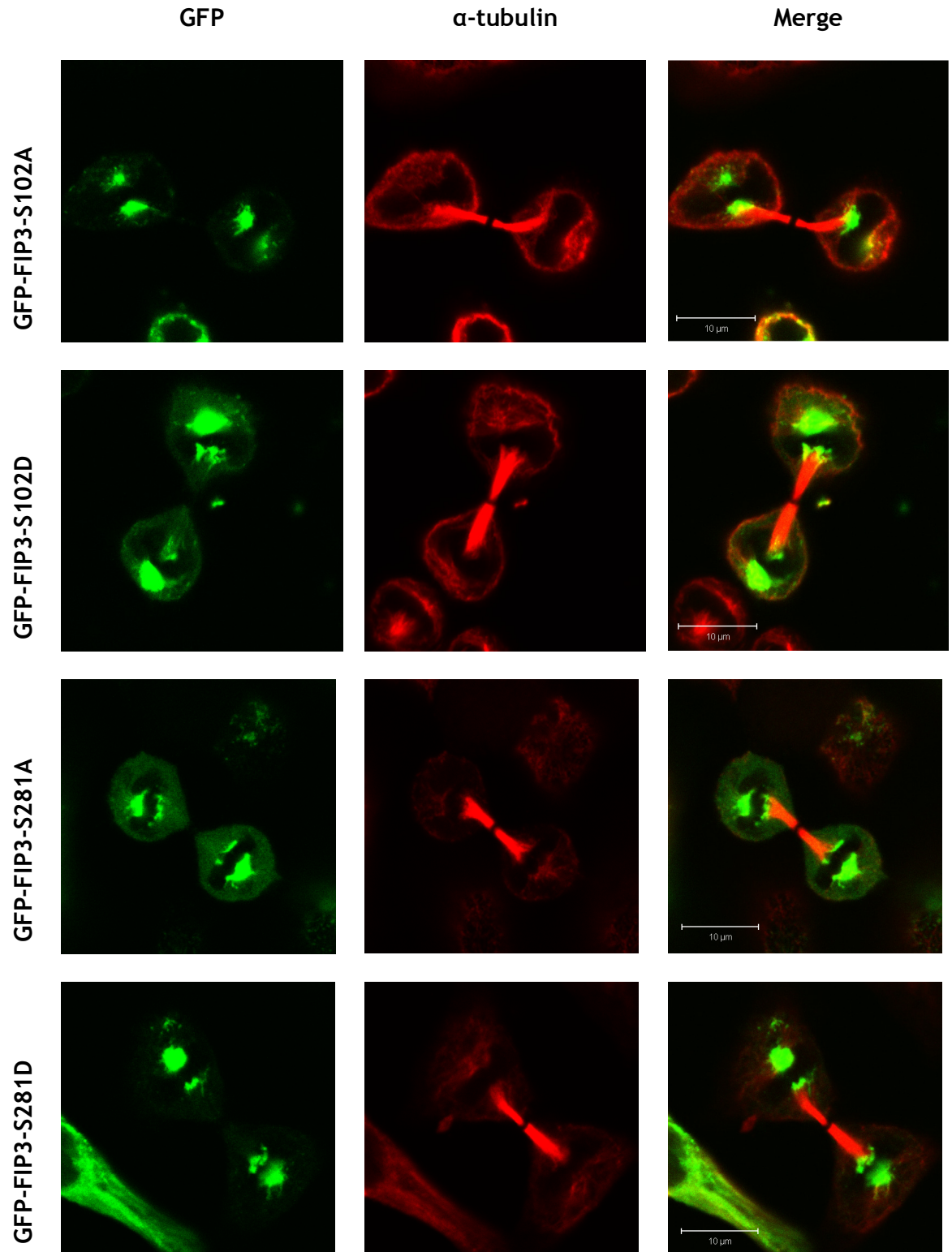


Figure 5-20 Immunofluorescence analysis of HeLa cells in early telophase expressing GFP-FIP3-S102A/D and GFP-FIP3-S281A/D plasmids for 48 hours.

HeLa cells were transfected with plasmid DNA or the relevant controls (section 2.4.6). Cells were fixed with 4% (w/v) ρ -formaldehyde and processed for immunofluorescence 48 hours after transfection (section 2.5). Cells were stained for microtubules using a rat monoclonal antibody to α -Tubulin, followed by Alexa Fluor® 568 (red channel). This figure details HeLa cells in early telophase expressing GFP-FIP3-S102A/D and GFP-FIP3-S281A/D plasmids for 48 hours. These images represent the majority of cells viewed.

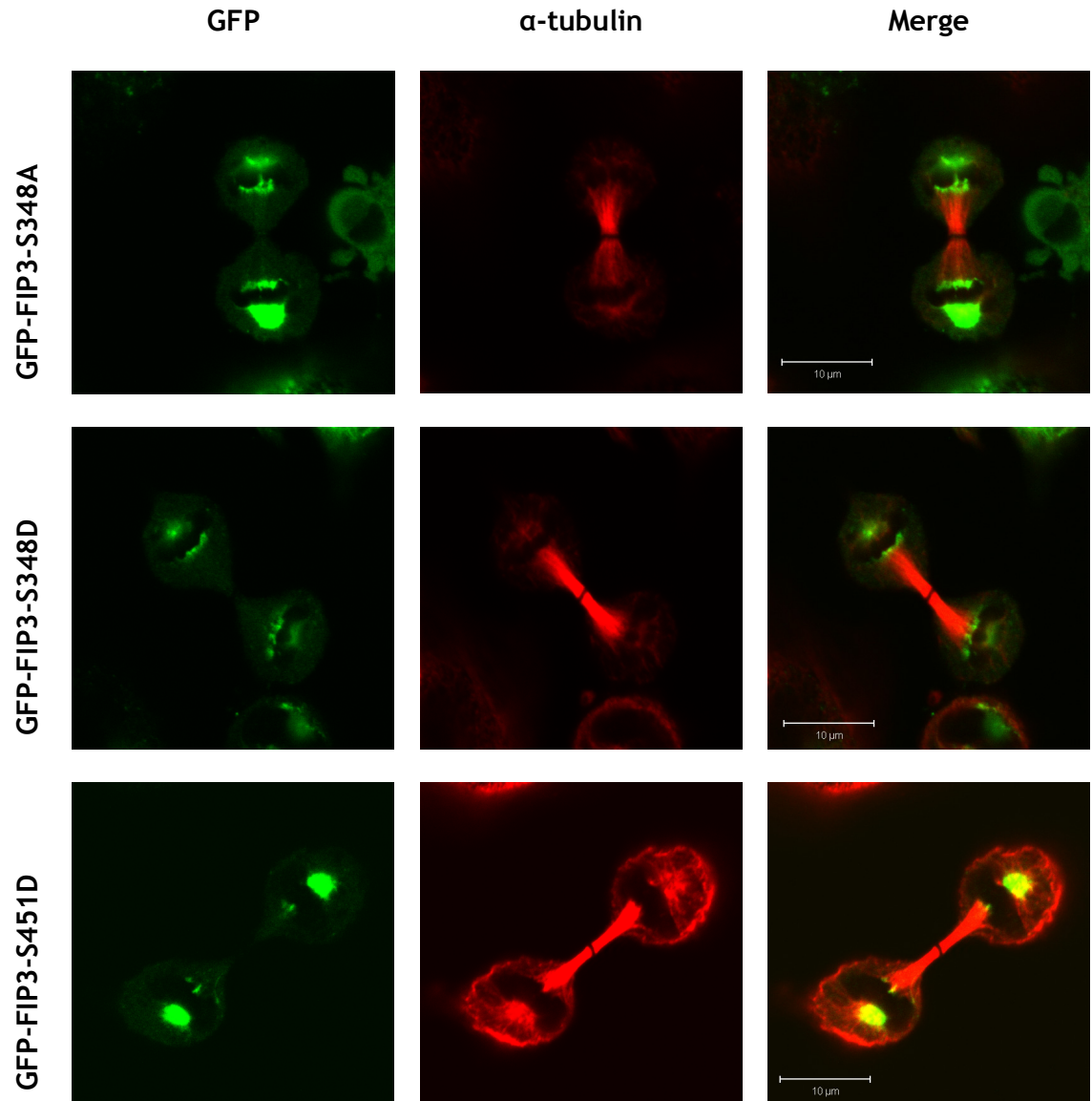


Figure 5-21 Immunofluorescence analysis of HeLa cells in early telophase expressing GFP-FIP3-S348A/D and GFP-FIP3-S451D plasmids for 48 hours.

HeLa cells were transfected with plasmid DNA or the relevant controls (section 2.4.6). Cells were fixed with 4% (w/v) ρ -formaldehyde and processed for immunofluorescence 48 hours after transfection (section 2.5). Cells were stained for microtubules using a rat monoclonal antibody to α -Tubulin, followed by Alexa Fluor® 568 (red channel). This figure details HeLa cells in early telophase expressing GFP-FIP3-S348A/D and GFP-FIP3-S451D plasmids for 48 hours. These images represent the majority of cells viewed.

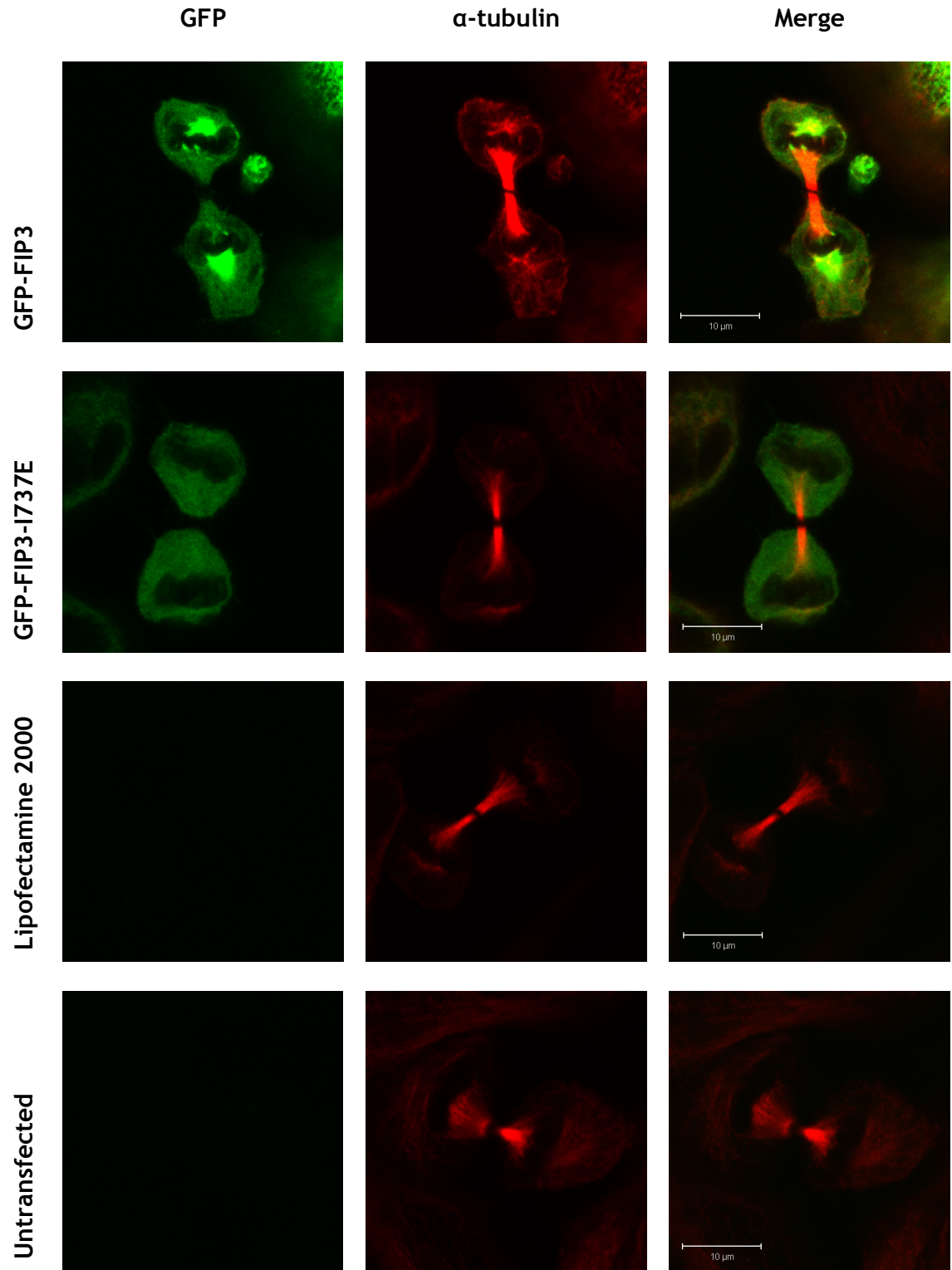


Figure 5-22 Immunofluorescence analysis of HeLa cells in early telophase expressing wild-type GFP-FIP3 and GFP-FIP3-I737E plasmids, in addition to Lipofectamine 2000 only and untransfected controls, for 48 hours.

HeLa cells were transfected with plasmid DNA or the relevant controls (section 2.4.6). Cells were fixed with 4% (w/v) ρ -formaldehyde and processed for immunofluorescence 48 hours after transfection (section 2.5). Cells were stained for microtubules using a rat monoclonal antibody to α -Tubulin, followed by Alexa Fluor® 568 (red channel). This figure details HeLa cells in early telophase expressing wild-type GFP-FIP3 and GFP-FIP3-I737E plasmids, in addition to control transfections, for 48 hours. These images represent the majority of cells viewed.

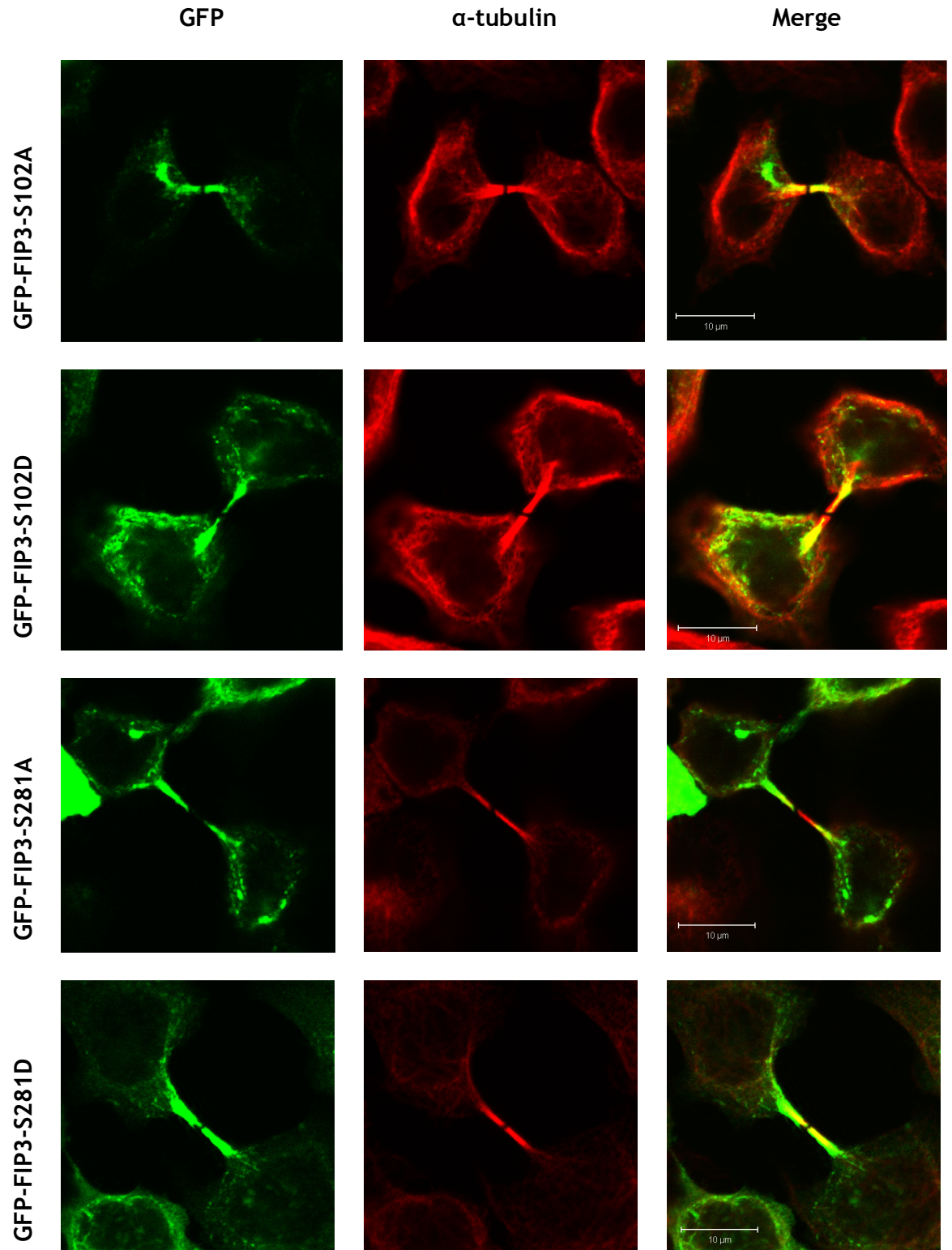


Figure 5-23 Immunofluorescence analysis of HeLa cells in late telophase expressing GFP-FIP3-S102A/D and GFP-FIP3-S281A/D plasmids for 48 hours. HeLa cells were transfected with plasmid DNA or the relevant controls (section 2.4.6). Cells were fixed with 4% (w/v) ρ -formaldehyde and processed for immunofluorescence 48 hours after transfection (section 2.5). Cells were stained for microtubules using a rat monoclonal antibody to α -Tubulin, followed by Alexa Fluor® 568 (red channel). This figure details HeLa cells in late telophase expressing GFP-FIP3-S102A/D and GFP-FIP3-S281A/D plasmids for 48 hours. These images represent the majority of cells viewed.

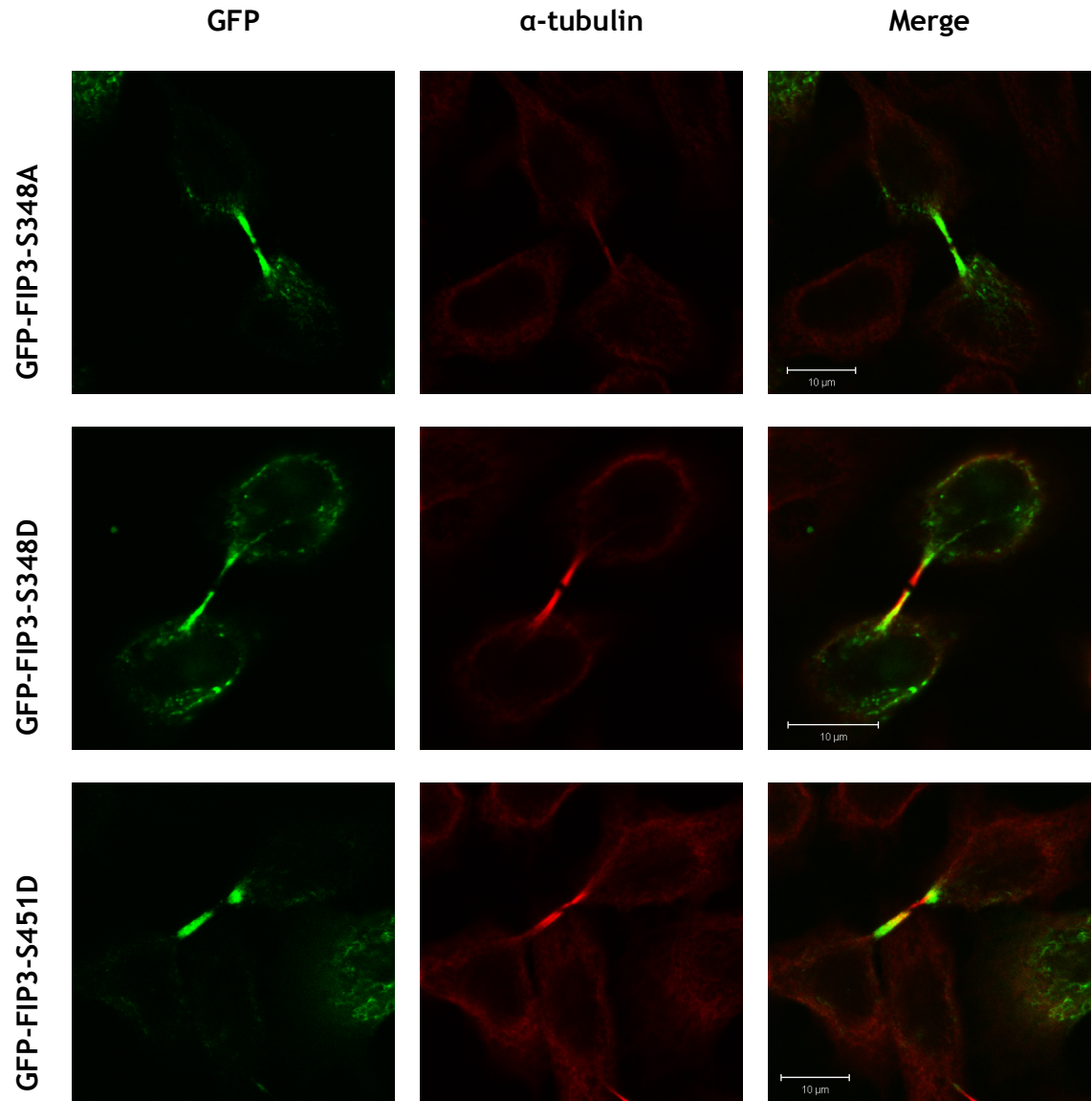


Figure 5-24 Immunofluorescence analysis of HeLa cells in late telophase expressing GFP-FIP3-S348A/D and GFP-FIP3-S451D plasmids for 48 hours.

HeLa cells were transfected with plasmid DNA or the relevant controls (section 2.4.6). Cells were fixed with 4% (w/v) ρ -formaldehyde and processed for immunofluorescence 48 hours after transfection (section 2.5). Cells were stained for microtubules using a rat monoclonal antibody to α -Tubulin, followed by Alexa Fluor® 568 (red channel). This figure details HeLa cells in late telophase expressing GFP-FIP3-S348A/D and GFP-FIP3-S451D plasmids for 48 hours. These images represent the majority of cells viewed.

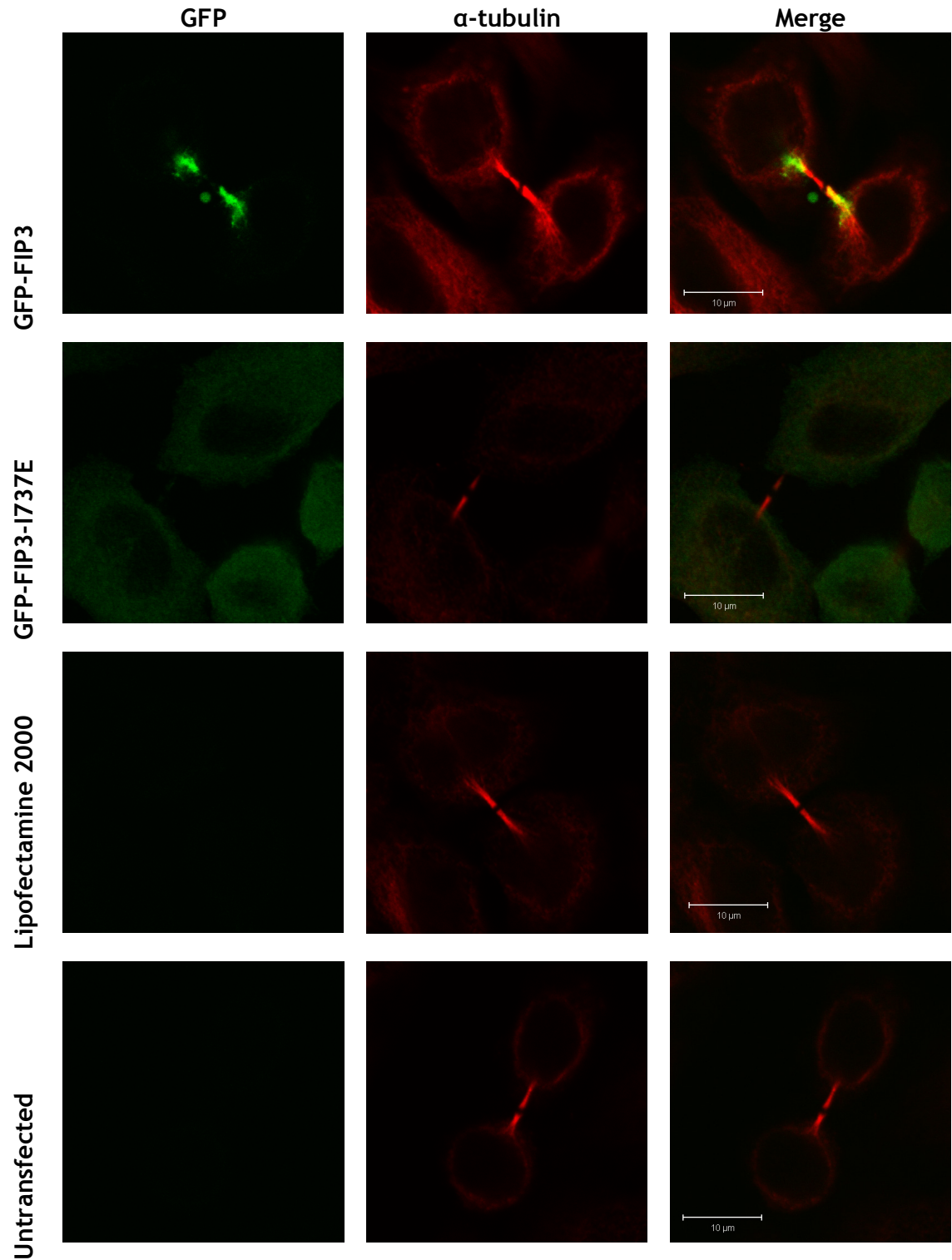


Figure 5-25 Immunofluorescence analysis of HeLa cells in late telophase expressing wild-type GFP-FIP3 and GFP-FIP3-I737E plasmids, in addition to Lipofectamine 2000 only and untransfected controls, for 48 hours.

HeLa cells were transfected with plasmid DNA or the relevant controls (section 2.4.6). Cells were fixed with 4% (w/v) ρ -formaldehyde and processed for immunofluorescence 48 hours after transfection (section 2.5). Cells were stained for microtubules using a rat monoclonal antibody to α -Tubulin, followed by Alexa Fluor® 568 (red channel). This figure details HeLa cells in late telophase expressing wild-type GFP-FIP3 and GFP-FIP3-I737E plasmids, in addition to control transfections, for 48 hours. These images represent the majority of cells viewed.

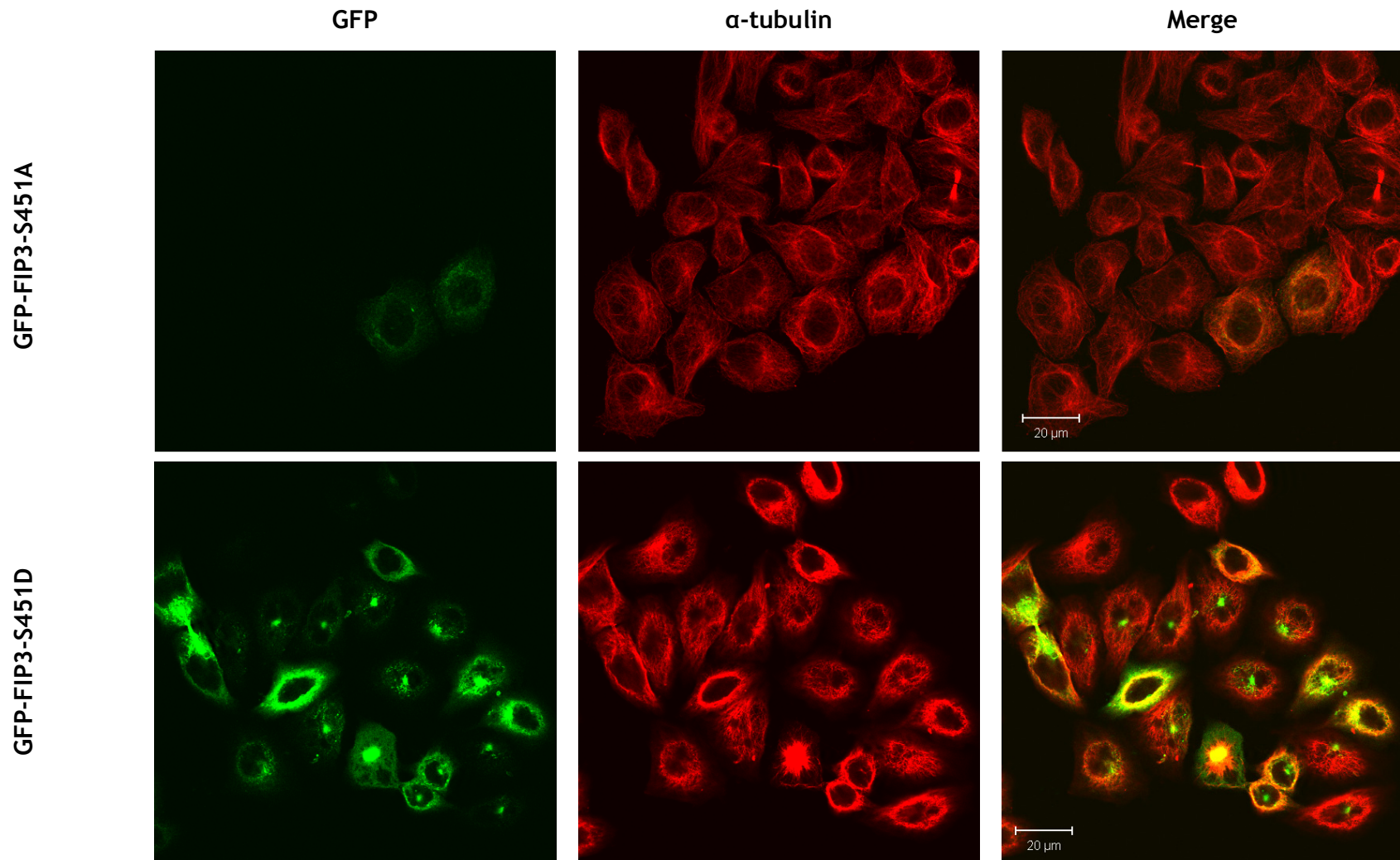


Figure 5-26 Immunofluorescence analysis of HeLa cells expressing GFP-FIP3-S451A/D plasmids for 48 hours. Cells were stained for microtubules using a rat monoclonal antibody to α -Tubulin, followed by Alexa Fluor® 568 (red channel). These images represent an average field of view.

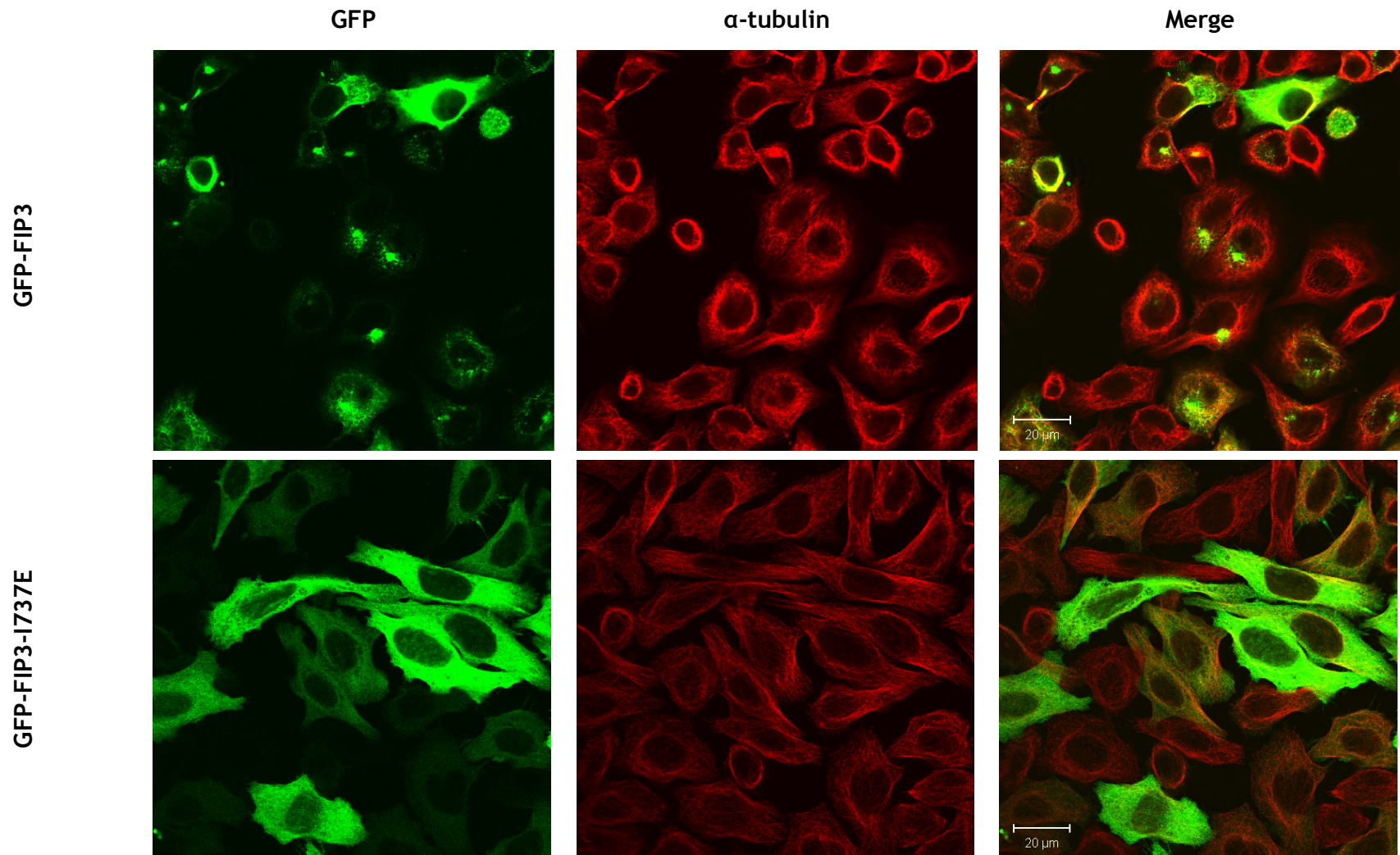


Figure 5-27 Immunofluorescence analysis of HeLa cells expressing wild-type GFP-FIP3 and GFP-FIP3-I737E plasmids for 48 hours. Cells were stained for microtubules using a rat monoclonal antibody to α -Tubulin, followed by Alexa Fluor® 568 (red channel). These images represent an average field of view.

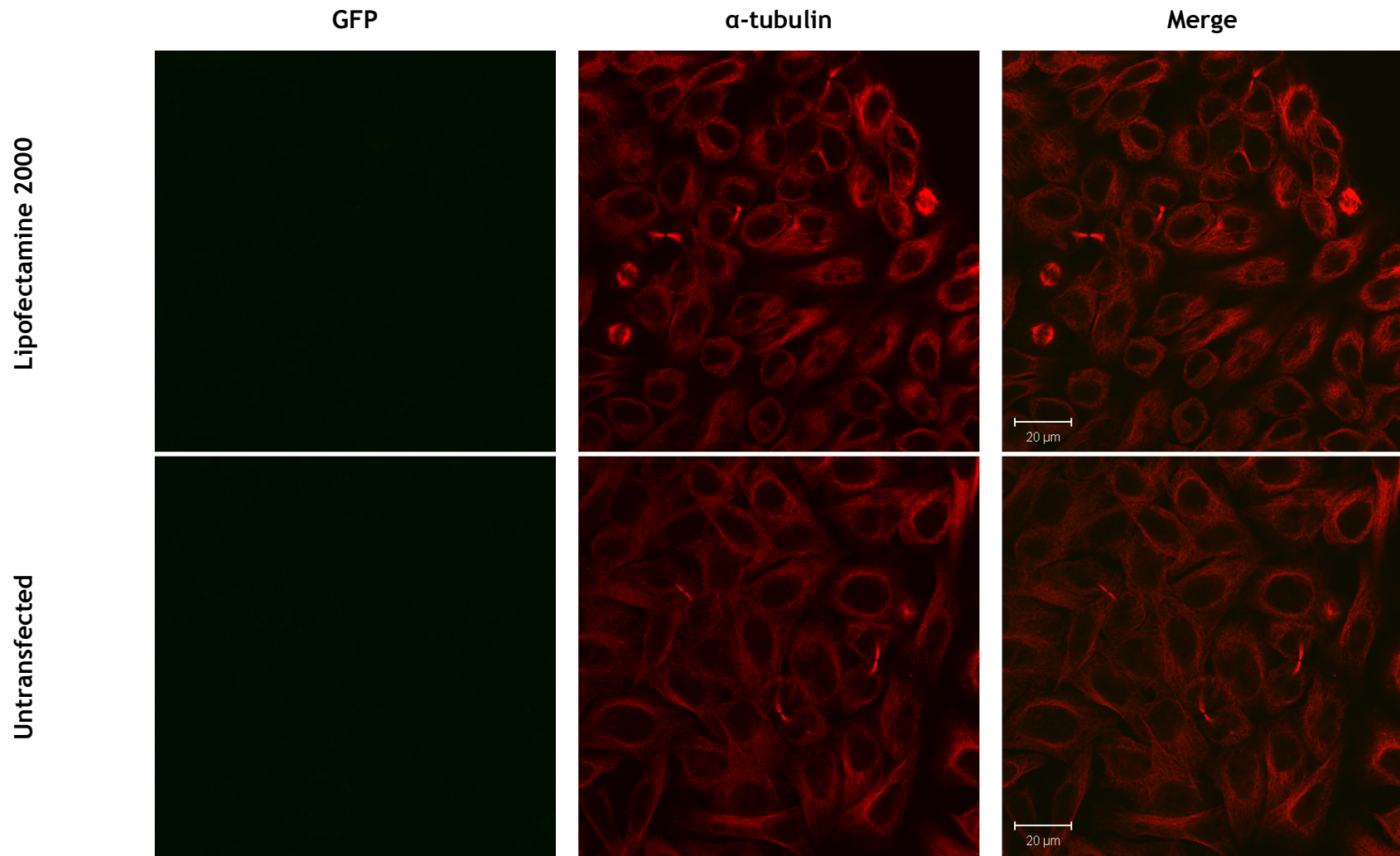


Figure 5-28 Immunofluorescence analysis HeLa cells treated with control transfections for 48 hours. Cells were stained for microtubules using a rat monoclonal antibody to α -Tubulin, followed by Alexa Fluor® 568 (red channel). These images represent an average field of view.

6 Discussion

Cytokinesis involves abscission of the intracellular bridge between two daughter cells, thus completing mitosis (Steigemann and Gerlich, 2009). The cellular dynamics at the midbody resulting in abscission are the subject of intense investigation. However, recent research has placed membrane traffic at the heart of mammalian cytokinesis (Albertson *et al.*, 2005; Barr and Gruneberg, 2007; Prekeris and Gould, 2008; Ai and Skop, 2009). Understanding the mechanisms of cytokinesis is of importance since failure of cytokinesis results in genomic instability and tumourigenesis (Fujiwara *et al.*, 2005).

Time-lapse microscopy of HeLa cells expressing GFP-FIP3 has shown that FIP3 undergoes spatial and temporal dynamics during mitosis (Wilson *et al.*, 2005). During metaphase and early anaphase FIP3 is largely cytosolic with some localised to endosomal membrane structures. During late anaphase, following furrow initiation, FIP3 localises to the centrosome. At late cytokinesis, FIP3 relocates to the cleavage furrow and midbody. On separation of daughter cells, FIP3 relocates to the centrosome. It has been proposed that FIP3 in complex with Rab11 plays a key role in the delivery and targeting of recycling endosomes to the furrow; this is essential for completion of cytokinesis (Wilson *et al.*, 2005; Fielding *et al.*, 2005).

The regulatory mechanisms governing the spatial and temporal dynamics of FIP3 during mitosis are unknown. The cell-cycle is regulated by a network of protein kinases which control the activity, localisation and interactions of proteins involved in cell-cycle progression (Nigg, 2001). This work aimed to determine if FIP3 can be phosphorylated by the mitotic kinases and whether this has an impact on its spatial and temporal dynamics. Work from a collaborating lab suggests that FIP3 is a phospho-protein, which can exist in different, reversible phosphorylation states (R. Prekeris, personal communication). Proteomic analysis of FIP3 immunoprecipitated from metaphase cells identified the serines 102, 281, 348 and 451 as sites of phosphorylation (R. Prekeris, personal communication).

We first sought to determine whether candidate cell-cycle kinases phosphorylate FIP3 *in vitro* and found that FIP3 was phosphorylated by cyclin B-CDK1, Plk1, Aurora A and weakly by Aurora B. A proteomic approach showed that within the limits of our experimental approach, only cyclin B-CDK1 phosphorylated FIP3 significantly, at serine 102. This parallels the site identified by Prekeris *et al.*, in metaphase HeLa lysates. Analysis of the amino acid sequence surrounding serine 102 identifies it as a potential target of the CDKs, owing to the presence of a proline residue immediately following the phospho-serine (Shetty *et al.*, 1993; Brown *et al.*, 1999; Ubersax and Ferrell Jr, 2007). This work does not discount the role of the Plk1, Aurora A, Aurora B or other mitotic kinases in the regulation of FIP3.

Analysis of the role of phosphorylation in the membrane and cytosol distribution of FIP3 throughout the cell-cycle has shown that phosphorylation and dephosphorylation of FIP3 during mitosis may regulate FIP3 association with membranes (unpublished data from the Prekeris and Gould labs). Synchronised HeLa cells fractionated at metaphase and telophase show that during prometaphase and metaphase, FIP3 is predominantly cytosolic. FIP3 is membrane associated in telophase cells. This work was performed by Prekeris *et al.*, and subsequently replicated in this thesis. This association of FIP3 with membranes is dependent upon dephosphorylation of FIP3, as phosphatase treatment of cell extracts from metaphase results in FIP3 associating with membranes. Interestingly, FIP3 phosphorylation appears to decrease at telophase (R. Prekeris, personal communication). Such data offer the hypothesis that FIP3 is phosphorylated during early stages of the cell-cycle, and that dephosphorylation of FIP3 is the trigger for the association of FIP3 with membranes. This may have implications for the regulation of FIP3's dynamics during the cell-cycle.

We sought to explore further the role that phosphorylation plays in the membrane association of FIP3. A phospho-specific antibody to serine 102 (pS102) detected CDK1 phosphorylated FIP3. This further supports our findings that cyclin B-CDK1 phosphorylates FIP3 at serine 102. Screening of crude cell lysates from synchronised HeLa cells shows that serine 102 is phosphorylated in metaphase and becomes dephosphorylated as the cell progresses through to telophase. Further analysis of membrane and cytosol fractions from these cells

reveal that cytosolic levels of pS102 peak in metaphase and decrease towards telophase to negligible levels. pS102 is absent in the membrane fraction. This work suggests that FIP3 may be directly phosphorylated by CDK1 at serine 102 in early mitosis. This may affect the membrane and cytosol distribution of FIP3 by preventing membrane association of FIP3 in metaphase.

Dephosphorylated FIP3 does not associate randomly with HeLa membranes or protein-free liposomes, as assayed by density gradient fractionation. Thus we suggest that the dephosphorylation event required for membrane association must in some way be coupled to a change in affinity for membranes, perhaps affinity for another protein. Proteins known to interact with FIP3 include Rab11 (Prekeris *et al.*, 2001; Eathiraj *et al.*, 2006; Shiba *et al.*, 2006), ARF6 (Shin *et al.*, 2001; Fielding *et al.*, 2005), CYK-4 (Simon *et al.*, 2008) and ASAP1 (Inoue *et al.*, 2008). Interestingly, Rab11 knock-down with RNAi results in translocation of FIP3 from the membranes to the cytosol, suggesting that the Rab11 mediates the association of FIP3 with endosomes (Wilson *et al.*, 2005). The link between FIP3 and the cell membrane and how this is modulated via phosphorylation warrants further investigation. Interestingly serine 102 is located within this proline rich region of FIP3; this type of region is known to mediate a large number of protein to protein interactions (Kay *et al.*, 2000).

The role of phosphorylation at serines 102, 281, 348 and 451 of FIP3 was investigated by creating phospho-null and phospho-mimetic mutants in the context of GFP-FIP3. It would appear that when mutated singly the potential phospho-sites of serines 102, 281, 348 and 451 (phospho-mimetic mutant only for serine 451) have no significant effect on the spatial and temporal regulation of FIP3 during mitosis as their localisations mirror that of the wild type GFP-FIP3 protein. Mutations of these phospho-sites had no effect on cytokinesis, as assayed via binuclear cell counts. However, this requires further analysis. Ongoing work in our lab aims to create a FIP3 knockdown system in HeLa cells which would allow the phospho-mutants to be expressed in the absence of endogenous FIP3. Also, to ensure that potential defects in mitosis are not overlooked, time lapse microscopy could be performed on cells expressing GFP-FIP3 phospho-mutants. Further work to produce double/triple/quadruple mutants for these four sites would explore the role of these phospho-sites further. It would also be of interest to analyse the membrane and cytosol ratios

of these GFP-FIP3 phospho-mutants. A phospho-null mutation of serine 451 produced an interesting phenotype. Very few cells expressed this protein. The ones which did so were often unhealthy and the protein failed to localise in the same way as wild-type GFP-FIP3. The role of phosphorylation at serine 451 warrants further investigation. Mitotic catastrophe resulting from expression of a phospho-mimetic form of CK2 has been previously reported (St Denis *et al.*, 2009).

Preliminary kinase inhibition studies show that inhibition of CDK1 by the inhibitor BMI-1026 results in a mis-localisation of GFP-FIP3 in HeLa cells. This could also be interpreted as a delay in cytokinesis, since CDK1 inhibition resulted in more cells displaying GFP-FIP3 in a localisation characteristic of an earlier stage of telophase, compared to the controls. However, since CDK1 is chiefly responsible for the orchestration of mitosis (Nigg, 2001), perhaps inhibiting the action of this kinase disrupts other factors in the cell, leading to mis-localisation of FIP3. Interestingly, knockdown of Aurora B with RNAi results in a similar mis-localisation of GFP-FIP3 (Simon *et al.*, 2008). Further work could employ the use of time lapse microscopy to study the effect of BMI-1026 on GFP-FIP3 localisation. Owing to the growing number of small molecule inhibitors of mitotic kinases, the role of other kinases such as Plk1 and Aurora B in GFP-FIP3 localisation could be examined by time lapse microscopy, allowing their roles in late mitosis to be examined by avoiding their earlier cell-cycle functions (Petronczki *et al.*, 2007). Also these inhibitors could be used to analyse the effect of kinase inhibition on the membrane and cytosol distribution of FIP3.

This work opens up another avenue of research. FIP3 is a phospho-protein and the current thinking suggests that dephosphorylation of FIP3 in late anaphase results in its association with membranes. The next step would be to identify the phosphatase responsible for this event. The role of phosphatases in the spatial and temporal regulation of mitosis is as important as that of the kinases, although less well studied (Bollen *et al.*, 2009).

In summary, FIP3 undergoes spatial and temporal dynamics during mitosis (Wilson *et al.*, 2005; Fielding *et al.*, 2005). The current working model suggests that Rab11 recruits FIP3 onto recycling endosome-derived vesicles at the centrosome. In telophase FIP3-Rab11 vesicles traffic to the furrow and at later

stages the midbody. These vesicles are directed along the microtubules of the mitotic spindle, possibly via the motor protein kinesin I. These vesicles are tethered to the midbody prior to abscission via interactions with ARF6, Rab11, CYK-4 and components of the Exocyst. These vesicles may serve as an organisation platform for the assembly of the abscission machinery or they may deliver the cargo required for abscission. FIP3-Rab11 vesicles may also be involved in a compound fusion event which seals the intracellular bridge, thus resolving the two daughter cells (Prekeris and Gould, 2008).

Work from this thesis has added a new dimension to this model. FIP3 dynamics may be regulated by phosphorylation, potentially by CDK1. CDK1 in complex with its regulatory subunit, cyclin B1, is chiefly responsible for the orchestration of mitosis (Nigg, 2001). Cyclin B1-CDK1 activity peaks in the early stages of mitosis and is inactivated via degradation of cyclin B as the last chromosome lines up on the metaphase plate, just after inactivation of the spindle-assembly checkpoint (Clute and Pines, 1999). Cyclin B1-CDK1 negatively regulates many of the protein complexes required for cytokinesis, until anaphase onset when the sister chromatids have successfully separated and CDK1 is inactivated (Barr and Gruneberg, 2007). Interestingly, phosphorylation by CDK1 can affect the membrane and cytosol distribution of proteins involved in mitosis: cyclin B1-CDK1 phosphorylation of the microtubule motor cytoplasmic dynein releases the protein from membranes, *in vitro* (Addinall *et al.*, 2001).

Work from our lab and Prekeris *et al.*, suggests that during prometaphase and metaphase FIP3 is phosphorylated, preventing its association with endosomes. FIP3 is dephosphorylated in late anaphase, allowing it to associate with endosomes and subsequently traffic to the furrow and midbody. We suggest that CDK1 phosphorylates FIP3 in the early stages of mitosis, at serine 102. This perhaps modulates the affinity of FIP3 for another protein which recruits it to vesicles derived from the recycling endosome at the centrosome. Recent research has placed membrane traffic at the heart of mammalian cytokinesis and data from this thesis suggests that membrane dynamics may be regulated by the orchestrators of mitosis: the cell-cycle kinases.

7 Appendix

7.1 Rab11-FIP3 Proteomic Data

7.1.1 Rab11-FIP3 solution analysed via nLC-ESI-MS/MS by Sir Henry Wellcome Functional Genomics Facility (SHWFGF), University of Glasgow

Protein	Score	Database Accession Number
Rab11-family interacting protein 3	1602	gi 7662234
Beta tubulin	580	gi 135490
Beta tubulin	538	gi 57429
Beta tubulin	531	gi 12851187
Beta tubulin	502	gi 49456871
Beta tubulin	495	gi 90075322
Alpha tubulin	466	gi 2843123
Beta tubulin	452	gi 223486
Beta tubulin	450	gi 149440634
Beta tubulin	440	gi 74212109
Beta tubulin	431	gi 223429
Rab11-family interacting protein 3	418	gi 26006197
Alpha tubulin	343	gi 66730465
Alpha tubulin	323	gi 135435
Alpha tubulin	305	gi 114649125
Alpha tubulin	293	gi 74186501
Alpha tubulin	266	gi 119878872
Hsp70	252	gi 428
Rab11-family interacting protein 3	236	gi 126335383
Rab11-family interacting protein 3	200	gi 116667015
Hsp70	198	gi 640325
Hsp70	187	gi 62897129
Beta tubulin	170	gi 225480
Alpha tubulin	163	gi 73960249

Alpha tubulin	146	gi 149626356	
Trypsin precursor	125	gi 136429	
Histone H2B	107	gi 76630991	
Histone H2B	103	gi 1568557	
Histone H2B	102	gi 28173554	
Beta tubulin	97	gi 114575797	
Ribosomal protein S3	92	gi 32532	
Alpha tubulin	88	gi 10436240	
Ribosomal protein L9	82	gi 607793	
Ribosomal protein S15a	81	gi 55586139	
T-complex protein 1 subunit eta (TCP-1-eta)	81	gi 549060	
Beta actin	74	gi 89257929	
PREDICTED: actin, gamma 1 propeptide	65	gi 114670968	
PREDICTED: similar to complement receptor (Cr2)	63	gi 119923979	
Beta tubulin	62	gi 2144007	
Ribosomal protein S9	62	gi 146424326	
Alpha tubulin	61	gi 119587277	
PREDICTED: similar to laminin, alpha 2	60	gi 149636827	
Ribosomal protein S4	60	gi 4432939	
PREDICTED: similar to serine/threonine protein phosphatase 2A, 55 kDa regulatory subunit B, alpha isoform (PP2A, subunit B, B-alpha isoform)	58	gi 73993713	★
Translation elongation factor 1 alpha	58	gi 31092	
Abnormal spindle-like microcephaly-associated protein	57	gi 38155726	
PREDICTED: similar to golgi autoantigen, golgin subfamily a, 4	54	gi 109484079	
PIG48 (proliferation-inducing gene 48)	52	gi 46411195	
rCG39164	51	gi 149015707	
PREDICTED: similar to phospholipase C-beta-3	51	gi 119919228	
PREDICTED: similar to macrophin 1	50	gi 149608639	
Serine/threonine protein phosphatase 2A, 55 kDa regulatory subunit B, beta isoform (PP2A, subunit B, B-beta isoform)	50	gi 26347737	★
PREDICTED: similar to tubulin tyrosine ligase-like family, member 6	49	gi 109488871	
PREDICTED: similar to copper-transporting ATPase	49	gi 149730284	

Table 7.1 Protein identification of recombinant FIP3 solution by nLC-ESI-MS/MS, searching the *Mammalia* database, performed by SHWFGF, University of Glasgow. Individual ion scores greater than the probability based MASCOT cut off score of 49 indicate homology or extensive identity ($p < 0.05$). Protein hits of interest are marked with a star.

Protein	Score	Database Accession Number
Beta tubulin	379	gi 24655737
Alpha tubulin	356	gi 17136564
Beta tubulin	224	gi 158743
Beta tubulin	131	gi 21428640
TCP-1eta chaperonin	118	gi 24645179
TCP1 chaperonin	109	gi 125775778
Heat shock cognate 4	83	gi 157665
Heat shock protein cognate 72	82	gi 157658
Histone H2b	71	gi 7436
Ribosomal protein L9	70	gi 1208910
Ribosomal protein S3	62	gi 296094
Ribosomal protein S3	62	gi 38048231
Kinesin heavy chain	62	gi 157778
TCP1 Chaperonin	60	gi 125778070
Heat shock protein cognate 1, isoform A	58	gi 17647515
Ribosomal protein S10a	58	gi 21357663
Acetyl CoA carboxylase	52	gi 24586458
Ribosomal protein S19	50	gi 396531
Actin	48	gi 156763
Actin	47	gi 156773
Ribosomal protein S9, isoform A	46	gi 24661707
DGP-1 protein	46	gi 5764409
Ribosomal protein S2	44	gi 288084
Ribosomal protein L17, isoform D	44	gi 18921137
N-acetyltransferase 1, isoform B (NAT1)	43	gi 22026966
RNA helicase	43	gi 157594
Innexin	42	gi 125981821
Ribosomal protein S4	41	gi 440853
Ribosomal protein S9	41	gi 125808610

★

Ribosomal protein S15Aa, isoform D	40	gi 17975567
------------------------------------	----	-------------

Table 7.2 Protein identification of recombinant FIP3 solution by nLC-ESI-MS/MS, searching the *Drosophila* database, performed by SHWFGF, University of Glasgow. Individual ion scores greater than the probability based MASCOT cut off score of 39 indicate homology or extensive identity ($p < 0.05$). Protein hits of interest are marked with a star.

7.1.2 Rab11-FIP3 gel slices analysed via nLC-ESI-MS/MS by Sir Henry Wellcome Functional Genomics Facility (SHWFGF), University of Glasgow

Protein	Score	Database Accession Number
Rab11-family interacting protein 3	1868	gi 7662234
Rab11-family interacting protein 3	775	gi 119916632
Rab11-family interacting protein 3	583	gi 149750990
Alpha tubulin	536	gi 2843123
Alpha tubulin	505	gi 46409270
Beta tubulin	486	gi 135490
Beta tubulin	479	gi 224839
Beta tubulin	470	gi 12851187
Beta tubulin	453	gi 49456871
Beta tubulin	448	gi 40018568
Alpha tubulin	441	gi 135435
Beta tubulin	426	gi 90080399
Alpha tubulin	421	gi 66730465
Beta tubulin	408	gi 149440634
Hsp70	364	gi 126326875
Alpha tubulin	350	gi 74186501
Alpha tubulin	350	gi 119878872
Heat shock-related 70 kDa protein 2	338	gi 123621
Rab11-family interacting protein 3	332	gi 126335383
Beta tubulin	323	gi 223429
Hsp70	306	gi 640325
Alpha tubulin	287	gi 149626356
Alpha tubulin	283	gi 77539752

Chain E, Leech-Derived Trypsin Inhibitor TRYPSIN COMPLEX	282	gi 3318722
Trypsin precursor	272	gi 136429
Hsp70	227	gi 62897129
Alpha tubulin	179	gi 73960249
Rab11-family interacting protein 3	164	gi 116667015
Beta tubulin	151	gi 225480
Alpha tubulin	134	gi 57099745
Ribosomal protein S3	117	gi 32532
Beta tubulin	103	gi 114575797
78 kDa glucose-regulated protein precursor (GRP78 precursor)	90	gi 386758
SWI/SNF related, matrix associated, actin dependent regulator of chromatin, subfamily c, member 2	83	gi 15341763
SWI/SNF related, matrix associated, actin dependent regulator of chromatin, subfamily c, member 1	80	gi 119585235
Ribosomal protein L9	76	gi 607793
Alpha tubulin	64	gi 10436240
40S Ribosomal protein S3	60	gi 73982323
Chaperonin containing t-complex polypeptide 1, delta subunit; CCT-delta	56	gi 126303810
TCP1 Chaperonin	53	gi 201723
rCG39164	52	gi 149015707
Eukaryotic translation initiation factor 3, subunit 10	51	gi 114326234
Fatty acid coenzyme A ligase 5	49	gi 6174877
Cytochrome b	48	gi 22652250

Table 7.3 Protein identification of recombinant FIP3 gel slice 1 by nLC-ESI-MS/MS searching the *Mammalia* database, performed by SHWFGF, University of Glasgow. Individual ion scores greater than the probability based MASCOT cut off score of 48 indicate homology or extensive identity (p<0.05).

Protein	Score	Database Accession Number
Beta tubulin	234	gi 24655737
Alpha tubulin	223	gi 17136564
Beta tubulin	166	gi 860916
Hsp70	159	gi 125778264
Beta tubulin	148	gi 158749
Beta tubulin	131	gi 158743
Heat shock protein cognate 72	125	gi 157658
Beta tubulin	85	gi 21428640
Ribosomal protein S3	82	gi 38048231
TCP1 gamma chaperonin	78	gi 125775778
Ribosomal protein L9	76	gi 1208910
GA15060-PA	67	gi 125776432
Moirra (contains DNA binding domain)	67	gi 4220848
Heat shock protein 68	63	gi 34420080
Heat shock protein cognate 1, isoform A	63	gi 17647515
Heat shock protein Hsp70c	63	gi 38325846
Heat shock protein 68 short form	63	gi 34420086
Heat shock protein 68 long form	63	gi 34420082
TCP1 chaperonin	62	gi 125778070
RNA helicase	58	gi 157594
RE65203p	54	gi 17946379
T complex protein	53	gi 158534
eIF3-S9, isoform B	48	gi 19922458
eIF3-S8	47	gi 19922464
CG11198-PA, isoform A	47	gi 24586458
AT15052p	44	gi 18446976
LD07301p	41	gi 16768826

Table 7.4 Protein identification of recombinant FIP3 gel slice 1 by nLC-ESI-MS/MS searching the *Drosophila* database, performed by SHWFGF, University of Glasgow. Individual ion scores greater than the probability based MASCOT cut off score of 38 indicate homology or extensive identity ($p < 0.05$).

Protein	Score	Database Accession Number
Rab11-family interacting protein 3	1292	gi 7662234
Rab11-family interacting protein 3	653	gi 119916632
Beta tubulin	546	gi 135490
Beta tubulin	529	gi 224839
Alpha tubulin	514	gi 2843123
Beta tubulin	506	gi 12851187
Beta tubulin	504	gi 49456871
Beta tubulin	501	gi 5174735
Alpha tubulin	412	gi 66730465
Beta tubulin	404	gi 149440634
Beta tubulin	399	gi 223429
Alpha tubulin	396	gi 135435
Beta tubulin	391	gi 74212109
Chain E, Leech-Derived Trypsin Inhibitor TRYPSIN COMPLEX	331	gi 3318722
Alpha tubulin	326	gi 74186501
Alpha tubulin	290	gi 119878872
Alpha tubulin	277	gi 149626356
Beta tubulin	272	gi 126321861
Beta tubulin	232	gi 73962097
Beta tubulin	213	gi 10433717
Alpha tubulin	178	gi 73951159
Alpha tubulin	147	gi 73960249
Beta tubulin	126	gi 225480
Ribosomal protein S3	109	gi 6755372
Beta tubulin	98	gi 147223311
T-complex protein 1 isoform b (TCP1b)	92	gi 57863259
PREDICTED: similar to retinoblastoma binding protein 4, isoform 5	81	gi 88982346
Ribosomal protein L9	76	gi 607793
Translation elongation factor EF-1 alpha	75	gi 31092
Alpha tubulin	69	gi 10436240
PREDICTED: similar to BMK1 alpha kinase	68	gi 126334010
Alpha tubulin	57	gi 13376181



PREDICTED: similar to laminin, alpha 2	55	gi 149636827
Solute carrier family 25, member 41	54	gi 115495681
Replication factor C (activator 1) 2, isoform CRA_c	52	gi 148687478
rCG40478, isoform CRA_e	52	gi 149068843

Table 7.5 Protein identification of recombinant FIP3 gel slice 2 by nLC-ESI-MS/MS searching the *Mammalia* database, performed by SHWFGF, University of Glasgow. Individual ion scores greater than the probability based MASCOT cut off score of 49 indicate homology or extensive identity ($p < 0.05$). Protein hits of interest are marked with a star.

Protein	Score	Database Accession Number
Beta tubulin	273	gi 24655737
Alpha tubulin	200	gi 17136564
Beta tubulin	181	gi 860916
Beta tubulin	169	gi 158749
Beta tubulin	135	gi 158743
Alpha tubulin	116	gi 17865841
Beta tubulin	87	gi 21428640
Ribosomal protein S3	78	gi 296094
Ribosomal protein L9	76	gi 1208910
TCP1 Chaperonin	73	gi 125810511
t-complex polypeptide 1	68	gi 7716854
TCP1 Chaperonin	64	gi 125775778
Lasp protein	58	gi 27526238
CG11198-PA, isoform A	54	gi 24586458
GA11482-PA	52	gi 125777031
RNA helicase	51	gi 157594
Int6 homologue	50	gi 17137592
Chromatin assembly factor 1 subunit	46	gi 17933648
Elongation factor 1-alpha (EF-1-alpha)	42	gi 7915

Table 7.6 Protein identification of recombinant FIP3 gel slice 2 by nLC-ESI-MS/MS searching the *Drosophila* database, performed by SHWFGF, University of Glasgow. Individual ion scores greater than the probability based MASCOT cut off score of 38 indicate homology or extensive identity ($p < 0.05$).

Protein	Score	Database Accession Number
Rab11-family interacting protein 3	1088	gi 7662234
Rab11-family interacting protein 3	564	gi 119916632
Keratin	424	gi 1346343
Keratin	420	gi 109096823
Chain E, Leech-Derived Trypsin Inhibitor TRYPSIN COMPLEX	402	gi 3318722
Ribosomal protein S3	143	gi 6755372
Beta actin	138	gi 49868
Keratin	129	gi 453155
Keratin	127	gi 547754
PREDICTED: similar to casein kinase II alpha 1 subunit isoform a isoform 1	121	gi 73991517
Keratin	116	gi 81891716
Keratin	102	gi 4159806
Keratin	99	gi 45597458
PREDICTED: similar to casein kinase II alpha 1 subunit isoform b	98	gi 114603982
Ribosomal protein L9	92	gi 607793
Keratin	90	gi 119892108
Ribosomal protein L9	83	gi 109503459
Keratin	80	gi 47059013
Keratin	76	gi 148747492
Keratin	73	gi 52789
Keratin	69	gi 398168
Alpha tubulin	69	gi 2843123
Alpha actin	64	gi 49864
Keratin	64	gi 115528975
Beta actin	61	gi 27687455
Beta actin	61	gi 57043600
PREDICTED: similar to laminin, alpha 2	61	gi 149636827
Beta tubulin	59	gi 57429
Trypsin 10	58	gi 84781771
Alpha tubulin	57	gi 66730465

★

★

Keratin 4	56	gi 148356276	
Cationic trypsinogen	56	gi 27465583	
PREDICTED: similar to ribosomal protein S6 kinase, 52kDa, polypeptide 1	54	gi 73960898	★
PREDICTED: hypothetical protein	51	gi 119914297	
PREDICTED: astrotactin	51	gi 114565537	
Transition protein	51	gi 110056	
PREDICTED: hypothetical protein	51	gi 126307650	

Table 7.7 Protein identification of recombinant FIP3 gel slice 3 by nLC-ESI-MS/MS searching the *Mammalia* database, performed by SHWFGF, University of Glasgow. Individual ion scores greater than the probability based MASCOT cut off score of 48 indicate homology or extensive identity ($p < 0.05$). Protein hits of interest are marked with a star.

Protein	Score	Database Accession Number	
Ribosomal protein S3	83	gi 296094	
CKII-alpha	78	gi 17016246	★
Ribosomal protein L9	70	gi 1208910	
GA17990 (Superfamily II RNA helicase)	52	gi 125984810	
Actin	49	gi 156773	
Trip1	44	gi 17648041	
Hu-li tai shao protein (homolog of adducin)	39	gi 157747	
CG32528	39	gi 24643390	

Table 7.8 Protein identification of recombinant FIP3 gel slice 3 by nLC-ESI-MS/MS searching the *Drosophila* database, performed by SHWFGF, University of Glasgow. Individual ion scores greater than the probability based MASCOT cut off score of 38 indicate homology or extensive identity ($p < 0.05$). Protein hits of interest are marked with a star.

Protein	Score	Database Accession Number
Chain E, Leech-Derived Trypsin Inhibitor TRYPSIN COMPLEX	331	gi 3318722
Trypsin precursor	306	gi 136429
Rab11-family interacting protein 3	246	gi 7662234
Ribosomal protein S3	221	gi 6755372
Keratin	192	gi 146741486
Keratin	133	gi 73996498
Keratin	110	gi 126343630
Keratin 4	103	gi 148356276
Keratin	74	gi 113420086
Trypsin 10	60	gi 84781771
Keratin	57	gi 148672070
BBC1	56	gi 29383
Acetyl-CoA carboxylase 2	54	gi 40019048
Ribosomal protein L9	53	gi 607793
Sema domain, seven thrombospondin repeats (type 1 and type 1-like), transmembrane domain (TM) and short cytoplasmic domain, (semaphorin) 5B	52	gi 109493368
Acetyl-CoA carboxylase	52	gi 2138330
PREDICTED: similar to aortic preferentially expressed gene 1	52	gi 113413482
PREDICTED: similar to Acetyl-CoA carboxylase 2	50	gi 149720500
PREDICTED: similar to phospholipase C, beta 3 (phosphatidylinositol-specific) isoform 6	50	gi 73983251
Ribosomal protein S9 isoform 2	50	gi 55661270
hCG41114, isoform CRA d	49	gi 119580811

Table 7.9 Protein identification of recombinant FIP3 gel slice 4 by nLC-ESI-MS/MS searching the *Mammalia* database, performed by SHWFGF, University of Glasgow. Individual ion scores greater than the probability based MASCOT cut off score of 49 indicate homology or extensive identity (p<0.05)

Protein	Score	Database Accession Number
Ribosomal protein S3	114	gi 17136324
Ribosomal protein S10a	64	gi 21357663
Ribosomal protein L9	53	gi 1208910
Ribosomal protein S9, isoform A	53	gi 24661707
Ribosomal protein S16	43	gi 19922746
Phospholipase C	40	gi 158131

Table 7.10 Protein identification of recombinant FIP3 gel slice 4 by nLC-ESI-MS/MS searching the *Drosophila* database, performed by SHWFGF, University of Glasgow. Individual ion scores greater than the probability based MASCOT cut off score of 38 indicate homology or extensive identity ($p < 0.05$).

Protein	Score	Database Accession Number
Keratin	583	gi 1346343
Chain E, Leech-Derived Trypsin Inhibitor TRYPSIN COMPLEX	335	gi 3318722
Trypsin precursor	314	gi 136429
Keratin	277	gi 453155
Keratin	151	gi 73996498
Keratin	140	gi 148356276
Keratin	122	gi 126343630
Rab11-family interacting protein 3	122	gi 7662234
Keratin	113	gi 114644554
Keratin	112	gi 149714742
Keratin	105	gi 149417889
Keratin	101	gi 57012352
Ribosomal protein S9 isoform 2	99	gi 55661270
Keratin	89	gi 81891716
Ribosomal protein S23	84	gi 3088342
PREDICTED: similar to calmodulin	84	gi 149255339
Keratin	82	gi 109099462
Keratin	78	gi 46485130
Keratin	75	gi 24753845

Keratin	75	gi 109096855
Keratin	71	gi 62122767
Keratin	69	gi 52789
Ribosomal protein L31	66	gi 1655596
Histone H2A.2	59	gi 31979
Ribosomal protein L9	59	gi 607793
Keratin	58	gi 547754
Keratin	57	gi 27764561
Histone cluster 1, H2ba	57	gi 24586679
Keratin	53	gi 73996461
Histone H2B	53	gi 119879706
PREDICTED: hypothetical protein	52	gi 126341903
Keratin	52	gi 398168

Table 7.11 Protein identification of recombinant FIP3 gel slice 5 by nLC-ESI-MS/MS searching the *Mammalia* database, performed by SHWFGF, University of Glasgow. Individual ion scores greater than the probability based MASCOT cut off score of 49 indicate homology or extensive identity ($p < 0.05$).

Protein	Score	Database Accession Number
Ribosomal protein S23	84	gi 22024141
Ribosomal protein S16	77	gi 19922746
60S ribosomal protein L31	66	gi 6094051
Chain A, Solution Structure of a Calmodulin-Target Peptide Complex By Multidimensional Nmr	64	gi 494737
Similar to <i>Drosophila melanogaster</i> Ribosomal protein L9	59	gi 38047669
Ribosomal protein S9, isoform A	56	gi 24661707
Ribosomal protein S10a	55	gi 21357663
CG32275-PA	43	gi 24656683

Table 7.12 Protein identification of recombinant FIP3 gel slice 5 by nLC-ESI-MS/MS searching the *Drosophila* database, performed by SHWFGF, University of Glasgow. Individual ion scores greater than the probability based MASCOT cut off score of 39 indicate homology or extensive identity ($p < 0.05$).

**7.1.3 Rab11-FIP3 gel slices analysed via LC-MS/MS by Aberdeen
Proteomics, University of Aberdeen**

Sample Details	Summary of Sample Results from Human database	Summary of Sample Results from <i>Spodoptera Frugiperda</i> database
Gel Slice 1	gi 30411061 Rab11 family interacting protein 3 (class II)	No hits
Gel Slice 2	gi 386854 Type II keratin subunit protein	No hits
Gel Slice 3	gi 7662234 Rab11-family interacting protein 3	No Hits
Gel Slice 4	gi 7662234 Rab11-family interacting protein 3	No Hits
Gel Slice 5	gi 7662234 Rab11-family interacting protein 3	No Hits
Gel Slice 6	gi 7662234 Rab11-family interacting protein 3	gi 12585261 Heat shock 70 kDa protein cognate 4 (Hsc 70-4)
Gel Slice 7	gi 7662234 Rab11-family interacting protein 3	No Hits
Gel Slice 8	gi 4507729 Tubulin, beta 2	gi 121987496 Tubulin beta-1 chain
Gel Slice 9	gi 7662234 Rab11-family interacting protein 3	gi 91091212 PREDICTED: similar to tar RNA binding protein
Gel Slice 10	gi 7662234 Rab11-family interacting protein 3	No Hits
Gel Slice 11	gi 7765076 S3 ribosomal protein	gi 16566719 Ribosomal protein S3
Gel Slice 12	gi 7662234 Rab11-family interacting protein 3	gi 74844658 40S ribosomal protein S4

Gel Slice 13	gi 607793 Ribosomal protein L9	gi 21759393 60S ribosomal protein L9
Gel Slice 14	No Significant Hits	No Significant Hits
Gel Slice 15	gi 1655596 Ribosomal protein L31	gi 51701794 60S ribosomal protein L31
Gel Slice 16	No Significant Hits	No Significant Hits

Table 7.13 Protein identification of recombinant FIP3 gel slices by LC-MS/MS searching Human and *Spodoptera Frugiperda* databases, performed by Aberdeen Proteomics at the University of Aberdeen. The major FIP3 band is found in gel slice 4.

List of References

- Addinall, S.G., Mayr, P.S., Doyle, S., Sheehan, J.K., Woodman, P.G., Allan, V.J. (2001). Phosphorylation by cdc2-CyclinB1 Kinase Releases Cytoplasmic Dynein from Membranes. *Journal of Biological Chemistry* **276**, 15939-15944.
- Ai, E., Skop, A.R. (2009). Endosomal recycling regulation during cytokinesis. *Commun Integr Biol.* **2**, 444-447.
- Albertson, R., Cao, J., Hsieh, T.s., Sullivan, W. (2008). Vesicles and actin are targeted to the cleavage furrow via furrow microtubules and the central spindle. *The Journal of Cell Biology* **181**, 777-790.
- Albertson, R., Riggs, B., Sullivan, W. (2005). Membrane traffic: a driving force in cytokinesis. *Trends in Cell Biology* **15**, 92-101.
- Alessi, D.R., Cuenda, A., Cohen, P., Dudley, D.T., Saltiel, A.R. (1995). PD 098059 Is a Specific Inhibitor of the Activation of Mitogen-activated Protein Kinase Kinase in Vitro and in Vivo. *Journal of Biological Chemistry* **270**, 27489-27494.
- Altan-Bonnet, N., Phair, R.D., Polishchuk, R.S., Weigert, R., Lippincott-Schwartz, J. (2003). A role for Arf1 in mitotic Golgi disassembly, chromosome segregation, and cytokinesis. *Proceedings of the National Academy of Sciences of the United States of America* **100**, 13314-13319.
- Amanchy, R., Periaswamy, B., Mathivanan, S., Reddy, R., Tattikota, S.G., Pandey, A. (2007). A curated compendium of phosphorylation motifs. *Nat Biotech* **25**, 285-286.
- Anjum, R., Blenis, J. (2008). The RSK family of kinases: emerging roles in cellular signalling. *Nat Rev Mol Cell Biol* **9**, 747-758.
- Bajorek, M., Morita, E., Skalicky, J.J., Morham, S.G., Babst, M., Sundquist, W.I. (2009). Biochemical Analyses of Human IST1 and Its Function in Cytokinesis. *Molecular Biology of the Cell* **20**, 1360-1373.
- Barr, A.R., Gergely, F. (2007). Aurora-A: the maker and breaker of spindle poles. *Journal of Cell Science* **120**, 2987-2996.
- Barr, F.A., Gruneberg, U. (2007). Cytokinesis: Placing and Making the Final Cut. *Cell* **131**, 847-860.
- Barr, F.A., Sillje, H.H.W., Nigg, E.A. (2004). Polo-like kinases and the orchestration of cell division. *Nat Rev Mol Cell Biol* **5**, 429-441.
- Bement, W.M., Benink, H.A., von Dassow, G. (2005). A microtubule-dependent zone of active RhoA during cleavage plane specification. *The Journal of Cell Biology* **170**, 91-101.

- Blom, N., Gammeltoft, S., Brunak, S. (1999). Sequence and structure-based prediction of eukaryotic protein phosphorylation sites. *Journal of Molecular Biology* 294, 1351-1362.
- Blom, N., Sicheritz-Pontén, T., Gupta, R., Gammeltoft, S., Brunak, S. (2004). Prediction of post-translational glycosylation and phosphorylation of proteins from the amino acid sequence. *Proteomics* 4, 1633-1649.
- Bluemink, J.G., de Laat, S.W. (1973). NEW MEMBRANE FORMATION DURING CYTOKINESIS IN NORMAL AND CYTOCHALASIN B-TREATED EGGS OF XENOPUS LAEVIS: I. Electron Microscope Observations. *The Journal of Cell Biology* 59, 89-108.
- Bollen, M., Gerlich, D.W., Lesage, B. (2009). Mitotic phosphatases: from entry guards to exit guides. *Trends in Cell Biology* 19, 531-541.
- Bonifacino, J.S., Glick, B.S. (2004). The Mechanisms of Vesicle Budding and Fusion. *Cell* 116, 153-166.
- Boucrot, E., Kirchhausen, T. (2007). Endosomal recycling controls plasma membrane area during mitosis. *Proceedings of the National Academy of Sciences* 104, 7939-7944.
- Brandeis, M., Rosewell, I., Carrington, M., Crompton, T., Jacobs, M.A., Kirk, J., Gannon, J., Hunt, T. (1998). Cyclin B2-null mice develop normally and are fertile whereas cyclin B1-null mice die in utero. *Proceedings of the National Academy of Sciences of the United States of America* 95, 4344-4349.
- Brandie, F.M., Aran, V., Verma, A., McNew, J.A., Bryant, N.J., Gould, G.W. (2008). Negative Regulation of Syntaxin4/SNAP-23/VAMP2-Mediated Membrane Fusion by Munc18c *In Vitro*. *PLoS ONE* 3, e4074.
- Bridges, D.J., Pitt, A.R., Hanrahan, O., Brennan, K., Voorheis, H.P., Herzyk, P., de Koning, H.P., Burchmore, R.J. (2008). Characterisation of the plasma membrane subproteome of bloodstream form *Trypanosoma brucei*. *Proteomics* 8, 83-99.
- Brown, N.R., Noble, M.E.M., Endicott, J.A., Johnson, L.N. (1999). The structural basis for specificity of substrate and recruitment peptides for cyclin-dependent kinases. *Nat Cell Biol* 1, 438-443.
- Burgess, D.R., Chang, F. (2005). Site selection for the cleavage furrow at cytokinesis. *Trends in Cell Biology* 15, 156-162.
- Burkard, M.E., Maciejowski, J., Rodriguez-Bravo, V.n., Repka, M., Lowery, D.M., Clauser, K.R., Zhang, C., Shokat, K.M., Carr, S.A., Yaffe, M.B., Jallepalli, P.V. (2009). Plk1 Self-Organization and Priming Phosphorylation of HsCYK-4 at the Spindle Midzone Regulate the Onset of Division in Human Cells. *PLoS Biol* 7, e1000111.
- Cao, J., Albertson, R., Riggs, B., Field, C.M., Sullivan, W. (2008). Nuf, a Rab11 effector, maintains cytokinetic furrow integrity by promoting local actin polymerization. *The Journal of Cell Biology* 182, 301-313.

- Cheeseman, I.M., Anderson, S., Jwa, M., Green, E.M., Kang, J.s., Yates III, J.R., Chan, C.S.M., Drubin, D.G., Barnes, G. (2002). Phospho-Regulation of Kinetochore-Microtubule Attachments by the Aurora Kinase Ipl1p. *Cell* **111**, 163-172.
- Chen, Y.A., Scales, S.J., Patel, S.M., Doung, Y.-C., Scheller, R.H. (1999). SNARE complex formation is triggered by Ca²⁺ and drives membrane fusion. *Cell* **97**, 165-174.
- Clute, P., Pines, J. (1999). Temporal and spatial control of cyclin B1 destruction in metaphase. *Nat Cell Biol* **1**, 82-87.
- Cohen, P. (2000). The regulation of protein function by multisite phosphorylation - a 25 year update. *Trends in Biochemical Sciences* **25**, 596-601.
- Colanzi, A., Suetterlin, C., Malhotra, V. (2003). Cell-cycle-specific Golgi fragmentation: how and why? *Current Opinion in Cell Biology* **15**, 462-467.
- D'Souza-Schorey, C., Li, G., Colombo, M.I., Stahl, P.D. (1995). A regulatory role for ARF6 in receptor-mediated endocytosis. *Science* **267**, 1175-1178.
- D'Souza-Schorey, C., Chavrier, P. (2006). ARF proteins: roles in membrane traffic and beyond. *Nat Rev Mol Cell Biol* **7**, 347-358.
- Danilchik, M.V., Bedrick, S.D., Brown, E.E., Ray, K. (2003). Furrow microtubules and localized exocytosis in cleaving *Xenopus laevis* embryos. *Journal of Cell Science* **116**, 273-283.
- Dhariwala, F., Rajadhyaksha, M. (2008). An Unusual Member of the Cdk Family: Cdk5. *Cellular and Molecular Neurobiology* **28**, 351-369.
- Ditchfield, C., Johnson, V.L., Tighe, A., Ellston, R., Haworth, C., Johnson, T., Mortlock, A., Keen, N., Taylor, S.S. (2003). Aurora B couples chromosome alignment with anaphase by targeting BubR1, Mad2, and Cenp-E to kinetochores. *The Journal of Cell Biology* **161**, 267-280.
- Dollar, G., Struckhoff, E., Michaud, J., Cohen, R.S. (2002). Rab11 polarization of the *Drosophila* oocyte: a novel link between membrane trafficking, microtubule organization, and oskar mRNA localization and translation. *Development* **129**, 517-526.
- Dudley, D.T., Pang, L., Decker, S.J., Bridges, A.J., Saltiel, A.R. (1995). A synthetic inhibitor of the mitogen-activated protein kinase cascade. *Proc Natl Acad Sci U S A*. **92**, 7686-7689.
- Dutertre, S., Cazales, M., Quaranta, M., Froment, C., Trabut, V., Dozier, C., Mirey, G., Bouche, J.P., Theis-Febvre, N., Schmitt, E., Monsarrat, B., Prigent, C., Ducommun, B. (2004). Phosphorylation of CDC25B by Aurora-A at the centrosome contributes to the G2-M transition. *Journal of Cell Science* **117**, 2523-2531.
- Dyer, N., Rebollo, E., Dominguez, P., Elkhatib, N., Chavrier, P., Daviet, L., Gonzalez, C., Gonzalez-Gaitan, M. (2007). Spermatocyte cytokinesis requires

rapid membrane addition mediated by ARF6 on central spindle recycling endosomes. *Development* **134**, 4437-4447.

Eathiraj,S., Mishra,A., Prekeris,R., Lambright,D.G. (2006). Structural Basis for Rab11-mediated Recruitment of FIP3 to Recycling Endosomes. *Journal of Molecular Biology* **364**, 121-135.

Echard,A., Hickson,G.R.X., Foley,E., O'Farrell,P.H. (2004). Terminal Cytokinesis Events Uncovered after an RNAi Screen. *Current Biology* **14**, 1685-1693.

Eggert,U.S., Kiger,A.A., Richter,C., Perlman,Z.E., Perrimon,N., Mitchison,T.J., Field,C.M. (2004). Parallel Chemical Genetic and Genome-Wide RNAi Screens Identify Cytokinesis Inhibitors and Targets. *PLoS Biol* **2**, e379.

Eggert,U.S., Mitchison,T.J., Field,C.M. (2006). Animal Cytokinesis: From Parts List to Mechanisms. *Annual Review of Biochemistry* **75**, 543-566.

Elia,A.E.H., Cantley,L.C., Yaffe,M.B. (2003a). Proteomic Screen Finds pSer/pThr-Binding Domain Localizing Plk1 to Mitotic Substrates. *Science* **299**, 1228-1231.

Elia,A.E.H., Rellos,P., Haire,L.F., Chao,J.W., Ivins,F.J., Hoepker,K., Mohammad,D., Cantley,L.C., Smerdon,S.J., Yaffe,M.B. (2003b). The Molecular Basis for Phosphodependent Substrate Targeting and Regulation of Plks by the Polo-Box Domain. *Cell* **115**, 83-95.

Feng,B., Schwarz,H., Jesuthasan,S. (2002). Furrow-Specific Endocytosis during Cytokinesis of Zebrafish Blastomeres. *Experimental Cell Research* **279**, 14-20.

Fielding,A.B., Schonteich,E., Matheson,J., Wilson,G.M., Yu,X., Hickson,G.R.X., Srivastava,S., Baldwin,S.A., Prekeris,R., Gould,G.W. (2005). Rab11-FIP3 and Rab11-FIP4 interact with Arf6 and the Exocyst to control membrane traffic during cytokinesis. *EMBO J.* **24**, 3389-3399.

Fujiwara,T., Bandi,M., Nitta,M., Ivanova,E.V., Bronson,R.T., Pellman,D. (2005). Cytokinesis failure generating tetraploids promotes tumorigenesis in p53-null cells. *Nature* **437**, 1043-1047.

Fung,T.K., Poon,R.Y.C. (2005). A roller coaster ride with the mitotic cyclins. *Seminars in Cell & Developmental Biology* **16**, 335-342.

Fürthauer,M., González-Gaitán,M. (2009). Endocytosis and mitosis: a two-way relationship. *Cell Cycle* **8**, 3311-3318.

Girio,A., Montero,J.C., Pandiella,A., Chatterjee,S. (2007). Erk5 is activated and acts as a survival factor in mitosis. *Cellular Signalling* **19**, 1964-1972.

Glotzer,M. (2004). Cleavage furrow positioning. *The Journal of Cell Biology* **164**, 347-351.

Glotzer,M. (2005). The Molecular Requirements for Cytokinesis. *Science* **307**, 1735-1739.

- Glotzer, M. (2009). The 3Ms of central spindle assembly: microtubules, motors and MAPs. *Nat Rev Mol Cell Biol* 10, 9-20.
- Goss, J.W., Toomre, D.K. (2008). Both daughter cells traffic and exocytose membrane at the cleavage furrow during mammalian cytokinesis. *The Journal of Cell Biology* 181, 1047-1054.
- Gould, G.W., Lippincott-Schwartz, J. (2009). New roles for endosomes: from vesicular carriers to multi-purpose platforms. *Nat Rev Mol Cell Biol* 10, 287-292.
- Grabarek, Z. (2006). Structural Basis for Diversity of the EF-hand Calcium-binding Proteins. *Journal of Molecular Biology* 359, 509-525.
- Grant, B.D., Donaldson, J.G. (2009). Pathways and mechanisms of endocytic recycling. *Nat Rev Mol Cell Biol* 10, 597-608.
- Gromley, A., Yeaman, C., Rosa, J., Redick, S., Chen, C.T., Mirabelle, S., Guha, M., Sillibourne, J., Doxsey, S.J. (2005). Centriolin Anchoring of Exocyst and SNARE Complexes at the Midbody Is Required for Secretory-Vesicle-Mediated Abscission. *Cell* 123, 75-87.
- Gruneberg, U., Neef, R., Honda, R., Nigg, E.A., Barr, F.A. (2004). Relocation of Aurora B from centromeres to the central spindle at the metaphase to anaphase transition requires MKlp2. *The Journal of Cell Biology* 166, 167-172.
- Guertin, D.A., Trautmann, S., McCollum, D. (2002). Cytokinesis in Eukaryotes. *Microbiology and Molecular Biology Reviews* 66, 155-178.
- Guse, A., Mishima, M., Glotzer, M. (2005). Phosphorylation of ZEN-4/MKLP1 by Aurora B Regulates Completion of Cytokinesis. *Current Biology* 15, 778-786.
- Hales, C.M., Griner, R., Hobdy-Henderson, K.C., Dorn, M.C., Hardy, D., Kumar, R., Navarre, J., Chan, E.K.L., Lapierre, L.A., Goldenring, J.R. (2001). Identification and Characterization of a Family of Rab11-interacting Proteins. *Journal of Biological Chemistry* 276, 39067-39075.
- Harper, J.V. (2005). Synchronization of cell populations in G1/S and G2/M phases of the cell cycle. *Methods Mol Biol.* 296, 157-166.
- Hickson, G.R.X., Matheson, J., Riggs, B., Maier, V.H., Fielding, A.B., Prekeris, R., Sullivan, W., Barr, F.A., Gould, G.W. (2003). Arfophilins are dual Arf/Rab 11 binding proteins that regulate recycling endosome distribution and are related to *Drosophila* nuclear fallout. *Mol. Biol. Cell.* 14, 2908-2920.
- Hirokawa, N., Noda, Y., Tanaka, Y., Niwa, S. (2009). Kinesin superfamily motor proteins and intracellular transport. *Nat Rev Mol Cell Biol* 10, 682-696.
- Horgan, C.P., McCaffrey, M.W. (2009). The dynamic Rab11-FIPs. *Biochem Soc Trans* 37, 1032-1036.
- Horgan, C.P., Oleksy, A., Zhdanov, A.V., Lall, P.Y., White, I.J., Khan, A.R., Futter, C.E., McCaffrey, J.G., McCaffrey, M.W. (2007). Rab11-FIP3 Is Critical

for the Structural Integrity of the Endosomal Recycling Compartment. *Traffic* **8**, 414-430.

Hümmer,S., Mayer,T.U. (2009). Cdk1 Negatively Regulates Midzone Localization of the Mitotic Kinesin Mklp2 and the Chromosomal Passenger Complex. *Current Biology* **19**, 607-612.

Inoue,H., Ha,V.L., Prekeris,R., Randazzo,P.A. (2008). Arf GTPase-activating Protein ASAP1 Interacts with Rab11 Effector FIP3 and Regulates Pericentrosomal Localization of Transferrin Receptor-positive Recycling Endosome. *Molecular Biology of the Cell* **19**, 4224-4237.

Ishizaki,T., Uehata,M., Tamechika,I., Keel,J., Nonomura,K., Maekawa,M., Narumiya,S. (2000). Pharmacological Properties of Y-27632, a Specific Inhibitor of Rho-Associated Kinases. *Molecular Pharmacology* **57**, 976-983.

Jackman,M., Firth,M., Pines,J. (1995). Human cyclins B1 and B2 are localized to strikingly different structures: B1 to microtubules, B2 primarily to the Golgi apparatus. *EMBO J* **14**, 1646-1654.

Jagoe,W.N., Lindsay,A.J., Read,R.J., McCoy,A.J., McCaffrey,M.W., Khan,A.R. (2006). Crystal Structure of Rab11 in Complex with Rab11 Family Interacting Protein 2. *Structure* **14**, 1273-1283.

Jahn,R., Scheller,R.H. (2006). SNAREs - engines for membrane fusion. *Nat Rev Mol Cell Biol* **7**, 631-643.

Jeyaprakash,A.A., Klein,U.R., Lindner,D., Ebert,J., Nigg,E.A., Conti,E. (2007). Structure of a Survivin-Borealin-INCENP Core Complex Reveals How Chromosomal Passengers Travel Together. *Cell* **131**, 271-285.

Jing,J., Tarbutton,E., Wilson,G., Prekeris,R. (2009). Rab11-FIP3 is a Rab11-binding protein that regulates breast cancer cell motility by modulating the actin cytoskeleton. *European Journal of Cell Biology* **88**, 325-341.

Junutula,J.R., Schonteich,E., Wilson,G.M., Peden,A.A., Scheller,R.H., Prekeris,R. (2004). Molecular Characterization of Rab11 Interactions with Members of the Family of Rab11-interacting Proteins. *Journal of Biological Chemistry* **279**, 33430-33437.

Jürgens,G. (2005). Plant cytokinesis: fission by fusion. *Trends in Cell Biology* **15**, 277-283.

Kahn,R.A., Cherfils,J., Elias,M., Lovering,R.C., Munro,S., Schurmann,A. (2006). Nomenclature for the human Arf family of GTP-binding proteins: ARF, ARL, and SAR proteins. *The Journal of Cell Biology* **172**, 645-650.

Kaitna,S., Mendoza,M., Jantsch-Plunger,V., Glotzer,M. (2000). Incenp and an Aurora-like kinase form a complex essential for chromosome segregation and efficient completion of cytokinesis. *Current Biology* **10**, 1172-1181.

Kay,B.K., Williamson,M.P., Sudol,M. (2000). The importance of being proline: the interaction of proline-rich motifs in signaling proteins with their cognate domains. *The FASEB Journal* **14**, 231-241.

- Kim, J.E., Billadeau, D.D., Chen, J. (2005). The Tandem BRCT Domains of Ect2 Are Required for Both Negative and Positive Regulation of Ect2 in Cytokinesis. *Journal of Biological Chemistry* **280**, 5733-5739.
- Kouranti, I., Sachse, M., Arouche, N., Goud, B., Echard, A. (2006). Rab35 Regulates an Endocytic Recycling Pathway Essential for the Terminal Steps of Cytokinesis. *Current Biology* **16**, 1719-1725.
- Lee, M.T., Mishra, A., Lambright, D.G. (2009). Structural Mechanisms for Regulation of Membrane Traffic by Rab GTPases. *Traffic* **10**, 1377-1389.
- Lindon, C., Pines, J. (2004). Ordered proteolysis in anaphase inactivates Plk1 to contribute to proper mitotic exit in human cells. *The Journal of Cell Biology* **164**, 233-241.
- Lindqvist, A., Rodriguez-Bravo, V., Medema, R.H. (2009). The decision to enter mitosis: feedback and redundancy in the mitotic entry network. *The Journal of Cell Biology* **185**, 193-202.
- Liu, Q., Ruderman, J.V. (2006). Aurora A, mitotic entry, and spindle bipolarity. *103*, 5811-5816.
- Low, S.H., Li, X., Miura, M., Kudo, N., Quiñones, B., Weimbs, T. (2003). Syntaxin 2 and Endobrevin Are Required for the Terminal Step of Cytokinesis in Mammalian Cells. *Developmental Cell* **4**, 753-759.
- Loyet, K.M., Stults, J.T., Arnott, D. (2005). Mass Spectrometric Contributions to the Practice of Phosphorylation Site Mapping through 2003: A Literature Review. *Molecular Cellular Proteomics* **4**, 235-245.
- Malumbres, M., Barbacid, M. (2009). Cell cycle, CDKs and cancer: a changing paradigm. *Nat Rev Cancer* **9**, 153-166.
- Marumoto, T., Honda, S., Hara, T., Nitta, M., Hirota, T., Kohmura, E., Saya, H. (2003). Aurora-A Kinase Maintains the Fidelity of Early and Late Mitotic Events in HeLa Cells. *Journal of Biological Chemistry* **278**, 51786-51795.
- Matsumura, F. (2005). Regulation of myosin II during cytokinesis in higher eukaryotes. *Trends in Cell Biology* **15**, 371-377.
- Maxfield, F.R., McGraw, T.E. (2004). Endocytic recycling. *Mol. Cell Biol.* **5**, 121-132.
- Mazumdar, A., Mazumdar, M. (2002). How one becomes many: blastoderm cellularization in *Drosophila melanogaster*. *Bioessays* **24**, 1012-1022.
- Meyers, J.M., Prekeris, R. (2002). Formation of Mutually Exclusive Rab11 Complexes with Members of the Family of Rab11-interacting Proteins Regulates Rab11 Endocytic Targeting and Function. *Journal of Biological Chemistry* **277**, 49003-49010.
- Minoshima, Y., Kawashima, T., Hirose, K., Tonozuka, Y., Kawajiri, A., Bao, Y.C., Deng, X., Tatsuka, M., Narumiya, S., May, J., Nosaka, T., Semba, K., Inoue, T., Satoh, T., Inagaki, M., Kitamura, T. (2003). Phosphorylation by Aurora B

Converts MgcRacGAP to a RhoGAP during Cytokinesis. *Developmental Cell* **4**, 549-560.

Mishima,M., Pavicic,V., Gruneberg,U., Nigg,E.A., Glotzer,M. (2004). Cell cycle regulation of central spindle assembly. *Nature* **430**, 908-913.

Mollinari,C., Kleman,J.P., Jiang,W., Schoehn,G., Hunter,T., Margolis,R.L. (2002). PRC1 is a microtubule binding and bundling protein essential to maintain the mitotic spindle midzone. *The Journal of Cell Biology* **157**, 1175-1186.

Montagnac,G., Echard,A., Chavrier,P. (2008). Endocytic traffic in animal cell cytokinesis. *Current Opinion in Cell Biology* **20**, 454-461.

Morgan,D.O. (2007). *The Cell Cycle: Principles of Control*. New Scientist Press Ltd.

Munson,M., Novick,P. (2006). The exocyst defrocked, a framework of rods revealed. *Nat Struct Mol Biol* **13**, 577-581.

Neef,R., Klein,U.R., Kopajtich,R., Barr,F.A. (2006). Cooperation between Mitotic Kinesins Controls the Late Stages of Cytokinesis. *Current Biology* **16**, 301-307.

Neef,R., Gruneberg,U., Kopajtich,R., Li,X., Nigg,E.A., Sillje,H., Barr,F.A. (2007). Choice of Plk1 docking partners during mitosis and cytokinesis is controlled by the activation state of Cdk1. *Nat Cell Biol* **9**, 436-444.

Neef,R., Preisinger,C., Sutcliffe,J., Kopajtich,R., Nigg,E.A., Mayer,T.U., Barr,F.A. (2003). Phosphorylation of mitotic kinesin-like protein 2 by polo-like kinase 1 is required for cytokinesis. *The Journal of Cell Biology* **162**, 863-876.

Neumüller,R.A., Knoblich,J.A. (2009). Dividing cellular asymmetry: asymmetric cell division and its implications for stem cells and cancer. *Genes & Development* **23**, 2675-2699.

Ng,M.M., Chang,F., Burgess,D.R. (2005). Movement of Membrane Domains and Requirement of Membrane Signaling Molecules for Cytokinesis. *Developmental Cell* **9**, 781-790.

Nigg,E.A. (2001). Mitotic kinases as regulators of cell division and its checkpoints. *Nat Rev Mol Cell Biol* **2**, 21-32.

Niiya,F., Xie,X., Lee,K.S., Inoue,H., Miki,T. (2005). Inhibition of Cyclin-dependent Kinase 1 Induces Cytokinesis without Chromosome Segregation in an ECT2 and MgcRacGAP-dependent Manner. *Journal of Biological Chemistry* **280**, 36502-36509.

Nurse,P. (2000). A Long Twentieth Century of the Cell Cycle and Beyond. *Cell* **100**, 71-78.

Otegui,M.S., Verbrugghe,K.J., Skop,A.R. (2005). Midbodies and phragmoplasts: analogous structures involved in cytokinesis. *Trends in Cell Biology* **15**, 404-413.

- Paradela,A., Albar,J.P. (2008). Advances in the Analysis of Protein Phosphorylation. *Journal of Proteome Research* 7, 1809-1818.
- Pelissier,A., Chauvin,J.P., Lecuit,T. (2003). Trafficking through Rab11 Endosomes Is Required for Cellularization during *Drosophila* Embryogenesis. *Current Biology* 13, 1848-1857.
- Perkins,D.N., Pappin,D.J.C., Creasy,D.M., Cottrell,J.S. (1999). Probability-based protein identification by searching sequence databases using mass spectrometry data. *Electrophoresis* 20, 3551-3567.
- Petronczki,M., Glotzer,M., Kraut,N., Peters,J.M. (2007). Polo-like Kinase 1 Triggers the Initiation of Cytokinesis in Human Cells by Promoting Recruitment of the RhoGEF Ect2 to the Central Spindle. *Developmental Cell* 12, 713-725.
- Petronczki,M., Lönnerst,P., Peters,J.M. (2008). Polo on the Rise--from Mitotic Entry to Cytokinesis with Plk1. *Developmental Cell* 14, 646-659.
- Pfeffer,S.R. (1999). Transport-vesicle targeting: tethers before SNAREs. *Nat Cell Biol* 1, E17-E22.
- Piekny,A., Werner,M., Glotzer,M. (2005). Cytokinesis: welcome to the Rho zone. *Trends in Cell Biology* 15, 651-658.
- Pines,J. (2006). Mitosis: a matter of getting rid of the right protein at the right time. *Trends in Cell Biology* 16, 55-63.
- Prekeris,R., Davies,J.M., Scheller,R.H. (2001). Identification of a Novel Rab11/25 Binding Domain Present in Eferin and Rip Proteins. *Journal of Biological Chemistry* 276, 38966-38970.
- Prekeris,R., Gould,G.W. (2008). Breaking up is hard to do - membrane traffic in cytokinesis. *Journal of Cell Science* 121, 1569-1576.
- Prekeris,R., Klumperman,J., Scheller,R.H. (2000). A Rab11/Rip11 Protein Complex Regulates Apical Membrane Trafficking via Recycling Endosomes. *Molecular Cell* 6, 1437-1448.
- Riggs,B., Rothwell,W., Mische,S., Hickson,G.R.X., Matheson,J., Hays,T.S., Gould,G.W., Sullivan,W. (2003). Actin cytoskeleton remodeling during early *Drosophila* furrow formation requires recycling endosomal components Nuclear-fallout and Rab11. *The Journal of Cell Biology* 163, 143-154.
- Rothwell,W.F., Fogarty,P., Field,C.M., Sullivan,W. (1998). Nuclear-fallout, a *Drosophila* protein that cycles from the cytoplasm to the centrosomes, regulates cortical microfilament organization. *Development* 125, 1295-1303.
- Rothwell,W.F., Zhang,C.X., Zelano,C., Hsieh,T.S., Sullivan,W. (1999). The *Drosophila* centrosomal protein Nuf is required for recruiting Dah, a membrane associated protein, to furrows in the early embryo. *Journal of Cell Science* 112, 2885-2893.

- Ruchaud,S., Carmena,M., Earnshaw,W.C. (2007). Chromosomal passengers: conducting cell division. *Nat Rev Mol Cell Biol* **8**, 798-812.
- Santamaria,A., Neef,R., Eberspacher,U., Eis,K., Husemann,M., Mumberg,D., PrechtI,S., Schulze,V., Siemeister,G., Wortmann,L., Barr,F.A., Nigg,E.A. (2007). Use of the Novel Plk1 Inhibitor ZK-Thiazolidinone to Elucidate Functions of Plk1 in Early and Late Stages of Mitosis. *Molecular Biology of the Cell* **18**, 4024-4036.
- Scholey,J.M., Brust-Mascher,I., Mogilner,A. (2003). Cell division. *Nature* **422**, 746-752.
- Schonteich,E., Pilli,M., Simon,G.C., Matern,H.T., Junutula,J.R., Sentz,D., Holmes,R.K., Prekeris,R. (2007). Molecular characterization of Rab11-FIP3 binding to ARF GTPases. *European Journal of Cell Biology* **86**, 417-431.
- Schonteich,E., Wilson,G.M., Burden,J., Hopkins,C.R., Anderson,K., Goldenring,J.R., Prekeris,R. (2008). The Rip11/Rab11-FIP5 and kinesin II complex regulates endocytic protein recycling. *Journal of Cell Science* **121**, 3824-3833.
- Schweitzer,J.K., Burke,E.E., Goodson,H.V., D'Souza-Schorey,C. (2005). Endocytosis Resumes during Late Mitosis and Is Required for Cytokinesis. *Journal of Biological Chemistry* **280**, 41628-41635.
- Schweitzer,J.K., D'Souza-Schorey,C. (2002). Localization and Activation of the ARF6 GTPase during Cleavage Furrow Ingression and Cytokinesis. *Journal of Biological Chemistry* **277**, 27210-27216.
- Schweitzer,J.K., D'Souza-Schorey,C. (2004). Finishing the job: cytoskeletal and membrane events bring cytokinesis to an end. *Experimental Cell Research* **295**, 1-8.
- Schweitzer,J.K., D'Souza-Schorey,C. (2005). A requirement for ARF6 during the completion of cytokinesis. *Experimental Cell Research* **311**, 74-83.
- Seong,Y.S., Min,C., Li,L., Yang,J.Y., Kim,S.Y., Cao,X., Kim,K., Yuspa,S.H., Chung,H.H., Lee,K.S. (2003). Characterization of a Novel Cyclin-Dependent Kinase 1 Inhibitor, BMI-1026. *Cancer Research* **63**, 7384-7391.
- Sessa,F., Mapelli,M., Ciferri,C., Tarricone,C., Areces,L.B., Schneider,T.R., Stukenberg,P.T., Musacchio,A. (2005). Mechanism of Aurora B Activation by INCENP and Inhibition by Hesperadin. *Molecular Cell* **18**, 379-391.
- Sharp,D.J., Rogers,G.C., Scholey,J.M. (2000). Microtubule motors in mitosis. *Nature* **407**, 41-47.
- Shetty,K.T., Link,W.T., Pant,H.C. (1993). cdc2-like kinase from rat spinal cord specifically phosphorylates KSPXK motifs in neurofilament proteins: isolation and characterization. *Proc Natl Acad Sci U S A.* **90**, 6844-6888.
- Shiba,T., Koga,H., Shin,H.W., Kawasaki,M., Kato,R., Nakayama,K., Wakatsuki,S. (2006). Structural basis for Rab11-dependent membrane

recruitment of a family of Rab11-interacting protein 3 (FIP3)/Arfophilin-1. *Proceedings of the National Academy of Sciences* **103**, 15416-15421.

Shin, O.H., Couvillon, A.D., Exton, J.H. (2001). Arfophilin Is a Common Target of both Class II and Class III ADP-Ribosylation Factors. *Biochemistry* **40**, 10846-10852.

Shin, O.H., Ross, A.H., Mihai, I., Exton, J.H. (1999). Identification of Arfophilin, a Target Protein for GTP-bound Class II ADP-ribosylation Factors. *Journal of Biological Chemistry* **274**, 36609-36615.

Shuster, C.B., Burgess, D.R. (2002). Targeted new membrane addition in the cleavage furrow is a late, separate event in cytokinesis. *Proceedings of the National Academy of Sciences of the United States of America* **99**, 3633-3638.

Siller, K.H., Doe, C.Q. (2009). Spindle orientation during asymmetric cell division. *Nat Cell Biol* **11**, 365-374.

Simon, G.C., Prekeris, R. (2008). Mechanisms regulating targeting of recycling endosomes to the cleavage furrow during cytokinesis. *Biochemical Society Transactions* **036**, 391-394.

Simon, G.C., Schonteich, E., Wu, C.C., Piekny, A., Ekiert, D., Yu, X., Gould, G.W., Glotzer, M., Prekeris, R. (2008). Sequential Cyk-4 binding to ECT2 and FIP3 regulates cleavage furrow ingression and abscission during cytokinesis. *EMBO J* **27**, 1791-1803.

Sisson, J.C., Field, C., Ventura, R., Royou, A., Sullivan, W. (2000). Lava Lamp, a Novel Peripheral Golgi Protein, Is Required for *Drosophila melanogaster* Cellularization. *The Journal of Cell Biology* **151**, 905-918.

Skop, A.R., Bergmann, D., Mohler, W.A., White, J.G. (2001). Completion of cytokinesis in *C. elegans* requires a brefeldin A-sensitive membrane accumulation at the cleavage furrow apex. *Current Biology* **11**, 735-746.

Skop, A.R., Liu, H., Yates, J., III, Meyer, B.J., Heald, R. (2004). Dissection of the Mammalian Midbody Proteome Reveals Conserved Cytokinesis Mechanisms. *Science* **305**, 61-66.

Sollner, T., Whiteheart, S.W., Brunner, M., Erdjument-Bromage, H., Geromanos, S., Tempst, P., Rothman, J.E. (1993). SNAP receptors implicated in vesicle targeting and fusion. *Nature* **362**, 318-324.

Song, S.J., Kim, S.J., Song, M.S., Lim, D.S. (2009). Aurora B-Mediated Phosphorylation of RASSF1A Maintains Proper Cytokinesis by Recruiting Syntaxin16 to the Midzone and Midbody. *Cancer Research* **69**, 8540-8544.

St Denis, N.A., Derksen, D.R., Litchfield, D.W. (2009). Evidence for Regulation of Mitotic Progression through Temporal Phosphorylation and Dephosphorylation of CK2{alpha}. *Molecular and Cellular Biology* **29**, 2068-2081.

Steigemann, P., Gerlich, D.W. (2009). Cytokinetic abscission: cellular dynamics at the midbody. *Trends in Cell Biology* **19**, 606-616.

Stenmark,H. (2009). Rab GTPases as coordinators of vesicle traffic. *Nat Rev Mol Cell Biol* 10, 513-525.

Strickland,L.I., Burgess,D.R. (2004). Pathways for membrane trafficking during cytokinesis. *Trends in Cell Biology* 14, 115-118.

Sullivan,M., Morgan,D.O. (2007). Finishing mitosis, one step at a time. *Nat Rev Mol Cell Biol* 8, 894-903.

Sunkel,C.E., Glover,D.M. (1988). polo, a mitotic mutant of *Drosophila* displaying abnormal spindle poles. *Journal of Cell Science* 89, 25-38.

The Arabidopsis Genome Initiative (2000). Analysis of the genome sequence of the flowering plant *Arabidopsis thaliana*. *Nature* 408, 796-815.

The UniProt Consortium (2009). The Universal Protein Resource (UniProt) 2009. *Nucleic Acids Research* 37, D169-D174.

Thompson,H.M., Skop,A.R., Euteneuer,U., Meyer,B.J., McNiven,M.A. (2002). The Large GTPase Dynamin Associates with the Spindle Midzone and Is Required for Cytokinesis. *Current Biology* 12, 2111-2117.

Touré,A., Mzali,R., Liot,C., Seguin,L., Morin,L., Crouin,C., Chen-Yang,I., Tsay,Y.G., Dorseuil,O., Gacon,G., Bertoglio,J. (2008). Phosphoregulation of MgcRacGAP in mitosis involves Aurora B and Cdk1 protein kinases and the PP2A phosphatase. *FEBS Letters* 582, 1182-1188.

Ubersax,J.A., Ferrell Jr,J.E. (2007). Mechanisms of specificity in protein phosphorylation. *Nat Rev Mol Cell Biol* 8, 530-541.

Uehata,M., Ishizaki,T., Satoh,H., Ono,T., Kawahara,T., Morishita,T., Tamakawa,H., Yamagami,K., Inui,J., Maekawa,M., Narumiya,S. (1997). Calcium sensitization of smooth muscle mediated by a Rho-associated protein kinase in hypertension. *Nature* 389, 990-994.

Ullrich,O., Reinsch,S., Urbe,S., Zerial,M., Parton,R.G. (1996). Rab11 regulates recycling through the pericentriolar recycling endosome. *The Journal of Cell Biology* 135, 913-924.

Vader,G., Medema,R.H., Lens,S.M.A. (2006). The chromosomal passenger complex: guiding Aurora-B through mitosis. *The Journal of Cell Biology* 173, 833-837.

Vagnarelli,P., Earnshaw,W.C. (2004). Chromosomal passengers: the four-dimensional regulation of mitotic events. *Chromosoma* 113, 211-222.

van Vliet,C., Thomas,E.C., Merino-Trigo,A., Teasdale,R.D., Gleeson,P.A. (2003). Intracellular sorting and transport of proteins. *Progress in Biophysics and Molecular Biology* 83, 1-45.

Wallace,D.M., Lindsay,A.J., Hendrick,A.G., McCaffrey,M.W. (2002). The Novel Rab11-FIP/Rip/RCP Family of Proteins Displays Extensive Homo- and Hetero-Interacting Abilities. *Biochemical and Biophysical Research Communications* 292, 909-915.

Wang,X., Tournier,C. (2006). Regulation of cellular functions by the ERK5 signalling pathway. *Cellular Signalling* **18**, 753-760.

Wang,Y.I. (2005). The mechanism of cortical ingression during early cytokinesis: thinking beyond the contractile ring hypothesis. *Trends in Cell Biology* **15**, 581-588.

Weber,T., Zemelman,B.V., McNew,J.A., Westermann,B., Gmachl,M., Parlati,F., Sollner,T.H., Rothman,J.E. (1998). SNAREpins: Minimal machinery for membrane fusion. *Cell* **92**, 759-772.

Werner,M., Glotzer,M. (2008). Control of cortical contractility during cytokinesis. *Biochemical Society Transactions* **036**, 371-377.

Wilson,G.M., Fielding,A.B., Simon,G.C., Yu,X., Andrews,P.D., Hames,R.S., Frey,A.M., Peden,A.A., Gould,G.W., Prekeris,R. (2005). The FIP3-Rab11 Protein Complex Regulates Recycling Endosome Targeting to the Cleavage Furrow during Late Cytokinesis. *Molecular Biology of the Cell* **16**, 849-860.

Xu,H., Brill,J.A., Hsien,J., McBride,R., Boulianne,G.L., Trimble,W.S. (2002). Syntaxin 5 Is Required for Cytokinesis and Spermatid Differentiation in *Drosophila*. *Developmental Biology* **251**, 294-306.

Yde,C.W., Olsen,B.B., Meek,D., Watanabe,N., Guerra,B. (2008). The regulatory [beta]-subunit of protein kinase CK2 regulates cell-cycle progression at the onset of mitosis. *Oncogene* **27**, 4986-4997.

Yu,X., Prekeris,R., Gould,G.W. (2007). Role of endosomal Rab GTPases in cytokinesis. *European Journal of Cell Biology* **86**, 25-35.

Yüce,O., Piekny,A., Glotzer,M. (2005). An ECT2-centralspindlin complex regulates the localization and function of RhoA. *The Journal of Cell Biology* **170**, 571-582.

Zerial,M., McBride,H. (2001). Rab proteins as membrane organizers. *Nat Rev Mol Cell Biol* **2**, 107-117.

Zhu,C., Lau,E., Schwarzenbacher,R., Bossy-Wetzel,E., Jiang,W. (2006). Spatiotemporal control of spindle midzone formation by PRC1 in human cells. *103*, 6196-6201.